KONINKLIJKE NEDERLANDSE AKADEMIE VAN WETENSCHAPPEN

PROCEEDINGS

SERIES B

PHYSICAL SCIENCES

VOLUME LXIII - No. 4

NORTH-HOLLAND PUBLISHING COMPANY - AMSTERDAM - 1960

The complete Proceedings consist of three Series, viz.:

SERIES A: MATHEMATICAL SCIENCES

SERIES B: PHYSICAL SCIENCES

SERIES C: BIOLOGICAL AND MEDICAL SCIENCES

Articles for these Series cannot be accepted unless formally communicated for publication by one of the members of the Royal Neth. Academy of Sciences.

BIOCHEMISTRY

SILICON TETRACHLORIDE-TREATED PAPER IN THE PAPER CHROMATOGRAPHY OF PHOSPHATIDES

IIIa. COMPARISON BETWEEN CHROMATOGRAPHY OF EGG PHOSPHATIDES ON $SiCl_4$-TREATED PAPER AND ON NON-IMPREGNATED PAPER. ROLE OF THE GRADIENT IN THE MOBILE PHASE AND INFLUENCE OF ADSORBENT

BY

H. G. BUNGENBERG DE JONG AND J. TH. HOOGEVEEN

(Communicated at the meeting of February 27, 1960)

1. *Introduction*

The chromatography of egg phosphatides on non-impregnated paper will now be treated in similar detail as the chromatography of egg phosphatides on $SiCl_4$-treated paper (Part II [5]).

Subsequently we proceed to deal with the question whether there exists a gradient in the mobile phase in non-impregnated and in different kinds of $SiCl_4$-treated papers. The role of the gradient and the influence of the nature of the adsorbent will be discussed in the final sections, as well as the location of the adsorbent effective in chromatography with $SiCl_4$-treated papers.

2. *Methods*

In the present study we use exclusively Schleicher and Schüll paper no 2043*b* cut into sheets of 17 × 27 cm, in such a way that the 27 cm direction coincides with the direction of the smaller suction rate of the paper. Part of the experiments is performed with non-impregnated paper, part with $SiCl_4$-treated paper. For preparing the latter we follow the directions given in Part I [1]. By means of a self-filling capillary pipette (of about 5 mm^3 capacity) the phosphatide solution is applied on the starting points. Chromatography is performed with di-isobutyl-ketone—acetic acid—H_2O (50:25:5; by volume) in a dark room at constant temperature (20° C), with the large slit-feeding apparatus described in a former communication [2]. After drying, the chromatogram is stained with the Acid-Fuchsin—$UO_2(NO_3)_2$—0.01 N HCl staining solution described in former communications [3, 4].

After drying once more, the spots are circumlined with a pencil.

The phosphatide preparations [1]) used are:

1) Pure lecithin obtained by column fractionation.

2) "Reference mixture", a mixture of column fractions containing lecithin, cephalin, lysolecithin, lysocephalin and sphingomyelin in not very different concentrations.

---

1) We thank Dr. G. J. M. Hooghwinkel for putting these preparations (dissolved in chloroform-methanol = 4:1) at our disposal.

3) A mixture of lecithin, lysolecithin and sphingomyelin (also mixed column fractions) in which components are not present in roughly comparable concentrations, but in which lecithin > lysolecithin $\gg$ sphingomyelin.

The method used for determining the gradient in the mobile phase wetting the paper has already been given in outline and for a special case only, in Part II of this series [5]. Further details and modifications which are necessary in determining the gradient in neutralized $SiCl_4$-treated paper are given in section 4.

3. *Some characteristics of the chromatography of egg phosphatides on non-impregnated paper*

a) Lecithin

Apart from a single observation on the chromatography of the reference mixture (see below in paragraph *b*) our knowledge of the chromatography of egg phosphatides with di-isobutylketone—acetic acid—H_2O (50:25:5) on non-impregnated paper is restricted to the laws which govern the displacement of lecithin spots (5 mm^3 of 0.12 % lecithin) [6].

In these experiments chromatograms with nine starting points on an oblique line cutting the frontline have been run by means of the large slit-feeding apparatus. An example of such a chromatogram is given in fig. 1.

It appeared that the transported spots do not lie on a straight line with the oblique line through the starting points. Any straight line through this intersection point (for instance the broken line in fig. 1) represents a definite R_f value. It was therefore evident that R_f values (which are constant in the case of ideal partition chromatography) are in our case not at all constant. The fact that the curve through the transported spots approximates a horizontal level, indicated that, the lower the starting point is situated, the position of the transported spots becomes more and more independent of it. The results suggest that a gradient is present in the composition of the mobile phase on the paper. The horizontal part of the curve on which the transported spots are situated may denote a particular composition of the mobile phase at which the upward migration of lecithin reaches its maximum value relative to the velocity of the front. Experiments in which the front-height was varied showed that the horizontal part (asymptote) through the transported spots always lies approximately at the same fraction of the distance from front to immersion line. This leads to the notion R_{f_i}, a (practically) constant number for lecithin (with the given paper, mobile phase and chromatographic apparatus), which is defined as follows

$$R_{f_i} = \frac{\text{distance from asymptote to immersion line}}{\text{distance from front to immersion line}}$$

In part II of the present series we have shown that the same applies for the chromatography of lecithin on neutralized $SiCl_4$-treated paper, though the numerical value of R_{f_i} is different (0.47) from that on non-impregnated paper (0.65) [5].

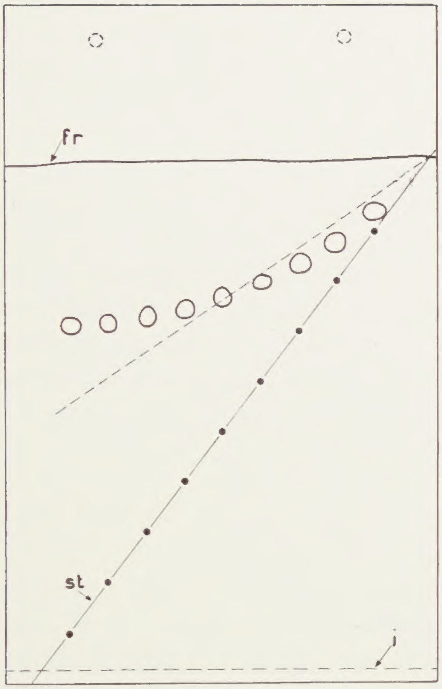

Fig. 1.

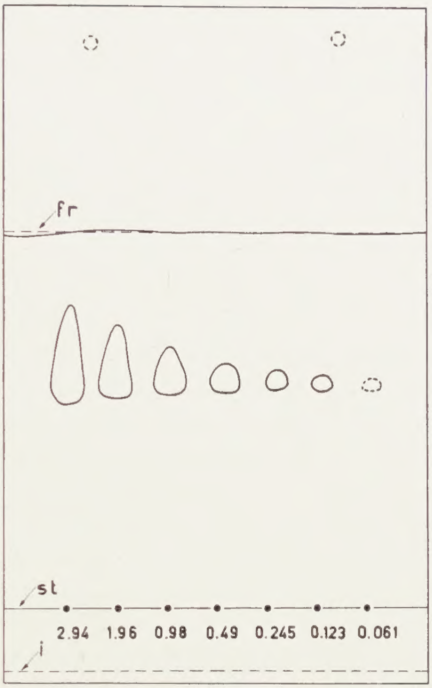

Fig. 2.

Fig. 1. Chromatogram of lecithin on non-impregnated Schleicher and Schüll 2043*b*, provided with nine starting points on a sloping line (*st*). The front (*fr*) has risen 20 cm above the immersion line (*i*).

Fig. 2. Influence of the amount of lecithin applied at the starting points (figures below the starting points give concentrations of the lecithin solution of which 5 mm^3 has been applied. Non-impregnated paper has been used). The front has risen 17.5 cm above the immersion line.

In the communication just mentioned another type of chromatograms was described giving additional information about the mechanism of chromatography on $SiCl_4$-treated paper. On the starting points lying on a horizontal line 5 mm^3 of lecithin solution of increasing concentration were applied. It appears that with increasing amounts of lecithin applied on the paper

a) the area of the transported spot increases with a power of the concentration smaller than one (namely 0.65),
b) the lower margins of the spots lie on a nearly horizontal line,
c) the gain in area is due to some broadening, but mainly to increase in length, whereby the spots acquire a roughly triangular shape,
d) small spots are evenly stained (with the Acid Fuchsin—$UO_2(NO_3)_2$—0,01 N HCl staining bath). The same intensity of staining is present in the lower part of the triangular spots. In the latter the colour intensity increases in upward direction, the more so as the total length of the triangular spot increases.

The above results, combined with the results concerning the importance of a gradient in the mobile phase led to a picture of the mechanism of chromatography of lecithin on $SiCl_4$-treated paper with our mobile phase. It is to be considered as adsorption chromatography operating with gradient elution.

We now return to the chromatography of lecithin on non-impregnated paper. It has been observed that the laws governing the displacement of lecithin spots on non-impregnated paper are the same as on $SiCl_4$-treated paper. We now want to know whether the influence of the concentration of the lecithin solution applied on the points of a horizontal starting line is also similar. In our experiments the same pure lecithin fraction (column fraction) has been used as for the analogous investigation on $SiCl_4$-treated papers of different kinds (Part II) [5].

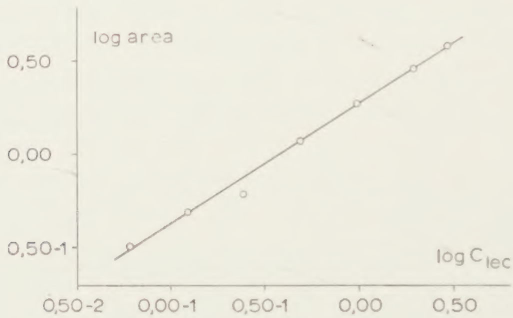

Fig. 3. Double logarithmic plot of spot area in relation to lecithin concentrations applied.

Various dilutions of the stock solution were made with $CHCl_3$-methanol (80:20) ranging from 2.94 to 0.061 %. As always 5 mm^3 was applied on the paper. The front was allowed to ascend to 17.5 cm above the immersion line. The chromatogram obtained is given in fig. 2. With a planimeter the area of the spots was measured (see Table I). In fig. 3 the logarithm of the area has been plotted against the logarithm of the lecithin concentration. Apart from one probably erroneous point, the points in fig. 3 lie on a straight line, with a slope equal to 0.64.

When we compare this result and the shape of the spots with the previously given observations (points a, b and c) we note the same behaviour as in the case of $SiCl_4$-treated paper. Moreover, the intensity of staining increases in the triangular spots in upward direction (point d).

Taking all facts regarding the chromatography of lecithin on non-impregnated paper together, the conclusion must be that its mechanism is similar to that effective on $SiCl_4$-treated paper, namely adsorption chromatography with gradient elution.

TABLE I

Spot area in dependence on lecithin concentration

lec. conc. %	spot area cm^2	lec. conc. %	spot area cm^2
0.061	0.32	0.98	1.84
0.123	0.49	1.96	2.82
0.245	0.61	2.94	3.71
0.49	1.16	—	—

b) Mixtures of egg-phosphatides

We have investigated the chromatography of the Reference mixture on non-impregnated paper only once. (See part I of this series, fig. 1A and B[1]). When working with a small chromatographic apparatus of the conventional type (closed glass cylinder with strip dipping with its lower end in a layer of the mobile phase di-isobutylketone—acetic acid—H_2O, in the ratio 50:25:5 by volume), we obtained only two elongated spots of which the upper had a distinct constriction. With the aid of special tests described in a former communication it has been found that the upper spot consists of three components which partly cover one another, namely lecithin (L) at the top, then cephalin (C) and lowest (below the constriction) sphingomyelin (S) [4]. The lower elongated spot on untreated paper is a composite spot too, consisting of lysolecithin (LL) at the top and lysocephalin (LC) at the bottom. In the experiments now following the large slit-feeding apparatus has been used throughout. In the case of $SiCl_4$-treated paper this apparatus gave a better resolution than the smaller type of apparatus. We expect this also to apply for chromatography on non-impregnated paper. We have found that with the large slit-feeding apparatus the Reference mixture yields no longer two but three spots. Evidently the upper spot with constriction has now been resolved into two separate spots. The three spots reckoned from top to bottom thus consist of:

L+C (not resolved); S; LL+LC (not resolved).

A chromatogram with nine starting points on an oblique line has been run to a front height of 22.5 cm above the immersion line. Beforehand on each starting point 5 mm^3 of $\frac{1}{2}$ % Reference mixture had been applied. The chromatogram — see fig. 4 — shows that for each of the spots: L+C; S; LL+LC the same applies as was discussed in paragraph a) for lecithin alone (compare fig. 1). The spots lie on three curves which to the left reach or nearly reach three horizontal levels. So it is clear that the postulated gradient in the mobile phase does not only play an important role in the chromatographic displacement of lecithin but also in the displacement of the other components of the Reference mixture. In the next chromatogram (fig. 5) we investigated the influence of the total amount of a mixture of lecithin, sphingomyelin and lysolecithin.

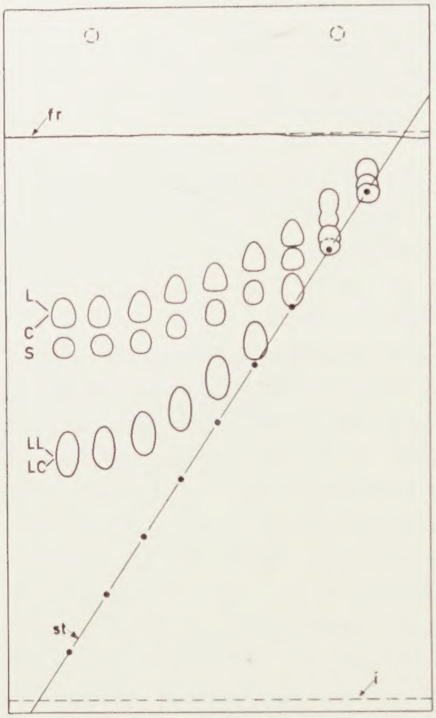

Fig. 4.

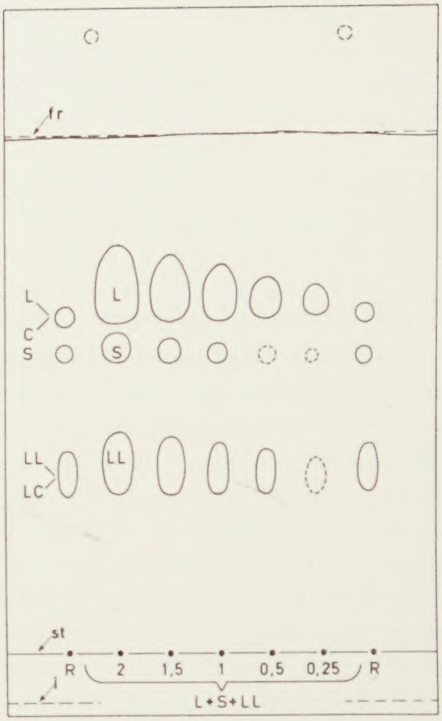

Fig. 5.

Fig. 4. Chromatogram of the Reference mixture on non-impregnated paper, with nine starting points on a sloping line. The front has risen 22.5 cm above the immersion line.

Fig. 5. Chromatogram of a mixture of lecithin (L), lysolecithin (LL) and sphingo myelin (S) on non-impregnated paper. Influence of the total concentration.

The concentration (%) of the 5 mm^3 portion brought up on the starting points is written underneath on the chromatogram. On the left and the right starting point 5 mm^3 of $\frac{1}{2}$ % Reference mixture has been applied When this chromatogram is compared with the one given in fig. 2 we find here in principle the same consequence of the increase of the amount applied:

a) Increase of spot area proportional to a power lower than one.
b) On each row the bases of the spots lie on one horizontal line.
c) The increase in area is mainly due to an increase in length of the spots.
d) The intensity of staining increases upwards in the larger spots.

We need not repeat here what was already said in paragraph a), and conclude this section with the statement that the chromatography of egg phosphatides on non-impregnated paper is of the same general character as that on $SiCl_4$-treated paper. So its mechanism must be considered to consist in adsorption chromatography by gradient elution.

When we compare the lecithin spots in fig. 5 with those in fig. 2 they appear to be broader and to have less pronounced triangular shapes. Besides, the contours of the spots are much vaguer, which gave difficulties in outlining the spots with a pencil.

This chromatogram was made with a stock solution of L + S + LL which had been stored some 4 months in the refrigerator. The same stock solution, when fresh, gave the characteristic, sharply defined triangular spots on $SiCl_4$-treated paper. See fig. 22–24 in Part II of this series [5].

We think that the less pronounced triangular shapes and vagues contours of the spots in fig. 5 are indications of a beginning deterioration. For this reason we give here no table for the spot areas, nor a double logarithmic plot.

4. *Determination of the acetic acid gradient in the mobile phase wetting the paper*

a) Method

In the following experiments paper sheets 17 × 27 cm were used, non-impregnated or $SiCl_4$-treated. The immersion line, and parallel to it lines 4.5; 9; 13.5; 18 and 22.5 cm above the immersion line were drawn on the paper beforehand.

In the large slit-feeding apparatus the sheets were run with di-isobutylketone—acetic acid—H_2O (50:25:5; by volume) until the front just reached the line 22.5 cm above the immersion line. The sheet was taken out of the apparatus and was cut with scissors along the pencil lines into five strips. As the strips were cut they were allowed to drop into wide flasks, each containing 50 ml distilled water. The weight of these flasks with their stoppers was known. All these manipulations were accomplished in the shortest possible time (20 seconds) to prevent evaporation losses. The flasks were now weighed so that the weight of the wetted strips became known. Extraction of the strips was accomplished by standing overnight. Two aliquots of 20 ml extract were titrated with 0.1 N NaOH. We calculated from this the weight of the acetic acid originally present in each strip. The strips were then dried in air at room temperature. Their weight became constant after at least 2 days. In our calculations we need, however, their weight without their hygroscopic moisture. In the case of non-impregnated paper, the moisture content of air-dry paper was 6 %. In the case of "acid" $SiCl_4$-treated paper which in the course of a week had lost all HCl, the moisture content was 5 %. To find the weight of the dry strips we subtracted in the cases mentioned 6 % and 5 % respectively of the air-dry weights.

The difference in weight of the wetted and dry strips gave us the weight of the mobile phase present in each strip. We finally calculated the mean acetic acid content in weight percent of the mobile phase in each of the five strips.

As it was necessary to cut the five strips as rapidly as possible, there is no garantee that the strips were cut exactly along the pencil lines. As the dry weight of each strip is known and therefore the sum of the dry weights of the five strips, we calculated the mean breadth of each strip expressed in % of the distance between front and immersion line.

Particulars concerning the determination of the gradient in the case of fresh acid $SiCl_4$-treated paper and of neutralized $SiCl_4$-treated paper are given in the paragraphs *d* and *e*.

b) Rate of loss of HCl to the air from freshly prepared $SiCl_4$-treated paper

We know already from Part I and II of this series that freshly prepared $SiCl_4$-treated paper contains free HCl, and that the HCl content diminishes with time when the paper hangs in air at room temperature [1], [5].

To be sure that the titrations following below in paragraph *d* will indicate only acetic acid we will use "acid" $SiCl_4$-treated paper which practically contains no HCl any more. It is not yet known how long the paper must hang in air until it is practically HCl-free.

Some 17 × 27 cm sheets with horizontal pencil lines at 4.5 cm distance were treated with a 2 % solution of $SiCl_4$ in CCl_4 [1], and were hung in air. At different times after the preparation, strips of 17 × 4.5 cm were cut off and were extracted with 50 ml water. Two aliquots of 20 ml extract were titrated with 0.1 N NaOH (at longer times of exposure with 0.01 N NaOH). The strips were dried and weighed. From these data we calculated the number of ml 0.1 N NaOH needed to neutralize the HCl present per gram of air dry $SiCl_4$-treated paper at increasing times of exposure to the air.

Age (hours)	ml NaOH 0.1 N	Age (hours)	ml NaOH 0.1 N
0.5	3.90	45	0.286
4	2.21	71	0.120
21	0.73	93	0.069

The decrease of the HCl content could not be followed further since results became unreliable by the titration error. We have tried to find an empirical relation between HCl content and time, and have found that when the logarithm of the NaOH 0.1 N is plotted against the square root of the time six points are obtained which lie practically on a straight line. Compare fig. 6.

The graph may be used to find at any time after preparation the amount of HCl still present in the paper.

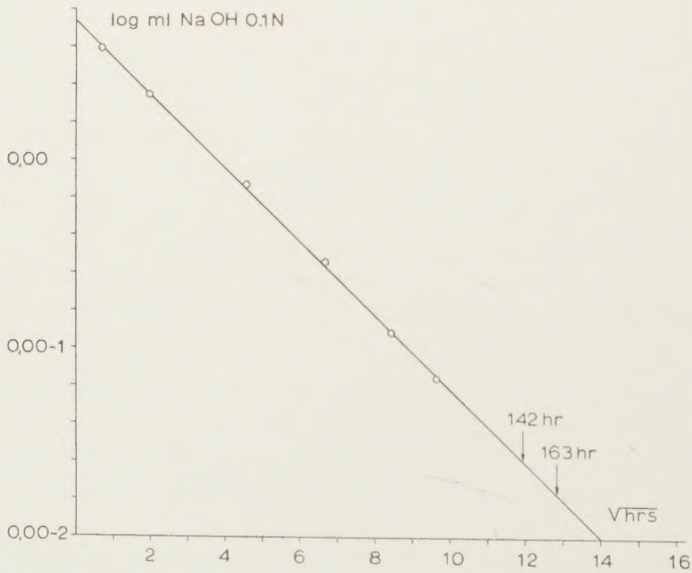

Fig. 6. Empirical relation for the loss of HCl from freshly prepared $SiCl_4$-treated paper (2 % $SiCl_4$ in CCl_4) and time of exposure of the paper to the air. Ordinate: Logarithm of ml NaOH 0.1 N needed for neutralizing the HCl present in 1 gr of air-dry paper. Abscissa: Square root of time in hours.

c) Non-impregnated paper

Two sheets were run. The results of each experiment are given in Table II. We see from the columns 1 and 5 that the calculated mean zone limits are only slightly different from 0–20; 20–40; 40–60; 60–80 and 80–100. The latter values would have been found if in cutting the strips the pencil lines on the paper would have been followed exactly.

As can be seen from the columns 2 and 6, for each zone the weight of the liquid wetting the paper diminishes appreciably in the direction of the front. The weight of acetic acid diminishes in frontward direction to a relatively much greater extent (columns 3 and 7). We are, however, interested in the change in concentration of the acetic acid in the direction of the front. The mean concentrations are found by dividing the values in columns 3 and 7 by those in columns 2 and 6 respectively.

When we compare the acetic acid concentrations thus found – see columns 4 and 8 – we see that experimental errors amounting to 1–2 weight percent of acetic acid may occur. For this reason the values in column 10 have as a rule been rounded off to whole percentages. The results (columns 9 and 10) are plotted in fig. 7. The gradient in the acetic acid concentration is given approximately by the broken curve.

The occurrence of a gradient in the mobile phase in chromatography with non-impregnated paper has been suggested in a former communication [6]. The results in section 3 of the present communication are in agreement with this view, while the results presented in this paragraph conclusively show that the supposed gradient exists. The mechanism

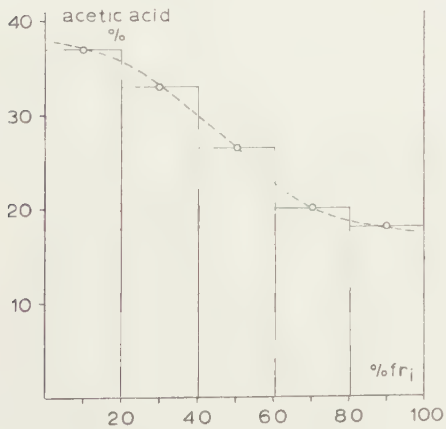

Fig. 7.

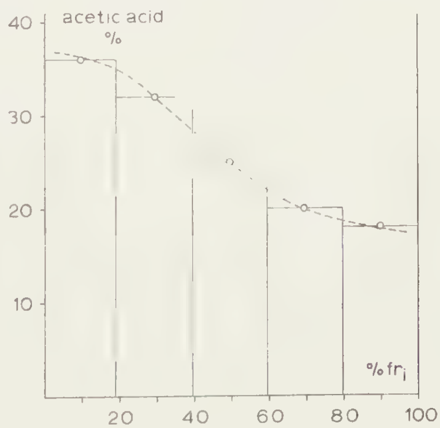

Fig. 8.

Fig. 7. Gradient in the mobile phase wetting a chromatogram on non-impregnated paper. Ordinate: weight percentage of acetic acid. The zone limits are expressed in percentages of f_{r_i}, that is the distance from front (f_r) to immersion line (i).

Fig. 8. Gradient in the acetic acid concentration of the mobile phase wetting HCl-free, $SiCl_4$-treated paper.

of chromatography of egg phosphatides on non-impregnated paper then may be assumed to be adsorption chromatography by gradient elution.

d) "Acid" $SiCl_4$-treated paper, which has lost practically all hydrochloric acid by hanging sufficiently long in air

In the two following determinations of the acetic acid gradient we have used $SiCl_4$-treated paper aged for 142 and 163 hours respectively (first and second experiment in Table III). We may use the graph given in fig. 6 to find the ml NaOH 0.1 N corresponding to the HCl content still left in 1 g of the paper (though by titration this can no longer be determined). We then find 0.025 and 0.017 ml NaOH. As the dry weight of the strips is somewhat less than 1 g (about 0.9–0.95 g), and the ml NaOH 0.1 N to neutralize 50 ml extract of the least acid strip (that beneath the front) appeared to be about 10 ml, we can completely neglect the very small amount of HCl remaining in the paper. So we are sure that the acidity which is titrated in the experiments of Table III concerns only acetic acid.

The results (Table III) show the same general trends as Table II, namely a strong decrease of the mean amount of mobile phase in the direction of the front and a still stronger decrease of the mean amount of acetic acid in the same direction, with the result that the mean acetic acid concentration decreases in that direction roughly by half.

TABLE II

Acetic acid gradient in non-impregnated paper

First experiment				Second experiment				Means	
upper margin of zone % of f_{r_i} *	wet strip -dry strip mg	acetic acid mg	acetic acid %	upper margin of zone of f_{r_i}	wet strip -dry strip mg	acetic acid mg	acetic acid %	position of zone % of f_{r_i}	acetic acid %
19.8	1005	371	36.9	20.3	1017	383	37.7	0–20.1	37
39.9	896	296	33.0	40.5	947	311	32.8	20.1–40.2	33
60.4	767	196	25.6	60.6	766	209	27.3	40.2–60.5	26^{5}
80.2	615	116	18.9	80.2	625	128	20.5	60.5–80.2	20
100	375	63	16.8	100	376	71	18.9	80.2–100	18

* In Tables II, III and IV: f_{r_i} means the distance of the front (f_r) from the immersion line (i).

In the last two columns of the Table the means of the two experiments have been given. They have been plotted in fig. 8, in which the broken line gives approximately the gradient in the acetic acid concentration. It is interesting to compare these results with those of Table II, and with fig. 7. We then find that the shape of the gradient is in principle the same, and further that quantitatively the differences do not differ more

than is compatible with the experimental errors (compare columns 10 in table II and III).

Thus the gradient in $SiCl_4$-treated paper appears to be about the same as in non-impregnated paper.

TABLE III

Acetic acid gradient in HCl-free $SiCl_4$-treated paper

First experiment				Second experiment				Means	
upper margin of zone % of f_{r_i}	wet strip -dry strip mg	acetic acid mg	acetic acid %	upper margin of zone % of f_{r_i}	wet strip -dry strip mg	acetic acid mg	acetic acid %	position of zone % of f_{r_i}	acetic acid %
19.0	800	289	36.1	19.2	849	301	35.5	0 19.1	36
39.4	769	250	32.5	39.7	792	256	32.3	19.1–39.6	32
59.6	693	174	25.1	59.5	670	168	25.1	39.6–59.6	25
79.8	553	112	20.3	79.6	536	107	20.0	59.6–79.7	20
100	338	61	18.0	100	331	61	18.4	79.7–100	18

e) Acid $SiCl_4$-treated paper used ½ hour after preparation

The experiment has been performed in the same way as that described in paragraph *d*. See Table IV, upper part. Here we have to reckon with the fact that in titrating the extracts we determine acetic acid + HCl. In column 3 we have given the amount of acetic acid derived from the titration data, supposing that no HCl is present. Compare fig. 9, broken curve. In doing so we make an error and the actual amount of acetic acid will be less.

As to the HCl present in the paper at the start of the experiment (corresponding to 3.90 ml 0.1 N NaOH per g air-dry paper) one calculates that in each strip of 4.5 × 17 cm (mean air-dry weight 0.923 g) the HCl present calculated as acetic acid amounts to 22 mg. When we subtract 22 mg from the values in column 3, the rounded-off acetic acid concentrations given in column 4, in downward direction, become 34; 29; 22^5; 17 and 14 % respectively. Compare fig. 9, dotted curve. It is not certain that the whole amount of HCl present at the start of the experiment must be subtracted. If the strips had been hung in air during the time of chromatography the HCl content would have diminished to half of its original value. Thus it is conceivable that during chromatography the still unwetted part of the paper continues to lose HCl. To obtain the true acetic acid concentration a smaller correction is needed as the zone is situated higher. Summarizing we can say that, though here the position of the curve representing the acetic acid gradient remains somewhat uncertain there is no doubt that such a gradient exists.

f) Neutralized $SiCl_4$-treated paper

With this paper complications arise from the NH_4Cl present in it, as a result of neutralizing the HCl with ammonia vapour. We cannot titrate the acetic acid with NaOH and phenolphthalein as the colour change of the indicator lies near the pK of NH_3. We have therefore added to the extract an excess of NaOH, boiled the NH_3 out and titrated back with HCl. The results are given in Table IV, lower part. Taking into account the more complicated method in determining the acetic acid, experimental errors in the results may be larger than in the experiments of the preceding paragraphs.

TABLE IV

Gradient in fresh $SiCl_4$-treated paper and in neutralized $SiCl_4$-treated paper

$SiCl_4$-treated paper (age = 30 min)			
upper margin of zone, % of fr_i	wet strip –dry strip mg	acetic* acid mg	acetic* acid %
19.5	1011	369	36.5
39.0	856	268	31
59.5	759	193	25
80.3	624	128	20^5
100	367	74	20

Neutralized $SiCl_4$-treated paper			
upper margin of zone, % of fr_i	wet strip –dry strip mg	acetic acid mg	acetic acid %
19.4	851	285	33^5
39.8	775	208	27
59.3	675	164	24
79.9	617	140	23
100	370	79	21

* Possibly present HCl also calculated as acetic acid. See text.

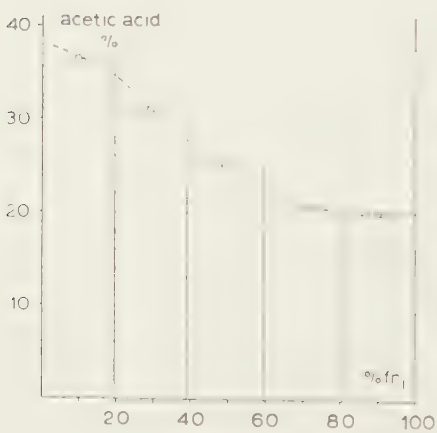

Fig. 9.

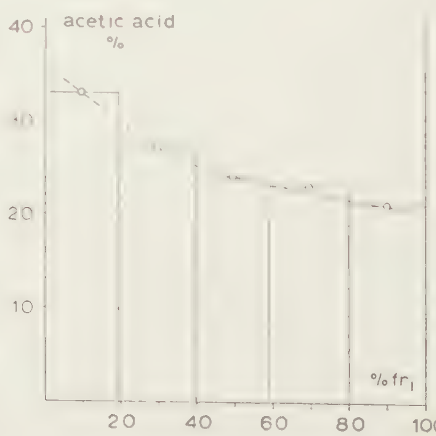

Fig. 10.

Fig. 9. Gradient (broken curve) in the total acid concentration of the mobile phase wetting $SiCl_4$-treated paper, starting chromatography ½ hr after preparation. The total acid (acetic acid + HCl) is here reckoned as acetic acid. The dotted curve gives the corrected gradient in the acetic acid concentration.

Fig. 10. Gradient in the acetic acid concentration of the mobile phase wetting neutralized $SiCl_4$-treated paper.

In any case it seems quite certain that a gradient is present in the acetic acid concentration in the direction of the front. When the results are plotted (fig. 10) and the gradient curve obtained is compared with those in figs. 7 and 8, its course seems to proceed differently (no longer distinctly S shaped and having in the middle of its course a smaller slope). Because of the greater errors this different course is however not certain.

5. *Chromatograms needed in the discussion following in section* 7

The determination of the gradient on non-impregnated paper (section 4, § b) and the running of the chromatograms on the same paper (fig. 4 and 5) were performed with a delay of one or two days. In both the same large slit-feeding apparatus has been used and the front has been allowed to ascend to the same height above the immersion line. These measures were taken in order that position of spots and gradient might be compared as best as possible.

The same measures were taken in the case of $SiCl_4$-treated papers. The chromatograms obtained from the Reference mixture are given in the figures 11 and 12 and are thus directly comparable with the gradients obtained in section 4, § d and e. A similar chromatogram on neutralized paper showed spots not lying on horizontal lines (possibly as a result of one-sided radiation) and can therefore not be trusted and will not be given here.

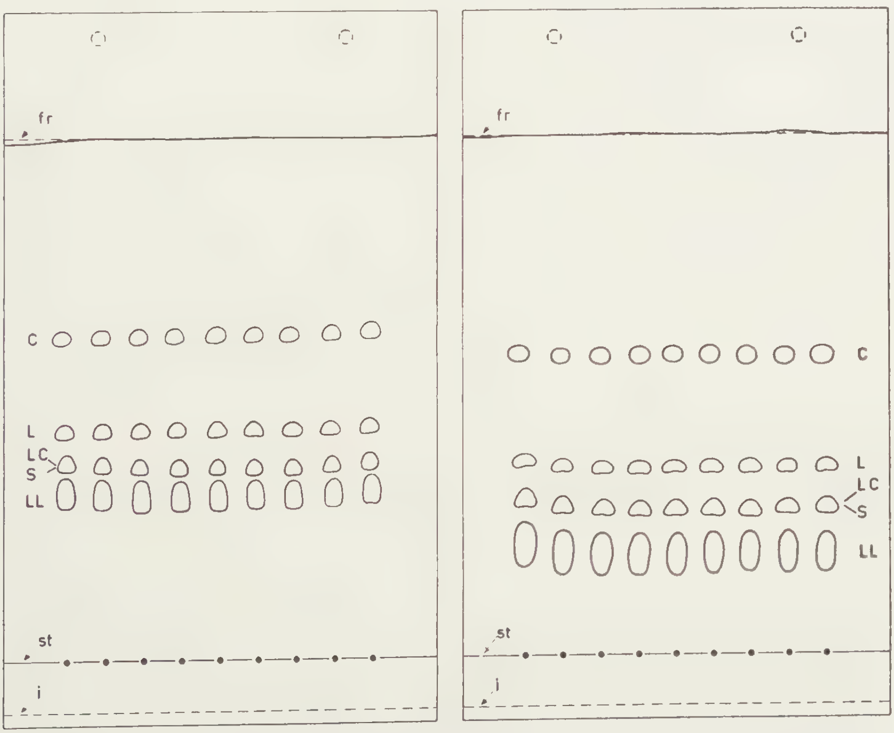

Figs. 11 and 12. Chromatograms of the reference mixture on $SiCl_4$-treated papers, 163 hours (fig. 11) and $\frac{1}{2}$ hour (fig. 12) after preparation respectively.

The next survey gives the R_{f_i} values for the spots on the chromatograms of fig. 4, 5, 11 and 12.

non-impregnated paper (mean of figs. 4 and 5)		HCl free $SiCl_4$-treated paper (fig. 11)		fresh $SiCl_4$-treated paper (fig. 12)	
L + C	0.66^5	C	0.64	C	0.60
S	0.60	L	0.48	L	0.40
LL + LC	0.38^5	LC + S	0.42	LC + S	0.33
		LL	0.35^5	LL	0.23

6. *Discussion of results in sections 4 and 5*

So far we have discussed a) the laws which govern the displacement of spots on the chromatograms, and b) the changes in area and in shape of the spots at increase of the amount brought up at the starting point. We found for $SiCl_4$-treated paper (Part II of this series) and for non-impregnated paper (section III of the present communication) the same picture of the mechanism of chromatography. Point a) suggests that a gradient in the composition of the mobile phase plays an important role, point b) suggests that the spots are present in adsorbed state on the paper, their displacement on the chromatogram being effected by elution at their base and readsorption higher up. In this way we arrived at the picture that the mechanism must be considered as adsorption chromatography operated by gradient elution.

The results in section 4 and 5 lead in independent ways to quite the same picture. In section 4 the postulated gradient in the mobile phase has been proved to exist both on $SiCl_4$-treated paper and on non-impregnated paper. That the spots on the chromatograms are in the adsorbed state will follow when the results of the gradient determinations are combined with the R_{f_i} values given in section 5. It must be emphasized that—though R_{f_i} values are data which needs must be taken from

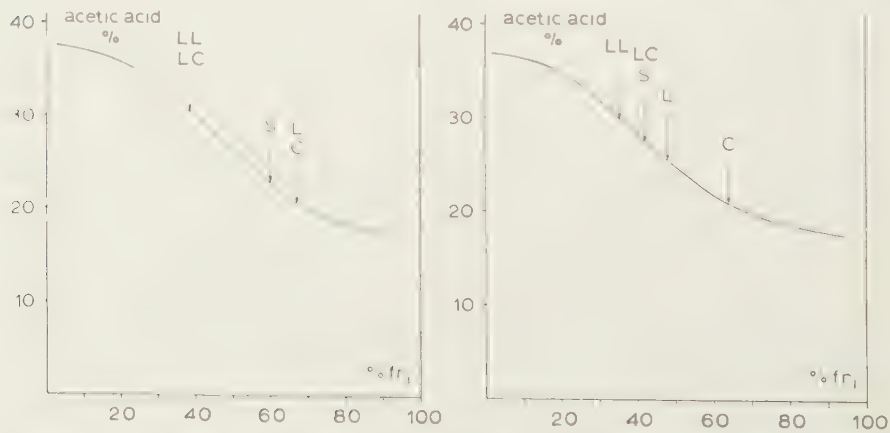

Figs. 13 and 14. Position of R_{f_i} values on the gradient curves for non-impregnated paper (fig. 13) and HCl-free, $SiCl_4$-treated paper (fig. 14) respectively.

chromatograms – they are really independent of the information given in the above-mentioned point b. (R_{f_i} refers to the position of the base of a spot. It has nothing to do with its area or shape, the R_{f_i} being the same for small and large spots).

We begin by comparing chromatography on non-impregnated paper and HCl-free $SiCl_4$-treated paper. For this purpose we have redrawn in figs. 13 and 14 the broken curves in figs. 7 and 8 representing the gradients in the acetic acid concentration in the mobile phase. We have further indicated by arrows the R_{f_i} values given in the survey in section 5.

Granted the importance of the gradient in the displacement of spots, the mechanism of the displacement of the spots might be assumed to consist of partition chromatography by a gradient in the mobile phase (partition between mobile phase and stationary phase, possibly "hygroscopic" H_2O in the paper; HCl-free $SiCl_4$-treated paper is hygroscopic too!) But if this applied, the succession and degree of resolution of the phosphatide components would not differ greatly on non-impregnated paper and on $SiCl_4$-treated paper respectively. As appears from a comparison of the figs. 13 and 14, there is a great difference. Not the hygroscopic water present on the two kinds of paper is the important factor but evidently the nature of the bearer itself. This can be explained without difficulty if we consider the spots to be adsorbed. Since the adsorbent is different (cellulose, impregnated cellulose) in the two papers, the succession and degree of resolution of the components of the mixture of phosphatides is not necessarily equal. This different sequence combined with the proved existence of a gradient leads to the conclusion that on both papers we have to do with adsorption chromatography operated by gradient elution.

The same conclusion holds if we compare chromatography on non-impregnated paper with that on $SiCl_4$-treated paper $\frac{1}{2}$ hour after preparation or on neutralized $SiCl_4$-treated paper. The sequence and degree of resolution for the just named $SiCl_4$-treated papers is the same as for HCl-free, $SiCl_4$-treated paper. Differences among the three $SiCl_4$-treated papers exist only with regard to the spread of R_{f_i} values of the spots.

We know already from former work (Part I, section 4 [1]) that the spread of the four spots on different kinds of $SiCl_4$-treated papers, diminishes in the order

Acid paper, age $\frac{1}{2}$ hr > Neutralized paper > HCl-free paper.

These differences must be ascribed to the presence of electrolytes in the former two papers, namely HCl in the first-mentioned and NH_4Cl in the second.

In adsorption chromatography by gradient elution, a foreign substance may modify R_{f_i} in two principally different ways, a) by influencing

the adsorption intensity, and b) by modifying the course of the gradient curve.

The cause of the greater spread of R_{f_i} values on freshly prepared (age $\frac{1}{2}$ hr) $SiCl_4$-treated paper (see fig. 11 and 12) and on neutralized $SiCl_4$-treated paper, as compared to HCl-free $SiCl_4$-paper, remains uncertain, since the course of the gradient curve in the former papers is not known with certainty (section 4, paragraphs e and f).

(To be continued)

SILICON TETRACHLORIDE-TREATED PAPER IN THE PAPER CHROMATOGRAPHY OF PHOSPHATIDES

IIIb. COMPARISON BETWEEN CHROMATOGRAPHY OF EGG PHOSPHATIDES ON $SiCl_4$-TREATED PAPER AND ON NON-IMPREGNATED PAPER. ROLE OF THE GRADIENT IN THE MOBILE PHASE AND INFLUENCE OF ADSORBENT

BY

H. G. BUNGENBERG DE JONG AND J. TH. HOOGEVEEN

(Communicated at the meeting of February 27, 1960)

7. *Amount, nature and location of the adsorbent effective in the chromatography of egg phosphatides on $SiCl_4$-treated paper*

a) Ash content and reaction product resulting from the $SiCl_4$ treatment

We remember that we impregnate the paper, by pulling the air-dry paper (Schleicher and Schüll 2043b) evenly in 10 seconds through a 2 % solution of $SiCl_4$ in CCl_4 [1]. It was supposed that the natural moisture in the air-dry paper (we found 6.2 %) reacts with the $SiCl_4$.

Paper made in the above-mentioned way was incinerated to determine its ash content, which was found to be about 0.85 %. The manufacturers give for the paper itself an ash content of 0.04–0.07 %. The difference of about 0.80 % is SiO_2. This does not yet prove that in the non-incinerated paper the reaction product with $SiCl_4$ is silica. One could also imagine that $SiCl_4$ reacts with hydroxyl groups of the cellulose. The reaction of $SiCl_4$ with water is, however, an extremely rapid reaction, the reaction with alcohol groups a much slower one. The chance that the latter will occur to an appreciable extent will be very small if the quantity of water present in the paper is much in excess to the quantity of $SiCl_4$ brought into the paper during the preparation. We have determined in duplo the increase in weight of the air-dry paper directly after pulling strips evenly in 10 seconds through CCl_4 (the solvent of $SiCl_4$ in the preparation). Taking into account the specific gravity of CCl_4 (1.595), we found that one gram of air-dry paper (moisture content 6.2 %) takes up 0.754 and 0.740 ml CCl_4. In our further calculations we take the mean: 0.75 ml CCl_4 per gram of air-dry paper.

As we use in the preparation a 2 % (by volume) solution of $SiCl_4$ in CCl_4, per gram of air-dry paper 0.015 ml $SiCl_4$ is taken up. Taking into

account the specific gravity (1.483) and the molecular weight (169.9) of $SiCl_4$, 0.131 *millimoles of $SiCl_4$ enter per gram into the air-dry paper.*

We may now first answer the question whether the moisture in the paper is in excess. For the total decomposition of one molecule of $SiCl_4$ are needed 4 molecules of H_2O (if orthosilicic acid is formed) or 2 molecules of H_2O (if SiO_2 is formed). The 0.131 millimoles of $SiCl_4$ in 1 g of air-dry paper would require 0.524 or 0.262 millimoles of H_2O. The moisture in the paper (6.2 %) represents 3.44 millimoles of H_2O per g of air-dry paper. This is roughly 6.5 times the amount required for the decomposition of the $SiCl_4$ soaked up by the paper, supposing the reaction ends with the formation of orthosilicic acid, and roughly 13 times if the orthosilicic acid during the preparation would completely polymerize to SiO_2. So there is a large excess of water in the air-dry paper. It seems reasonable to assume that the $SiCl_4$ soaked up in the paper will for far the greater part react with water (rapid reaction). The orthosilicic acid probably formed as first reaction product will, catalyzed by the HCl set free in the reaction, polymerize forming "silica". We may thus consider the $SiCl_4$-treated paper as a silica-impregnated paper with a low silica content.

b) Balance of the reaction involved in the impregnation with a 2 % solution of $SiCl_4$ in CCl_4

We now turn to the question whether all $SiCl_4$ soaked up in CCl_4 solution during the preparation reacts indeed as rapidly as assumed. We can check this by determining the SiO_2 content of the ash, and independently by determining the HCl formed. The 0.131 millimol of $SiCl_4$ taken up in 1 g of air-dry paper (see above) should form at incineration 0.131 millimol of SiO_2, that is 0.00788 g of SiO_2. The calculated ash-content of 0.79 % is in good agreement with the actually found ash content (after subtraction of the ash in the original paper), namely about 0.80 % (see above). Another control whether all $SiCl_4$ soaked up in the paper has already reacted with water, in the very short time the paper is pulled through the 2 % $SiCl_4$ solution in CCl_4, consists in measuring the HCl formed and compare it with the expected amount. As one molecule of $SiCl_4$ gives rise to 4 molecules of HCl, one should find that at the moment the paper has been pulled through the 2 % $SiCl_4$ solution it should contain $4 \times 0.131 = 0.524$ millimoles of HCl reckoned per 1 gr. of air-dry paper.

This has not been determined directly, but we may use the graph given in fig. 6 to find this content. We consider the crossing point of the straight line with the ordinate. We find then 0.74 for log ml NaOH 0.1 N (necessary to neutralize the HCl present in 1 g of air-dry paper) at $\sqrt{\text{hours}} = \text{zero}$. This value corresponds with 5.5 ml of NaOH 0.1 N. Thus the initial content of HCl present in 1 g air-dry paper would amount to 0.55 millimoles of HCl. This approximates the amount above calculated (0.524).

H. G. BUNGENBERG DE JONG AND J. TH. HOOGEVEEN: *Silicon tetrachloride-treated paper in the paper chromatography of phosphatides*

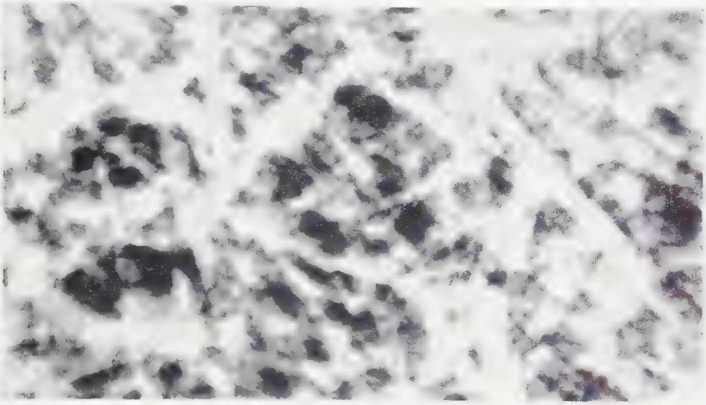

A

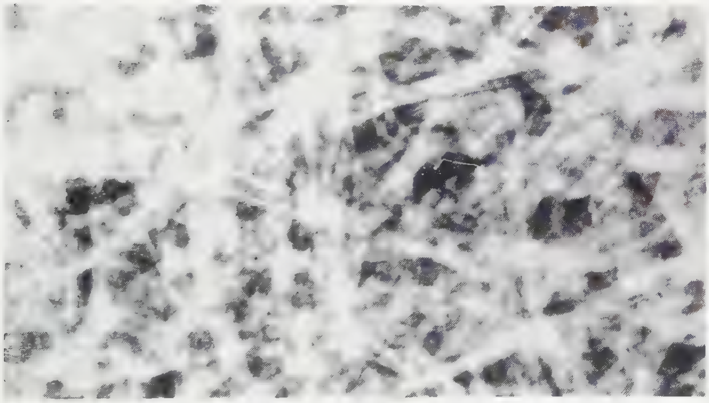

B

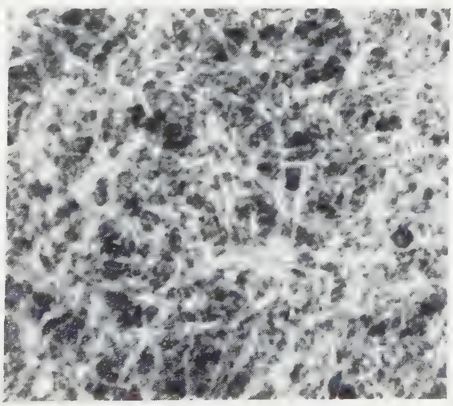

C

Contact-microradiograms of non-impregnated Schleicher and Schüll 2043*b* (A), of the same paper impregnated by means of a 2 % solution in CCl_4 (B) and of the ash of the $SiCl_4$-treated paper respectively (C). Magnification 150 ×.

One needs not take the small difference seriously as the empirical relationship between log ml NaOH 0.1 N and $\sqrt{}$ hours, suggested in fig. 6 to be linear might be an approximation to linear only. The position of the six points in fig. 6 suggests that a slightly bent curve can be drawn through the points, which cuts the ordinate axis at a slightly lower value than the straight line. It seems quite possible that this slightly bent curve will cut the ordinate axis at the logarithmic value of 0.72 (instead of 0.74), which corresponds with the calculated value of 0.524 millimoles per g of air-dry paper.

c) Location of the silica within the impregnated paper

In performing ash determinations of the $SiCl_4$-treated paper we incinerated a sufficient number of paper squares of about 1.5×1.5 cm. It is interesting that the resulting ash still consists of coherent squares. Microscopic investigation revealed that the ash consists of a meshwork of fibres. This suggests that in the preparation a mantle of silica is formed round the cellulose fibres.

The added Plate gives contact microradiograms obtained from non-impregnated Schleicher and Schüll paper 2043b(A), from the same paper after treatment in the usual way with a 2 % solution of $SiCl_4$ in CCl_4(B) and from the ash of the $SiCl_4$-treated paper (C) [1]).

As the magnification of the original contact microradiograms on Plate I is equal for A, B and C, they may be directly compared.

The non-impregnated paper (A) shows a meshwork of cellulose fibres which have double contours (optical cross section of the wall of the fibres).

The $SiCl_4$-treated paper (B) closely resembles the non-impregnated paper. No silica has been deposited as granules in the holes between the fibres. Evidently the silica forms a thin mantle around the cellulose fibres, while in addition superficial impregnation into the wall of the fibres may have taken place. Given an ash content of only 0.8 % SiO_2 the supposed mantle must be so thin, compared to the cellulose wall of the fibres, that it will not be visible as an apart layer. Indeed the aspect of the double contours of the fibres in A and B is equal.

Now turning to the picture of the ash (C), it is evident at once that the ash fibres have in general a much smaller diameter, and are much more bent in all directions. This need not contradict our assumption of a silica mantle around the cellulose fibres. At incineration, the enclosed cellulose decomposes and the mantle bursts to pieces, the length of which is likely to be greater than their thickness. These pieces are bent irregularly and sinter together into the observed meshwork of fibres. Here and there in C parallel lines are to be seen which remind of the double contours of the fibres in A and B. These may be places where the original location of the silica mantle was by chance preserved after incinerations.

The method used in preparing the $SiCl_4$-treated paper gives a plausible

---

[1]) We kindly thank Mr. O. C. Timmer for making these contact microradiograms for us.

explanation of these observations. In pulling the air-dry paper strip through the 2 % $SiCl_4$ solution in CCl_4, the air in the meshes between the cellulose fibres is replaced by the above-mentioned solution. Thus the conditions for a heterogeneous chemical reaction between the two reactants are given, the $SiCl_4$ being present in the carbon tetrachloride and the H_2O being present in the cellulose fibres (as natural moisture). The reaction will start at the contact surface of solution and fibres. Thus the fibres are coated by a thin layer of silica, possibly followed by superficial impregnation of the fibres.

8. *Comparison of $SiCl_4$-treated papers with different silica content*

a) Motive for the investigation

In part I of this series we gave chromatograms on $SiCl_4$-treated papers prepared by drawing paper strips evenly in 10 seconds through $SiCl_4$ solutions in which the $SiCl_4$ concentration amounted to 1.2; 3.7; 11.1 and 33.3 % (by volume) respectively [1]. About 2 hours after preparation chromatograms were made of the Reference mixture (small slit-feeding apparatus). Compare fig. 15, in which we have reproduced the figure given in Part I. Apart from minor details [1]) and the higher position of the C spots on the right chromatogram (presumably due to the larger content of HCl still present in the paper), the resemblance of the chromatograms is striking. In Part I no explanation of this resemblance was tried. We may assume that the silica content of the prepared strips increases as the concentration of the $SiCl_4$-solutions used in the preparation is higher. An indication for this is that in this direction the prepared strips decrease in suppleness. If it is true that the ash content increases (unfortunately no determinations were made) the close resemblance of the chromatograms suggests that the chromatographic properties of the prepared papers is independent of the silica content (within the range investigated). This would also be in agreement with our finding that the silica within the paper is present as a thin layer coating the fibres (section 7 paragraph c).

We decided to repeat these experiments on a larger scale, this time including determination of the ash content.

b) Ash

Four sets of strips have been prepared using 0.41; 1.24; 3.7; 11.1 and 33.3 % (by volume) solutions of $SiCl_4$ in CCl_4. The strips were pulled evenly, in 10 seconds, through the solutions and then left hanging in air. One set which had for more than a week been exposed to the air, was used to determine the ash content. The results are given in the next survey:

$SiCl_4$ % (*v*/*v*) . .	0.41	1.24	3.7	11.1	33.3
Ash %	0.27	0.57	1.11	1.92	2.66

[1]) The resolution of the two lower spots is better at low $SiCl_4$ concentrations.

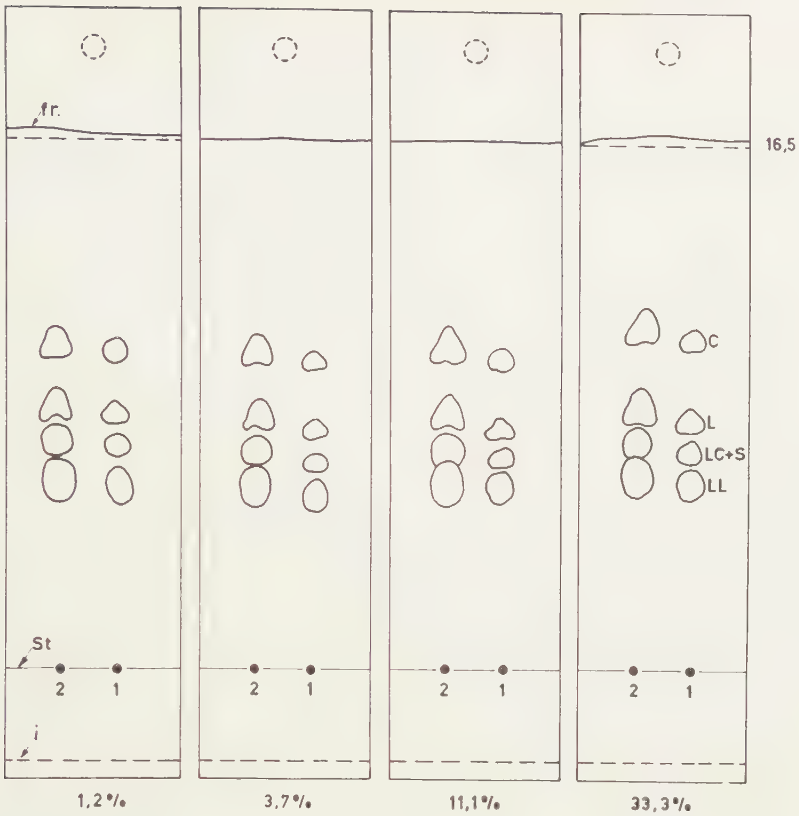

Fig. 15. Chromatography of the Reference mixture on Schleicher and Schüll 2043*b* treated 10 seconds with solutions of $SiCl_4$ of different concentration (% by volume). Chromatography has been started 2 hours after preparation.

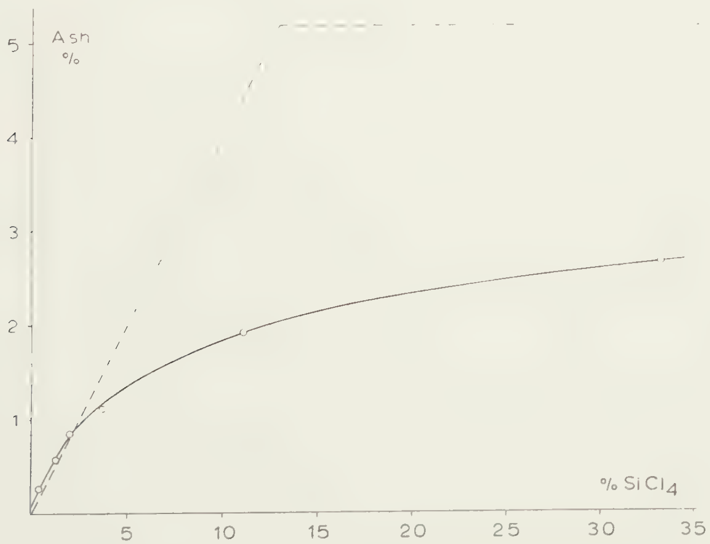

Fig. 16. Ash content of Schleicher and Schüll 2043*b* treated 10 seconds with solutions of $SiCl_4$ of different concentrations. With $SiCl_4$ solutions higher than 2 % the actually found ash (solid curve) remains below the theoretically possible SiO_2 ash (two broken straight lines meeting at the point 5.2 % ash and 13 % $SiCl_4$). For discussion see paragraph e).

The data of the survey and the value 0.85 % ash at 2 % $SiCl_4$ (found in section 7, paragraph a) have been plotted in fig. 16. The solid curve in fig. 16 gives the relation between ash content and concentration of the $SiCl_4$ solution. In this figure broken lines indicate the theoretical course of the curve for the SiO_2 ash, supposing that during the short time of preparation no polymerization of the original reaction product (orthosilicic acid) has taken place. This curve for the SiO_2 ash starts at the origin with a straight branch proceeding upwards to the right, until an ash content of 5.2 % is reached at 13 % $SiCl_4$. Here all H_2O in the paper is used up in the reaction with $SiCl_4$ [1]). From here the curve proceeds horizontally to the right.

We see that the curve for actually found ash content proceeds up to 2 % $SiCl_4$ as was expected, the distance between this curve and the oblique broken line corresponding to the ash content of the non-impregnated paper (about 0.05 %). From about 2 % $SiCl_4$ on, the curve for the actual ash content remains more and more behind the expected ash content. We will return to this discrepancy below in paragraph e. In the following discussion of the chromatograms in paragraphs c and d it will suffice to know that in the range of $SiCl_4$-concentrations used (0.41–33.3 %) the ash content increases about tenfold.

c) Chromatograms obtained on neutralized $SiCl_4$-treated paper

A second set of strips after 30 minutes hanging in air was neutralized by hanging 10 minutes in ammonia vapour. Chromatography (small slit-feeding apparatus) of the Reference mixture (5 mm³ of ½ and 1 % solutions were applied on the starting points spots) was started the next day. The chromatograms obtained – see fig. 17 – resemble one another very strikingly.

The R_{f_i} values (indicated by the basis of the spots) on each row are about the same. Further, the areas of the spots on each row are about equal too (variations may be due to errors made in circumlining the spots). It is very unlikely that the above can be explained when it is assumed that in preparing the strips the silica is deposited as a granular mass in the meshes between the cellulose fibres. Then we would have two

[1]) We have shown in section 7 that in preparing the paper with a 2 % $SiCl_4$ solution a), all $SiCl_4$ sucked up in the paper is used up in the reaction with the water in the paper, b) that this amount of $SiCl_4$ corresponds with practically 0.8 % SiO_2 ash, and c) that the water present in the paper is about 6.5 times the water necessary for the reaction with $SiCl_4$ to form $Si(OH)_4$. Hence, when all water present in the paper reacts with $SiCl_4$ the SiO_2 ash would amount to $6.5 \times 0.8 = 5.2$ %, and the necessary $SiCl_4$ concentration would be $6.5 \times 2 = 13$ %.

When during preparation the polymerization of $Si(OH)_4$ to SiO_2 proceeds so rapidly that the water set free reacts further with $SiCl_4$, the SiO_2 ash would at most be 10.2 % and the needed $SiCl_4$ concentration 26 %.

Fig. 17. Chromatography of the Reference mixture on Schleicher and Schüll 2043*b* treated for 10 seconds with solution of $SiCl_4$ of different concentrations followed by neutralization in ammonia vapour. Chromatography has been started next day.

adsorbents side by side, of which each one separately would give a different sequence of the components and degree of resolution.

It is difficult to believe that about 400 times less silica than cellulose will result in a chromatogram characteristic for silica. Besides, at the about tenfold increase of the amount of silica in the paper one would expect the spots to become very much smaller [1]). This is decidedly not the case.

The striking resemblance can, however, be simply explained if the conclusions drawn from the contact-microradiograms in section 7 paragraph c and are taken into account. We came to the conclusion that in

---

[1]) When the silica is deposited as loose granules in the meshes between the fibres we have to expect a large decrease of the spot areas when a number of granules increase tenfold; i.e. the effective adsorbent surface increase tenfold. In this case, taking into account that on paper treated with 2 % $SiCl_4$ solution the spot areas increase with the 2/3 power of the phosphatide brought up, we had to expect that the spot areas in fig. 17 would grow from left to right 4.7 times smaller.

the preparation the cellulose fibres become coated with a layer of silica. A thin layer — when complete — will already suffice to shield the surface of the cellulose fibres. Evidently this shielding is about complete with a strip containing only 0.27 % [1]). At further increase in thickness of the silica layer, the nature of the effective adsorbent remains the same. As long as the thickness of the layer is small compared to the diameter of the coated fibres (this still being the case at an ash content of 2.66 %) the surface of the effective adsorbent remains practically the same.

The fact that the effective adsorbent is of the same nature may account for the practically equal R_f values of the spots. The practically equal surface of the effective adsorbent, results in practically equal surfaces of the spots.

Fig. 18. Chromatography of the Reference mixture on Schleicher and Schüll 2043*b* treated for 10 seconds with solutions of $SiCl_4$ of different concentrations. Chromatography has been started 30 minutes after preparation.

[1]) There are signs that with 0.27 % the covering is not really complete on all cellulose fibres, because the spots lie already somewhat higher than on the other chromatograms. Strips prepared with a three times lower $SiCl_4$ concentration, showing an ash content of about 0.09 % gave already uncertain results. Sometimes we obtained the characteristic four spots, sometimes the three spots characteristic for untreated paper.

Fig. 19. Chromatography of the Reference mixture on Schleicher and Schüll 2043*b* treated for 10 seconds with solutions of $SiCl_4$ of different concentrations. Chromatography has been started 142 hours after preparation.

d) Chromatograms obtained on $SiCl_4$-treated paper $\frac{1}{2}$ hour and 142 hours respectively after preparation

The chromatograms belonging to these two sets are given in the figures 18 and 19. Compared with the chromatograms on neutralized paper (fig. 17) the effect of increasing silica content is less simple here. From left to right the difference of the R_{f_i} values of the upper and lower spot increases, slightly at first but pronouncedly in the two chromatograms at the right. As this is not present in the series on neutralized paper it must be due to HCl in the paper, the amount of which increases very markedly just in the two strips at the right.

It is interesting that this behaviour is still present in the series of strips which had hung in the air for 142 hrs (fig. 19). In section 4, paragraph b) it was found that strips prepared with 2 % $SiCl_4$ in CCl_4 have in 142 hrs become practically free of HCl. We must conclude that the time-span necessary for all HCl to escape into the air is much lengthened if a higher concentrated $SiCl_4$ solution is used for the preparation. This might be because of the larger quantity of HCl liberated. We

think, however, that it is mainly due to the greater thickness of the layer of silica surrounding the cellulose fibres (or alternatively the outer layer of the cellulose fibre impregnated with silica). At the start of the heterogeneous reaction the formation of silica begins at the contact surface between cellulose fibre and $SiCl_4$ solution in CCl_4. The HCl liberated will partly move inwards into the fibre. After completion of the silica layer it is shut up in the interior of the fibre. Its escape from the dried strip to the air will be increasingly more difficult as the silica layer is thicker.

e) Discussion of fig. 16

The growing thickness of the silica layer at the surface of the cellulose fibre (and possibly of the impregnated part of the cellulose fibre) may also explain why in the preparation with higher concentrated $SiCl_4$ solutions the amount of silica in the paper remains far below the theoretically possible amount. Compare fig. 16. This growing thickness will afford an increasingly greater barrier for the two reactants on either side ($SiCl_4$ dissolved in the CCl_4; H_2O in the cellulose fibre). It may thus come to pass that the available time for preparation (pulling the strips in 10 seconds through the $SiCl_4$ solution) is too short to complete the reaction.

The $SiCl_4$ present in the solution filling the meshwork then rapidly evaporates together with the solvent CCl_4 after hanging the strips in the air. It is not found as SiO_2 in the ash.

8. *Summary*

1. Concerning chromatography of egg phosphatides on non-impregnated paper similar information has been obtained as for chromatography on $SiCl_4$-treated paper, using the same mobile phase (di isobutylketone—acetic acid—H_2O = 50:25:5, by volume) and the same chromatographic device (large slit-feeding apparatus) (Compare Part II of this series).

2. The laws which govern the displacement of spots (R_{f_i}, not R_f, being an appropriate measure), the change in area and in shape at increase of the amount applied are in principle the same on non impregnated paper and on $SiCl_4$ treated paper. This leads to the same picture of the mechanism of the chromatography as was proposed in Part II for the chromatography on $SiCl_4$ treated paper: adsorption chromatography by gradient elution.

3. The succession and degree of resolution of the components is quite different. Reckoned from above to below we obtain:
non-impregnated paper: L + C (not resolved) – S – LL + LC (not resolved)
$SiCl_4$-treated paper: C – L – LC + S (not resolved) – LL.
in which the symbols mean: L = lecithin; C = cephalin; LL and LC their lysoproducts; S = sphingomyelin.

4. The existence of a gradient in the mobile phase has been confirmed. Both in non-impregnated paper and in $SiCl_4$-treated papers of different

kinds the acetic acid concentration decreases considerably in upward direction (roughly by half). The gradient curves have the same shape and within the errors nearly coincide in the case of non-impregnated paper and HCl-free $SiCl_4$-treated paper.

5. The gradient curves thus are practically the same for non-impregnated paper and HCl-free $SiCl_4$-treated paper. The fact that the sequence and degree of resolution of the components is different (see point 3) must then, in accordance with the proposed mechanism of chromatography (see point 2), be due to the different adsorbent in the two cases.

6. The adsorbent effective in $SiCl_4$-treated paper has been investigated (analyses, contact microradiograms). The main result is that the effective adsorbent, consisting of silica, is formed as a thin coherent layer around the cellulose fibres (possibly followed by superficial impregnation into the fibre). This location of the silica is explained by considering that the reaction involved is heterogenous, the two reactants ($SiCl_4$ dissolved in CCl_4; H_2O present as moisture in the fibres) meet at the contact surface of fibres and solution.

7. Papers have been treated with $SiCl_4$ solutions in CCl_4 with increasing $SiCl_4$-concentration. Their chromatographic properties and ash contents have been determined. In the range of $SiCl_4$ concentrations investigated (0.41 to 33.3 %):

A) the chromatograms (neutralized papers) show practically the same R_{f_i} values and the same area of the spots.
B) the chromatograms (not neutralized) show that HCl escapes into the air more slowly as the concentration of $SiCl_4$ is higher.
C) the ash content increases proportionally to the $SiCl_4$ concentration up to 2 % $SiCl_4$; at higher $SiCl_4$ concentrations the ash contents remain far behind the theoretically possible ones.

8. The points A, B and C mentioned sub 7, can easily be explained from the location of the silica mentioned above sub 6), and in addition for B and C) from the increase in the thickness of the silica layer.

Department of Medical Chemistry,
University of Leyden

REFERENCES

1. Bungenberg de Jong, H. G. and J. Th. Hoogeveen, these Proceedings, Series **B 63**, 190 (1960).
2. ——— and ———, these Proceedings, Series **B 63**, 1 (1960).
3. ——— and G. R. van Someren, these Proceedings, Series **B 62**, 150 (1959).
4. Hooghwinkel, G. J. M., J. Th. Hoogeveen, M. J. Lexmond and H. G. Bungenberg de Jong, these Proceedings, Series **B 62**, 222 (1959).
5. Bungenberg de Jong, H. G. and J. Th. Hoogeveen, these Proceedings, Series **B 63**, 228 (1960).
6. ——— and ———, these Proceedings, Series **B 63**, 15 (1960).

GEOPHYSICS

CONTINENTAL AND OCEAN-FLOOR TOPOGRAPHY; MANTLE-CONVECTION CURRENTS

BY

F. A. VENING MEINESZ

(Communicated at the meeting of May 28, 1960)

In a paper in the Proceedings of this Academy of 1959 [1]) the writer dealt with the development in spherical harmonics up to the 31st order of the earth's topography. This development, for which prof. Ir. G. J. BRUINS of the Geodetical Laboratory of the Polytechnical University at Delft and his collaborators provided the 40680 figures of the topographic elevation, was carried out by the Mathematical Centre in Amsterdam under the supervision of Dr. Ir. D. J. HOFSOMMER and Mr. M. L. POTTERS. A similar development was already made in 1919–1922, by Prof. Dr. A. PREY of Prague University, who carried it out up to the 16th order. Since that time the method of echo-sounding made an enormous advance in our knowledge of the ocean-floor topography possible, and thus the second development could be much more efficient in representing this topography. By pushing it up to the 31st order the new development represents more details.

Both in Prey's case and in that of the recent work done in the Netherlands, two developments were carried out, one of the complete topography of the earth and one of the ocean floor topography for which the continental elevation was put zero. In the paper of the writer mentioned above he used the $2n+1$ coefficients derived for the order n for each of the two developments, to deduce the root mean square of the total topography represented by all $2n+1$ terms of the development for the order n; he carried this out for all values of n from 1 to 31. He thus obtained for the total topography a series of 31 representative values, which he represented as ordinates in a curve for this development of the total topography which he indicated by t. In the same way he obtained a curve of 31 ordinates, indicated by s, representing only the topography of the ocean-floor. From these two curves he deduced a similar curve of 31 ordinates, indicated by l, for the topography of only the continents, putting zero the ocean-floor topography. The three curves were given in the same figure, viz. in fig. 1.

[1]) F. A. VENING MEINESZ, The results of the development of the earth's topography in spherical harmonics up to the 31st order; provisional conclusions, Proc. Kon. Ned. Acad. v. Wetens., Ser. B, 62, No. 2, 1959.

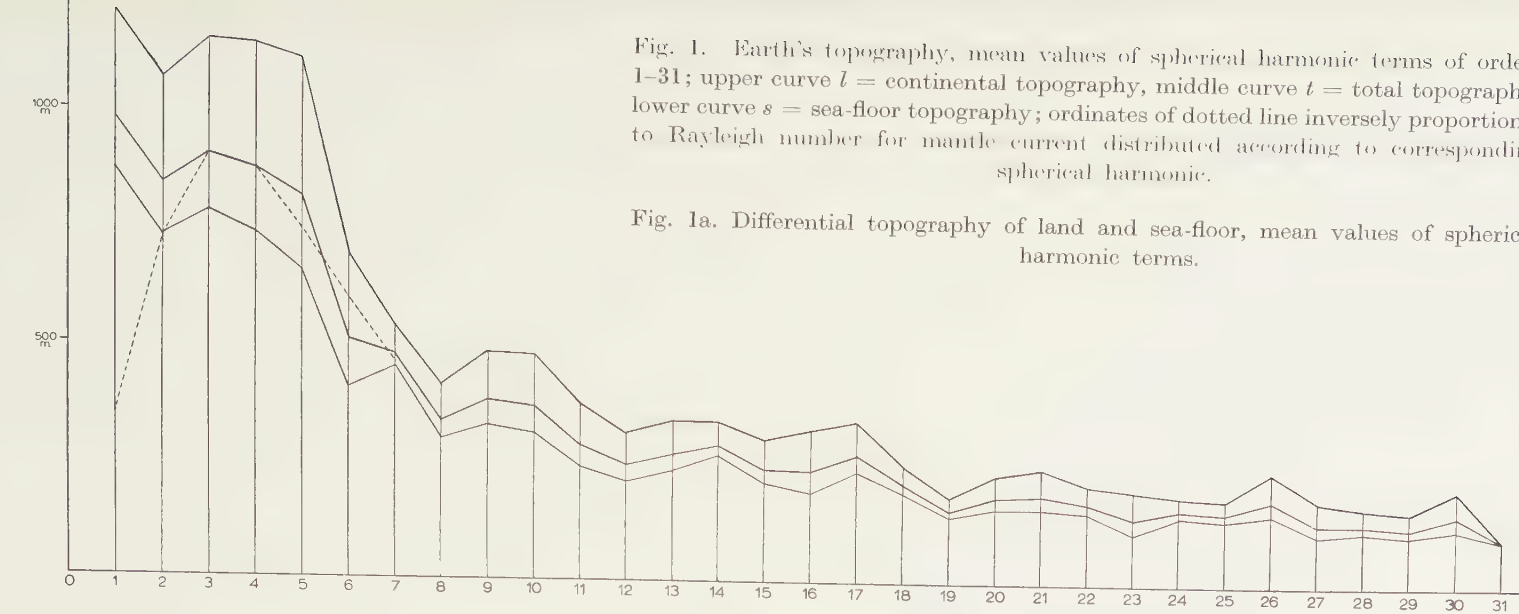

Fig. 1. Earth's topography, mean values of spherical harmonic terms of orders 1–31; upper curve l = continental topography, middle curve t = total topography, lower curve s = sea-floor topography; ordinates of dotted line inversely proportional to Rayleigh number for mantle current distributed according to corresponding spherical harmonic.

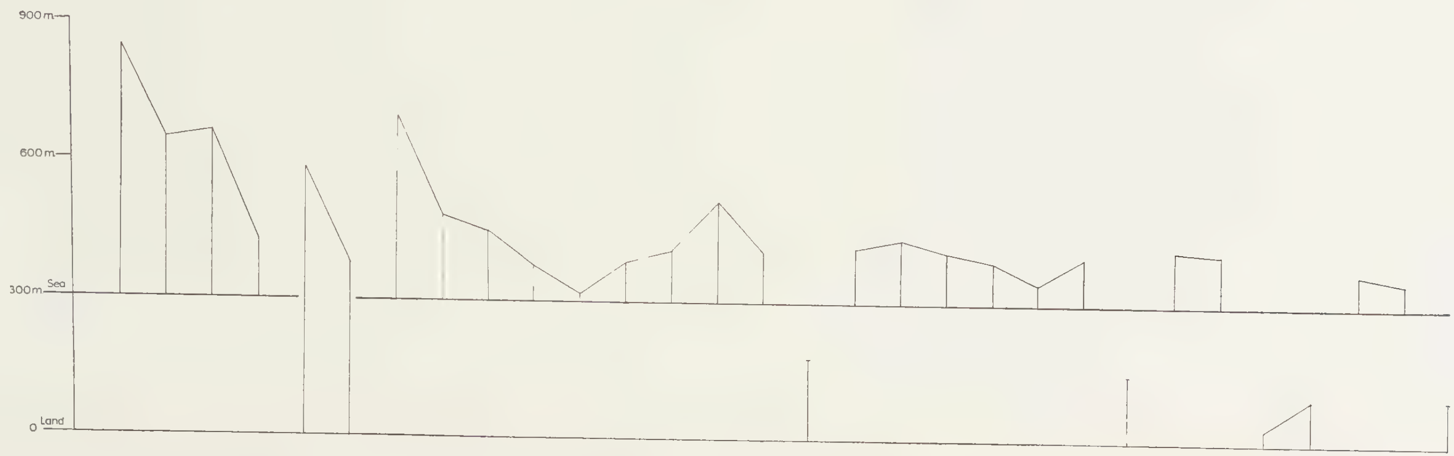

Fig. 1a. Differential topography of land and sea-floor, mean values of spherical harmonic terms.

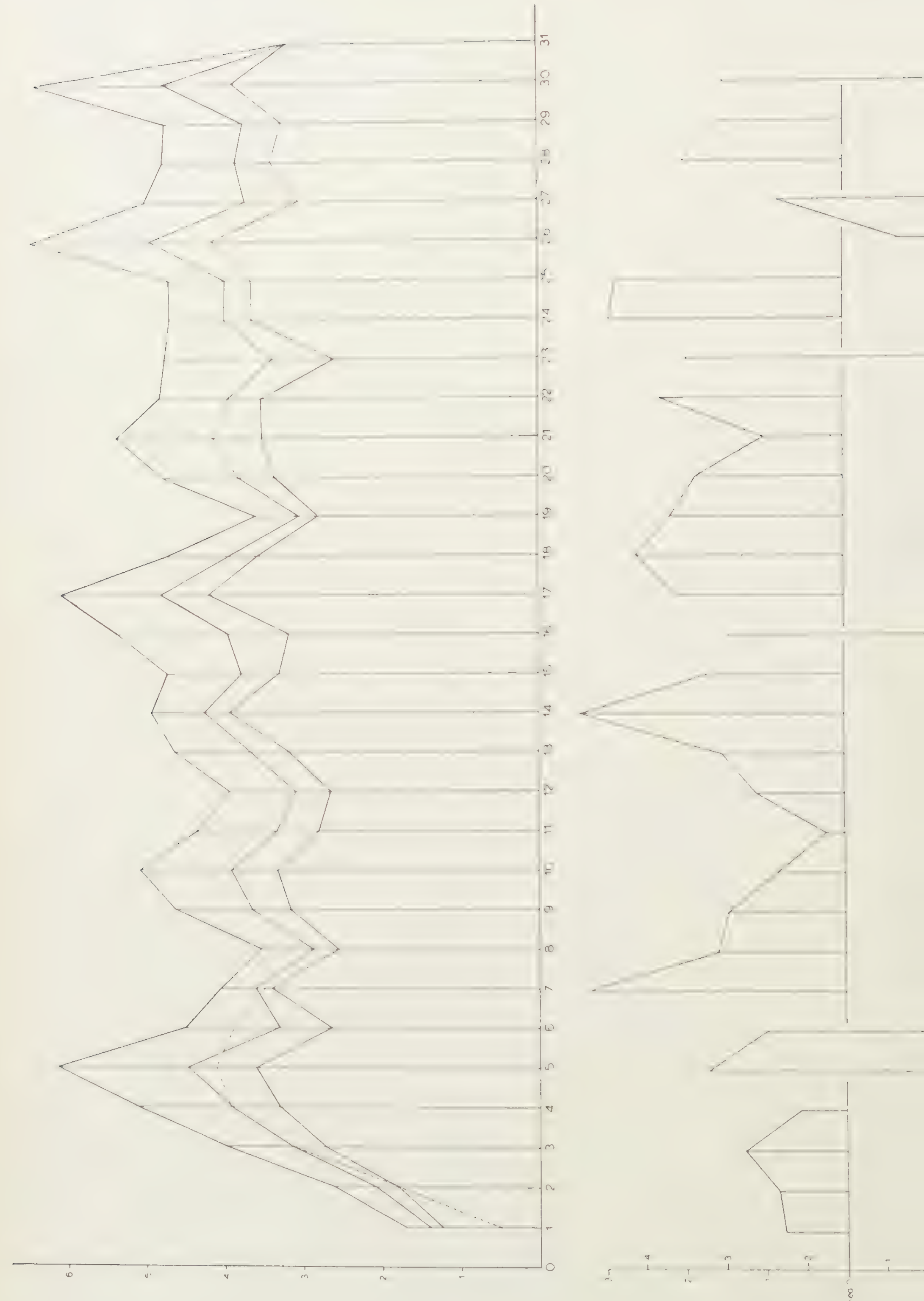

As the ordinates of these three curves diminish with increasing value of n, and, roughly speaking, in about inverse ratio to n, he also gave a second figure, viz. fig. 2, with three curves — ordinates indicated by T, S, L resp. — in which this effect was eliminated by multiplying each ordinate by $\sqrt{n(n+1)}$. For low values of n this seriously affects the character of the curves; the first order peaks disappear entirely and the maxima for $n=3$ shift to $n=5$. The figures 1 and 2 of the former paper are given here again.

In studying the earth's topography we realize that the main part of it is the presence of high continental blocks and of low ocean-floors with a more or less steep transition between. We may consider this transition topography as being common to both areas, the continental and the oceanic areas, or at least approximately so. So, for the corresponding part of the elevations, the integral of the squares of the elevations of the continental areas must equal the integral of the squares of the elevations of the oceanic areas, which can also be expressed in this way that the continental area multiplied by l^2 must equal the oceanic area multiplied by s^2 and also half of the total area multiplied by t^2. The same must be true for L^2, S^2, T^2. As we know that 0.2917 of the earth's surface is land and, therefore, 0.7083 of it sea, we can write

$$0.2917\ l^2 = 0.7083\ s^2 = 0.5\ t^2$$

$$0.2917\ L^2 = 0.7083\ S^2 = 0.5\ T^2$$

This leads to the relations

$$\text{(1A)} \qquad s^2 = 0.4118\ l^2;\quad s = 0.6417\ l;\quad t = 0.7638\ l;$$

$$\text{(1B)} \qquad S^2 = 0.4118\ L^2;\quad S = 0.6417\ L;\quad T = 0.7638\ L.$$

In all these formulas the values of l, s, t, L, S and T have regard to the main parts of these quantities, corresponding to the common topography along the coasts of the continental and oceanic areas. In the figures 1 and 2 we see that this checks with the three curves; the ordinates fairly well correspond to these ratios.

In the paper of 1959 the writer discussed the shape of the different curves and the peaks fig. 2 displays for $n=5$, 10, 14, 17, 21, 26 and 30. He showed that they can be explained by the presence of convection-currents in the mantle, viz. the peak for $n=5$ ($n=3$ for fig. 1) by a current over the whole mantle, the peak for $n=10$ by currents in two layers in which the mantle is divided, and so on, up to currents in seven layers of the mantle explaining the peak for $n=30$. He also gave many other arguments for the hypothesis of convection-currents in the mantle. The correlation between these currents and the transition topography between the continental blocks and the ocean floors can easily be understood; it is clear that the subsiding columns of the mantle convection-currents must tend to concentrate the light continental matter

at the surface above these columns and that, therefore, the location of the continental blocks must more or less coincide with that of the subsiding columns. In more recent times the currents have no doubt had the character of currents making only a half turn and lasting about 50–100 million years with periods of rest between of 200–400 million years [1]).

In this paper the writer wants to study the relatively small deviations of the curves of figures 1 and 2 from the ratios given by the formulas (1A) and (1B); he has not yet done this in the previous paper. These deviations must be caused by the topography inside the continents and inside the oceans but they can not be considered as the complete expression of these topographic features; part of their effects can obey the formulas (1A) and (1B) and, therefore, not show up as a deviation from the formulas. In two directions we may expect clear deviations.

In the first place they must be disclosed by the topography resulting from a pattern of geosynclines running through continents and oceans. In several publications [2]) the writer has pointed out that the difference of density of the rigid crust in the continents and under the oceans must lead to a great difference of elevation of the surface ridge which, after the stopping of the horizontal compression in the crust, originates. Assuming that the thickening of the continental and oceanic rigid crust is about the same, the isostatic readjustment, which at that moment sets in, must lead to a surface elevation which for the continental crust of a mean density of about 2.83 must amount to several kilometers, while for the oceanic crust of a mean density very near to that of the subcrustal mantle layer cannot be more than a few hundred meters. The resulting topography must, therefore, be much higher in the continents than for the ocean–floor.

In the second place the Atlantic and the Indian Oceans display mid ocean ridges which are different in character from any topographic features in the continents. In general they show elevations of several kilometers. The rifts found on these ridges by Ewing and his collaborators point to tension in the crust and this checks well with the great number of volcanoes located on the ridges. The volcanoes of Iceland, of the Azores and of Tristan da Cunha, high enough to show up to considerable height above sea level are instances of this; soundings display also a great number of submarine ones. On the continents we likewise find topography which we may assume to be caused by tension in the crust.

[1]) The Earth and its Gravity Field, by W. A. Heiskanen and the writer, p. 400, 1958.

[2]) Plastic Buckling of the Earth's Crust: The Origin of Geosynclines; "Crust of the Earth" Spec. Paper Geol. Soc. o. Amer. 62, pp. 319–330, esp. p. 328; 1955.

Geophysical History of a Geosyncline, Proc. Kon. Ned. Akad. v. Wetensch., Ser. B, vol. 60, pp. 126–140, 1956.

The Earth and its Gravity Field, by W. A. Heiskanen and the writer, p. 343, McGraw–Hill, 1958.

as e.g. the graben which we find in the belt of the great African lakes, in the Dead Sea belt and in the Rhine valley between the Vosges and the Black Forest and in the area north of Coblentz. With the exception of the volcanoes the height of the topography here is not much more than one kilometer and usually less; it depends on the isostatic adjustment of crustal blocks delimited by fault planes under angles of hade of the order of 25°–30°. As in the oceans the density of the rigid crust is so much closer to that of the substratum, the same feature caused by isostatic adjustment can in the oceans only bring about graben of a topography of a few hundreds of meters at the highest.

It can, therefore, hardly be doubted that the mid-ocean ridges mentioned above have another origin than the continental graben. Realizing that the Atlantic and Indian Oceans in which they occur have probably come into being by a breaking apart, in a very early stage of the earth's history during which the mantle surface had not yet consolidated, of an urcontinent, the question may be put whether during this process part of the continental matter could have been left behind above the rising currents which led to the breaking apart. Such a process may also explain the connection, south of S. Africa, of the Mid-Atlantic ridge system and the Mid-Indian Ocean ridge system, which has been found by Ewing and his collaborators. They likewise found a ridge continuing south of Australia. As also the Antarctic continent originally belonged to the urcontinent, these last ridges probably belong to the same system of mid-ocean ridges.

The explanation of these mid-ocean ridges given here appears acceptable; we may understand that above a rising current we find a neutral zone where part of the continental matter above this current has neither a tendency to flow off towards one side nor to the other.

We shall now take up the main subject of our paper, the study of the deviations of the ratios s/l and S/L from the values given by the formulas (1A) and (1B). As the quantities s and l are the roots of mean squares of the elevations for each order n over the ocean and land areas, respectively, we shall derive the quantities $\sqrt{s^2-0.4118\, l^2}$ for those values of n for which the difference is positive and, therefore, the root real, and the quantities $\sqrt{l^2-2.428\, s^2}$ for the other values of n. The first group, denoted by s_d, represents the root of the mean square of the topographic elevations found in the ocean areas and the second group, denoted by l_d, the root of the mean square of the topographic elevations found in the land areas. As it has already been mentioned, these figures do not comprise the common topography of land and sea along the coasts between both areas, nor the topography inside these areas which, in taking the differences of the squares, compensate each other.

In the table we have also added a column giving the results multiplied by $\sqrt{n(n+1)}$; the sea values of this column are denoted by S_d and the land values by L_d.

The values of s_d and l_d are expressed in km; they are represented by fig. 1a. They can be compared to the values given by fig. 1. In the same way the values of S_d and L_d are given by fig. 2a; they can be compared with the values of fig. 2.

TABLE of l_d, s_d, L_d, S_d

n	l_d	s_d	L_d	S_d	n	l_d	s_d	L_d	S_d
1		0.546		0.774	16	0.1787		2.946	
2		0.349		0.856	17		0.1196		2.091
3		0.365		1.265	18		0.1400		2.588
4		0.126		0.565	19		0.1115		2.173
5	0.587		3.211		20		0.0903		1.849
6	0.380		2.462		21		0.0458		0.983
7		0.403		3.019	22		0.1017		2.287
8		0.188		1.598	23	0.1469		3.453	
9		0.1531		1.453	24		0.1194		2.923
10		0.0787		0.826	25		0.1116		2.846
11		0.0186		0.214	26	0.0293		0.778	
12		0.0869		1.085	27	0.0841		2.310	
13		0.1135		1.531	28		0.0702		2.001
14		0.2209		3.197	29		0.0521		1.537
15		0.1115		1.727	30	0.0981		2.991	

Examining this table as well as the figures 1a and 2a, we see that in the same way as it was the case for the figures 1 and 2, the figures 1a and 2a are remarkably regular; see e.g. the parts 1–4, 7–15 and 17–22. This again points to physical processes in the background. The following features strike us:

1° a fairly strong first order term in the ocean topography, as given by fig. 1a;

2° a strong fifth order term in the continental topography;

3° strong seventh and fourteenth order terms in the ocean topography;

4° 16th, 23rd and 30th order terms in the continental topography;

5° an irregular mixture of land and sea topography terms in the orders higher than 20.

In discussing these results we must realize that the land values l_d and L_d and the sea values s_d and S_d have regard to different areas of the earth's surface and that, therefore, for similar topographic features we may expect the same difference in scale as given for l and s in the formulas (1).

We shall start by examining the strong 7th and 14th order terms in the sea-floor topography; there are several reasons to suppose that both these terms are caused by the mid-ocean ridges. In the first place they were not conspicuous in the development of the earth's topography in

spherical harmonics by Prey in the years 1919–1922 [1]). This is explained by the fact that at that time the mid-ocean ridges were not yet discovered, though of course the volcanic islands on those ridges, as e.g. Iceland, the Azores, Tristan da Cunha, Mauritius, Réunion, etc. were known. This argument is obviously valid for all sea-floor topography unknown at that time, but as the mid-ocean ridges are by far the most important of that unknown topography, it is indicated to consider them responsible for the 7th and 14th order terms.

Another argument is given by the hypothesis about their originating above the mantle-currents rising in the middle of the rupture oceans, denoting by this indication the oceans, which came into being by the breaking apart of the urcontinent. We must suppose this to have occurred in the beginning of the earth's history when the ocean-floors had not yet consolidated and the urcontinent had already done so.

For making this clear, we may shortly summarize here the first part of the earth's history, as we may suppose it to have occurred [2]). We shall start by the stage that the earth was still an undifferentiated fluid body, in which the cooling at the surface caused instability. This must have led to a current through the earth's centre, which returned along the earth's surface. It must be surmised that this current left the heavy matter in the centre, where it gradually formed the core, while the light matter was brought to the surface and was by the current itself concentrated in a more or less round urcontinent, extending over about one third of the earth's surface. The formation of the core forced the current to pass around it and thus gradually brought it to a stop. A period of rest ensued, during which the urcontinent crystallized and consolidated, but during which the free surface of the mantle must have remained fluid; if the cooling at the surface somewhere brought about consolidation, the increase of density made it subside again and melt. The matter of the urcontinent, though consolidating, remained lighter and thus stayed at the surface. We may conclude that the consolidation of the free mantle's surface must have been delayed for a long time, which it is difficult to form an estimate of.

When after the period of rest the cooling at the surface again brought about instability, a new system of currents must have originated in the mantle, which distributed itself according to the thickness of the mantle. It tore the urcontinent apart in the way it was discussed above and transported the parts more or less towards the places now shown by the continents; we may leave it an open question whether this distribution was reached at once or whether this took more than one period of convection-currents. We may perhaps even assume that still the relative

---

1) The Earth and its Gravity Field, by Heiskanen and Vening Meinesz, pp. 425, 428.

2) The Earth and its Gravity Field, by Heiskanen and Vening Meinesz, pp. 430–440.

positions of the continents are not stable. During the first part of the earth's history, however, the transportation of the continents through the unconsolidated mantle's surface must have been a simpler phenomenon than more recent changes of relative position.

During that early period we can easily understand that the mantle-current rising under the middle of the rupture oceans flowed off at the surface to both sides and left some of the lighter matter behind in the centre of these oceans, thus forming the middle ocean ridges. From this hypothesis it would follow that the origin of these ridges dates from about the same period as the origin of the continents.

Coming back to our problem, we may remark that, as the convection-currents in the mantle leading to the mid-ocean ridges must have had the character of a current in a more or less viscous mantle, its distribution may be expected to have corresponded with the dotted curve given in fig. 1, the ordinates of which are inversely proportional to the Rayleigh numbers belonging to currents of that type distributed according to the spherical harmonic of the order indicated below. We see that the spherical harmonics of the third and fourth orders are the most probable. As our hypothesis assumes positive topographic elevations above the subsiding as well as over the rising columns we may expect this topography to have a distribution according to an order of spherical harmonic of the double value, i.e. around the seventh order. This confirms our hypothesis; if we assume that the topography rising above the subsiding current belongs to what is common to continent and ocean areas, viz. to the transition zone between, this checks with the fact that this seventh order appears in the ocean topography and not in the continental topography.

The fairly strong first order term in the ocean-floor topography is an indication that the main part of this topography – which no doubt is the system of mid-ocean ridges – is principally situated in the hemisphere where the land abounds, viz. in that where the first order term gives positive elevations. The centre of this hemisphere is located in the Black Sea, east of Constanza and south of Odessa. This conclusion regarding the mid-ocean ridges checks with their being situated in the middle of the rupture oceans, which originated by the breaking apart of the urcontinent.

We shall now examine the particularly strong fifth and sixth order terms in the continental topography. We can hardly doubt that they are caused by the topography in geosyncline zones in which we may expect a great difference between the high elevations originating in continental geosynclines when the mantle currents come to a stop and the horizontal compression in the crust, therefore, likewise relaxes, and the low elevations then coming into being in the oceanic geosynclines. This great difference must lead to a large continental term in our differential spherical harmonic development of the topography.

This evidently leads to the conclusion that the strong fifth and sixth order terms in the continental spherical development must be attributed to the pattern of geosynclines which led to the present mountain-ranges. As there are so many arguments in favour of the hypothesis that the horizontal compression of the earth's crust causing these geosynclines has been brought about by mantle convection-currents, the problem arises why in the beginning of the earth's history these currents were mainly distributed according to spherical harmonic terms of the third and fourth orders while in recent periods they obeyed a fifth and sixth order distribution.

We have already mentioned that convection in a mantle consisting of a viscous fluid must mainly be distributed according to a third and fourth spherical harmonic. In the present period, however, the mantle is no longer likely to be viscous. The density increase at a depth from 500–900 km is probably for a great part brought about by a difference of crystal phase of the principal mantle constituent, $(Fe, Mg)_2SiO_4$, viz. the orthorhombic phase of olivine in the upper 500 km and the cubic phase of spinel in the lower 2000 km of the mantle, with a transition-layer in between [1]).

These views imply a crystalline structure throughout the whole, or at least throughout the greatest part of the mantle and it is likely that this leads to another distribution of the mantle convection-currents. In the following way we can show that it is likely to assume a fifth and sixth order spherical harmonic distribution as we have here found it to be probably the case. For making this acceptable we shall examine the properties of crystalline matter. The most important for our purpose is the presence of an elastic limit σ_l which the stress-deviator σ has to exceed before movement comparable to flow can take place; the velocity V of this pseudo-flow can often be assumed to be proportional to σ–σ_l. If σ is smaller than σ_l a purely elastic deformation, proportional to σ, comes into being, which disappears when σ vanishes. The pseudo-viscous flow is probably accompanied by an elastical deformation proportional to σ, which likewise disappears when σ vanishes.

It is likely we may suppose that the pseudo-viscous flow of a crystalline substance tends to assume such a pattern, that in great parts σ does not attain the elastic limit σ_l; in this way these parts are transported and rotated without flow. For convection this no doubt means that the central part of a cell of such a current rotates and makes a half turn, while around this cell a kind of flow occurs which adapts itself to the boundaries inside of which the cell moves. We may, therefore, surmise that the cell tends to assume a shape the boundaries of which are more or less tangential to a circle.

---

[1]) Meijering, J. L. and C. J. M. Rooymans, On the olivine-spinel transition in the earth's mantle, Proc. Kon. Ned. Akad. v. Wetensch., Ser. B, 61, No. 5, 1958, pp. 333–344.

Applying this to our problem it seems likely that the distribution of the convection system often assumes the character of a sectorial spherical harmonic and that the cross-sections of each cell in the equator of this system, which need not coincide with the equator of the earth, shows a series of circles tangent to the system's equator, to the core and to each other. Thus we find that ten circles more or less fill the whole equator cross-section in the way as shown by fig. 3. This means a fifth order spherical harmonic distribution. Perpendicular to this equator-plane we may suppose that the cells extend over some distance to both sides. We may repeat that the equator mentioned here need not coincide with the earth's equator.

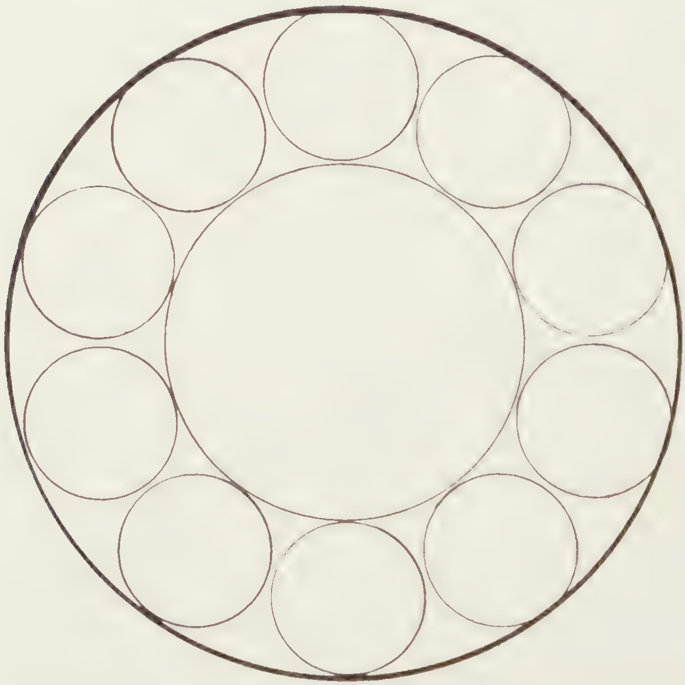

Fig. 3. Schematic representation of mantle currents in a crystalline mantle.

Studying the distribution more accurately, we find that, if the circles are tangent to each other, we in fact have 10.8 circles over the whole equator circumference, which would correspond to an order of spherical harmonic of 5.4, or, as fractions are impossible, to an order varying between 5 and 6. This appears to check remarkably well with the orders 5 and 6 present in the land development of the figures 1a and 2a.

The sectorial spherical harmonic distribution appears in harmony with the linear character, over great distances, of the folded mountain ranges at the earth's surface. During the earlier periods of the earth's history, when the mantle had not yet crystallized, the mantle currents can not have had this two-dimensional character; they must in general

have been of a three-dimensional type and this must have led to the formation in the crust of the old sialic shields well known to the geologists.

We shall not examine the higher order terms of the continental parts of the differential development here; they are anyhow much smaller than those which have been discussed here.

Summary

From the spherical harmonic development of the land and sea-floor topography we have derived that probably during the beginning of the earth's history the spherical harmonic distribution of mantle convection-currents corresponded to what we must expect to occur for a mantle consisting of a viscous fluid. We further found that during more recent periods and during the present time the convection-currents were and are distributed according to other orders of spherical harmonics, which may be explained by assuming that the entire mantle, or at least the greatest part of it, is now crystalline. These results are in favour of the supposition that the earth has been cooling.

This same hypothesis has already been used for accounting for the origin of the continents; by our present study it finds further support.

PHYSICAL CHEMISTRY

INFLUENCE OF GRAIN SIZE ON THE RATE OF ABSORPTION OF HYDROGEN BY PALLADIUM

BY

T. J. TIEDEMA [1]), B. C. DE JONG AND W. G. BURGERS

(Communicated at the meeting of May 28, 1960)

Summary

Palladium wires of different grain-size, if charged under identical conditions with hydrogen gas, show a pronounced difference in rate of absorption of the hydrogen, this difference being such that the smaller the grains the higher the rate of absorption. Most likely this difference is caused by a difference in rate of dissociation of the hydrogen molecules at the surface of the specimens. Probably the grain boundaries act as favoured places for this dissociation. An influence of the rate of internal diffusion could not be established. Palladium wires of different grainsize but charged with electrolytically developed hydrogen do not show a difference in rate of absorption.

Introduction

It is well known that palladium can take up large quantities of hydrogen, as well from the gas phase as from aqueous solution. In the latter case the hydrogen may be developed either electrolytically at a palladium electrode used as a cathode, or it may be directly absorbed from a gas stream bubbling through the solution (FLANAGAN and LEWIS [1]). In all these cases the rate of absorption depends markedly on the condition of the surface of the metal which is exposed to the gas.

There are numerous observations of this fact, which are, however, not always concordant. For example, according to TAMMANN and SCHNEIDER [2], the rate of absorption of hydrogen by palladium foil from the gas phase decreases if the metal comes into contact with air. WORSHAM, WILKINSON and SHULL [3] on the other hand, find that the absorption of hydrogen by palladium powder is much better in case the metal has been in contact with dry air.

In considering such apparent differences in results, it must be kept in mind that the rate of absorption depends moreover on the purity of the gas used. For example the presence of hydrogensulphide may prevent the absorption completely as was shown by OWEN and JONES [10].

[1]) Associate Worker of the Dutch Foundation for Fundamental Research (F.O.M.).

Purification of the hydrogen gas used is therefore essential (see also Flanagan and Lewis [1], Lewis, Roberts and Ubbelohde [7], Smith and Derge [11], Krause and Kahlenberg [12]).

For absorption from a solution, either after electrolysis or directly, the observations agree that activation of the surface by a preliminary anodic treatment increases the rate of absorption considerably: See for example Clamroth and Knorr [4], Breiter, Kammermaier and Knorr [5], von Stackelberg and Bischoff [6], Lewis ,Roberts and Ubbelohde [7], Hoare and Schuldiner [8], Duhm [9], Flanagen and Lewis [1].

In this note we are concerned with another factor, namely the grain-size of the metal. There are indications in the literature that the rate of absorption under similar circumstances decreases with increasing grain-size. At least one might interpret in this sense the observation of Tammann and Schneider [2] that the rate of absorption of rolled palladium foil decreases after a heat treatment at 400° C, a temperature at which, according to our experience, considerable grain growth can occur.

Tammann and Schneider, however, attribute the effect to a change in the texture of the foil, caused by the recrystallization process. Due to this change in texture the number of (110)-lattice planes parallel to the surface of the foil increases at the cost of (112)-planes. According to these authors the rate of absorption thus depends on the crystallographic nature of the lattice planes exposed to the surface of the foil. In the next paragraph we shall describe some experiments which were carried out in order to test this conception and the results obtained.

Experimental

On charging palladium with hydrogen, first the so-called α-phase comes into existence which contains hydrogen up to about 3 at%. The lattice parameter of this phase is only slightly larger than that of pure palladium (3,984 Å instead of 3,883 Å for pure palladium). After this phase has been formed, palladium can still take up large quantities of hydrogen under formation of the so-called β-phase which contains about 37,5 at% hydrogen ($PdH_{0,6}$) and which has a lattice parameter of about 4,02 Å. Due to this large difference in lattice parameter between the α- and the β-phase, the easiest method to discern between these two phases is by means of X-rays (see for example Tiedema, Kooy and Burgers [13]). This method has been used in this investigation.

In order to be able to decide whether the above-mentioned conception of Tammann and Schneider is correct or whether the change in rate of absorption must be ascribed merely to a difference in grain-size, palladium wires of a diameter of 1 mm were charged at room temperature with purified hydrogen under an increased pressure. Figures 1*a*–*c* represent a series of Debye–Scherrer photographs of three such specimens of nearly the same dimensions and charged simultaneously at room temperature at a pressure of 35 atm. during 4½h. The only difference between these

specimens was the grain-size which increased from specimen 1*a* to specimen 1*c*.

As can be seen clearly from the photographs, specimen 1*a* has been transformed into β-palladium entirely, at least the surface layer[1]), specimen 1*b* into a mixture of α- and β-palladium, whereas specimen 1*c* shows α-palladium only. Furthermore it can be derived from these photographs that the specimens practically show no texture at all. A very weak texture may perhaps be present as the first low-order Debye Scherrer circles are not altogether blackened homogeneously, but the difference in blackening is very small. The remarkable difference in rate of absorption (specimen 1*a* must have taken up at least 20 times as much hydrogen as specimen 1*c*) therefore can be ascribed only to a difference in grain-size.

Of course these experiments do not refute the conclusion of Tammann and Schneider, but they show clearly that, apart from a possible influence of texture upon the rate of absorption, also a remarkable influence of grain-size exists. This influence is gradual: the photographs reproduced in figures 2*a*–*c* show that a wire with large grains (1–5 mm in length, obtained by straining the fine-grained wires for 3–4 % and subsequent heating at about 1400° C for several hours) did not transform its surface layer into β-palladium after 3 hours charging at 20–25 atmospheres hydrogen, but did so after charging for 15 hours under the same conditions.

The difference in rate of absorption of hydrogen between fine-grained and coarse-grained palladium was not observed in case of electrolytic charging. This is shown in figure 3 for two wires, charged under identical conditions in 0,1 n H_2SO_4 at a current density of 1 mA/cm² during 1 hour. The presence of the α-phase beside the β-phase is evident in both photographs.

On the other hand it might be supposed that the difference in hydrogen content observed in the surface layers of the wires charged from the gas

[1]) The depth of penetration of CuK-radiation in palladium amounts to about 18 μ.

Fig. 1. Debye–Scherrer photographs (taken according to Straumanis method; CuK_α-radiation) of palladium wires charged with hydrogen from the gas phase under identical conditions of temperature, pressure and duration of charging. The grain-size of the wires increases from $a \to b \to c$ (due to reproduction the very fine spots on the D-S-circles of Fig. 1*b* are not distinguishable); *a:* diagram of β-palladium; *b:* diagram of a mixture of α- and β-palladium; *c:* diagram of α-palladium.

Fig. 2. Rotating crystal photographs (CuK_α-radiation) of palladium wires with large crystals (1–5 mm in length); *a:* before charging with hydrogen; *b:* charged with hydrogen from the gas phase at room temperature and 20–25 atmospheres pressure during 3 hours. The diagram shows lines of the α-phase only.; *c:* charged during 15 hours: α- and β-palladium lines.

T. J. TIEDEMA, B. C. DE JONG AND W. G. BURGERS: *Influence of grain-size on the rate of absorption of hydrogen by palladium*

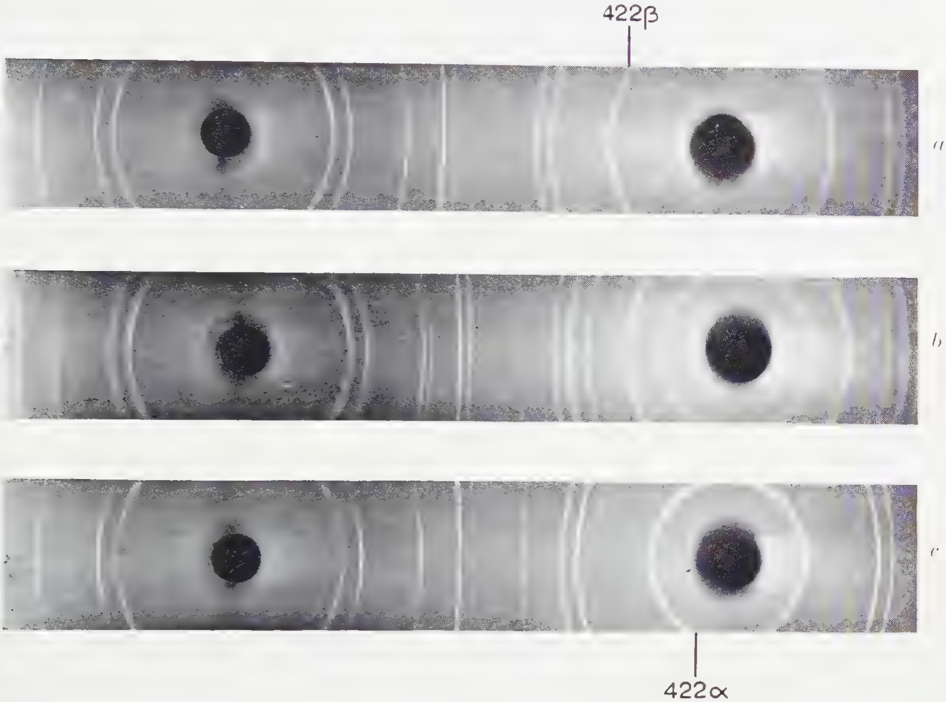

Fig. 1

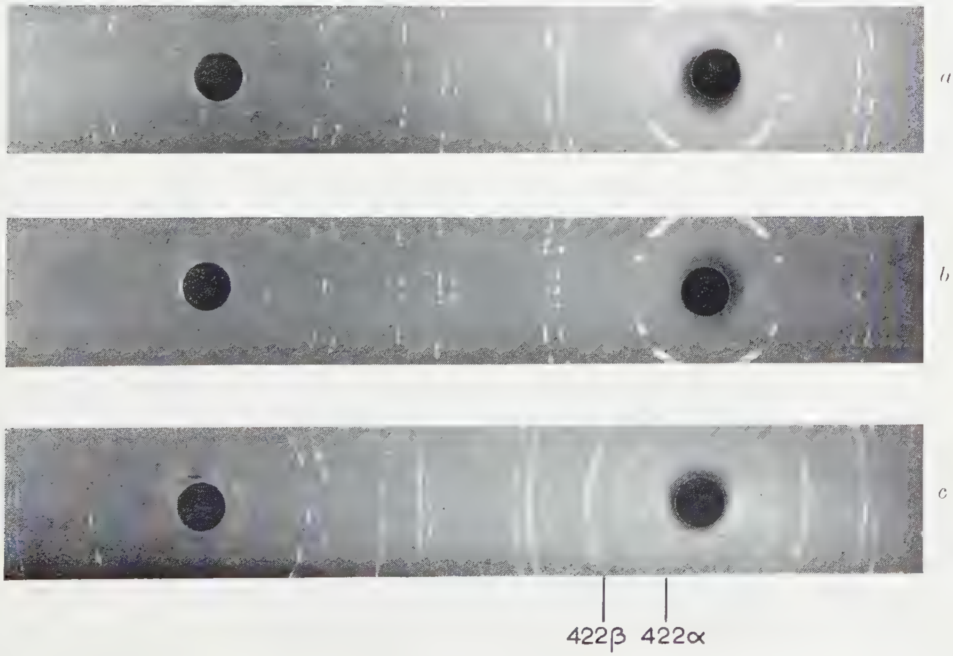

Fig. 2

Fig. 3

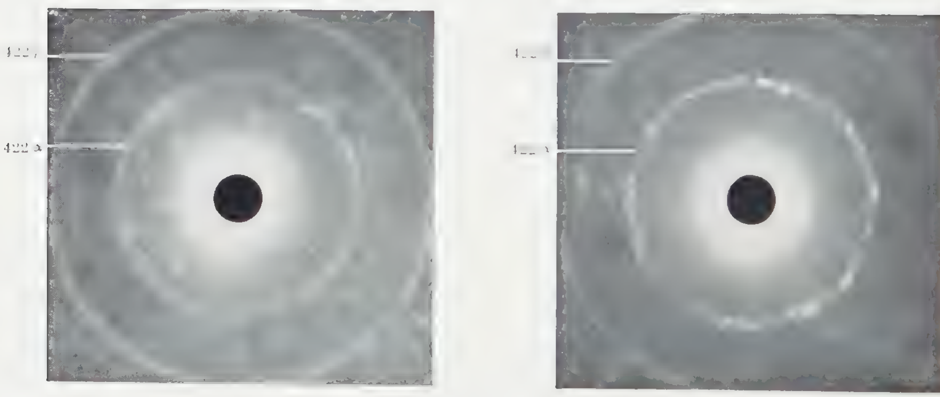

a Fig. 4 *b*

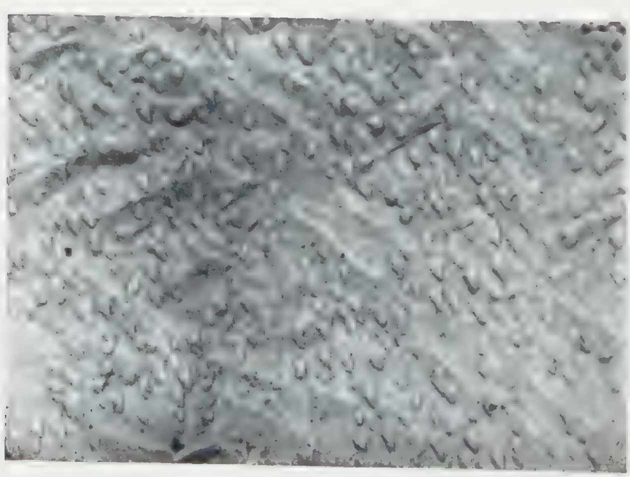

Fig. 5

phase may be due to a difference in rate of diffusion of the hydrogen through the palladium caused by an influence of the crystal boundaries in the fine-grained wire. In order to obtain information about the influence of grain-size on the process of internal diffusion, palladium foils of 0.1 mm thickness and of different grain-size were charged with electrolytically developed hydrogen in such a way that only one side of the foil was in contact with the solution. After charging during a certain time under identical circumstances, X-ray exposures (figure 4) were made from that side of the foils which had *not* been in direct contact with the hydrogen. In all cases it turned out that the hydrogen content of the foils was independent of the grain-size.

It is therefore most likely that the difference in rate of absorption is caused by a difference in dissociation velocity of the hydrogen molecules at the surface of the fine-grained and the coarse-grained palladium. This conclusion finds some confirmation in an observation of Stackelberg and Bischoff [6], according to which hydrogen bubbles at a palladium cathode are formed almost exclusively at grain-boundaries, during or after interruption of the current.

In this connection it is of some interest to remark that experiments with single crystal surfaces reveal that the first observable surface roughness is localized along definite planes (see Tiedema, Kooy and Burgers [13]) or at definite points of a certain crystallographic plane. The latter fact is demonstrated by figure 5, showing a (111)-plane as cut on a large single crystal prepared after the method of Czochralski. From this photograph it can be seen that quaint triangular figures appear on the polished surface in the first stages of charging with hydrogen.

Laboratory of Physical Chemistry,
Technological University, Delft,
The Netherlands

Fig. 3. Debye–Scherrer photographs (CuK_α-radiation) of fine-grained and coarse-grained palladium wires, charged electrolytically with hydrogen under identical conditions (see text): both photographs show the presence of lines of the α- and of the β-phase, indicating that in this case the difference in grain size has no influence on the rate of absorption.

Fig. 4. Back reflection X-ray photographs (CuK_α-radiation) of *a*) a fine-grained and *b*) a coarse-grained palladium foil (thickness 0.1 mm), both charged electrolytically at one side (the "front") under identical conditions (2.8 mA/cm^2; $3\frac{1}{2}$ h). The photographs were taken from the non-exposed "back" of the foils. Both photographs show the presence of the α-phase beside the β-phase, indicating that there is no marked difference in rate of internal diffusion.

Fig. 5. Microphotograph of (111)-plane of large single crystal after charging electrolytically with hydrogen (8 mA/cm^2; 20 min). Magnification 270 $\times$. The surface roughness starts at certain points and the figures developed give the impression of parallel triangles.

REFERENCES

1. Flanagan, T. B. and F. Lewis, Trans. Faraday Soc. **55**, 1400 (1959); J. Chem. Physics **29**, 1417 (1958).
2. Tammann, G. and J. Schneider, Z. anorg. allg. Chemie **172**, 43 (1928).
3. Worsham, J. E., M. K. Wilkinson and C. G. Shull, J. Phys. Chem. Solids 3, 309 (1957).
4. Clamroth, R. and C. A. Knorr, Z. Elektrochem. **57**, 399 (1953).
5. Breiter, M., H. Kammermaier and C. A. Knorr, Z. Elektrochem. **58**, 702 (1954).
6. Stackelberg, M. von and H. Bischoff, Z. Elektrochem. **59**, 467 (1955).
7. Lewis, F. A., G. Roberts and A. R. Ubbelohde, Proc. Roy. Soc. London **A 220**, 279 (1953).
8. Hoare, J. P. and S. Schuldiner, J. Electrochem. Soc. **102**, 485 (1955).
9. Duhm, B., Z.f. Physik **94**, 434 (1935).
10. Owen, E. A. and J. I. Jones, Proc. Phys. Soc. London **49**, 587 (1937).
11. Smith, D. P. and G. J. Derge, Trans. Electrochem. Soc. **66**, 253 (1934).
12. Krause, W. and L. Kahlenberg, Trans. Electrochem. Soc. **68**, 449 (1935).
13. Tiedema, T. J., C. Kooy and W. G. Burgers, Proc. Acad. Sc. Amsterdam **B 62**, 34 (1959).

CHEMISTRY

ALKALOIDS OF *LUNASIA AMARA*

STRUCTURE AND SYNTHESIS OF LUNASIA I

BY

H. C. BEYERMAN AND R. W. ROODA

(Communicated by Prof. P. E. VERKADE at the meeting of March 26, 1960)

1. *Introduction*

In a previous communication we submitted a preliminary report on the isolation, characterization, and structural investigations of six alkaloids, which on that occasion we named Lunasia I–VI, from the bark of *Lunasia amara* Blanco, originating from Java [1]). This was followed up by a supplementary proof of the complete structure of Lunasia II [2]).

In our first communication we already pointed out that the *Lunasia* alkaloids can be classified according to their relative hydrogen content into *two groups*, one containing less and the other more hydrogen. The latter group, to which, among others, the alkaloids Lunasia II, probably III, and IV–VI belong, comprises compounds derived from furano-quinoline and/or pyrano-quinoline; this group might also be called "isoprene-quinoline alkaloids". The former group, to which Lunasia I belongs, appears to be derived from 2-phenylquinoline.

Since we started our investigation several 2-phenylquinolines were isolated from Rutaceae; formerly it was unknown that they occur in nature. GOODWIN *et al.* in the leaves of Philippine *Lunasia amara* found 4-methoxy-2-phenylquinoline (Fig. 1) [3]), 4-methoxy-2-(3′, 4′-methylenedioxyphenyl)-quinoline (Fig. 2) [4]), and 7-methoxy-1-methyl-2-(3′, 4′-methylenedioxyphenyl)-quinolone (Fig. 4) [4]); the latter compound is, in all probability the lunamarine of earlier investigators [5]). GOODWIN *et al.* [4]) also found the compound 7-methoxy-1-methyl-2-phenyl-4-quinolone (Fig. 3), which is closely related to lunamarine (Fig. 4) and which had already been isolated by JOHNSTONE, PRICE and TODD from

---

1) H. C. BEYERMAN and R. W. ROODA, Proc. Kon. Nederl. Akad. Wetensch., Series **B 62**, 187–199 (1959).

2) H. C. BEYERMAN and R. W. ROODA, Proc. Kon. Nederl. Akad. Wetensch., Series **B 63**, 154 (1960).

3) S. GOODWIN, A. F. SMITH and E. C. HORNING, J. Am. Chem. Soc. **79**, 2239 (1957).

4) S. GOODWIN, A. F. SMITH. A. A. VELASQUEZ and E. C. HORNING, J. Am. Chem. Soc. **81**, 6209 (1959).

5) F. A. STELDT and K. K. CHEN, J. Am. Pharm. Assoc., Sci. Ed. 32, 107 (1943).

the bark of *Lunasia quercifolia* collected in northern Australia [6]). The latter compound (Fig. 3) was also found by SONDHEIMER *et al.* as a bark component of *Casimiroa edulis*, a Mexican tree of the Rutaceae and called eduleine by them [7]). From the seed of the same plant SONDHEIMER *et al.* obtained another alkaloid of unknown structure, which they called eduline [8]). As appears from the subsequent communication, we were able to elucidate the structure by a comparison with synthetic material; eduline is 6-methoxy-1-methyl-2-phenyl-4-quinolone (Fig. 5) [9]).

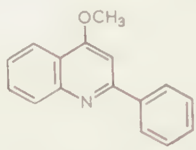

Fig. 1.
(Lunasia amara).

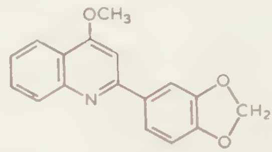

Fig. 2.
(Lunasia amara).

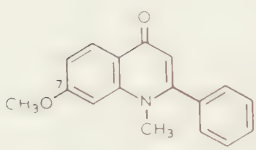

Fig. 3. Eduleïne
(Lunasia amara, Lunasia quercifolia, Casimiroa edulis)

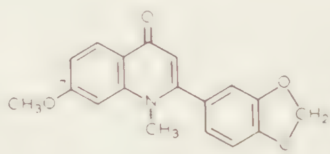

Fig. 4. Lunamarine
(Lunasia amara)

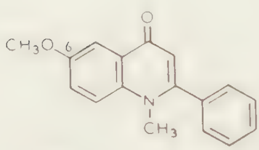

Fig. 5. Eduline
(Casimiroa edulis)

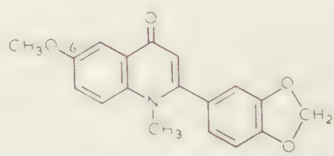

Fig. 6. Lunasia I
(Lunasia amara)

Figs. 1–6. Derivatives of 2-phenylquinoline found in nature.

2. *Structure of Lunasia I*

In our first communication we uttered our expectation that to Lunasia I ($C_{18}H_{15}NO_4$) might have to be assigned the structure of a 1-methyl-

6) R. JOHNSTONE, J. R. PRICE and A. R. TODD, Australian J. Chem. **11**, 562 (1958); J. R. PRICE, "Progress in the Chemistry of Organic Natural Products", Ed., L. ZECHMEISTER, 13, 302 (1956).

7) F. SONDHEIMER and A. MEISELS, J. Org. Chem. 23, 762 (1958); compare also J. IRIARTE, F. A. KINCL, G. ROSENKRANZ and F. SONDHEIMER, J. Chem. Soc. **1956**, 4170.

8) F. A. KINCL, J. ROMO, G. ROSENKRANZ and F. SONDHEIMER, J. Chem. Soc. **1956**, 4163.

9) H. C. BEYERMAN and R. W. ROODA, Proc. Kon. Nederl. Akad. Wetensch., Series B **63**, 432 (1960).

2-phenyl-4-quinolone substituted with one methoxyl and one methylene dioxy group, *i.e.* one out of thirty-four formally possible isomers [1]). From a mixed melting point determination (m.p. 204–230°) Lunasia I (m.p. 228–230°) was found not to be identical with Goodwin's lunamarine (m.p. 245–247°, Fig. 4) [10]); furthermore there are some differences in the ultra-violet and infra-red spectra.

Since then we synthesized a number of compounds, including 1-methyl-2-phenyl-4-quinolone and its 6-, 7-, and 8-methoxy derivatives, in order to obtain indications about the position of the methoxyl substituent in Lunasia I by a comparison of the spectra of the synthetic compounds with those of the natural product [11]).

TABLE A

Ultra-violet spectral data *) and melting points of Lunasia I and of some related compounds

Compound	M.p.	λ max, mμ	log max	λ min, mμ	log min
Lunasia I (Fig. 6)	228–230°	247	4.47	230	4.34
		289	4.05	283	4.02
		338	4.08	304	3.92
		352	4.06	344	4.04
6-Methoxy-1-methyl-2-phenyl-4-quinolone (Eduline, Fig. 5)	186–187°	257	4.54	227	4.26
		338	4.01	313	3.66
		352	4.04	343	4.00
7-Methoxy-1-methyl-2-phenyl-4-quinolone (Eduleïne, Fig. 3)	200–201°	251	4.52	256	4.49
		258	4.50	276	3.38
		324	4.11		
8-Methoxy-1-methyl-2-phenyl-4-quinolone	170–171°	249	4.47	227	4.23
		340	4.05	295	3.62
1-Methyl-2-phenyl-4-quinolone	144–145°	251	4.53	227	4.23
		325	4.12	278	3.43
		337	4.17	329	4.11

*) Measurements were made in ethanol; only the most conspicuous maxima and minima are mentioned.

From the ultra-violet spectral data listed in Table A the following fact appeared, among other things. The maximum at longer wave-length of

[10]) We thank Dr. Sidney Goodwin for making this comparison and for kindly putting a sample of synthetic 7-methoxy-1-methyl-2-(3′,4′-methylenedioxyphenyl)-4-quinolone (synthetic lunamarine) at our disposal (communication of Dec. 1, 1958).

[11]) The synthesis of 6-methoxy-1-methyl-2-phenyl-4-quinolone is described in our next communication (ref. 9). The other compounds were prepared analogously. 7-Methoxy-2-phenyl-4-quinolinol, an intermediate in one of the last-mentioned syntheses, was prepared not only according to Conrad–Limpach (compare ref. 9), but also by following the synthetic route indicated by Fuson and Burness (J. Am. Chem. Soc. **68**, 1270 (1946); this is contrary to the experience of Johnstone, Price and Todd (compare ref. 6).

Lunasia I, *like that of the said 6-methoxy compound*, has shifted considerably towards the red in relation to the unsubstituted 1-methyl-2-phenyl-4-quinolone and is split into two peaks, in contrast to the spectrum of the 7- and the 8-methoxy compound respectively.

Dr. SIDNEY GOODWIN was so kind as to have the nuclear magnetic resonance spectrum of Lunasia I taken and to interpret this. This interpretation, which was independent of our conclusion, pointed to the structure of 6-methoxy-1-methyl-2-(3′, 4′-methylenedioxyphenyl)-4-quinolone (Fig. 6) [12]:

In this paper we wish to present an unambiguous synthesis of the last-mentioned compound, which upon comparison of the ultra-violet and infra-red spectra and a mixed melting point determination proved to be identical with the natural product. Lunasia I therefore has the structure shown in Fig. 6.

3. *Synthesis of Lunasia I*

The synthesis of 6-methoxy-1-methyl-2-(3′, 4′-methylenedioxyphenyl)-4-quinolone (Lunasia I) is outlined in a flow-sheet.

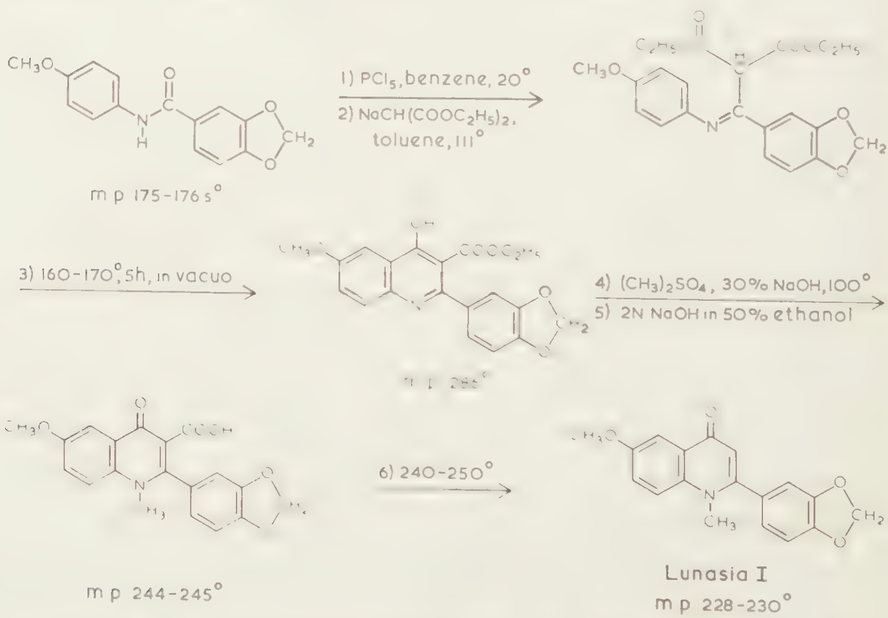

Starting from piperonyloyl *p*-anisidide, the first three steps form a synthesis according to JUST [13]), as improved by ELDERFIELD *et al.* [14])

[12]) We are indebted to Dr. SIDNEY GOODWIN and her colleagues at the Laboratory of Chemistry of Natural Products, National Heart Institute, Bethesda, Md., for this spectrum. We are very grateful to Dr. GOODWIN for writing to us about the analysis of the nuclear magnetic resonance spectrum (communication of April 23, 1959).

[13]) F. JUST, Ber. 18, 2632 (1885).

[14]) R. C. ELDERFIELD, W. J. GENSLER, T. H. BEMBRY, C. B. KREMER, J. D. HEAD, F. BRODY and R. FROHARDT, J. Am. Chem. Soc. 68, 1272 (1946).

and by Šorm and Novotný [15]. The overall yield of these three steps was about 40 %. The subsequent methylation, followed by alkaline hydrolysis of the ester group, gave the carboxylic acid (yield about 80 %). This decarboxylated upon being heated above its melting point [16].

Summary

After some spectral evidence had been obtained, the structure of the alkaloid Lunasia I, obtained previously by us from the bark of *Lunasia amara*, originating from Java, was proved by synthesis. Lunasia I is 6-methoxy-1-methyl-2-(3', 4'-methylenedioxyphenyl)-4-quinolone (Fig. 6).

Laboratory of Organic Chemistry,
Technische Hogeschool, Delft,
The Netherlands

---

15) F. Šorm and L. Novotný, Coll. Czech. Chem. Comm. **20**, 1206 (1955).
16) We hope to publish complete experimental details in Rec. trav. chim.

CHEMISTRY

ALKALOIDS OF *CASIMIROA EDULIS*

STRUCTURE AND SYNTHESIS OF EDULINE

BY

H. C. BEYERMAN AND R. W. ROODA

(Communicated by Prof. P. E. VERKADE at the meeting of March 26, 1960)

1. *Introduction*

In connection with our investigations about the alkaloid constituents from the bark of Javanese *Lunasia amara*, and more in particular in connection with the elucidation of the structure of the alkaloid Lunasia I (6-methoxy-1-methyl-2-(3', 4'-methylenedioxyphenyl)-4-quinolone), we became interested in substituted 2-phenylquinolines [1,2]). Compounds of this type were found in nature only since we started our investigations [3]).

7-Methoxy-1-methyl-2-phenyl-4-quinolone —also called eduleine— is found in Australian *Lunasia quercifolia* [4]), in Philippine *Lunasia amara* [5]), and in Mexican *Casimiroa edulis* [6,7b]), plants belonging to the Rutaceae. The compound was synthesized by JOHNSTONE, PRICE and TODD [4]).

Besides eduleine obtained from the bark, SONDHEIMER *et al.* from seed of *Casimiroa edulis* obtained, among others, another alkaloid with a structure that was unknown at the time, which compound they called eduline [7a]). The simplest composition of eduline was given as $C_{17}H_{15}NO_2$ and the compound was characterized by the said investigators not only by the melting point (m.p. 187–188°) and the ultra-violet spectrum, but also by a picrate and a perchlorate.

[1]) H. C. BEYERMAN and R. W. ROODA, Proc. Kon. Nederl. Akad. Wetensch., Series B 62, 187–199 (1959).

[2]) *a.* H. C. BEYERMAN and R. W. ROODA, Proc. Kon. Nederl. Akad. Wetensch., Series B 63, 154 (1960).

b. *ibid.* B 63, 427 (1960).

[3]) Compare ref. 2*b* for a short review.

[4]) R. JOHNSTONE, J. R. PRICE and A. R. TODD, Australian J. Chem. 11, 562 (1958); J. R. PRICE, "Progress in the Chemistry of Organic Natural Products", Ed., L. ZECHMEISTER, 13, 302 (1956).

[5]) S. GOODWIN, A. F. SMITH, A. A. VELASQUEZ and E. C. HORNING, J. Am. Chem. Soc. 81, 6209 (1959).

[6]) F. SONDHEIMER and A. MEISELS, J. Org. Chem. 23, 762 (1958).

[7]) *a.* F. A. KINCL, J. ROMO, G. ROSENKRANZ and F. SONDHEIMER, J. Chem. Soc. 1956, 4163;

b. J. IRIARTE, F. A. KINCL, G. ROSENKRANZ and F. SONDHEIMER, J. Chem. Soc. 1956, 4170.

2. *Structure of eduline*

In relation with the elucidation of the structure of Lunasia I we synthesized a number of compounds, including the isomer of eduleine: 6-methoxy-1-methyl-2-phenyl-4-quinolone [2b]). The latter compound has physical constants (m.p. 186–187°; ultra-violet spectrum: λ max 257, 338, 352 mμ, log max 4.54, 4.01, 4.04) which come close to those of eduline (m.p. 187–188°; ultra-violet spectrum: λ max 256, 336, 350 mμ, log max 4.56, 4.04, 4.06) [7a]). A determination of the mixed melting point (186–188°) and a direct comparison of the infra-red spectra (in potassium bromide pellets) showed the identity of the two compounds [8]).

3. *Synthesis of eduline*

This compound was obtained (m.p. 186–187°, yield 85 %) by alternate treatments, with methyl sulphate and 30 % aqueous sodium hydroxide, of 6-methoxy-2-phenyl-4-quinolinol [9]). The latter compound was formed by condensation of *p*-anisidine with ethyl benzoyl acetate according to the procedure of Conrad and Limpach [10]) in the modified form of Kaslow and Lawton [11]). The procedure was as follows: after formation of the anil (in refluxing chloroform with continuous separation of water), cyclization by refluxing in "dowtherm" (255–260°) with simultaneous distillation of the ethanol formed (m.p. 309–312°, yield about 50 %).

The derivatives prepared were the picrate: m.p. 218–221° (dec.) and perchlorates: m.p. 258.5–261° (1 equivalent of $HClO_4$), m.p. 231.5–233° ($\frac{1}{2}$ equivalent of $HClO_4$) [12]).

Summary

The structure of the alkaloid eduline of *Casimiroa edulis* was elucidated by synthesis. Eduline is 6-methoxy-1-methyl-2-phenyl-4-quinolone.

Laboratory of Organic Chemistry,
Technische Hogeschool, Delft,
The Netherlands

---

[8]) We are indebted to Dr. F. A. Kincl, Syntex S.A., Mexico City, for making these comparisons and to Prof. Dr. F. Sondheimer, The Weizmann Institute of Science, Rehovoth, Israel, for communicating these results, including a copy of the pertinent infra-red spectra, to us (communication of October 27, 1959).

[9]) For this we are indebted to Mr. J. van Westerveld.

[10]) M. Conrad and L. Limpach, Ber. **21**, 521 (1888).

[11]) C. E. Kaslow and W. R. Lawton, J. Am. Chem. Soc. **72**, 1723 (1950). Compare also R. U. Schock and H. J. Eichel, U.S.P. 2, 785, 165; C.A. **51**, 9713 g (1957).

[12]) We hope to publish the experimental details in Rec. trav. chim.

THE MOULDS OF FOOT PRINTS ON TRIASSIC SANDSTONE SLABS IN THE TEYLER MUSEUM, WITH NOTES ON THE NOMENCLATURE AND TYPES OF SOME *CHIROTHERIUM* SPECIES

BY

C. O. VAN REGTEREN ALTENA [1])

(Communicated by Dr. L. D. BRONGERSMA at the meeting of March 26, 1960)

1. INTRODUCTION

In his well-known "Histoire de l'ichnologie" WINKLER described and figured a series of eleven sandstone slabs with moulds of foot prints, presumably from Hessberg, Thuringia, which are kept in the Teyler Museum. I have lately re-examined these slabs with the purpose of bringing the explicative labels up to date, and, WINKLER's figures being sometimes used for reference, it seems worth while to publish the revised identifications. As I was anxious to use a correct nomenclature, the early literature on these Triassic foot prints was studied. The result of this study forms the third part of the present paper.

WINKLER was well aware of the fact that the slabs contained prints of several kinds of animals. In fact he distinguished the following species: (1) *Chirotherium majus*, (2) *Chirotherium minus*, (3) "petites traces tridactyles et pectiniformes", (4) "[impression] se distinguant particulièrement par la forme arrondie des bouts des doigts", and (5) "traces de pas qui se distinguent considérablement des empreintes des deux espèces de *Chirotherium* que nous venons d'étudier". The following table shows how, according to WINKLER, the five species are distributed over the slabs:

Catalogue no.:		1315	1316	1317	1318	1319	1320	1321	1322	1323	1324	1325
Species	(1)	+	—	—	—	—	+	+	+	+	+	+
,,	(2)	—	—	+	—	+	+	—	[illegible]	[illegible]	—	—
,,	(3)	+	—	—	+	—	—	—	+	—	—	—
,,	(4)	—	—	—	+	—	—	—	—	—	—	—
,,	(5)	+	—	—	+	—	—	—	+	—	—	—

Except in one case (cat. no. 1320) the two *Chirotherium* species were correctly identified by WINKLER, but the names he used are invalid when the International Rules of Zoological Nomenclature are applied to them. The species should be called *Chirotherium barthii* Kaup and *Ch. bipes* Berthold, respectively (see section 3).

[1]) Teyler Museum, Haarlem.

The "petites traces tridactyles et pectiniformes" are scattered over some of the slabs, and it is not possible to find a coherent trackway among them. They are, therefore, insufficient for exact identification, and, following PEABODY (1948, p. 318), I shall refer to them as lacertoid prints.

Originally I thought that the prints described as "[impression] se distinguant particulièrement par la forme arrondie des bouts des doigts" might be those of the feet of turtles. Closer examination revealed, however, that they certainly belong to a small *Chirotherium*. On these slabs there is considerable variation in size of the *Chirotherium* prints which are too small and relatively too narrow to belong to *Ch. barthii*. It seems probable, however, that all the differences in shape have been caused by differences in the way the animals moved and in the condition of the prints on the moment they were moulded in the sand. Therefore, all the small *Chirotherium* prints on these slabs have been attributed to *Ch. bipes*, though some of them with doubt.

WINKLER was right in considering his fifth species identical with that figured by SICKLER (1836) on his plate VII. The prints figured by SICKLER were assigned to a dicynodont and described as *Dicynodontipus hildburghausensis* by RÜHLE VON LILIENSTERN in 1944.

2. REVISED IDENTIFICATIONS OF THE FOOT PRINTS ON TRIASSIC SANDSTONE SLABS IN THE TEYLER MUSEUM [1]

No. 1315. WINKLER, 1886, p. 431, pl. V.

Chirotherium barthii Kaup: right pes and manus. WINKLER is probably right in considering an indistinct mould visible in the lower right corner of the slab to be that of the left pes.

Chirotherium bipes Berthold: a left pes and manus slightly below and to the left of the middle of the slab, and a right pes at the middle of the left border. This track was not recognized by WINKLER, and the left pes and manus have been poorly figured. Length of pes about 8 cm, pace about 32 cm.

Small lacertoid prints passim.

No. 1316. WINKLER, 1886, p. 431, pl. VII.

Chirotherium bipes Berthold: along the upper edge of the slab (the right side in WINKLER's figure) a right pes, a left pes and manus, and another right pes can be discerned. The track was not recognized by WINKLER, and the first right pes and the left manus have not been figured. Length of pes about 9.5 cm, stride about 70 cm.

No. 1317. WINKLER, 1886, p. 431, pl. VI.

Chirotherium bipes Berthold: two tracks: (1) at the left side a left pes and manus, and a right pes and manus; (2) at the right side a right pes and manus. In all these pedes the digits II–IV are distinctly moulded

---

[1] Unless otherwise stated the prints are inner moulds.

with their claws, while digit I is less distinct and V is lacking. Well figured by WINKLER. Length of digit III slightly more than 8 cm, pace about 41 cm.

1318. WINKLER, 1886, p. 431, pl. VIII.

Chirotherium bipes Berthold (?): from the lower left corner of the slab toward the right and slightly upward: right pes and manus (indistinct), left pes and manus, right pes and manus (indistinct). The track was not recognized by WINKLER, who described the left pes as "[impression] se distinguant particulièrement par la forme arrondie des bouts des doigts". Digit V of this pes is, however, distinctly visible, and I have no doubt that the track belongs to a *Chirotherium*. Length of pes almost 7 cm, stride almost 40 cm.

Dicynodontipus hildburghausensis Rühle: left manus and pes, right manus and pes, left manus.

Small lacertoid prints passim.

1319. WINKLER, 1886, p. 431, pl. IV, fig. 2 (upper figure).

Chirotherium bipes Berthold: two tracks: (1) right pes probably with manus (8 cm in front of the tip of digit III of the pes); (2) right pes (length about 7.5 cm) and manus, and left pes (pace about 25 cm). The second track was not recognized by WINKLER; he distinctly figures the right manus only.

A print figured by WINKLER below the middle of the slab with the digits pointing downward remains unidentified.

1320. WINKLER, 1886, p. 430, pl. III, fig. 2 (upper figure).

Chirotherium bipes Berthold: right pes (length about 11.5 cm) and manus, and left pes and manus. The left manus, though quite distinct, has not been figured. The left pes and manus belong to a slightly smaller animal than the right pes and manus.

A single small print with the digits pointing downward on the left side of the slab remains unidentified.

1321. WINKLER, 1886, p. 432, pl. IX, fig. 1 (lower figure).

Chirotherium barthii Kaup: outer moulds of right pes and manus.

1322. WINKLER, 1886, p. 429, p.l III, fig. 1 (lower figure).

Chirotherium barthii Kaup: left pes and manus.

Chirotherium bipes Berthold: from top of slab downward: much disturbed and consequently indistinct left pes and manus, less disturbed right pes and manus, and distinct left pes and manus. This track was not recognized by WINKLER and its elements have been poorly figured. Length of pes almost 8 cm, stride about 48 cm.

Small lacertoid prints passim.

1323. WINKLER, 1886, p. 429, pl. II.

Chirotherium barthii Kaup: left pes and manus, and right pes and manus.

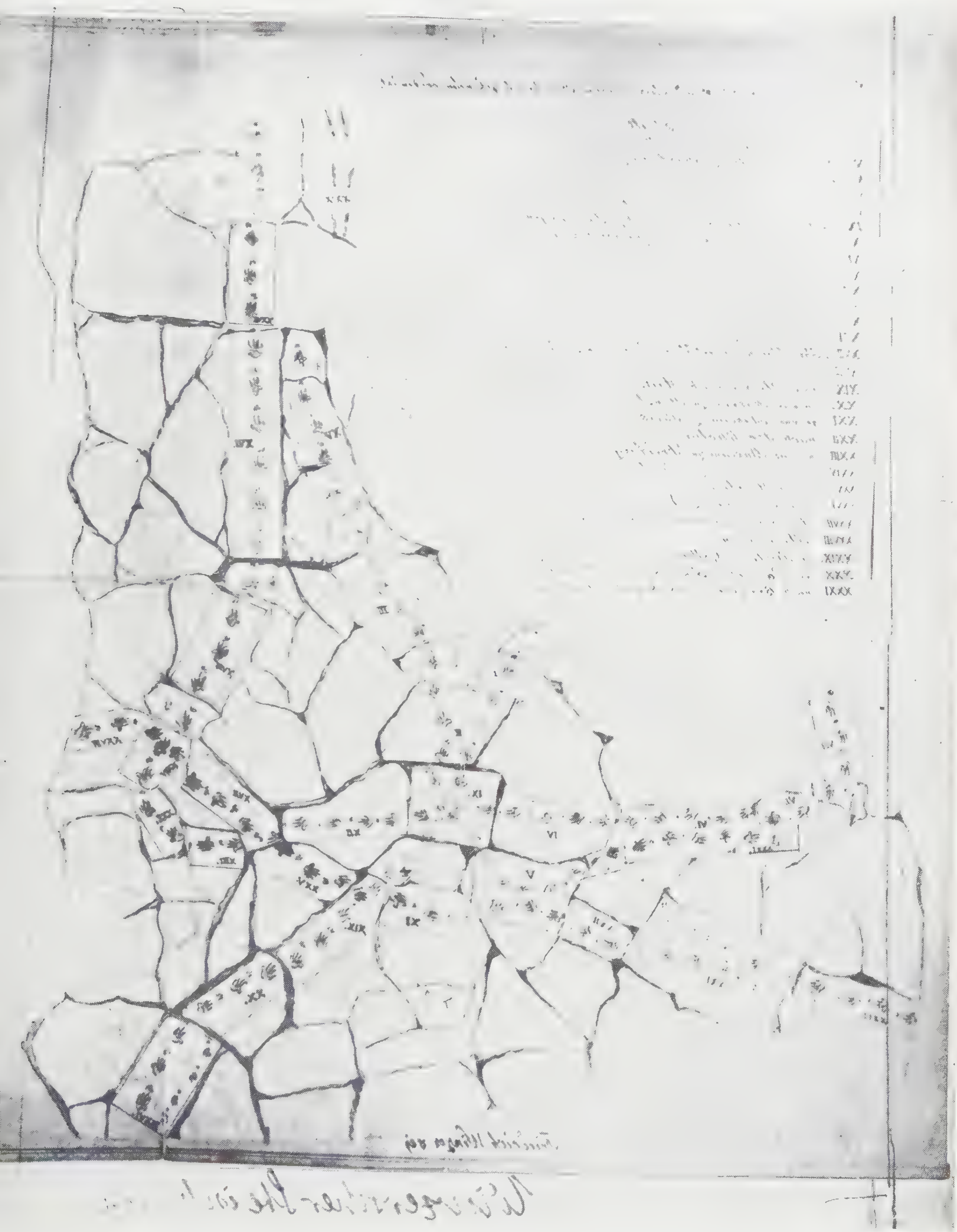

Plate 1. Reversed image of the photograph of the map of Mr. Winzer's sandstone quarry at Hessberg, Thuringia.

1324. Winkler, 1886, p. 189, pl. I.

Chirotherium barthii Kaup: right pes and manus, left pes and manus, and another right pes and manus.

Chirotherium bipes Berthold: left pes and manus, and right pes and manus in the left lower corner of the slab; rather indistinct. This track was not mentioned by Winkler, but it has been figured, although somewhat roughly. Length of pace almost 26 cm.

Scattered small indistinct prints remain unidentified.

1525. Winkler, 1886, p. 430, pl. IV, fig. 1 (lower figure).

Chirotherium barthii Kaup: part of left pes and manus, and right pes, and further a second left pes and manus which probably belong to another trackway.

The revised identifications are summarized in the following table, in which circles indicate the prints which were not or wrongly identified by Winkler.

Catalogue no.:	1315	1316	1317	1318	1319	1320	1321	1322	1323	1324	1325
Ch. barthii	+	—	—	—	—	⊖	+	+	+	+	+
Ch. bipes	⊕	⊕	+	⊕	+	+	—	⊕	—	⊕	—
Dicynodontipus	—	—	—	+	—	—	—	—	—	—	—
lacertoid	+	—	—	+	—	—	—	+	—	—	—

3. Notes on the nomenclature and type specimens of some species of Chirotherium.

The genus *Chirotherium* is generally attributed to Kaup, 1835, N. Jahrb., p. 328. If this really were the first publication of the name, it might be considered preoccupied by *Palaeopithecus* Voigt, 1835, N. Jahrb., p. 324. Fortunately, however, Kaup's name had already been published earlier in the same year in a paper by Hohnbaum in "Die Dorfzeitung", no. 34, of February 18, 1835. The pages 324 and 328 belong to the third part of the "Jahrbuch" of 1835. This part contains a letter dated March 6, 1835, and was, consequently, certainly published later than the issue of "Die Dorfzeitung" just mentioned. The latter journal is extremely rare in libraries, and I am very much indebted to the Director of the "Geschwister-Scholl-Oberschule" at Hildburghausen for providing me a type-written copy of Hohnbaum's paper [1]).

In Hohnbaum's paper attention is drawn to the foot prints of *Chirotherium* which had been discovered in sandstone quarries at Hessberg near Hildburghausen, Thuringia. It contains a description of *Chirotherium* prints from the same slab as that which was described and figured by Sickler in December of the preceding year, and people are encouraged to contribute to the fund necessary for the excavation of more specimens.

1) The kind assistance of Prof. Dr. F. von Huene and Dr. F. Westphal in procuring literature necessary for writing this paper is here gratefully acknowledged.

HOHNBAUM cites a letter of KAUP, and this part of his paper is copied here, because of its nomenclatural importance.

Ein anderer, durch seine Abhandlungen über fossile Thierknochen hinreichend bekannte Naturforscher, Hr. D. KAUP in Darmstadt, dessen Stimme mir in dieser Angelegenheit von besonderem Gewicht zu sein scheint, äussert sich folgendermassen darüber:

"Schon vor einigen Monaten besass ich durch die güte meiner Freunde, des Hrn. Kupferstechers Barth (der erste, der auf den seltenen Fund aufmerksam wurde) und des MR. D. Hohnbaum eine sehr exacte Zeichnung der vorhandenen grossen Platte, eine 5 Fuss grosse Originalplatte und geognostische Notizen, die ich zur Ausarbeitung einer Abhandlung benützt habe, welche ich später herauszugeben gedenke, wenn ich erst Knochen dieses Thieres kennen lernen werde".

"Die Fussabdrücke, so ähnlich sie auch Fussspuren von Affen sind, gehören ganz gewiss nicht Thieren dieser Ordnung an, die bis jetzt, selbst in dem Diluvium, fossil nicht gefunden worden sind. Im Sandstein einer viel älteren Bildung, er mag Namen haben, welchen er will, sind bis jetzt nur Amphibien gefunden worden, allein dass die Fährten von Amphibien herrühren, dagegen spricht der säugethierähnliche Gang. Das Wahrscheinlichst bleibt dies, dass sie Thieren zugehören, welche vielleicht in der Ordnung der Beutelthiere ihre Stelle finden, denn auch bei diesen findet sich der den Fingern entgegengesetzte Daumen der Hinterfüsse, und es wäre keine Unmöglichkeit, dass diese abnormen Geschöpfe mit den Amphibien des Sandsteins zu gleicher Zeit gelebt hätten".

"Das erste Vorkommen von Fussspuren, allein undeutlich vertieft, hat man in New Red Sandstone in dem Steinbruch Corncocle Muir in Dumfriesshire (Schottland) entdeckt. Bukland hält sie für Fährten von Krocodilen und Schildkröten, die bergauf und bergab gingen, allein wegen der Steilheit der Lage ausglitten."

"Das Genus des grossen Thieres habe ich einstweilen wegen seiner volkommen Handbildung sowohl des Vorder- als Hinterfusses: Handthier, Chirotherium, und die Art nach meinem Freunde Barth Chirotherium Barthii genannt. Die Pflanzenreste scheinen einem Equisetum anzugehören, das nicht abgebildet ist. Die kleinen Fussspuren bedürfen einer näheren Prüfung, besonders was die manschettenartige Form am hinteren Rand der Fusswurzel bedeutet. Der Sandstein besteht aus sehr kleinen krystallisch-eckigen Quarzkörnern, die, nicht ohne Zwischenräume, durch ein sparsames kalkiges Bindemittel verkittet sind".

So weit unser Freund Kaup.

The following is a list of the early names given to the genus:

Chirotherium KAUP in HOHNBAUM, 18 II 1835, Die Dorfzeitung no. 34 (monotype *Ch. barthii* Kaup in HOHNBAUM, 1835).

Palaeopithecus VOIGT, 1835, N. Jahrb., p. 324 (no species named; based on the publication of SICKLER, 1834, and on a slab received in Jena, probably no. VII of WINZER's map, see below).

Chirosaurus KAUP, 1835, N. Jahrb., p. 328 (proposed as an alternative for *Chirotherium*, if it would prove to be a reptile).

Cheirotherium SICKLER, 1836, Die vorz. Fährten-Abdrucke, &c., p. 1, 8 (for *Chirotherium* Kaup).

Cheirotherion SICKLER, 1836, Op. cit., p. 7, 8 (for *Chirotherium* Kaup).

An excellent survey of the species of *Chirotherium* was given by PEABODY in 1948. As PEABODY was not acquainted with some very rare early publications on the subject, some of his statements are incomplete or not

quite correct. Therefore, the earliest described nominal species of *Chirotherium* will be discussed here, but their type locality needs to be discussed first.

The type locality of all the nominal species of *Chirotherium* described shortly after the discovery of fossil reptile tracks in Germany in 1833 is the quarry of Mr. WINZER at Hessberg near Hildburghausen. Of this quarry Mr. WINZER drew a map in which all the large slabs sent to museums and private collections were indicated by a number and listed. A partly faded photograph of this map exists in the Geological-Palaeontological Institution of the Martin Luther University at Halle, and has been reproduced by WILLRUTH (1917). The late Prof. H. GALLWITZ was so kind as to send me that photograph on loan in 1958, so that I was able to have it copied. A reflected image of this photograph, on which the slabs are more easily recognized because they are the counterparts of the original relief, is reproduced here (Pl. 1). It may serve as a proof that the specimens considered types come from this locality, and also help in providing correct locality labels for incompletely labelled slabs in many a museum.

The list of collections to which the slabs were sent is only partly readable; WILLRUTH gave the following interpretation of it: I ?, II probably Trier, III Darmstadt, IV Göttingen, V Berlin, VI certainly Strassburg, VII Jena, VIII Darmstadt, IX Meiningen, X ?, XI certainly Freiberg, XII ?, XIII ?, XIV prof. WEISS (Berlin), XV ?, XVI certainly Meiningen, XVII certainly Cassel, XVIII Gotha, XIX Halle, XX Strassburg, XXI Paris, XXI Stockholm, XXIII Freiberg, XXIV Berlin, XXV Haarlem, XXVI Vienna, XXVII Göttingen, XVXIII Meiningen, XXIX Berlin and Gotha, XXX Poppelsdorf, XXXI Bonn.

The following are some notes on this list:

I: it seems that the sentence bearing on this number reads "das erste Stück welches im Winzerschen Steinbruch gefunden worden ist".

II: this is the slab figured by SICKLER (1834), and said by him to have been placed in the "Gymnasium" at Hildburghausen. It is still in that school, now the "Geschwister-Scholl-Oberschule", and to the kindness of its Director I owe a series of photographs of this interesting slab. WILLRUTH's supposition that it was sent to Trier thus proved to be wrong.

VIII: this probably is the slab figured by KAUP (1835, Das Thierreich, vol. 1, p. 247), which was sent by him to the British Museum (Natural History), and studied there by BUCKLAND, who figured one of the prints (1837, pl. 26'', cf. LYDEKKER, 1890, p. 216 no. R 728). It is remarkable, however, that the print of the left manus, visible at the top of KAUP's figure, is lacking on the map. On the other hand slab no. XV, which according to WILLRUTH was sent to London, bears the correct number of pes and manus prints, but they are reversed.

XVI: though WILLRUTH states that this slab had certainly been sent to Meiningen, it is the only one answering HUMBOLDT's description of a specimen sent to Berlin (DE HUMBOLDT, 1835, p. 135: "la grande pierre de dix à douze pieds de long sur trois à quatre de large, que vient d'acquérir le cabinet de minéralogie de Berlin", and p. 137: "le pouce détaché, dirigé trois fois alternativement vers la droite et vers la gauche").

XXI: this is the famous slab in the Paris Museum figured by SICKLER (1836, pl. 1), and by RÜHLE VON LILIENSTERN (1944, pl. 22, fig. 1).

XXV: this slab is clearly indicated to have been sent to Haarlem, but none of the slabs in the Teyler Museum agrees with it. Cat. no. 1324, figured by WINKLER (1886, pl. 1), bears the correct number of manus and pes prints, but they are reversed.

Consequently the indications on the map were confirmed in some cases, but seem to be incorrect in others.

The following is a discussion of some early described nominal species of *Chirotherium* in chronological order.

Chirotherium barthii Kaup

Chirotherium Barthii Kaup in Hohnbaum, 18 II 1835, Die Dorfzeitung, no. 34.

The species is based on "eine sehr exacte Zeichnung der vorhandenen grossen Platte", and "eine 5 Fuss grosse Originalplatte". The drawing was presumably of no. II of Winzer's map. The original slab must have been no. III of the same map, which was sent to Darmstadt, as is still to be read on the list on the map. These two slabs have the prints of one individual of the large species of *Chirotherium* in common, though the prints of a second are visible on slab no. II. I propose to consider the track which no. II and no. III have in common the lectotype of the species. Consequently parts of this track are to be found on the slabs no. XXIII (Freiberg), XXI (Paris), XXII (Stockholm), V (Berlin), IX (Meiningen, but I doubt if this name is correctly interpreted by WILLRUTH), II (Hildburghausen), III (Darmstadt), XIV (Berlin), XV (?).

Chirotherium bipes Berthold

Chirotherium bipes Berthold, 4 IV 1835, Göttingische gel. Anz., p. 520.

The name was created for the smaller of the two species figured by SICKLER, 1834. SICKLER figured slab no. II of WINZER's map, on which two divergent tracks of *Ch. barthii*, and two parallel tracks of a much smaller species are visible. No manus prints are figured in the latter tracks. On a series of photographs of the original slab, most kindly provided by the Director of the "Geschwister-Scholl-Oberschule" at Hildburghausen, I cannot find any indication of the presence of manus prints. KAUP (1835, Das Thierreich, vol. 1, p. 248), however, considered *Ch. bipes* identical with his *Ch. sickleri* based on a specimen showing both

pes and manus prints, although not every pes print is accompanied by one of the manus. On the other hand Abel (1935, p. 45, fig. 24), who copied Buckland's (1837, pl. 26′, cf. footnote p. 265) copy of Sickler's figure, but wrongly stated the slab to be from Corn Cockle Muir, Scotland, thought these tracks to be from a short-legged animal with a broad trunk and belonging to a systematic group totally different from *Chirotherium*. The accurate figure of one foot print in natural size in Sickler's plate leaves no doubt as to the appurtenance of the species to the genus *Chirotherium*. Size and form of these prints are strikingly similar to those of the species referred to as *Ch. minus* by Peabody (1948). As this small species is known to have left tracks in which the manus prints are partly lacking (cf. the remark of Kaup, 1835, Das Thierreich, vol. 1, p. 248, on his *Ch. sickleri*, and of Soergel, 1925, p. 42, on *Ch. bornemanni*, both synonyms of *Ch. minus*), it seems very likely that what is preserved on no. II of Winzer's sandstone slabs are two bipedal tracks of *Ch. minus*. Consequently this name must fall as a synonym of *Ch. bipes*.

Chirotherium sickleri Kaup

Chirotherium sickleri Kaup, 1835, Das Thierreich, vol. 1, p. 248, fig. on p. 247.

This species is based on a track consisting of small prints in a sandstone slab which also bears prints of *Ch. barthii*. This slab was sent to the British Museum (Natural History) by Kaup and was catalogued by Lydekker (1890, p. 216) under no. R 728. It probably is no. VIII of Winzer's map (see, however, my remarks under that number). I have no doubt that this is the species referred to as *Ch. minus* by Peabody (1948, p. 358). Soergel (1925, p. 46), apparently unaware of Kaup's earlier use, gave the same name to the same species.

Chirotherium majus Sickler

Cheirotherion majus Sickler, 1836, Die vorzügl. Fährten-Abdrucke, &c., p. 7, 8, pl. 1, 2, 3, 4, 5.

This species was based on the track of large prints in slab no. XXI of Winzer's map, which slab is in the Muséum National d'Histoire Naturelle at Paris. If my proposal to consider the track which the slabs no. II and III have in common the lectotype of *Ch. barthii* Kaup is accepted, *Ch. majus* becomes an objective synonym of *Ch. barthii*.

Chirotherium minus Sickler

Cheirotherion minus Sickler, 1836, Die vorzügl. Fährten-Abdrucke, &c., p. 7, pl. 1.
Cheirotherium minus Sickler, 1836, op. cit., p. 8, pl. 6.

Peabody (1948, p. 358) says that a type was not designated by Sickler and, therefore, considers the species to be represented by the slabs nos. 1317, 1319 and 1320 of the Teyler Museum (Belgium [sic.!],

recte Netherlands) as figured by WINKLER [1]). The species was, however, based on a track in the large sandstone slab in the Muséum National d'Histoire Naturelle at Paris, no. XXI of WINZER's map, which track must, consequently, be considered the type specimen of this species. SICKLER's name, however, falls as a synonym of *Ch. bipes* Berthold.

REFERENCES

ABEL, O., Vorzeitliche Lebensspuren. Jena (1935).

BERTHOLD, (Review of Sickler's publication of 1834). Göttingische Gelehrten Anzeigen, 1835, 1, 514–520 (4.IV.1835).

BUCKLAND, W., Geology and Mineralogy considered with reference to Natural Theology (Bridgewater Treatise no. VI). London, 2 vols. (1837).

HOHNBAUM, D. C., Urwelt-Händel. Die Dorfzeitung Nr. 34 (18.II.1835). (copied in Allgemeine Preussische Staatszeitung, 22.II.1835, review in: Berlinische Nachrichten 24.II.1835).

HUMBOLDT, DE, Note sur les empreintes de pieds d'un Quadrupède dans la formation de grès bigarré de Hildburghausen en Allemagne. Ann. Sc. Nat. (2) **4** (Zool.), 135–138, pl. 5 (1835).

[KAUP, J. J.], (Letter of 2.II.1835 to Prof. BRONN.) N. Jahrb. Miner., &c. 1835, 327–328 (1835).

KAUP, J. J., Das Thierreich, 1 Darmstadt (1835).

LYDEKKER, R., Catalogue of the fossil Reptilia and Amphibia in the British Museum (Natural History), Cromwell Road, S.W., Part IV. London (1890).

PEABODY, F. E., Reptile and Amphibian trackways from the Lower Triassic Moenkopi formation of Arizona and Utah. Univ. Calif. Publ., Bull. Dep. Geol. Sci., **27**, no. 8, 295–468, 40 figs., pls. 23–45 (1948).

RÜHLE VON LILIENSTERN, H., Eine Dicynodontierfährte aus dem Chirotherium Sandstein von Hessberg bei Hildburghausen (aufbewahrt im Palaeontologischen Museum des Jardin des Plantes in Paris). Palaeont. Zeitschr., **23**, 368–385, 7 figs., pls. 22, 23 (1944).

SICKLER, F. K. L., Sendschreiben an . . . Dr. J. F. BLUMENBACH, . . . über die höchst merkwürdigen, vor einigen Monaten erst entdeckten Reliefs der Fährten urweltlicher, grosser und unbekannter Thiere in den Hessberger Sandsteinbrüchen bei der Stadt Hildburghausen. Hildburghausen, 16 pp., 1 pl. Reprint from a "Schulprogramm" issued 17 XII 1834 (1834).

———, Die vorzüglichsten Fährten-Abdrucke Urweltlicher Thiere in buntem Sandstein, aus den Sandsteinbrüchen in der Umgegend von Hildburghausen; treu nach der Natur gezeichnet und lithographirt von C. Kessler, . . . mit einem Vorwort herausgegeben. Erstes Heft. Hildburghausen, 8 pp., 7 pls., map (1836).

SOERGEL, W., Die Fährten der Chirotheria. Jena (1925).

VOIGT, FR. S., (letter of 14 II 1835 to Geheimrath v. LEONHARD.) N. Jahrb. Miner., &c. 1835, 322–326 (1835).

WILLRUTH, K., Die Fährten von Chirotherium. Thesis, Halle (1917).

WINKLER, T. C., Histoire de l'ichnologie. Etude ichnologique sur les empreintes de pas d'animaux fossiles suivie de la description des plaques à impressions d'animaux qui se trouvent au Musée Teyler. Arch. Mus. Teyler (2) **2**, 241–440, pls. 8–19 (1886).

[1]) PEABODY refers to the plates III (2), IV, and VI, and to the specimens 1320 and 1317. It seems likely that he meant the plates III (2), IV (2), and VI representing the specimens 1320, 1319, and 1317 respectively.

PHYSICAL CHEMISTRY

REACTIONS OF THE PENTACYANOCOBALTATE(II)-ION

BY

B. DE VRIES

(Communicated by Prof. J. H. DE BOER at the meeting of April 30, 1960)

Introduction

When solutions of potassium cyanide and a cobaltous salt, in molar ratio $\frac{(CN)^-}{Co^{++}} > 5$ and in the absence of oxygen, are added together, the pentacyanocobaltate(II)-ion is formed [1, 2]. Concentrated solutions of this complex ion display several interesting properties. They are able not only to give spontaneous hydrogen evolution, but also to absorb and activate molecular hydrogen even in dilute solutions. Since the latter property was discovered by IGUCHI [3] in 1942, various fundamental investigations into these two aspects of the cobalt complex have been carried out [4, 5, 6].

Inter alia it was found that a dilute solution of the cobalt complex, stored under nitrogen and which had not yet evolved hydrogen, showed a rapidly decreasing ability with time to absorb hydrogen [6] (the so-called ageing process).

Some years ago it was found in this laboratory [7] that sorbic acid in a hydrogen-saturated pentacyanocobaltate(II) solution quantitatively absorbed one equivalent of hydrogen under formation of 2-hexenoic acid. The discovery of this selective catalytic hydrogenation gave rise to a more extensive investigation into the reaction of this cobalt complex with sorbic acid with and without molecular hydrogen. In connection with the above-mentioned ageing process some results of this investigation will be mentioned here.

Reaction between sorbate and pentacyanocobaltate(II)

Results

When sodium sorbate is added to a hydrogen-saturated freshly prepared aqueous solution of the complex, the sorbate absorbs one equivalent of hydrogen (see curves A and B, Fig. 1a). By infra-red and ultra-violet analysis of the reaction product, it was demonstrated that the sorbic acid had been quantitatively converted into 2-hexenoic acid, in accordance with the following scheme.

(1) $$\mathrm{CoH} + \text{sorbic acid} \rightarrow \mathrm{Co} + \text{hexenoic acid}$$

(2) $$2\mathrm{Co} + \mathrm{H_2} \rightarrow 2\mathrm{CoH}$$

in which Co and CoH represent the non-hydrogenated and the hydrogenated cobalt complex respectively.

If the reaction is carried out with at least 10 times as much cobalt complex as sorbic acid, it was found, from the course of the hydrogen absorption with time, that the reaction is of 1st order in sorbic acid (curves A and B, Fig. 1b).

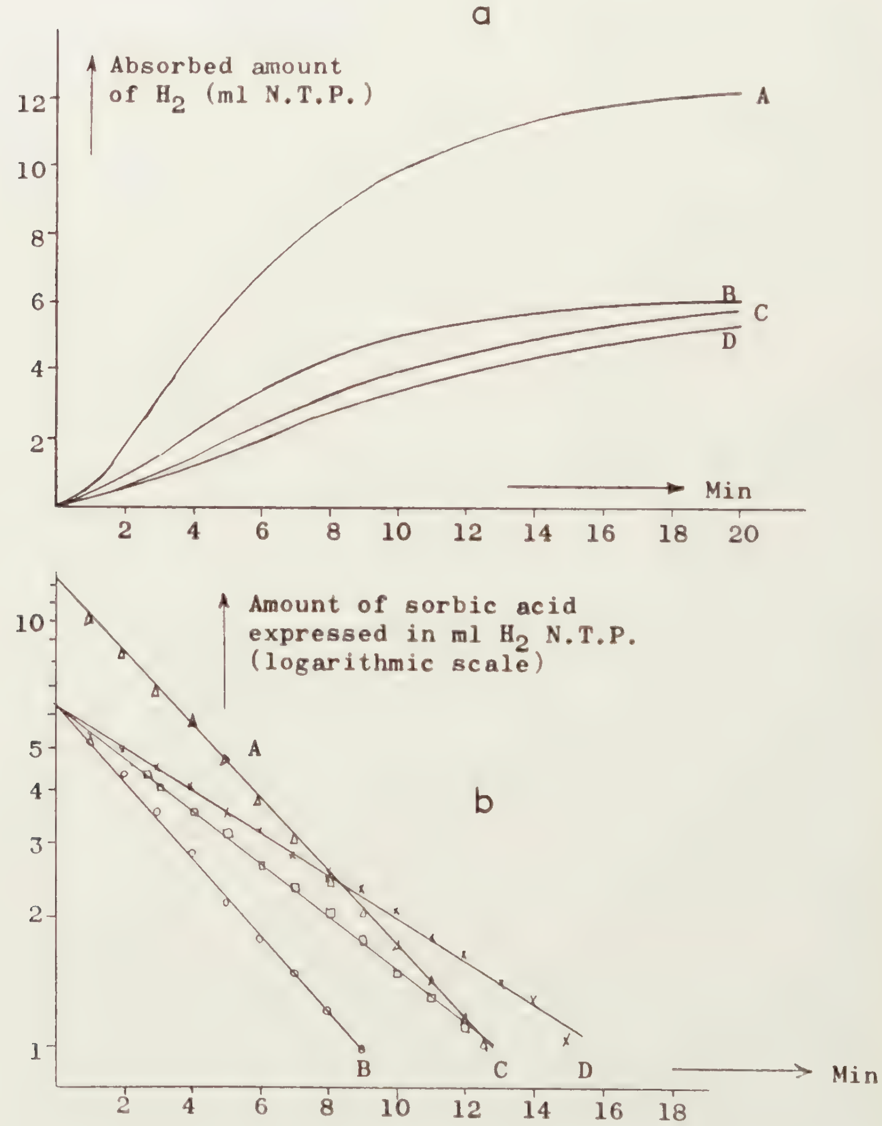

Figs. 1*a*, *b*. Reaction between sorbic acid and hydrogenated pentacyanocobaltate (II) in hydrogen atmosphere. For all reactions: $CoCl_2$ 6.14 mmole; KCN 34.9 mmole; KCl 17.2 mmole; Volume 78 ml; temperature 25° C; H_2 pressure 735 mm Hg. Initial amount of sorbate: A, 0.562 mmole, corr. to 12.54 ml H_2 N.T.P., B, C and D, 0.281 mmole, corr. to 6.27 ml H_2 N.T.P. Ageing time: A and B, 0 h; C, 3 h; D, 41 h.

For the amount of free sorbic acid to be calculated the hydrogen absorption had to be corrected for the non-hydrogenated cobalt complex which is formed back according to (1) during the reaction.

The dependence of the reaction rate on the concentration of the hydrogenated complex could be established, although less accurate, from hydrogen absorption measurements. From experiments with varying concentrations of Co complex, values of the second order rate constant were calculated based on the reaction being of 1st order both in sorbate and in cobalt. The results shown in Table 1 indicate a somewhat higher order, namely 1.1, in the cobalt complex.

In view, however, of the relatively large experimental errors which are possible with low cobalt concentrations, a pure 1st order with respect to cobalt would appear to be most probable.

TABLE 1

Reaction between sorbic acid and hydrogenated Co-complex (2 N NaOH; 1 M KCN; temp. 25.0° C)

Sorbic acid 10^{-3} mole/l	Hydrogenated Co-complex 10^{-3} mole/l *)	Rate (dH_2/dt) 10^{-3} mole/l. min	Rate constant k **) l/mole. min
5.45	29.4	0.665	4.1
5.57	18.4	0.427	4.2
5.73	11.7	0.270	4.1
5.64	5.93	0.122	3.6
6.13	2.88	0.056	3.2

*) Calculated for mono-nuclear Co-complex.

**) The influence of the Co-concentration upon the rate constant, due to variation of the ionic strength, has been neglected because of the high value of the latter.

In order, however, to hydrogenate sorbic acid in a solution of potassium cyanide and cobalt chloride, the presence of molecular hydrogen was not necessarily required. Even in the case of a solution of sorbate and pentacyanocobaltate(II), prepared in and stored under nitrogen, the sorbic acid had completely converted into 2-hexenoic acid after two days. The infra-red spectra of the reaction products of the solutions stored under nitrogen and those treated with hydrogen, were completely identical.

Kinetic measurements were also made of the hydrogenation of sorbic acid in a Co-complex solution aged under nitrogen. The conditions of temperature, and concentrations of Co, KCN, and sorbic acid under which these experiments were carried out were otherwise identical with those using hydrogenated freshly prepared solutions. Such aged cobalt-complex solutions absorbed only a few percents of the theoretically possible amount of hydrogen.

After the addition of sodium sorbate the hydrogen absorption was measured as a function of time. Here again, an amount of hydrogen

equivalent to the sorbic acid was absorbed (Fig. 1a, curve C and D).

The results of the experiments with hydrogenated, fresh and aged solutions, are summarized in Table 2.

TABLE 2

Effect of ageing on the rate of sorbic acid hydrogenation (conditions as in Fig. 1)

Exp.	Ageing time of Co-complex solutions (h)	H_2 absorption by Co-complex (% of theory)	CoH, calculated amount of hydrogenated Co-complex (% of theory)	Apparent first order rate constant $k(min^{-1})$	$\frac{k}{CoH}$
A	0	77.6	84.3	0.20	0.24
B	0	77.6	84.3	0.21	0.25
E	0	78.5	84.7	0.22	0.26
C	3	30.8	62.0	0.14	0.23
F	16	8.5	51.3	0.11	0.21
D	41	3.7	49.6	0.12	0.23

Discussion

It appears from Table 2 that despite the strongly reduced amount of hydrogen absorbed by the aged complex, the apparent first order rate constant for the hydrogenation of sorbic acid is not less than 50 % of that for a hydrogenated fresh solution. This fact, together with the striking agreement in selective hydrogenation of sorbic acid by non-hydrogenated, aged and hydrogenated, fresh solutions of the Co-complex, strongly indicate that the same active molecules are present in both solutions.

The simplest explanation of this phenomenon seems to be a disproportionation of the pentacyanocobaltate(II)-ion during ageing, hydrogenation and disproportionation being represented by the following overall reaction schemes:

(3) Hydrogenation: $2[Co(CN)_5H_2O]^{3-} + H_2 \rightleftarrows 2[Co(CN)_5H]^{3-} + 2H_2O$

(4) Disproportionation:

$$2[Co(CN)_5H_2O]^{3-} \rightarrow [Co(CN)_5H]^{3-} + [Co(CN)_5OH]^{3-} + H_2O.$$

The concentrations of the active Co-complex in the hydrogenated, fresh and aged solutions were calculated in accordance with the stoechiometry of this disproportionation [1]) (see Table 2). These calculated values are, in good approximation, proportional to the corresponding apparent first order rate constants observed.

[1]) A minor amount of non-hydrogenated Co(II)-complex in equilibrium with its hydrogenated form according to (3) was taken into account, their ratio being about 0.11 at 25° C. Results of the investigation into this equilibrium reaction will be published in due course.

The observations of MILLS *et al.* [6], namely, that in fresh and aged pentacyanocobaltate(II) solutions, the D_2-H_2O exchange proceeds at rates of the same order of magnitude, are also in agreement with this explanation. In a recent publication, GRIFFITH and WILKINSON [8] also concluded from the close agreement between the U.V. spectra of aged and hydrogenated fresh solutions, that a disproportionation of the Co-complex occurred during the ageing process.

Experimental part

The kinetic experiments were carried out in a 85 ml glass reaction vessel, fitted with an efficient vibration stirrer, and connected to a gas burette.

The vessel and burette were surrounded by a mantle through which liquid flowed from a thermostat ($\pm$ 0.01° C). The dead space of the system was ca. 10 ml.

The required amount of cobalt chloride solution was introduced in the reaction vessel and saturated with oxygen-free hydrogen or nitrogen. Other oxygen-free, hydrogen- or nitrogen-saturated solutions of potassium cyanide, sodium hydroxide and sodium sorbate were pressed into the reaction vessel. Each of these operations was completed in ca. 10 sec. After the addition of the KCN solution, the hydrogen absorption was measured as a function of time. The pressure in the system was automatically kept constant. Subsequently sodium sorbate was added to the hydrogen-saturated solution of the cobalt complex and the absorption of hydrogen measured as a function of time.

The amount of hydrogenated sorbic acid present at any given time could be calculated as the sum of the corresponding amount of absorbed hydrogen and the amount of non-hydrogenated Co-complex—equivalent to H_2—which had formed back at that moment. This followed from comparison of the hydrogenation curve thus obtained with the curve for a Co-complex solution without sorbate, under otherwise identical conditions (sodium valerate instead of sodium sorbate).

Points, on these curves, of equal H_2 absorption rate (dH_2/dt) correspond with solutions of the same amount of non-hydrogenated Co-complex.

Summary

Aqueous solutions of the pentacyanocobaltate(II)-ion both hydrogenated and stored under nitrogen are able to hydrogenate 2,4-hexadienoic acid (sorbic acid) quantitatively and selectively to 2-hexenoic acid. This reaction between sorbic acid and hydrogenated cobalt complex is first order in both reactants. In spite of the strong decrease of hydrogen absorption after storing the solution of the cobalt complex under nitrogen (ageing), the subsequent hydrogenation of sorbic acid proceeds with a rate of the same order of magnitude as with hydrogenated fresh solutions.

It is suggested that in both aged and hydrogenated freshly prepared solutions of the pentacyanocobaltate(II)-ion identical molecules containing activated hydrogen are present. The overall ageing process is most likely represented by a disproportionation of the pentacyanocobaltate(II)-ion into its hydrogenated form and a cobalt(III) complex.

Acknowledgement. The author wishes to express his thanks to the Management of Unilever N.V., Rotterdam for their kind permission to publish this paper.

Unilever Research Laboratory,
Vlaardingen, The Netherlands

REFERENCES

1. Hume, D. N. and I. M. Kolthoff, J. Am. Chem. Soc. **71**, 867 (1949).
2. Adamson, A. W., J. Am. Chem. Soc. **73**, 5710 (1951).
3. Iguchi, M., J. Chem. Soc. Japan **63**, 634 (1942). Chem. Abstr. **41**, 2975 (1947).
4. Bayston, J., N. K. King and M. E. Winfield, Adv. in Catalysis **9**, 312 (1957).
5. King, N. K. and M. E. Winfield, J. Am. Chem. Soc. **80**, 2060 (1958).
6. Mills, G. A., S. Weller and A. Wheeler, J. Phys. Chem. **63**, 403 (1959).
7. Jonge, A. de, unpublished results.
8. Griffith, W. P. and G. Wilkinson, J. Chem. Soc. **1959**, 2757.

PALEONTOLOGY

MICROFAUNA AND AGE OF THE BASSES PLAINES FORMATION OF FRENCH GUYANA. I

BY

C. W. DROOGER

(Communicated by Prof. G. H. R. VON KOENIGSWALD at the meeting of May 28, 1960)

ABSTRACT

A Paleocene age is concluded for the recently discovered sediments of the Basses Plaines formation. This age assignment is supported with more or less weight by the three groups of the microfauna. Especially the rotaliid Foraminifera appear to be very important. The fauna points to a very shallow marine environment with imperfect back-reef conditions, with but slight deposition of material from the hinterland and possibly with occasional salinity fluctuations.

INTRODUCTION

In between the Quaternary deposits and the basement complex of northwestern French Guyana, near Mana, a number of wells encountered a hitherto unknown series of 10 to 45 metres of marls and limestones, the Basses Plaines formation. Several details of the character of the sediments and a general account of the microfauna were communicated by CRUYS (1959).

A number of selected samples, coming from three of the borings (DROOGER, 1960, p. 288), were sent to Utrecht for a detailed microfaunal analysis:

XF–TP, samples at depths of 28, 34, and 34.50 m,

XF–15, at depths of 61.50, 62, 62.50, 67.50 and 86.75 m, and

XF–16, at depths of 81–82, 86.40, 90, and 97 m.

The director of the Bureau Minier Guyanais (Paris) kindly authorized us to publish the details, on which a report had been given in 1958.

The fauna consists of numerous Foraminifera and Ostracoda together with undeterminable macrofaunal elements, mainly oyster fragments and echinoid spines. The rotaliid Foraminifera have been the subject of a separate paper (DROOGER, 1960).

Two of the investigated samples were poor in microfossils. XF–15, 86.75 m mainly contains angular quartz in the wash residues; XF–16, 97 m predominantly consisted of hard rock. Thin sections of the latter show many fragments of molluscs and a few Foraminifera and Ostracoda. The fauna of the other samples is fairly homogeneous. Minor differences in presence or absence of some of the species distinguish certain samples or even wells, but they are probably only due to slight variations of an

otherwise uniform environment. Local transports of faunal elements have occurred, but there is no reason to assume large-scale reworking from older deposits.

AGE

Evaluating the microfauna, the rotaliid Foraminifera have to be given prevalence for age determination, as they are better characterized and have been studied in more detail.

The genus *Ranikothalia* is restricted to the Paleocene-Early Eocene of central America and southern Asia. Our species *R. soldadensis* is known from Paleocene beds in Trinidad, Barbados, Venezuela and Georgia. *Lockhartia* of the Paleocene-Early Eocene was so far unknown from America. The species *L. haimei* is known from the Paleocene Ranikot beds of India and from the lower part of the Paleocene series of Qatar. *Smoutina cruysi* is thought to be a descendent of the Late Cretaceous *S. bermudezi* of Cuba. The genus is closely related to *Kathina* from the Paleocene of Qatar. *Storrsella haastersi* has been described from the Paleocene-Lower Eocene series of Guatemala and British Honduras. *Rotalia hensoni* is again known from the Paleocene beds of Qatar. The striking resemblance of Paleocene faunas of the Caribbean to those of southern Asia is thus once more confirmed.

The remainder of the foraminiferal fauna shows great affinity with Paleocene American associations, such as those of the Paleocene-Lower Eocene series of Guatemala and British Honduras, and of the Madruga formation of Cuba; as for the latter especially by the presence of the genus *Boldia*, which genus again seems to be restricted to the Paleocene and possibly the Early Eocene. There is much relationship with faunas of deposits of Midway age of the southern United States, of formations such as Aquia, Salt Mountain, Naheola, Porters Creek, Clayton, etc. (see the stratigraphic review of LOEBLICH and TAPPAN, based on planktonic Foraminifera). Species formerly known only from Cretaceous deposits seem to be absent, but there are some more distinct Eocene affinities. *Asterigerina texana* is known from several Middle Eocene deposits of the United States, though it has been mentioned from the older deposits of Guatemala and British Honduras. Finally both *Valvulina* species have originally been described from Eocene deposits of the Paris basin.

The Ostracoda are less valuable for age determination, because of the less well-defined specific limits and since part of our determinations are certainly debatable. The assemblage again shows a good many affinities with those of Paleocene-Eocene age of the United States. There is remarkable agreement with the Paleocene fauna described from Soldado Rock and the Guasare formation of Venezuela, but it must be kept in mind that there are but few other important references in the adjoining areas.

With more or less weight all three parts of the microfauna point to a Paleocene age of the Basses Plaines formation of Guyana.

ENVIRONMENT

It is difficult to draw conclusions about the environment of a Paleocene fauna, so far back from recent associations. The assemblages of relatively few species and often many individuals indicate special marine conditions. The dominance of species of *Rotalia* and related genera (*Lockhartia*, *Storrsella*, *Smoutina*, and even *Ranikothalia*) fits in with an environment of very shallow water, in which slight salinity fluctuations may have occurred. This assumption is supported by the absence of Discocyclinidae or other contemporaneous orbitoidal Foraminifera, which probably preferred more open marine conditions. Similar conclusions may be drawn from the absence of planktonic Foraminifera and the abundance of oyster remains. Algal life probably flourished, considering the relative abundance of Ostracoda, and of *Discorbis* and Anomalinidae among the smaller Foraminifera.

Summarizing it follows that the sediments of the Basses Plaines formation have been deposited under not too rigorous back-reef conditions with occasional invasions of river water coming from an adjacent hinterland with slight erosion.

Local transport in this sedimentation area can account for the sorting of the fossils in XF–15, 61.50 m and 62.50 m. In the upper sample most individuals of *Ranikothalia soldadensis* and *Lockhartia haimei* are big, whereas at 62.50 m they are always small, though accompanied by numerous fragments of large individuals, which fragments do not exceed the weight of the small, complete specimens.

SYSTEMATIC DESCRIPTION

The determinations of the smaller Foraminifera and the Ostracoda have mainly been based on American literature. For the order of discussion of the species we mainly followed the classification of SIGAL (1952) for the Foraminifera, and that of POKORNÝ (1958) for the Ostracoda.

FORAMINIFERA

Valvulina triangularis D'ORBIGNY

Pl. 1, fig. 1

Valvulina triangularis D'ORBIGNY, 1826, Ann. Sci. Nat., vol. 7, p. 270, no. 1; CUSHMAN, 1937, Cushm. Lab. Foram. Res., Sp. Publ. 8, p. 5, pl. 1, fig. 8–10.

Remarks. Our specimens are somewhat smaller than the typical, hardly attaining a length of 1 mm. Among the bigger ones some are too elongated.

Age. Originally described from the Eocene of the Paris basin. No similar species are known from the American Early Tertiary.

Valvulina pupa D'ORBIGNY

Pl. 1, fig. 2

Valvulina pupa D'ORBIGNY, 1826, Ann. Sci. Nat., vol. 7, p. 270, no. 2; CUSHMAN, 1937, Cushm. Lab. Foram. Res., Sp. Publ. 8, p. 6, pl. 1, fig. 11–13.

Remarks. There is little doubt about the assignment of our few specimens to this European species. *V. germeraadi* VAN DEN BOLD (1946, p. 122, pl. 18, fig. 1) from the Lower Eocene of Guatemala and British Honduras is hardly different. The original material of the latter species shows that the rounded part of the test is commonly much longer – three quarters to nine tenths of the total length – than it is seen in the type figure. Also *V. rugidia* CUSHMAN (1937, p. 7, pl. 1, fig. 16–18) from the Eocene of the Paris basin belongs to this group, being more coarsely arenaceous.

Age. Originally described from the Eocene of the Paris basin.

Quinqueloculina spp.

Remarks. The ill-preserved specimens do not allow more than a generic determination.

Guttulina problema D'ORBIGNY

Guttulina problema D'ORBIGNY, 1826, Ann. Sci. Nat., vol. 7, p. 266, no. 14; CUSHMAN and OZAWA, 1930, Proc. U.S. Nat. Mus., vol. 77, art. 6, p. 19, pl. 2, fig. 1–6, pl. 3, fig. 1.

Remarks. Our few big specimens also show affinities with *G. hantkeni* CUSHMAN and OZAWA, and with *G. jarvisi* CUSHMAN and OZAWA.

Age. The species is considered to range from the Cretaceous to recent.

Discorbis midwayensis CUSHMAN

Pl. 1, fig. 3

Discorbis midwayensis CUSHMAN, 1940, Contrib. Cushm. Lab. Foram. Res., vol. 16, p. 70, pl. 12, fig. 6; CUSHMAN, 1951, U.S. Geol. Surv., Prof. Paper 232, p. 48, pl. 13, fig. 20.

Remarks. Our few specimens commonly show better resemblance with *D. midwayensis* var. *soldadoensis* CUSHMAN and RENZ (1942, Contrib. Cushm. Lab. Foram. Res., vol. 18, p. 10, pl. 3, fig. 4) than with the type of the species.

Age. The species and its variety have been described from the Midway of Alabama, and from Paleocene beds of Soldado Rock, respectively.

Siphonina prima PLUMMER

Pl. 1, fig. 4

Siphonina prima PLUMMER, 1926, Texas Univ. Bull. 2644, p. 148, pl. 12, fig. 4.

Remarks. It is thought that our specimens differ from the type (though its figures are poor) by the greater size (up to 0.38 mm), by the ventral side which is often more convex than the dorsal side, and by the slight, but distinct apertural lip of several individuals. Moreover, bigger specimens have relatively greater chambers. Especially the latter individuals resemble *S. elegans* BROTZEN (1948, p. 107, pl. 17, fig. 4). Affinities seem to be present also with *S. wilcoxensis* CUSHMAN from the Wilcox of Alabama, the ventral sutures of which are straighter. BROTZEN remarked that several species of the Cretaceous-Eocene are probably no more than varieties of a single species. We chose the oldest name that corresponds to the central type of the group.

Age. Although described from the Midway of Texas, the range is known to be from the Cretaceous (Navarro) to the Earely Eocene (Wilcox) of central America. *S. elegans* was described from Paleocene beds (Seelandian) of southern Sweden.

Anomalinoides cf. **danica** (BROTZEN)

Pl. 1, fig. 5

Cf. *Cibicides danica* BROTZEN, 1942, Sver. Geol. Unders., ser. C, no. 435, p. 31, textfig. 7:2.

Anomalinoides danica (Brotzen), BROTZEN, 1948, Sver. Geol. Unders., ser. C, no. 493, p. 87, pl. 14, fig. 1, textfig. 22.

Remarks. Our few specimens clearly belong to the group around *A. danica*, which group includes *A. grosserugosa* (GÜMBEL), *A. granosa* (HANTKEN) and *A. vanbelleni* TEN DAM and SIGAL. Probably *Anomalina cubana* CUSHMAN and BERMUDEZ, and *A. madrugaensis* CUSHMAN and BERMUDEZ (1948, Contrib. Cushm. Lab. Foram. Res., vol. 24, p. 86, pl. 15, fig. 7–9, and fig. 4–6, respectively) from the Madruga formation of Cuba must also be placed in this group. Our individuals are distinctly evolute on the dorsal side, approaching the type of *Gavelinella lellingensis* BROTZEN (1948, p. 75, pl. 11, fig. 1, 2, textfig. 20).

Age. The entire group occurs in the Late Cretaceous to Eocene.

Anomalinoides midwayensis (PLUMMER)

Pl. 1, fig. 6, 7

Truncatulina midwayensis PLUMMER, 1926, Texas Univ. Bull. 2644, p. 141, pl. 9, fig. 7, pl. 15, fig. 3.

Anomalina midwayensis (Plummer), CUSHMAN, 1951, U.S. Geol. Surv., Prof. Paper 232, p. 62, pl. 17, fig. 17–19.

Anomalinoides midwayensis (Plummer), BROTZEN, 1948, Sver. Geol. Unders., ser. C, no. 493, p. 88, pl. 14, fig. 2, 3.

Remarks. Typical individuals in our material are small, up to 0.4 mm. They are not separable from the greater (up to 0.55 mm), more frequent and more distinct representatives of the variety *A. midwayensis* var. *trochoidea*

(Plummer) (*Truncatulina midwayensis* Plummer var. *trochoidea* Plummer, 1926, Texas Univ. Bull. 2644, p. 142, pl. 9, fig. 8).

Age. Both the species and the variety have been described from the Midway of Texas. They are widely distributed in Paleocene sediments of America, but also in Europe and other areas.

Cibicides browni Kline

Pl. 1, fig. 8

Cibicides browni Kline, 1943, Miss. Geol. Surv., Bull. 53, p. 62, pl. 7, fig. 18–20; Cushman, 1951, U.S. Geol. Surv., Prof. Paper 232, p. 67, pl. 20, fig. 6–8.

Remarks. The few individuals of this general *Cibicides* type resemble the original fairly well. They have five or six chambers in the final coil.

Age. The species was described from the Clayton formation of Mississippi. It is also known from other Paleocene deposits of the United States.

Boldia carinata Cushman and Bermudez

Pl. 1, fig. 9–13

Boldia carinata Cushman and Bermudez, 1948, Contrib. Cushm. Lab. Foram. Res., vol. 24, p. 75, pl. 11, fig. 11–13.

Remarks. This is the most common species among the smaller Foraminifera. Small specimens are more or less *Cibicides*-like. They often

Plate 1

For all figures, except 1 and 2: *a* = ventral view, *b* = dorsal view, *c* = peripheral view.

Figs. 1*a*, *b*. *Valvulina triangularis* d'Orbigny. *a* = side view, *b* = apertural view. XF-TP, 28 m. × 25.
,, 2*a*, *b*. *Valvulina pupa* d'Orbigny. *a* = side view, *b* = apertural view. XF-TP, 28 m. × 25.
,, 3*a*, *b*. *Discorbis midwayensis* Cushman var. *soldadoensis* Cushman and Renz. XF-TP, 34 m. × 40.
,, 4*a*–*c*. *Siphonina prima* Plummer. XF-16, 90 m. × 40.
,, 5*a*–*c*. *Anomalinoides* cf. *danica* (Brotzen). XF-TP, 34 m. × 40.
,, 6*a*–*c*. *Anomalinoides midwayensis* (Plummer). XF-TP, 34 m. × 50.
,, 7*a*–*c*. *Anomalinoides midwayensis* (Plummer) var. *trochoidea* (Plummer). XF-15, 67.50 m. × 50.
,, 8*a*–*c*. *Cibicides browni* Kline. XF-15, 62 m. × 50.
,, 9*a*–*c*. *Boldia carinata* Cushman and Bermudez, juvenile specimen. XF-16, 90 m. × 40.
,, 10*a*–*c*. *Boldia carinata* Cushman and Bermudez, adult specimen. XF-15, 61.50 m. × 40.
,, 11*a*–*c*. *Boldia carinata* Cushman and Bermudez var. 1. XF-TP, 28 m. × 40.
,, 12*a*–*c*. *Boldia carinata* Cushman and Bermudez var. 2. XF-16, 86.40 m. × 40.
,, 13*a*–*c*. *Boldia carinata* Cushman and Bermudez var. 2. XF-TP, 28 m. × 40.
,, 14*a*–*c*. *Asterigerina texana* (Stadnichenko). XF-TP, 34 m. × 25.

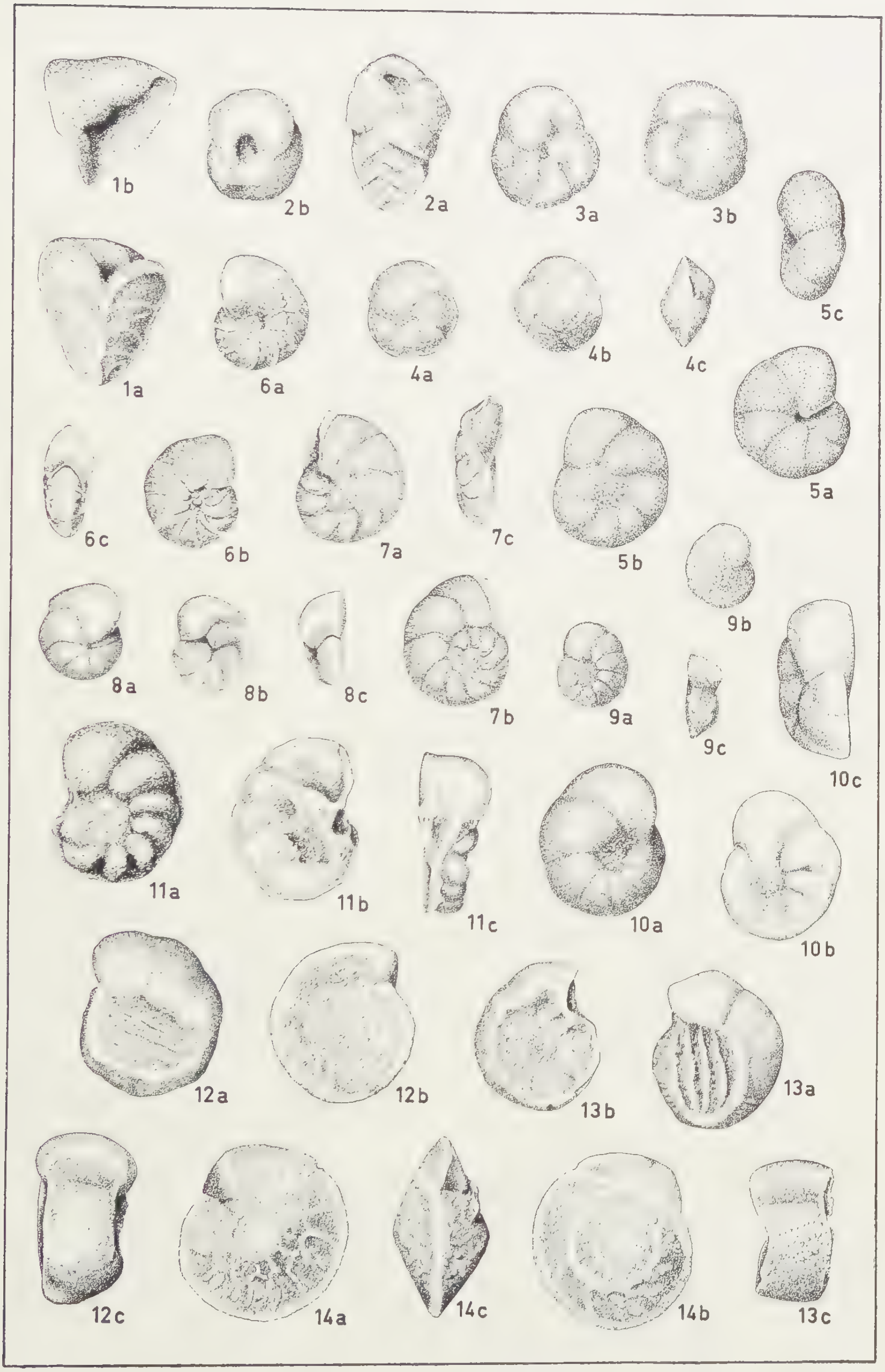
1b
2b
2a
3a
3b
5c
1a
6a
4a
4b
4c
5a
6c
6b
7a
7c
5b
9b
8a
8b
8c
7b
9a
9c
10c
11a
11b
11c
10a
10b
12a
12b
13b
13a
12c
14a
14c
14b
13c

Plate I

resemble *C. blanpiedi* TOULMIN, as figured by CUSHMAN (1951, pl. 20, fig. 3–5, not fig. 1, 2). Among the bigger individuals, those closely agreeing with the type of *B. carinata*, are most frequent. Even the size of about 0.5 mm is comparable.

Especially in sample XF–TP, 28 m, big variants, up to 0.65 mm, are different by the strong dorsal keel and the thickened, inflated median parts of the ventral chamber walls with deeply depressed sutures in between. The ventral spiral is fairly evolute, showing the irregular ornamentation of the previous coils (*B. carinata* var. 1).

Yet another variant of great size (*B. carinata* var. 2) is found. It is characterized by a completely truncated periphery and a costate ornamentation of the ventral side. The ridges are parallel, but independent of the position of the final chamber. This suggests that they are an accomodation to similarly striated surfaces, to which the animals adhered. Echinoid spines with an identical striated pattern are frequent.

Age. All American species of *Boldia* occur in Paleocene and possibly Early Eocene deposits. *B. carinata* was described from the Madruga formation (Paleocene) of Cuba.

Asterigerina texana (STADNICHENKO)

Pl. 1, fig. 14

Eponides texana STADNICHENKO, 1927, Jour. Pal., vol. 1, p. 232, pl. 38, fig. 1–5.
Asterigerina texana (Stadnichenko), CUSHMAN and THOMAS, 1929, Jour. Pal., vol. 3, p. 181, pl. 24, fig. 5; VAN DEN BOLD, 1946, p. 124, pl. 18, fig. 5; BANDY, 1949, Bull. Am. Pal., vol. 32, no. 131, p. 117, pl. 22, fig. 3.

Remarks. The individuals are biconvex. In immature ones the ventral side is most convex. Umbilical granules and raised ventral sutures are frequent elements of the ornamentation. The dorsal side often shows granules mainly on the central part and a raised spiral suture. Usually the chambers are hardly visible. Their number in the final whorl increases from eight to thirteen, the latter number observed in an individual of 0.95 mm diameter. This maximal number is somewhat greater than it is in the individuals of the North American Eocene, including the closely comparable *A. lisbonensis* CUSHMAN and TODD (1945, Contrib. Cushm.

PLATE 2

For all figures, except 12: *a* = ventral view, *b* = dorsal view, *c* = peripheral view.

Figs. 1*a*–*c*. *Rotalia hensoni* SMOUT. XF-16, 86.40 m. × 25.
,, 2*a*–*c*. *Rotalia* cf. *sigali* DROOGER. XF-15, 67.50 m. × 80.
,, 3*a*–*c*. *Storrsella haastersi* (VAN DEN BOLD). XF-TP, 34 m. × 40.
,, 4*a*–6*c*. *Lockhartia haimei* (DAVIES). XF-15, 62.50 m. × 20.
,, 7*a*–*c*. *Smoutina cruysi* DROOGER. XF-15, 62.50 m. × 20.
,, 8*a*–*c*. *Smoutina cruysi* DROOGER. XF-16, 90 m. × 20.
,, 9–12*b*. *Ranikothalia soldadensis* (VAUGHAN and COLE). 9, 10, 11, 12*a*, side views; 12*b* = peripheral view. XF-15, 62 m. × 10.

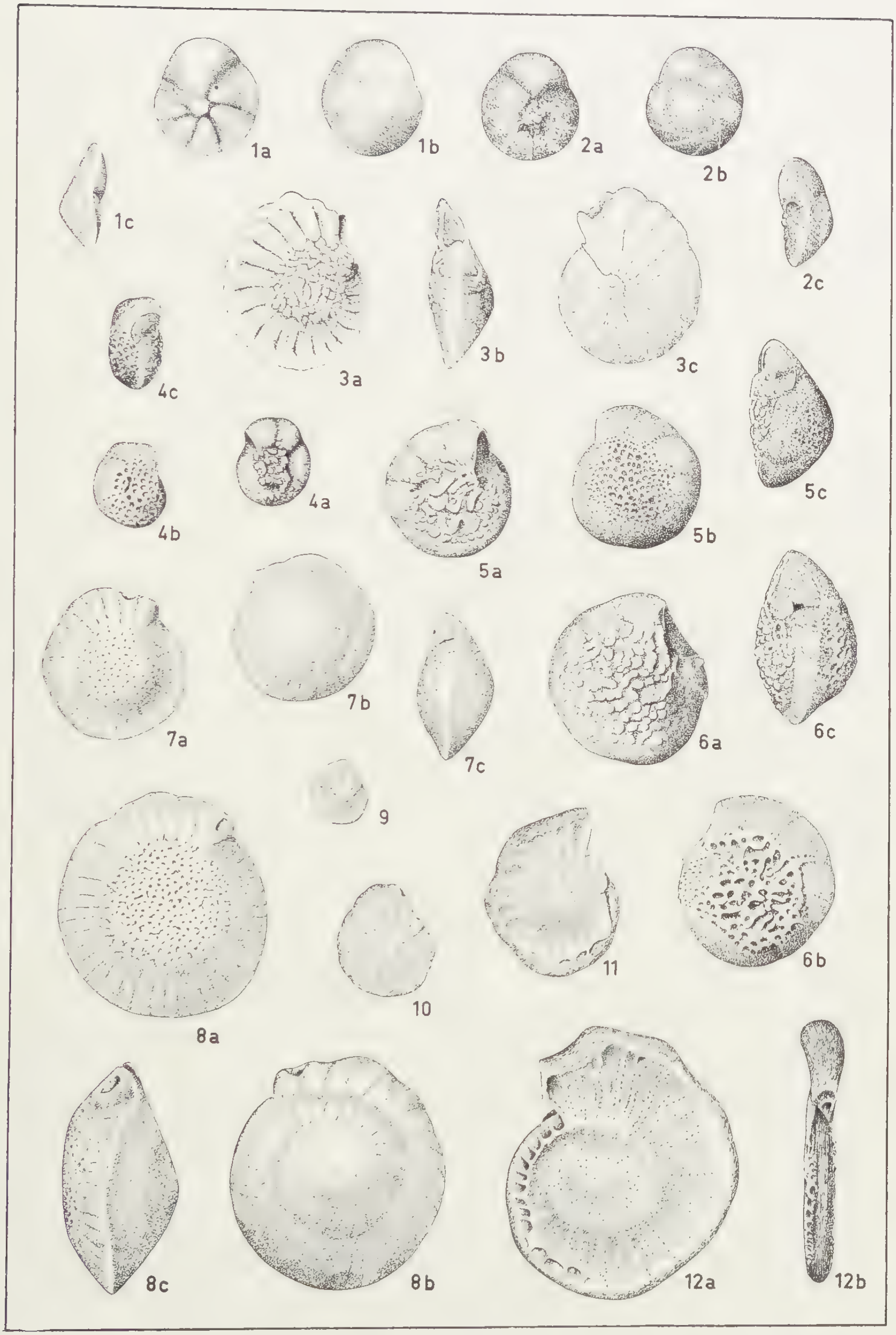
1a
1b
2a
2b
1c
2c
3a
3b
3c
4c
4a
4b
5a
5b
5c
7a
7b
7c
6a
6c
9
8a
10
11
6b
8c
8b
12a
12b

PLATE II

Lab. Foram. Res., vol. 21, p. 19, pl. 4, fig. 15–18) and *A. tatumi* HUSSEY (1951, Contrib. Cushm. Found. Foram. Res., vol. 2, p. 19, pl. 3, fig. 1–3), both from the Claiborne Eocene. Also *A. texana* from the Paleocene-Lower Eocene series of Guatemala and British Honduras seems to have more chambers in the final coil.

Age. The species is mainly known from the Gulf Coast Middle Eocene.

Rotalia hensoni SMOUT

Pl. 2, fig. 1

Rotalia hensoni SMOUT, 1954, p. 45, pl. 15, fig. 8; DROOGER, 1960, Proc. Kon. Ned. Ak. Wetensch., ser. B, vol. 63, p. 291, pl. 1, fig. 1–6.

Remarks. Our specimens closely resemble the figures of the type of this species.

Age. Originally described from zone 2 of the Paleocene series of Qatar.

Rotalia cf. **sigali** DROOGER

Pl. 2, fig. 2

Cf. *Rotalia sigali* DROOGER, 1952, Contrib. Cushm. Found. Foram. Res., vol. 3, p. 99, pl. 15, fig. 36, 37.

Rotalia cf. *sigali* Drooger, DROOGER, 1960, Proc. Kon. Ned. Ak. Wetensch., ser. B, vol. 63, p. 292, pl. 1, fig. 7.

Remarks. The very small size of our specimens, up to 0.25 mm, did not allow a good comparison with the original material of this African species.

Age. R. sigali was originally described from Cretaceous-Tertiary transitional strata of Algeria.

Storrsella haastersi (VAN DEN BOLD)

Pl. 2, fig. 3

Cibicides haastersi VAN DEN BOLD, 1946, p. 125, pl. 18, fig. 9.

Storrsella haastersi (Van den Bold), DROOGER, 1960, Proc. Kon. Ned. Ak. Wetensch., ser. B, vol. 63, p. 296, pl. 1, fig. 10, pl. 2, fig. 1–13.

Remarks. Our individuals fairly well resemble those of VAN DEN BOLD's collection.

Age. Originally described from the Paleocene-Lower Eocene series of Guatemala and British Honduras.

Lockhartia haimei (DAVIES)

Pl. 2, fig. 4–6

Dictyoconoides haimei DAVIES, 1927, Quart. Jour. Geol. Soc., vol. 83, p. 280, pl. 21, fig. 13–15.

Lockhartia haimei (Davies), SMOUT, 1954, p. 49, pl. 2, fig. 1–14; DROOGER, 1960, Proc. Kon. Ned. Ak. Wetensch., ser. B, vol. 63, p. 302, pl. 3, fig. 1–10.

Remarks. The features of our assemblages best resemble those of the variable populations of *L. haimei*, *L. diversa* SMOUT, and *L. prehaimei* SMOUT, described from zone 2 of the Paleocene series of Qatar.

Age. *L. haimei* is known from Paleocene beds of India, Qatar and other areas of southern Asia.

Smoutina cruysi DROOGER

Pl. 2, fig. 7, 8

Smoutina cruysi DROOGER, 1960, Proc. Kon. Ned. Ak. Wetensch., ser. B, vol. 63, p. 307, pl. 4, fig. 1–13.

Remarks. This species probably is a descendent of "*Lockhartia*" *bermudezi* COLE (1942, Jour. Pal., vol. 16, p. 641, pl. 92, fig. 1–5) from the Upper Cretaceous of Cuba.

Ranikothalia soldadensis (VAUGHAN and COLE)

Pl. 2, fig. 9–12

Miscellanea soldadensis VAUGHAN and COLE, 1941, Geol. Soc. Am., Sp. Paper 30, p. 36, pl. 4, fig. 8, 9; VAUGHAN, 1945, Geol. Soc. Am., Mem. 9, p. 30, pl. 5, fig. 2–5.
Ranikothalia soldadensis (Vaughan and Cole), CAUDRI, 1944, Bull. Am. Pal., vol. 28, no. 114, p. 23, pl. 4, fig. 19, pl. 5, fig. 24, 26; DROOGER, 1960, Proc. Kon. Ned. Ak. Wetensch., ser. B, vol. 63, p. 312, pl. 5, fig. 1–14.
Operculinoides georgianus COLE and HERRICK, 1953, Bull. Am. Pal., vol. 35, no. 148, p. 52, pl. 1, fig. 1–21, pl. 2, fig. 1–3.

Remarks. The individuals are characterized by their relative thinness, being identical with *R. soldadensis* and *R. georgiana*.

Age. The species is known from Paleocene deposits in Venezuela, Trinidad, Soldado Rock, Barbados and Georgia.

(To be continued)

MICROFAUNA AND AGE OF THE BASSES PLAINES FORMATION OF FRENCH GUYANA. II

BY

C. W. DROOGER

(Communicated by Prof. G. H. R. von Koenigswald at the meeting of May 28, 1960)

OSTRACODA

Cytherella guasarensis Van den Bold

Pl. 3, fig. 1, 2

Cytherella guasarensis Van den Bold, 1957, Micropal., vol. 3, p. 4, pl. 1, fig. 1.

Remarks. Our individuals of variable shape partly correspond well with Van den Bold's species. They resemble this species better than *C. tumidosa* Alexander (1934, Jour. Pal., vol. 8, p. 209, pl. 32, fig. 1, 2, 5, 6, pl. 35, fig. 3, 4). Some individuals show a depression near the centre of the valves (fig. 2), as it is shown in *C. excavata* Alexander (id., p. 211, pl. 32, fig. 3, 4, pl. 35, fig. 5, 6).

Age. Originally described from the Guasare formation (Paleocene) of Venezuela.

Platella kellettae Munsey

Pl. 3, fig. 3

Platella kellettae Munsey, 1953, Jour. Pal., vol. 27, p. 5, pl. 1, fig. 4; Van den Bold, 1957, Micropal., vol. 3, p. 4, pl. 1, fig. 2.

Remarks. Only some closed carapaces have been found.

Age. Originally described from the Coal Bluff formation (Paleocene) of the southern United States. Also known from the Paleocene deposits of Soldado Rock and from the Guasare formation.

Bairdoppilata magna (Alexander)

Pl. 3, fig. 4–6

Bairdia magna Alexander, 1927, Jour. Pal., vol. 1, p. 32, pl. 6, fig. 7, 8; Alexander, 1934, Jour. Pal., vol. 8, p. 215.

Remarks. The hinge typical for this genus was seen in only a few of the largest valves. Such great valves and carapaces of 1 to 1.15 mm are rare. Their outline is somewhat intermediate between that of *B. magna*

and that of *B. pondera* JENNINGS, as figured by SCHMIDT (1948, Jour. Pal., vol. 22, p. 408, pl. 61, fig. 21, 22). These specimens also resemble *Bairdia cespedecensis* VAN DEN BOLD (1957, Micropal., vol. 3, p. 6, pl. 2, fig. 5). Molts smaller than 1 mm are numerous and they show considerable variation without a clear separation of various groups being possible. The majority again resemble *B. magna*. The dorsal outline may have one or two obtuse angles, one in the middle and the other farther behind. Such individuals resemble *Bairdia soldadensis* VAN DEN BOLD (1957, p. 6, pl. 2, fig. 3) and *B.* aff. *hondurasensis* VAN DEN BOLD (id., fig. 4). The variation of relative height and width of these carapaces is considerable, especially if one compares the individuals of different samples. Some specimens of several molts are more elongate (*Bairdia* sp., pl. 3, fig. 7), somewhat resembling *B. dolicha* VAN DEN BOLD (id., p. 5, pl. 2, fig. 2). They may represent the only species in this group, distinct from *Bairdoppilata magna*.

Age. *B. magna* is known from Late Cretaceous and Paleocene deposits of the United States. The other types mentioned are mainly known from the Paleocene deposits of Soldado Rock and Venezuela.

Clithrocytheridea tombigbeensis (STEPHENSON)

Pl. 4, fig. 1, 2

Cytheridea (Clithrocytheridea) tombigbeensis STEPHENSON, 1938, Jour. Pal., vol. 12, p. 579, pl. 67, fig. 1, 2, textfig. 30, 31.
Clithrocytheridea tombigbeensis (Stephenson), SCHMIDT, 1948, Jour. Pal., vol. 22, p. 428, pl. 64, fig. 30, 31.

Remarks. Our specimens also show affinities with *Cytheridea* (*Clithrocytheridea*) *smithvillensis* STEPHENSON (1942, Jour. Pal., vol. 16, p. 113, pl. 18, fig. 2) from the Claiborne Eocene of Alabama. The valves are either smooth or they show a variable number of pores. There are many detached valves, but muscle scars are not clearly visible.

Age. Originally described from the Wilcox Eocene of Alabama. The species is also known from the Aquia formation (Late Paleocene) of the United States.

Krithe cf. **perattica** ALEXANDER

Pl. 4, fig. 3

Cf. *Krithe perattica* ALEXANDER, 1934, Jour. Pal., vol. 8, p. 229, pl. 34, fig. 1, 2.

Remarks. The seven specimens of XF–TP, 34.50 m, best resemble the male individual of ALEXANDER's figure 2. The dorsal outline is straight to slightly arched. The left valve overlaps the right one except at the posteroventral angle. Two detached valves show a wide anterior vestibule, the details of which are obscured by recrystallization. A left valve shows the simple hinge groove. Muscle scars are not visible. Some

closed carapaces of XF–TP, 28 m, have a more curved dorsal outline, but also the posterior end is more rounded, which makes the generic assignment still more doubtful.

Age. *K. perattica* has been originally described from the Wills Point formation of the Texan Midway.

Hermanites bassleri (Ulrich)

Pl. 3, fig. 8–13

Cythereis bassleri Ulrich, 1901, Maryland Geol. Surv., Eocene vol., p. 120, pl. 16, fig. 19–21.

Remarks. Our numerous individuals show several neighbouring types that are not clearly separable. Partly these types correspond with different molts, but they also show changes from one sample to the other. The literature on this group not being very clear, we chose the oldest name, though in all our individuals the vertical posterior ridge of typical *Cythereis bassleri* is nearly absent.

Type 1 has regularly inflated valves with distinct reticulation and distinct ridges. The ridges and subcentral swelling are clearly visible, but never prominent.

Plate 3

Figs. 1*a*, *b*. *Cytherella guasarensis* Van den Bold. *a* = side view left valve, *b* = dorsal view carapace. XF-15, 61.50 m. × 40.

,, 2*a*, *b*. *Cytherella guasarensis* Van den Bold. *a* = side view left valve, *b* = dorsal view carapace. XF-TP, 34.50 m. × 40.

,, 3*a*, *b*. *Platella kellettae* Munsey. *a* = side view left valve, *b* = dorsal view carapace. XF-16, 90 m. × 40.

,, 4*a*, *b*. *Bairdoppilata magna* (Alexander). *a* = side view right valve, *b* = dorsal view carapace. XF-15, 62.50 m. × 40.

,, 5. *Bairdoppilata magna* (Alexander), interior left valve. XF-TP, 34 m. × 25.

,, 6*a*, *b*. *Bairdoppilata magna* (Alexander). *a* = side view right valve, *b* = dorsal view carapace. XF-16, 86.40 m. × 40.

,, 7*a*, *b*. *Bairdia* sp. *a* = side view right valve, *b* = dorsal view carapace. XF-16, 86.40 m. × 40.

,, 8*a*, *b*. *Hermanites bassleri* (Ulrich) var. 1. *a* = side view left valve, *b* = dorsal view carapace. XF-TP, 28 m. × 40.

,, 9*a*, *b*. *Hermanites bassleri* (Ulrich) var. 2. *a* = side view left valve, *b* = dorsal view carapace. XF-TP, 28 m. × 40.

,, 10*a*, *b*. *Hermanites bassleri* (Ulrich) var. 3. *a* = side view left valve, *b* = dorsal view carapace. XF-15, 61.50 m. × 40.

,, 11*a*, *b*. *Hermanites bassleri* (Ulrich) var. 3. *a* = side view left valve, *b* = dorsal view carapace. XF-TP, 34 m. × 40.

,, 12*a*, *b*. *Hermanites bassleri* (Ulrich) var. 4. *a* = side view left valve, *b* = dorsal view carapace. XF-TP, 28 m. × 40.

,, 13. *Hermanites bassleri* (Ulrich) var. 3, interior right valve. XF-15, 86.75 m. × 40.

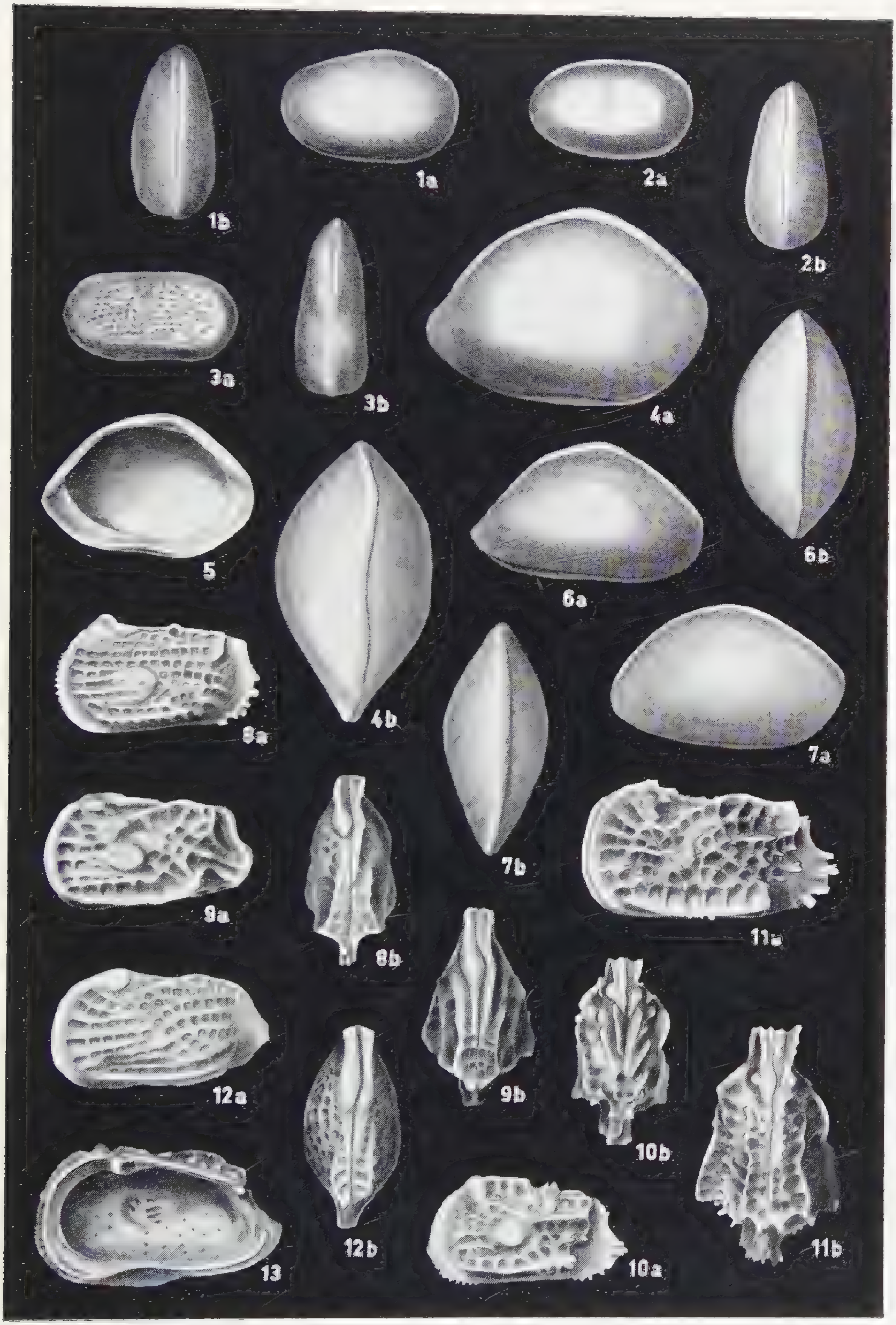
1b
1a
2a
2b
3a
3b
4a
5
6b
6a
8a
4b
7a
9a
8b
7b
11a
12a
9b
10b
12b
13
10a
11b

PLATE 3

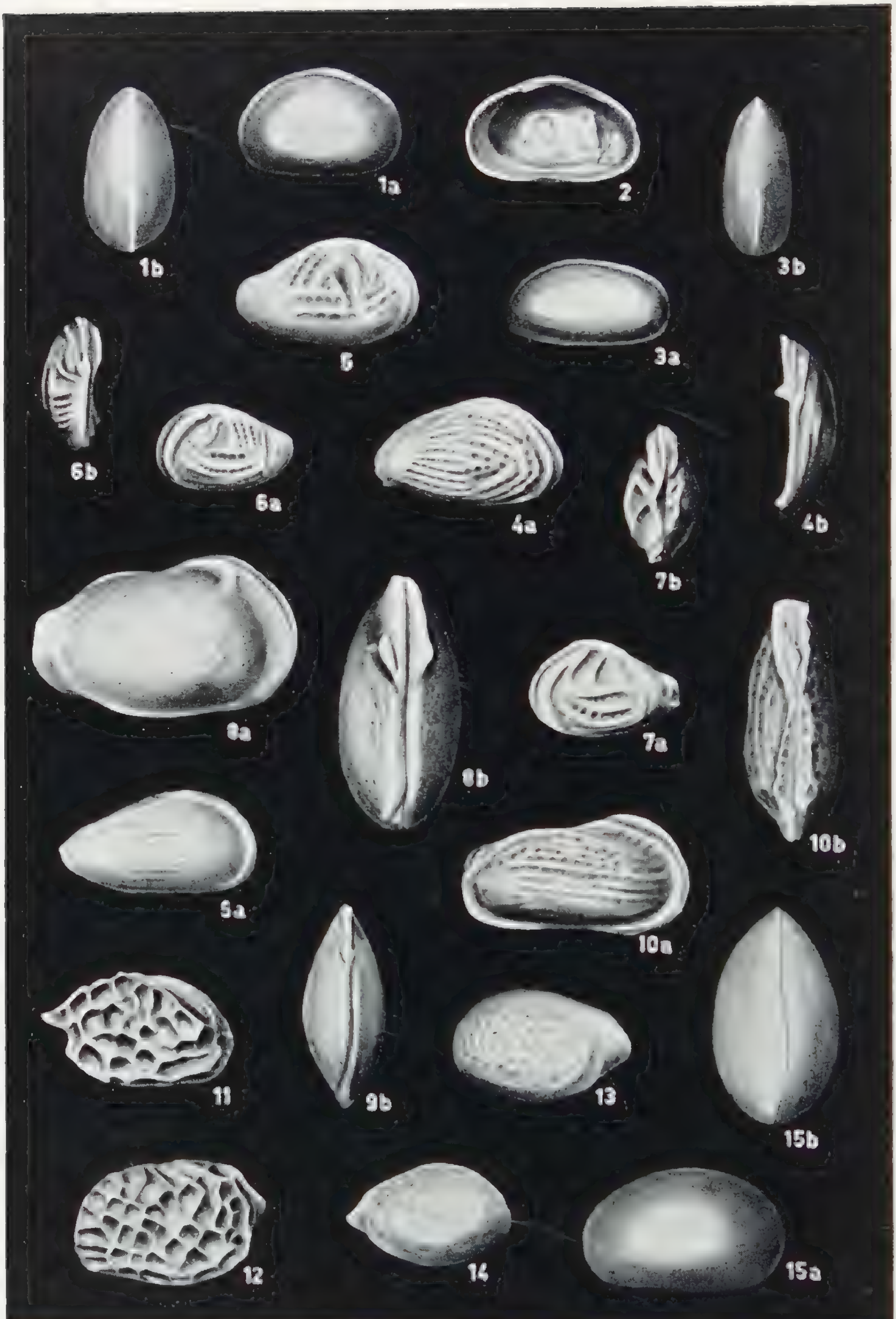
1a
2
1b
3b
5
3a
6b
6a
4a
4b
7b
8a
8b
7a
10b
5a
10a
11
9b
13
15b
12
14
15a

PLATE 4

The carapace of type 2 is more compressed in the anterodorsal part. The subcentral swelling and the dorsal and ventral ridges are prominent, the latter ridge bordering a distinct wing. The reticulation may be more or less reduced.

In type 3 the ornamentation of ridges and reticulation is most excessive, often being irregular and spinose. The dorsal ridge is often subdivided, the ventral ridge along the wing may be perforated.

Type 4 again resembles the first one with fairly regular reticulation and without pronounced dorsal and ventral ridges, while the subcentral swelling is hardly visible. The posterior compressed part is often rather small.

Smaller and middle-sized molts commonly belong to types 1 and 2. Their separation is quite possible in some samples (i.e. XF–TP, 28 m), whereas in others (i.e. XF–TP, 34.50 m) there is complete intergradation. The less frequent type 3 occurs mainly among the larger molts, while the equally rare type 4 is especially found among the middle-sized individuals. All four types show considerable variation in relative length

---

PLATE 4

Figs. 1*a*, *b*. *Clithrocytheridea tombigbeensis* (STEPHENSON). *a* = side view right valve. *b* = dorsal view carapace. XF-15, 34 m. × 40.

,, 2. *Clithrocytheridea tombigbeensis* (STEPHENSON), interior right valve. XF-15, 86.75 m. × 40.

,, 3*a*, *b*. *Krithe* cf. *perattica* ALEXANDER. *a* = side view right valve, *b* = dorsal view carapace. XF-TP, 34 m. × 40.

,, 4*a*, *b*. *Buntonia alabamensis* (HOWE and PYEATT) var. 1. *a* = side view right valve, *b* = dorsal view right valve. XF-15, 61.50 m. × 40.

,, 5. *Buntonia alabamensis* (HOWE and PYEATT) var. 2, side view right valve. XF-TP, 34 m. × 40.

,, 6*a*, *b*. *Buntonia alabamensis* (HOWE and PYEATT) var. 3. *a* = side view left valve, *b* = dorsal view carapace (damaged). XF-TP, 34 m. × 40.

,, 7*a*, *b*. *Buntonia alabamensis* (HOWE and PYEATT) var. 4. *a* = side view left valve, *b* = dorsal view carapace. XF-TP, 34 m. × 40.

,, 8*a*, *b*. *Brachycythere kugleri soldadensis* VAN DEN BOLD. *a* = side view right valve, *b* = dorsal view carapace. XF-TP, 34.50 m. × 40.

,, 9*a*, *b*. *Brachycythere kugleri soldadensis* VAN DEN BOLD. *a* = side view right valve, *b* = dorsal view carapace. XF-16, 81–82 m. × 40.

,, 10*a*, *b*. *Cytheretta arrugia* VAN DEN BOLD. *a* = side view right valve, *b* = dorsal view carapace. XF-TP, 28 m. × 40.

,, 11. *Eucytherura decorata* WEINGEIST, side view of a coarsely reticulated right valve. XF-15, 67.50 m. × 80.

,, 12. *Eucytherura decorata* WEINGEIST, side view left valve. XF-15, 67.50 m. × 80.

,, 13. *Cytheropteron midwayensis* ALEXANDER, side view left valve. XF-16, 90 m. × 80.

,, 14. *Cytheropteron midwayensis* ALEXANDER, side view right valve. XF-16, 90 m. × 80.

,, 15*a*, *b*. *Xestoleberis mauryae* VAN DEN BOLD. *a* = side view left valve, *b* = dorsal view carapace. XF-16, 97 m. × 40.

and width, which seems to exclude the possibility that some of the differences between the types are due to sexual dimorphism. Their mutual relationship is also clear from the individuals of sample XF 15, 16.50 m. Specimens of type 3 show more or less developed, median, longitudinal ridges (fig. 10), but the same tendency is found in the individuals of types 1 and 2 of this sample.

There are but very few isolated valves. The hinge is identical with that typical of the genus *Hermanites* PURI: the terminal teeth are not crenulated. A single valve, of type 3, shows the muscle scars, a vertical series of four more or less elongated scars with two others in front. This might indicate some preference for the genus *Bradleya* HORNIBROOK.

H. collei (Gooch)? VAN DEN BOLD (1957, Micropal., vol. 3, p. 9, pl. 3, fig. 6) from Paleocene beds of Soldado Rock resembles our types 1, 2 and 4. Comparison of the original material showed that type 2 is identical with *Cythereis collei* GOOCH var. *extrema* VAN DEN BOLD (1946, p. 94) from the Paleocene-Eocene beds of Guatemala and British Honduras. *C. bassleri* as figured by MUNSEY (1953, Jour. Pal., vol. 27, p. 8, pl. 4, fig. 12–14) from the Paleocene Naheola formation of Alabama shows the posterior vertical ridge, but otherwise figures 12 and 14 resemble our type 3, while the individual of figure 13 rather belongs to the group of types 1 and 2. *C. plusculmensis* SCHMIDT (1948, Jour. Pal., vol. 22, p. 422, pl. 64, fig. 2–4) from the Aquia formation of Maryland resembles our type 2. *C. bassleri reticulolira* SCHMIDT (id., p. 423, pl. 64, fig. 14, 15) from the same deposits is closer to our types 1 and 4, while *C. bassleri vacuitatis* SCHMIDT (id., p. 423, pl. 61, fig. 19, 20) from the Upper Cretaceous is more in resemblance with our type 4.

Age. The group of *C. bassleri* is frequent in strata of Late Cretaceous to Eocene age of America.

Buntonia alabamensis (HOWE and PYEATT)

Pl. 4, fig. 4–7

Cythereis? alabamensis HOWE and PYEATT, 1934, Louis. Dept. Cons., Geol. Bull. 4, p. 50, pl. 4, fig. 2, 5, 7–10.

Remarks. Several individuals of different molts belong to the group of *B. alabamensis*.

Type 1, the biggest and most regularly ornamented one, resembles *Pyricythereis alabamensis* (HOWE and PYEATT) of VAN DEN BOLD (1946, p. 103, pl. 11, fig. 6) from the Early Tertiary beds of Guatemala and British Honduras, though our individuals seem to be thicker.

Type 2 is slightly smaller, but especially more flattened, and the ornamentation is less regular and often weaker. It somewhat resembles figures 5 and 8 of HOWE and PYEATT.

Type 3 is still smaller and especially shorter than the previous one, but with similar ornamentation pattern.

Type 4 of small to middle size, is more angular and less finely ornamented with fairly heavy ridges. It resembles the forms, figured by STEPHENSON as *Pyricythereis alabamensis* (HOWE and PYEATT) from the Texan Claiborne Eocene (1944, Jour. Pal., vol. 18, p. 453, pl. 76, fig. 2, 3).

Intermediates between types 2 and 3 have been found, and possibly type 1 is an adult molt of the same species. Type 4, which is represented by individuals of several molts may belong to a different species. The number of detached valves is restricted. There are no observations on the muscle scar pattern. It has to be remarked that in one sample some valves of types 2 and 3 (five in total) show a reversed hinge, i.e. as might be expected of the opposite valve of a *Buntonia* species. Those of types 1 and 4 of the same sample (XF–TP, 34 m) show a normal hinge pattern, but also the valves of 2 and 3 in other samples are normal.

Age. The species group is known from several Eocene and Paleocene deposits of America.

Brachycythere kugleri VAN DEN BOLD **soldadensis** VAN DEN BOLD

Pl. 4, fig. 8, 9

Brachycythere? kugleri soldadensis VAN DEN BOLD, 1957, Micropal., vol. 3, p. 10, pl. 4, fig. 8.

Remarks. Especially among our larger specimens there is considerable variation of relative height. The posterior part of these carapaces is more rounded or truncated than it is shown in the type figure. Usually there are also distinct pores, and the anterodorsal tubercle may be very strong. Among the smaller molts types are found which better resemble *Brachycythere? kugleri* var. VAN DEN BOLD (id., p. 11, pl. 4, fig. 9) and more rarely *Brachycythere? kugleri* (id., p. 10, pl. 4, fig. 7). Detached valves have not been found.

Age. *B. kugleri* and its variants have been described from Paleocene beds of Venezuela and Soldado Rock.

Cytheretta arrugia VAN DEN BOLD

Pl. 4, fig. 10

Cytheretta arrugia VAN DEN BOLD, 1957, Micropal., vol. 3, p. 11, pl. 3, fig. 10.

Remarks. Generally our carapaces are thicker and more ornamented than the figured type. Variation of the relative length is considerable; an elongated specimen has been figured. There are no isolated valves.

Age. Originally described from Paleocene beds of Trinidad and Venezuela.

Eucytherura decorata WEINGEIST

Pl. 4, fig. 11, 12

Eucytherura decorata WEINGEIST, 1949, Jour. Pal., vol. 23, p. 373, pl. 73, fig. 9; VAN DEN BOLD, 1957, Micropal., vol. 3, p. 11, pl. 4, fig. 4.

RANGE CHART

Borings	NF TP			NF-15					NF-16			
Depth in metres	28	34	34.50	61.50	62	62.50	67.50	86.75	81.82	86.40	90	97
Valvulina triangularis	f	r	r			r			r		r	
Valvulina pupa	r								r			
Quinqueloculina spp.			f								r	
Guttulina problema									r	r	r	
Discorbis midwayensis	r	f									r	
Siphonina prima							r				f	
Anomalinoides cf. danica		r	r						r	r	r	r
Anomalinoides midwayensis		r			f		f		r		r	
Cibicides browni				r	r						r	
Boldia carinata		f		f	f		f		r	r	f	
Boldia carinata var. 1	f								r		r	
Boldia carinata var. 2	r								r	r	r	
Asterigerina texana		f							r		r	
Rotalia hensoni		r							f	f	r	
Rotalia cf. sigali		r			f		f					
Storrsella haastersi	A	f	f	A	f	r	f		f	f	f	r
Lockhartia haimei				r	r	A	r			r	r	
Smoutina cruysi	A	r	f	r	r	A	r	r	f	r	f	f
Ranikothalia soldadensis				A	A	A	f		r	r	r	
Cytherella guasarensis	r	r	f	r			r		r		r	
Platella kellettae											r	
Bairdoppilata magna		f	f	r		r	r		r	f	r	
Clithrocytheridea tombigbeensis		f	A	r			r	r	r		r	
Krithe cf. perattica	r		r									
Hermanites bassleri var. 1	f	f	r	r			r		r	r		
Hermanites bassleri var. 2	r	r	r	r			r	r	r	r		
Hermanites bassleri var. 3	r	r		r			r	r	r	r		
Hermanites bassleri var. 4	r		r	r					r			r
Buntonia alabamensis var. 1		r	r	r			r			r	r	
Buntonia alabamensis var. 2		r					r					
Buntonia alabamensis var. 3		r		r	r		r			r		
Buntonia alabamensis var. 4		r		r			r		r	r		
Brachycythere kugleri soldadensis	f		r				r		r	f		
Cytheretta arrugia	r			r							r	
Eucytherura decorata							r				r	
Cytheropteron midwayensis											r	
Xestoleberis mauryae			r							r		r

r = rare, f = frequent, A = abundant.

Remarks. Our few specimens show some variation in outline and much variation in the surface reticulation and its ridges. A splitting into more than one group is impossible. The ornamentation resembles best that of *E. decorata,* but the details of WEINGEIST's description cannot be followed. In specimens with coarse reticulation, ridges are prominent (fig. 11). With a finer reticulation, with never more than eight pits on a vertical line, the ridges become obscure. The posterior double alar prolongation is present, but probably less prominent than it is in WEINGEIST's type.

Age. The species has been described from the Paleocene Naheola formation of Alabama. It has been found on Soldado Rock.

Cytheropteron midwayensis ALEXANDER

Pl. 4, fig. 13, 14

Cytheropteron midwayensis ALEXANDER, 1934, Jour. Pal., vol. 8, p. 230, pl. 33, fig. 17.

Remarks. Only two specimens were found. They may differ from ALEXANDER's species in the nearly straight hinge line and a less wide ventral inflation. Shape and ornamentation seem to be identical.

Age. Originally described from the Wills Point formation of Midway age of Texas.

Xestoleberis mauryae VAN DEN BOLD

Pl. 4, fig. 15

Xestoleberis mauryae VAN DEN BOLD, 1957, Micropal., vol. 3, p. 12, pl. 1, fig. 6.

Remarks. There are only a few closed carapaces of different molts. They differ from *X. opina* SCHMIDT (1948, Jour. Pal., vol. 22, p. 410, pl. 61, fig. 15, 16, textfig. 2*b*) in the slightly concave ventral outline.

Age. Described from Paleocene beds of Soldado Rock and Venezuela.

REFERENCES

ALEXANDER, C. I., Ostracoda of the Midway (Eocene) of Texas. Jour. Pal., 8, 206–237 (1934).

BOLD, W. A. VAN DEN, Contribution to the study of Ostracoda. Thesis Utrecht (1946).

———, Ostracoda from the Paleocene of Trinidad. Micropal., 3, 1–18 (1957).

BROTZEN, F., The Swedish Paleocene and its foraminiferal fauna. Sver. Geol. Unders., C, **493**, Årsbok 42 (1948).

CAUDRI, C. M. B., The larger Foraminifera from San Juan de los Morros, State of Guarico, Venezuela. Bull. Am. Pal., **28**, 114 (1944).

CIZANCOURT, M. DE, Nummulites de l'ile de la Barbade. Mém. Soc. géol. France, n. ser., **27**, 57 (1948).

———, Grands Foraminifères du Paléocène, de l'Eocène inférieur et de l'Eocène moyen du Venezuela. id., **30**, 64 (1951).

Cole, W. S., *Lockhartia* in Cuba. Jour. Pal., **16**, 640–642 (1942).

—— and S. M. Herrick, Two species of larger Foraminifera from Paleocene beds in Georgia. Bull. Am. Pal., **35**, 148 (1953).

Cushman, J. A., Paleocene Foraminifera of the Gulf Coastal Region of the United States and adjacent areas. U.S. Geol. Survey, Prof. Paper 232 (1951).

—— and P. J. Bermudez, Some Paleocene Foraminifera from the Madruga formation of Cuba. Contrib. Cushm. Lab. Foram. Res., **24**, 68–75 (1948).

Cruys, H., Termes inférieures d'âge tertiaire et plio-quaternaire de la série sédimentaire côtière de la région Saint Laurent-Mana. Communic. 5e Conf. géol. Guyanes, Georgetown, Octobre (1959).

Davies, L. M., *Ranikothalia* in East and West Indies. Geol. Mag., **86**, 113–116 (1949).

Drooger, C. W., Some early rotaliid Foraminifera. Proc. Kon. Ned. Ak. Wetensch., **B 63** (1960).

Loeblich, A. R. and H. Tappan, Correlation of the Gulf and Atlantic Coastal Plain Paleocene and Lower Eocene formations by means of planktonic Foraminifera. Jour. Pal., **31**, 1109–1137 (1957).

Munsey, G. C., A Paleocene Ostracode fauna from the Coal Bluff Marl Member of the Naheola formation of Alabama. id., **27**, 1–20 (1953).

Plummer, H. J., Foraminifera of the Midway formation in Texas. Univ. Texas Bull. **2644** (1926).

Pokorný, V., Grundzüge der zoologischen Mikropaläontologie, 2 (1958).

Sachs, K. N., Restudy of some Cuban Foraminifera. Contrib. Cushm. Found. Foram. Res., **8**, 106–120 (1957).

Schmidt, R. A. M., Ostracoda from the Upper Cretaceous and Lower Eocene of Maryland, Delaware and Virginia. Jour. Pal., **22**, 398–431 (1948).

Sigal, J., Foraminifères. In J. Piveteau, Traité de Paléontologie, **1**, 133–178, 192–301 (1952).

Smout, A. H., Lower Tertiary Foraminifera of the Qatar Peninsula. Publ. Brit. Mus. Nat. History (1954).

Vaughan, T. W., American Paleocene and Eocene larger Foraminifera. Mem. Geol. Soc. Am., **9**, 1–175 (1945).

—— and W. S. Cole, Preliminary report on the Cretaceous and Tertiary larger Foraminifera of Trinidad, B.W.I.. Geol. Soc. Am., Spec. Paper 30 (1941).

BIOCHEMISTRY

QUANTITATIVE PAPER CHROMATOGRAPHY OF PHOSPHATIDES

THE ACID-BASE TYPE PHOSPHATIDES OF HEN'S EGG-YOLK AND HUMAN AORTA

BY

G. J. M. HOOGHWINKEL AND H. P. G. A. VAN NIEKERK

(Communicated by Prof. H. G. Bungenberg de Jong at the meeting of May 28, '60)

Introduction

Some investigators in the field of phospholipid research use a method for the quantitative analysis of paper chromatograms based on the determination of phosphorus in the eluted spots. (Marinetti [1], E. B. Smith [2]). The experimental procedure is rather elaborate and it is necessary to work with high precision to get accurate results and a good reproducibility. We are able to give a method for the quantitative paper chromatographic analysis of acid-base type phosphatides using the tricomplex staining procedure [3, 4, 5], which method is based on experimental results we published earlier.

The method has been tested with egg-yolk phosphatides extracts the composition of which is relatively well known from the work of Lea and Rhodes [6]. As a demonstration of its possible usability, the analysis of human aorta phospholipids of atherosclerotic arteries is given.

Experimental

1. *Phospholipid extraction*

The hen's egg-yolk phospholipids were prepared as follows: One egg (fresh) was boiled [1]) during 15 minutes and cooled. The egg-yolk was extracted with a mixture of methanol and chloroform (2:3, vol.:vol.).

The extraction was repeated with new solvent till no more lipids could be demonstrated in the extract. For this purpose we used a spot test on filter paper, carried out as follows: A drop of the extract is applied on a filter paper. After the solvent is evaporated, the filter paper is immersed in a staining solution as described under "paper-chromatography". No phosphatides are present in the extract when the spot on the spot test paper is not stained within 10 minutes. The extracts were combined and the methanol-chloroform was evaporated in a rotation film evaporator till dry. The lipids were dissolved in methanol-chloroform (20:80) to a concentration of 4 %.

[1]) Boiling eggs before extracting prevents the occurrence of enzymatic breakdown processes [9].

The human aorta phospholipid extract was prepared by extracting human atherosclerotic aorta (stage III; C. J. F. BÖTTCHER [8]) with methanol-chloroform (2:3). The extract was dialysed against a rubber membrane (C. J. F. BÖTTCHER [7]). The dialysed phospholipid solution was diluted to a concentration of 2 % in methanol-chloroform.

2. *Paper chromatography*

Using a capillary pipet with a volume of 4.7 mm³, the phospholipids are applied on silica impregnated filterpaper. Schleicher and Schüll 2043b.

Chromatography is carried out as described elsewhere (HOOGHWINKEL, [4]) using di-isobutylketone, acetic acid, water (40:25:5) as solvent (MARINETTI, [1]).

After finishing the chromatographic separation the paper is dried in a stream of warm air and stained by suspending the paper in a staining solution containing 0.005 % Edicol Supra Ponceau 4 RS, 0.2 % $UO_2(NO_3)_2$ and 0.01 n HCl. The paper is allowed to take up dye molecules for a period of 16 hours (the night over), necessary to get a staining which will secure proportionality between dye uptake and the phospholipid amount on the chromatographic spots (HOOGHWINKEL and VAN NIEKERK, [5]). At the end the papers are dried between filter paper and with a stream of warm air.

3. *Elution of the stained spots and colorimetric measurements of the eluates*

On the dried chromatograms the stained spots are outlined by pencil and subsequently cut out with a pair of scissors, exactly following the outline. The excised spots are suspended in 5 ml or 3 ml 50 % tert. butylalcohol containing 3.5 n HCl. The extinction of the eluate is measured after a period (about 3 hours) sufficient to ensure complete dissolution of the dye. The maximum absorption wavelength of Edicol Supra Ponceau 4 RS in the eluting solvent is 510 mμ.

RESULTS

Hen's egg-yolk phosphatides

This material is used to test the method because the composition is known from work of Lea and Rhodes (1957).

The chromatogram (see figure 1) shows 4 spots: phosphatidyl ethanolamine; phosphatidyl choline; sphingomyelin; lyso phosphatidyl choline.

In the same place where we find sphingomyelin also lyso phosphatidyl ethanolamine, might be present. The amount of lyso phosphatidyl ethanolamine in egg-yolk is very low if the extract is freshly prepared, as may be concluded from separations over Al_2O_3 columns of freshly prepared egg-yolk extracts. The analysis is carried out in 5 fold and the data are given below:

TABLE 1

Extinction values of eluates of hen's egg-yolk phosphatide spots

Chromatographic spot of:	measurements					mean	mol % of acid-base type phosphatides	
phosphatidyl ethanolamine	.067	.077	.059	.069	.065	.067	14.9	(15.0)
phosphatidyl choline	.213	.193	.200	.194	.186	.328 (.197)*	72.5	(72.8)
sphingomyelin	.030	.027	.029	.028		.029	6.4	(4.6)
lyso phosphatidyl choline	.030	.027	.029	.028	.026	.028	6.2	(5.8)

* The mean value 197 must be multiplied by 5/3 giving 328, to get a value comparable with the other extinction values because the lecithin spot is eluted with 5 ml eluting solvent while the other spots are eluted with 3 ml solvent.

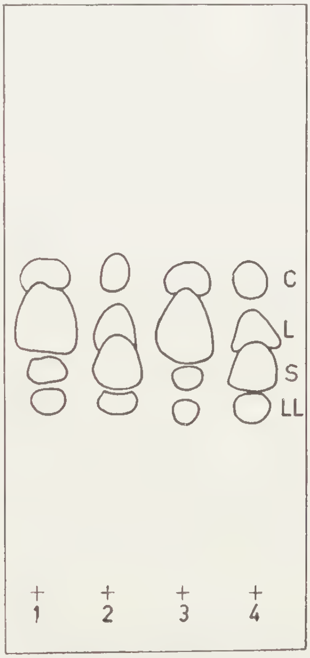

Fig. 1. A paper-chromatogram of hen's egg yolk phosphatides (1 and 3) and of arterial phosphatides (2 and 4).

In an earlier paper (5) we demonstrated on spot tests that using the staining solution as given here, the amount of dye bound by phosphatidyl choline is proportional to the molecular amount of the phospholipid. The amount of dye bound is expressed in the eluate-extinction. On theoretical grounds we can state that the same proportionality must exist for all the acid-base type phosphatides[2]). So it may be concluded that the eluate extinctions of chromatographic spots are proportional to the molecular amount of phosphatide present at the spot. Consequently it is possible to calculate molecular percentages of the acid-base type phosphatides from these extinction values. The result of the calculations are given in the fourth column of the above table.

[2]) This theoretical statement has also been confirmed by us experimentally.

The percentages mentioned in brackets are given by LEA and RHODES [6] as a result of an analysis using column separations and chemical analysis.

AORTA PHOSPHOLIPIDS

The chromatograms of a human aorta (atherosclerotic, stage III) phospholipid are made in the same way as the hen's egg phospholipid chromatograms (fig. 1).

The 2 % solution is applied 3 times at the origin of the chromatogram. Table 2 gives the results:

TABLE 2

Extinction values of Eluates of the human aorta phosphatides

Chromatographic spot of:	measurements				mean values	calculated mol percentages
phosphatidyl ethanolamine	.036	.036	.038	.040	.038	13.8
phosphatidyl choline	.077	.080	.083	.082	.081	29.5
sphingomyelin	.150	.136	.148	.143	.144	52.5
lyso phosphatidyl choline	.012	.011	.012	.012	.012	4.39

In a supplementary experiment we combined corresponding chromatographic spots of two chromatograms, which were eluted and the extinctions of the eluates measured (table 3).

TABLE 3

Extinction values of combined spots of two chromatograms

Chromatographic spot of:	Extinction	mol %
phosphatidyl ethanolamine	.071	13.9
phosphatidyl choline	.153	29.5
sphingomyelin	.278	53.5
lyso phosphatidyl choline	.019	3.65

The molecular percentages are calculated in the same way as in the analysis of hen's egg-yolk phosphatides.

By using the method it is not necessary to measure blank values. This, we studied extensively on spot test experiments with phosphatidyl choline (5). However, it is strictly necessary to outline the stained spot circumference on the chromatograms carefully to make sure that no more paper is cut out than contains stained phospholipid.

DISCUSSION

The high reproducibility of the method is remarkable as can be seen from the extinction values of the different determinations. The tricomplex stained spot is chemically to be regarded as formed by Coulomb interactions in which formation the reacting partners are involved on behalf of their ionic properties. Consequently we may expect that the components

of the "tricomplex system" are present in the complex in equivalent amounts. This is indeed true (5) if the concentrations of dye and of uranyl nitrate in the staining solution are chosen sufficiently high. For lecithin we studied in detail the relationship between dye uptake and lecithin amount, if the dye concentration in the staining solution is not sufficient to promote a tricomplex containing an equivalent amount of the dye. In such cases we still find a linear proportionality between dye uptake (eluate extinction) and lecithin amount on the spot. Consequently we may say that it is permissible to use lower dye concentrations for quantitative purposes.

On theoretical grounds there is no reason to expect that other phosphatides then phosphatidyl choline will stain, using the same conditions, in another way (see also note 2). Work is in progress to investigate this point.

On the basis of the above considerations we may claim a molecular proportionality of the different acid-base type phosphatides expressed in the mean extinctions obtained. If related to a total of 100, the extinctions will give the molecular percentual distribution.

An accuracy within 1 % of the calculated percentage must be permitted. Other methods based on the determination of phosphorus in the chromatographic spots, in our hands were less accurate and much more elaborate.

The absolute amount of phosphatides in a sample can be calculated if the total amount of the acid-base type phosphatides is known. The total acid-base type phosphatide amount in an extract can be measured by making a spot test of the extract and staining in the same way as described here for chromatograms. The eluate extinction of this spot test compared with the extinction of a spot test eluate from a phosphatidyl choline extract of known concentration, makes the calculation of the molecular concentration of the unknown extract possible.

Acknowledgements

We will express our thanks to Prof. Dr. C. J. F. Böttcher, Laboratory for Physiçal Chemistry, University of Leyden, and his co-worker C. M. van Gent for the interest in this work, especially concerning the analysis of the human aorta phosphatides. The samples of human aorta phospholipid extract were obtained from Prof. Böttscher's group working on the lipid composition of human arteries in relation to atherosclerosis. One of the members of this group, Miss H. A. M. ter Haar, must be thanked for her valuable technical assistance.

Summary

A method for the quantitative paper chromatographic analysis of acid-base type phosphatides is given, based on the staining of chromatograms, on silica-impregnated filter paper, with the tricomplex staining procedure.

Paper chromatograms which are developed with di-isobutylketone,

acetic acid, water (40:25:5) are dried and subsequently stained in a bath containing 0.005 % Edicol Supra Ponceau 4 RS, 0.2 % $UO_2(NO_3)_2$ and 0.01 n HCl. The extinction of the eluate is measured at 510 mμ in a spectrophotometer. The extinction value is proportional to the molecular amount present in the spot. If related to a total of 100 the molecular percentages of the acid-base type phosphatides of the sample can be calculated.

Hen's egg-yolk and a sample of human arterial phospholipids are analysed. The molecular compositions in percentages of the total are given in the table.

TABLE 4

	Molecular percentages of acid-base type phosphatides	
	hen's egg-yolk	human artery (atherosclerotic stage III)
phosphatidyl ethanolamine	14.9 %	13.8 –13.9 %
phosphatidyl choline	72.5 %	29.5 –29.5 %
sphingomyelin	6.4 %	52.5 –53.2 %
lyso phosphatidyl choline	6.2 %	3.65– 4.38 %

Department of Medical Chemistry,
University of Leyden

REFERENCES

1*a*. MARINETTI, G. V., J. ERBLAND, J. KOCHEN, Fed. Proc. **16**, 837 (1957).
1*b*. ———, M. ALBRECHT, T. FORD and E. STOTZ, Biochem. Biophys. Acta **36**, 4 (1959).
2. SMITH, E. B., The Lancet **1**, 799 (1960).
3. BUNGENBERG DE JONG, H. G., and G. R. VAN SOMEREN, These Proceedings Series **B 62**, 150 (1959).
4. HOOGHWINKEL, G. J. M., J. TH. HOOGEVEEN, M. J. LEXMOND and H. G. BUNGENBERG DE JONG, These Proc. Series **B 62**, 222 (1959).
5. HOOGHWINKEL, G. J. M. and H. P. G. A. VAN NIEKERL, These Proceedings Series **B 63**, 258 (1960) and Series **B 63**, 272 (1960).
6. RHODES, D. A. and C. H. LEA, Biochem. J. **56**, 526 (1957).
7. BÖTTCHER, C. J. F., F. P. WOODFORD, E. BOELSMA–VAN HOUTE and C. M. VAN GENT, Rec. Trav. Chim. T. **78**, 794 (1959).
8. ———, The Lancet **1**, 1378 (1960).
9. DE BAKKER, A., Thesis, 's-Gravenhage, 1957.

BIOCHEMISTRY

METHOD FOR THE MICRO-DETERMINATION OF PHOSPHORUS IN BIOLOGICAL SUBSTANCES. A MODIFICATION OF THE METHOD OF ZINZADSE

BY

G. J. M. HOOGHWINKEL AND H. P. G. A. VAN NIEKERK

(Communicated by Prof. H. G. Bungenberg de Jong at the meeting of May 28, '60)

1. Introduction

Most methods for the determination of phosphorus or phosphate in biological material are modifications of the method of C. H. Fiske and Y. Subbarow [1]. Especially in the field of lipid research and in clinical laboratories a great number of phosphorus determination methods are in use (Fiske and Subbarow [1], King [2], Lowry and Lopez [3], Berenblum and Chain [4]). The methods are based on the fact that the reaction product between phosphate and molybdate in acid medium will form a blue colour by reduction.

The published modifications of this method are generally based on:

1e. variations in the acidity of the medium,

2e. variations in the reducing substances added.

Instead of sulphuric acid (Fiske and Subbarow) King [2] used $HClO_4$ and Lowry and Lopez [3] used an acetate buffer of pH = 4. Many reducing substances have been proposed: hydroquinone, thiosulphate, $SnCl_4$, $FeSO_4$, ascorbic acid, 1-amino-2-naphtol-4-sulphuric acid and others.

The reducing substances in use for the Fiske and Subbarow modifications generally are instable and cause inaccuracies. The existence of so many variations for one, in principle unchanged, method, suggests that it may be useful to draw attention to a different method which in our hands gives accurate results and has some advantages above the methods generally used.

In 1930 Zinzadse [5] published a method for the determination of phosphorus based on a principle which differs from that of the Fiske and Subbarow method.

While Fiske and Subbarow reduced a preformed reaction product between phosphate and molybdate (phosphomolybdate), Zinzadse added the phosphate-containing sample to a molybdate solution reduced beforehand with Mo. The reduced molybdate reagent is stable over long periods, even for over 4 years as Zinzadse established. Zinzadse also noted that

the colour intensity of the reaction product between reduced molybdate and phosphate is stable for more than 7 days.

The old article of Zinzadse is the basis of our investigation which led to a micro method suitable for the routine determination of phosphorus. This micro method has a high sensitivity as well as a good reproducibility.

2. Method

a. *Reagents*

1. Reduced molybdate reagent: This is prepared as follows: 120 ml concentrated sulphuric acid is boiled under reflux with MoO_3 (molybdic acid). When all the molybdic acid has been dissolved the solution is allowed to cool. 80 ml destilled water is added and again the solution is allowed to cool. Now 0.56 g of Mo (p.a. metallic) is added and again under reflux the solution is softly boiled till all the molybdenum is dissolved. This will take about 20 minutes. The solution is now dark green-blue. After cooling again, 200 ml distilled water is added so that the volume is now 400 ml. *This reagent will be referred to as "Zinzadse reagent"* [1]).
2. Perchloric acid p.a. (Merck, ca. 60 %). It is necessary to use P-free perchloric acid to prevent the occurrence of "high" blanks.
3. Sulphuric acid concentrated p.a. (Merck).
4. 5n NaOH in distilled water.
5. ∝. dinitrophenol 0.1 % in ethylalcohol.

b. *Procedure*

A. Inorganic phosphorus

The phosphate sample containing 2–20 μg or 5–50 μg P is pipetted into 10 or 25 ml pyrex test tubes having a constriction in the upper part and a mark at exactly 10 ml or 25 ml. The sample must be nearly neutral [2]). 0.2 ml (10 ml test tubes) or 0.5 ml (25 ml test tubes) Zinzadse reagent is added and the volume is made up to 10 resp. 25 ml. It is necessary to mix the contents of the tubes thoroughly. The test tubes are now placed in a boiling water bath for 30 minutes. The solution has attained a blue colour. After cooling to room temperature, the volume is corrected to 10 or 25 ml. The extinction is measured at 825 mμ in a 10 mm cell. A blank containing no phosphorus and a standard phosphate solution are determined in the same way.

[1]) The grey-green coloured "Zinzadse reagent" looses its colour by dilution. Especially at the dilution (1:50) described to carry out the reaction no significant colour is present.

[2]) If this is not the case it is necessary to neutralise using two drops ∝ dinitro phenol as indicator and $5n$ NaOH in distilled water for acidic solutions. Alkaline solutions can be made acidic with $5n$ H_2SO_4 using the same indicator. Afterwards it is necessary to neutralise again with $5n$ NaOH till the colour is yellow again.

Calculation

The amount in μg of phosphorus in the sample can be calculated as follows:

$$\frac{\text{Ext. sample}}{\text{Ext. stand.}} \times \text{phosphorus amount of the standard in } \mu g.$$

The extinctions of the sample and of the standard are diminished with the extinction of the blank.

B. Organic phosphorus

In Kjeldahl destruction tubes, samples containing organic phosphorus (2–20 μg P), for instance: serum or phospholipid solution [1]), are combined with 0.5 ml perchloric acid and a few drops of concentrated sulphuric acid. The destruction is performed by heating the tubes for a short period, generally not longer then 20 minutes. The destruates are allowed to cool and then neutralised with 5n NaOH (about 20–25 drops) against α dinitrophenol as indicator.

The neutralised destruates are transferred into pyrex test tubes of 10 or 25 ml (see also the inorgame P determination). In the latter case the amount of phosphorus in a sample can be 5–50 γ P. Now 0.2 ml (10 ml test tube) or 0.5 ml (25 ml test tube) of the Zinzadse reagent is added. Distilled water is added up to 10 or 25 ml and the tubes are placed in a boiling water bath for 30 minutes. The solution has attained a blue colour. After cooling to room temperature the extinctions are measured in 10 mm cells at 825 mμ. Blank and standard solutions are determined in exactly the same way. The calculations are carried out as described for the inorganic P determination.

3. Experiments

a. *Absorption spectrum*

The absorption spectrum is given in figure 1. It was obtained by measuring in the range of 640 mμ–900 mμ. For this we made a determination of a 5 ml KH_2PO_4 standard solution containing 2 μg pro ml. The extinctions were measured against a blank determination containing no phosphorus. The measurements are carried out in 10 mm cells. The result is given in figure 1. The maximum absorption is at 825 mμ.

b. *Influence of heating time on colour development*

To investigate the influence of heating time on colour development, we carried out a determination as described under the method for inorganic phosphate with 7.5 μg phosphorus in the 10 ml test tubes. The heating time was varied between 3 and 60 minutes. Figure 2 demonstrates the result.

The conclusion we may draw is that a heating time of 30 minutes will no

---

[1]) The organic solvent must be evaporated in a boiling water bath before the reagents are added.

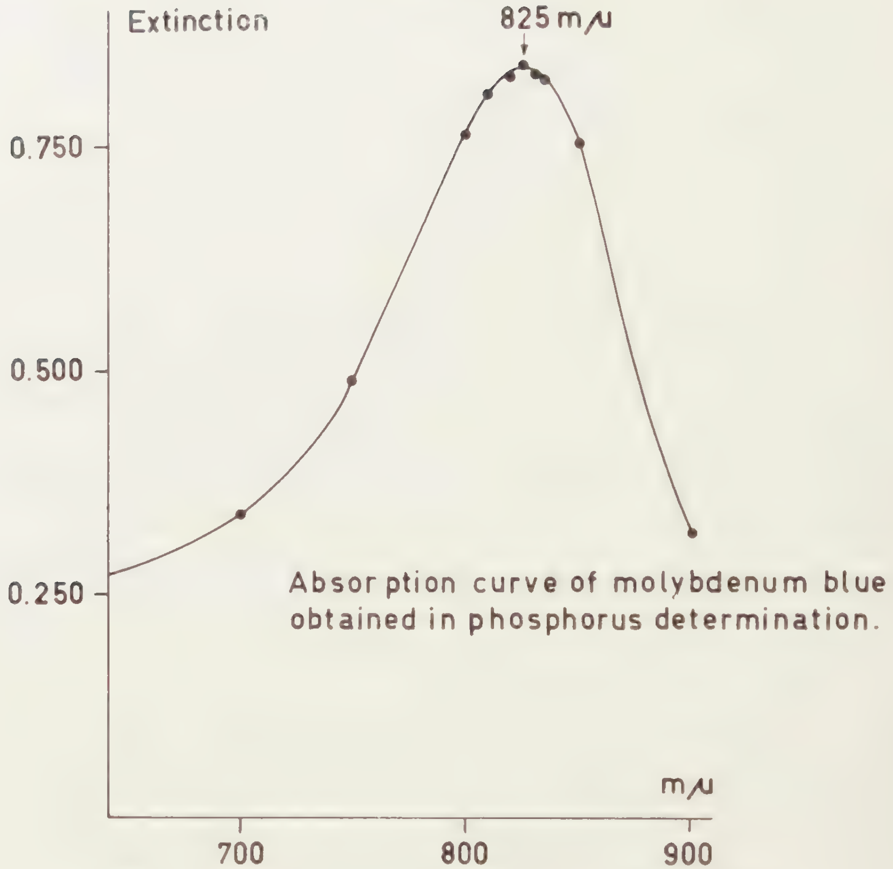

Fig. 1. Absorption Spectrum. Phosphorus determination.

doubt be sufficient for the routine determination. The measured extinction values do not change after the maximum extinction has been obtained, even if the extinction was measured again after 5 days. For instance: The extinctions of 3 determinations measured after heating 30 minutes were respectively 0.662, 0.662 and 0.658. We kept the tubes for 5 days and measured the extinctions: 0.654, 0.660 and 0.664. The mean extinction values were 0.661 when measured after 30 minutes heating and 0.659 after 5 days. This difference is within the experimental error.

c. *Standard curves*

Standard curves ranging between 2 μg and 20 μg P (10 ml test tubes) or 5 μg and 50 μg (25 ml test tubes) are obtained as a result of phosphate determinations in solutions prepared by dissolving KH_2PO_4 p.a. in distilled water and pipetting the required amount in test tubes (10 ml and 25 ml test tubes respectively).

The results of a representative experiment carried out in triplo is given in table 1. Total volume 10 ml. (Procedure as described for inorganic phosphate).

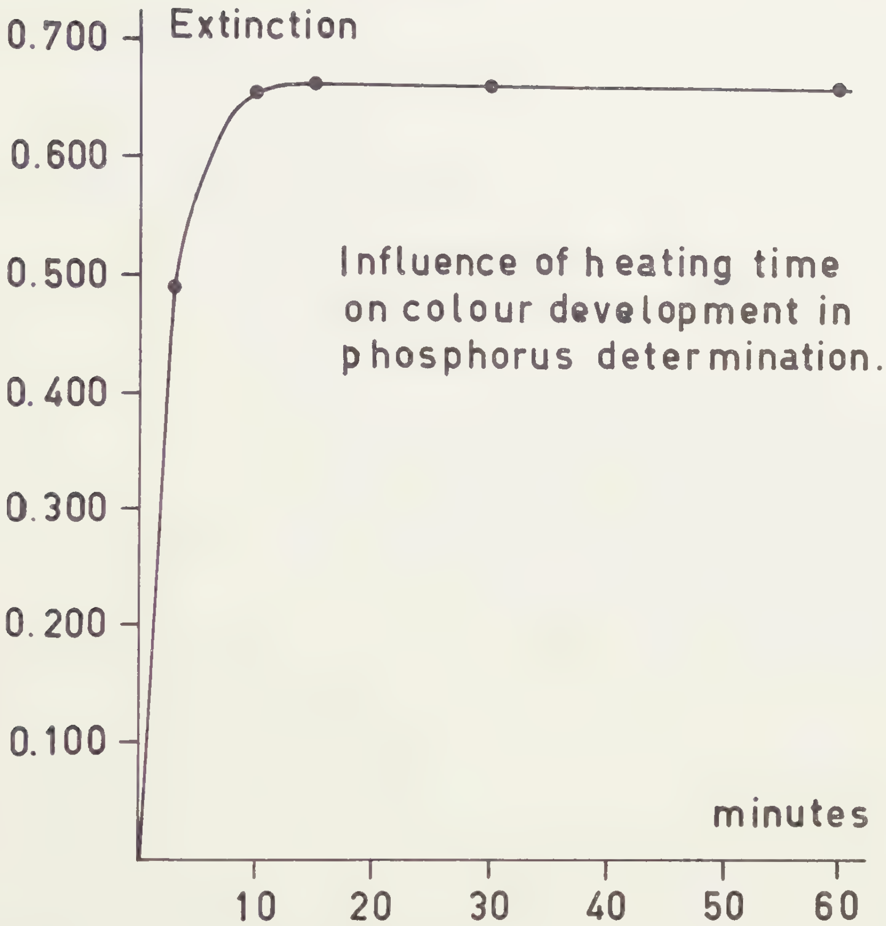

Fig. 2. Influence of heating time on colour development.

TABLE 1

Extinctions of P determinations in a standard series

Amount of P in μg	Extinction			mean diminished with the blank
0	0.018	0.018	0.013	—
2	0.171	0.166	·0.168	0.152
4	0.350	0.340	0.336	0.326
6	0.515	0.507	0.511	0.495
8	0.704	0.690	0.698	0.681
10	0.862	0.863	—	0.847
12	1.033	1.041	1.021	1.016
16	1.372	1.380	1.385	1.363
20	1.680	1.660	—	1.654

The standard line is given in figure 3 and is checked for the determination in both 10 ml and 25 ml test tubes.

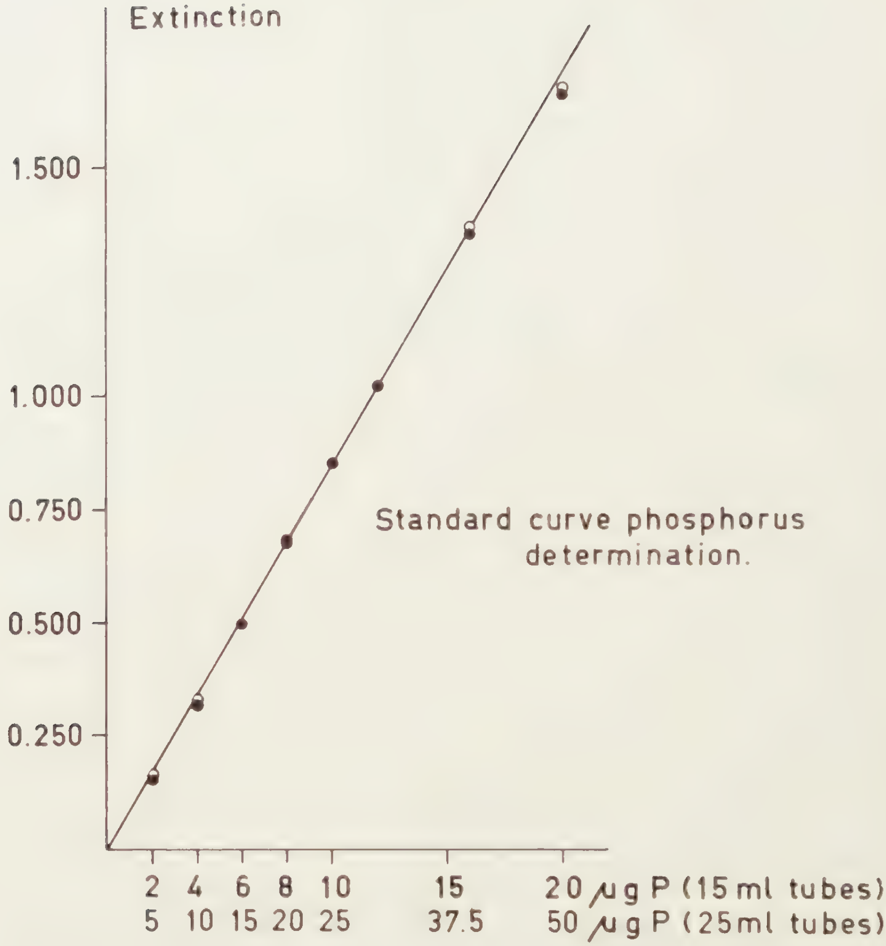

Fig. 3. Standard curve; Phosphorus determination.

As can be seen from the standard line, determinations are possible from about 2 μg P up to nearly 50 μg P.

The standard line is exactly the same for both procedures for inorganic and organic phosphorus. It is evident that smaller concentrations may be estimated with the method if the total volume in which the chromogenic reaction is performed is chosen smaller. It is necessary then accordingly to reduce the amounts of the reagents used.

d. *The required amount of Zinzadse reagent*

Concerning the volume of Zinzadse reagent that must be used to get a sufficient and accurate determination, we may say that 0.5 2.0 ml reagent (in total volume of 25 ml) gives a linear proportionality between colour intensity (extinction) and P-concentration in the range of the standard line.

With different amounts of reagent the extinction of the blank deter-

minations are different. For instance, if 2 ml reagent is used at a total volume of 25 ml for the reaction a blank extinction of about 0.085 will be measured while using 0.5 ml the blank extinction will be about 0.015. This is important especially if lower phosphate amounts are present in the sample where the phosphorus must be determined. Using less than 0.5 ml or more than 2 ml, the determination is no longer possible because in the first case the max. intensity of the coloured reaction product is not reached and in the last case because of disturbing effects of the blank reaction and the high amount of sulphuric acid.

4. Discussion

The phosphorus determination described in this paper has some advantages over other phosphorus determinations, like the modifications of the original Fiske and Subbarow method.

These advantages are:

1. The reduced molybdate reagent, "Zinzadse reagent", prepared at a given time and in a considerable quantity is stable for a very long time. We have used the same solution for 6 months. Zinzadse used the same solution for more than 4 years without any noticeable change in the quantitative results.
   It is important to prepare the Zinzadse reagent exactly as described, to make certain that the composition is $MoO_2 \cdot 4\ MoO_3$.
2. If the Zinzadse reagent is combined with the test solution no colour will develop at room temperature. But if heated in a boiling water bath for 30 minutes colour development is completed and the intensity of the colour obtained is highly reproducible. It has hardly changed even after some days waiting (we chequed this taking a period of 5 days).
3. The sensitivity of the reaction is rather high if compared with other methods for the determination of phosphorus. We can express the sensitivity, as suggested by Woods and Mellon [9], in "parts per million", phosphorus (μg/ml) giving 50 % transmission in a 10 mm cell.

Table 2 gives a survey of the sensitivity of some methods.

TABLE 2

Survey of the sensitivity of some methods for the determination of phosphorus

Method published by:	Sensitivity expressed as part per million phosphorus (μg/ml) giving 50 % transmission in the solution used for colorimetry
H. Weil-Malherbe, 1955 [6]	12.2
A. E. T. H. Meyer, 1957 [7]	2.4
A. A. Hirata and D. Appleman, 1959 [8]	0.47
G. J. M. Hooghwinkel and H. P. G. A. van Niekerk, this method	0.34

The method of Weil–Malherbe and Meyer are modifications of the original Fiske and Subbarow method. The method of Hirata and Appleman is a modification of the original Bernhart and Wreath method based on the fact that acetone enhances the absorbance of the phosphomolybdate complex; here no added reductant is necessary to give molybden blue. It is very important to use highly purified acetone to get reproducible results.

Our method has been used successfully in analysing the phosphorus contents of phospholipid preparations, and we also had good results in using, the method for analysing the P-amount in paper chromatographic spots in phosphatide chromatography. Investigations on the possible use of the method in clinical routine analysis are in progress.

Acknowledgements

We are indebted to Dr Riemersma of this laboratory for his interest in this investigation.

Summary

In this paper a method for the micro determination of phosphorus is described. The method is based on an old method originally published by Zinzadse in 1930. Instead of adding a reducing substance to a preformed phosphomolybdate complex. Fiske and Subbarow and its modifications). by our method, 0.2 ml of a reduced molybdate solution is added to the test tube containing the sample on a total volume of 10 ml.

For the determination of organic P it is necessary to perform a destruction of the material with $HClO_4$. The reduced molybdate solution is prepared as follows: 120 ml concentrated sulphuric acid is boiled under reflux with 6.02 gr. MoO_3. After diluting 0.56 gr. Mo is added and the mixture is boiled till all the Mo is dissolved. The dark blue solution is diluted by adding 200 ml of distilled water.

The determination described in this paper has some advantages over other phosphorus determinations like the modifications of the Fiske and Subbarow method. These advantages are:

1. A very considerable stability of the reduced molybdenum reagent. (4 years and more).
2. The intensity of the colour obtained after heating the test tubes for 30 minutes is highly reproducible, and even after waiting for 5 days the extinction has practically not changed.
3. The sensitivity of the method is high compared with other methods.

When expressed (Woods and Mellon) in "parts per Million" phosphorus in the solution used for colorimetry then we find a sensitivity of 0.34, for other methods we always find a higher value.

Department of Medical Chemistry,
University of Leyden

REFERENCES

1. Fiske, C. H. and Y. Subbarow, J. Biol. Chem. **66**, 275 (1925).
2. King, E. J., Biochem. J. **26**, 292 (1932).
3. Lowry, O. H. and Lopez, J. A., J. Biol. Chem. **162**, 421 (1946).
4. Berenblum, J. and E. Chain, Biochem. J. 32, 286 (1938).
5. Zinzadse, Sch. R., Ztschr. f. Pflanzenernährung Düngung und Bodenkunde XV, 129 (1930).
6. Weil-Malherbe, H., *Hoppe Seyler Thierfelder*, Handbuch der Physiologischen und Pathologischen Analyse, Berlin B. III, S. 460. Aufl. 10, 1955.
7. Meyer, A. E. T. H., these Proc. Series **B 60**, 37 (1957).
8. Hirata, A. A. and D. Appleman, Anal. Chem. **31**, 2097 (1959).
9. Woods, J. P. and M. G. Millon, Anal. Chem. **13**, 760 (1941).
10. Bernhart, D. N. and A. R. Wreath, Anal. Chem. **27**, 440 (1955).

MECHANICS

BENDING OF AN INFINITE BEAM RESTING ON AN ELASTIC HALF-SPACE

BY

J. G. LEKKERKERKER [1])

(Communicated by Prof. W. T. KOITER at the meeting of May 28, 1960)

1. *Introduction*

An infinite beam, having a constant bending stiffness B, rests on the plane boundary of an elastic half-space (modulus of elasticity E, POISSON's ratio ν). The area of contact between the beam and the elastic half space is an infinite strip of width $2b$ (fig. 1); the deflection of the beam is assumed to be constant over its width. We neglect shear deformations of the beam, and we restrict ourselves to the case of loading by a single concentrated load.

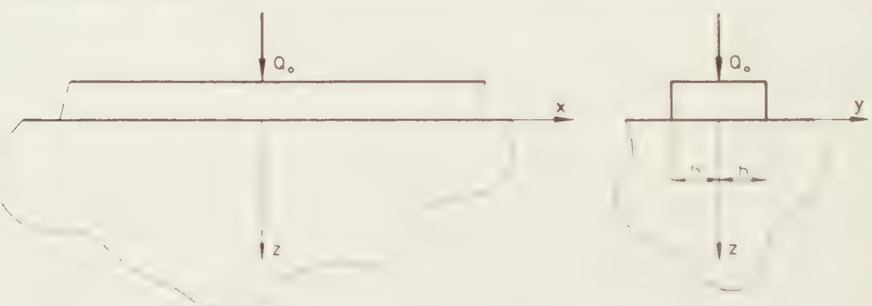

Fig. 1. Beam, resting on an elastic half-space, loaded by a concentrated load.

The classical approach to the problem of a beam on an elastic foundation is based on WINKLER's assumption [10] [2]). In this assumption the foundation is replaced by a system of springs, continuously distributed over the length of the beam, and the local deflection is uniquely determined by the local pressure. Actually, the deflection of the foundation depends of course on the entire distribution of pressure over the contact area between beam and half-space.

In order to allow for this interaction of load and deflection at different points, WIEGHARDT [9] introduces an improved assumption that the deflection at a point x due to the load $q\,d\xi$ at a point ξ is described by an exponential function

$$w(x) = q\,d\xi \cdot c \cdot e^{-\alpha|x-\xi|}. \tag{1}$$

[1]) Laboratory of Applied Mechanics, Technological University, Delft, the Netherlands.

[2]) Numbers in square brackets refer to the bibliography at the end of the paper.

which assumption is based on empirical data obtained by Föppl [2], and it has been applied and again confirmed experimentally by de Pater [4].

Wieghardt was fully aware that his assumption represents no more than a crude approximation because it reduces the actual two-dimensional problem of contact between beam and half-space to a one-dimensional problem. In fact, the deflection at a point x, y of the boundary of the half-space due to a load $p\,d\xi\,d\eta$ on an element of area at a point ξ, η, is given by Boussinesq's formula

$$w(x, y) = \frac{1-\nu^2}{\pi E} \frac{p\,d\xi\,d\eta}{\sqrt{(x-\xi)^2+(y-\eta)^2}}. \tag{2}$$

An important advance was achieved by Biot [1]. As a first approximation he assumed a constant contact pressure over the width of the contact area; the magnitude of the local contact pressure is found from the condition that the average deflection of the foundation over the width equals the beam deflection. In a second approximation the contact pressure was again assumed constant over $^3/_4$ of the width and slightly higher at the outer ends, in order to obtain approximately constant deflections over the contact width. A shortcoming of Biot's approach is that it cannot account for the effect of the singularities in the pressure distribution along the edges of the strip of contact.

Recently, Rvachev [5] attacked the problem anew, starting from the two-dimensional integral equation, resulting from Boussinesq's fundamental solution for the half-space

$$w(x, y) = \frac{1-\nu^2}{\pi E} \int\limits_{-\infty}^{+\infty} d\xi \int\limits_{-b}^{+b} \frac{p(\xi, \eta)}{\sqrt{(x-\xi)^2+(y-\eta)^2}}\, d\eta, \tag{3}$$

where $w(x, y)$ for $|y| \leqq b$ equals the beam deflection, the width of the beam being $2b$. Applying a Fourier-transformation, Rvachev obtains a one-dimensional integral equation for the Fourier-transform of the contact pressure. The solution of this integral equation is obtained in the form of a series of Mathieu-functions. Rvachev's solution is valid for arbitrary prescribed deflections over the contact area, but his numerical evaluation is restricted to the special case of a constant deflection over the width of the contact area. This numerical evaluation of the solution seems to be rather cumbersome, and Rvachev does not give any results on the distribution of bending moments and deflections of the beam; his graphs show only the distribution of contact pressure over the width of the contact area for several wave lengths of the Fourier-transform.

In the present paper we shall show how an approximate solution can be obtained by solving the basic integral equation for small and for large wave lengths and linking these asymptotic solutions. The result turns out to be completely satisfactory since a good accuracy is achieved while the numerical computation requires only a small effort.

2. FOURIER-*transforms of the basic equations*

The deflection of the beam will have to satisfy the equation

$$B\frac{d^4w}{dx^4} = Q_0\cdot\delta(0) - q(x), \tag{4}$$

where

$$q(x) = \int_{-b}^{+b} p(x, y)\, dy, \tag{5}$$

and $\delta(0)$ denotes the DIRAC delta function.

We now introduce the following FOURIER-transforms

$$\frac{1}{\sqrt{2\pi}}\int_{-\infty}^{\infty} w(x)\, e^{i\lambda x}\, dx = W(\lambda). \tag{6}$$

$$\frac{1}{\sqrt{2\pi}}\int_{-\infty}^{\infty} p(x, y)\, e^{i\lambda x}\, dx = P(\lambda, y), \tag{7}$$

$$\frac{1}{\sqrt{2\pi}}\int_{-\infty}^{\infty} q(x)\, e^{i\lambda x}\, dx = Q(\lambda). \tag{8}$$

Equations (4) and (5) are transformed into

$$\lambda^4 BW(\lambda) = \frac{Q_0}{\sqrt{2\pi}} - Q(\lambda). \tag{9}$$

$$Q(\lambda) = \int_{-b}^{+b} P(\lambda, y)\, dy. \tag{10}$$

In transforming the basic integral equation (3), we use the well-known BESSEL function relation

$$\int_{-\infty}^{+\infty} \frac{e^{i\lambda x}\, dx}{\sqrt{x^2+y^2}} = 2K_0(|\lambda y|), \tag{11}$$

where $K_0(z)$ denotes the modified BESSEL function of the second kind [8]. The resulting transformed equation is

$$W(\lambda) = \frac{2(1-\nu^2)}{\pi E}\int_{-b}^{+b} P(\lambda, \eta)\cdot K_0\{|\lambda(\eta - y)|\}\, d\eta. \tag{12}$$

The problem is now to find the solution $P(\lambda, y)$ of the integral equation (12). Once this solution has been obtained, we can insert $P(\lambda, y)$ in (10), which yields $Q(\lambda)$ in terms of $W(\lambda)$, and we next substitute $Q(\lambda)$ into (9), which gives $W(\lambda)$ in terms of the given load Q_0. The deflection $w(x)$ and the bending moment in the beam are finally obtained by the inverse FOURIER transformations.

3. *The solution of the integral equation for small values of λb*

For sufficiently small values of λb, we retain only the first two terms of the series expansion for the modified BESSEL function

$$K_0\{|\lambda(\eta-y)|\} = -\log\{\tfrac{1}{2}|\lambda(\eta-y)|\} - \gamma, \tag{13}$$

in which γ denotes EULER's constant (0,577216), and replace the kernel in the integral equation (12) by this expansion. The approximate solution of the integral equation is now

$$P(\lambda, y) = -\frac{EW(\lambda)}{2(1-\nu^2)\left\{\log\left|\frac{\lambda b}{4}\right| + \gamma\right\}\sqrt{b^2-y^2}}, \tag{14}$$

which is easily to be verified, using the results (A1) and (A2) of the Appendix.

In order to estimate the error of our approximation we calculate the right-hand member of our integral equation (12), using our approximate solution (14) and a *higher* approximation for the modified BESSEL function

$$\left\{\begin{aligned} K_0\{|\lambda(\eta-y)|\} &= -\log\{\tfrac{1}{2}|\lambda(\eta-y)|\} - \gamma \\ &\quad - \left\{\frac{\lambda(\eta-y)}{2}\right\}^2 [\log\{\tfrac{1}{2}|\lambda(\eta-y)|\} + \gamma - 1]. \end{aligned}\right. \tag{15}$$

Instead of a result $W(\lambda)$, independent of y, we obtain (cf. Appendix)

$$W(\lambda)\left[1 + \frac{\frac{1}{8}\left(2\gamma+1+2\log\left|\frac{\lambda b}{4}\right|\right)\lambda^2 y^2 + \frac{1}{16}\left(2\gamma-1+2\log\left|\frac{\lambda b}{4}\right|\right)\lambda^2 b^2}{\log\left|\frac{\lambda b}{4}\right| + \gamma}\right].$$

An improved approximate solution is now obtained by adding a first correction, obtained from the integral equation

$$\left\{\begin{aligned} &\frac{2(1-\nu^2)}{\pi E}\int_{-b}^{+b} P_1(\lambda,\eta)\,[-\log\{\tfrac{1}{2}|\lambda(\eta-y)|\} - \gamma]\,d\eta = \\ &\qquad = -W(\lambda)\,\frac{\frac{1}{8}\left(2\gamma+1+2\log\left|\frac{\lambda b}{4}\right|\right)\lambda^2 y^2 + \frac{1}{16}\left(2\gamma-1+2\log\left|\frac{\lambda b}{4}\right|\right)\lambda^2 b^2}{\log\left|\frac{\lambda b}{4}\right| + \gamma}. \end{aligned}\right. \tag{16}$$

The solution of this equation is (cf. Appendix)

$$\left\{\begin{aligned} P_1(\lambda, y) &= \frac{EW(\lambda)}{2(1-\nu^2)\left\{\log\left|\frac{\lambda b}{4}\right| + \gamma\right\}}\,\frac{1}{\sqrt{b^2-y^2}}\,\cdot \\ &\qquad \cdot\left[\left\{\frac{2\gamma+3}{8} + \tfrac{1}{4}\log\left|\frac{\lambda b}{4}\right|\right\}\lambda^2 b^2 - \left\{\frac{2\gamma+1}{4} + \tfrac{1}{2}\log\left|\frac{\lambda b}{4}\right|\right\}\lambda^2 y^2\right]. \end{aligned}\right. \tag{17}$$

Hence our second approximation to the solution of the integral equation (12) is

$$(18)\quad \left\{\begin{aligned} P(\lambda, y) &= \frac{EW(\lambda)}{2(1-\nu^2)\left\{\log\left|\frac{\lambda b}{4}\right|+\gamma\right\}}\frac{1}{\sqrt{b^2-y^2}}\Bigg[-1+\\ &+\left\{\frac{2\gamma+3}{8}+\tfrac{1}{4}\log\left|\frac{\lambda b}{4}\right|\right\}\lambda^2b^2-\left\{\frac{2\gamma+1}{4}+\tfrac{1}{2}\log\left|\frac{\lambda b}{4}\right|\right\}\lambda^2y^2\Bigg].\end{aligned}\right.$$

Inserting this result in (10) yields

$$(19)\qquad Q(\lambda) = -\frac{\pi E}{2(1-\nu^2)}\cdot\frac{W(\lambda)}{\log\left|\frac{\lambda b}{4}\right|+\gamma}\cdot(1-\tfrac{1}{4}\lambda^2b^2),$$

where the second term between brackets represents the first correction due to the solution of (17).

Substituting this value into (9) gives

$$(20)\qquad W(\lambda) = \frac{Q_0}{\sqrt{2\pi}\left[\lambda^4B-\dfrac{\pi E}{2(1-\nu^2)\left\{\log\left|\frac{\lambda b}{4}\right|+\gamma\right\}}(1-\tfrac{1}{4}\lambda^2b^2)\right]}.$$

4. *The solution of the integral equation for large values of λb*

In the integral equation (12) we make the substitution

$$(21)\qquad \lambda(y+b)=y^*,$$

and we shall obtain an approximate solution of the equation

$$(22)\qquad W(\lambda) = \frac{2(1-\nu^2)}{\pi E\lambda}\int_0^{2\lambda b} P^*(\lambda,\eta^*)\,K_0(|\eta^*-y^*|)\,d\eta^*,$$

in which P^* and η^* are substitutions in accordance with (21).

When λb is large we can obtain an approximate solution, if we replace this upper limit $2\lambda b$ by ∞. In view of the asymptotic behavior of $K_0(|\eta^*-y^*|)$, this approximation is valid except near the upper limit $2\lambda b$.

The solution of the integral equation

$$(23)\qquad \frac{1}{\pi}\int_0^\infty m(\xi)\,K_0(|x-\xi|)\,d\xi = 1,$$

is known in the form [3]

$$(24)\qquad m(x) = \frac{e^{-x}}{\sqrt{\pi x}}+\frac{2}{\sqrt{\pi}}\int_0^{\sqrt{x}} e^{-t^2}\,dt.$$

Hence the solution of (22) is approximately

$$P^*(\lambda, y^*) = \frac{E\lambda W(\lambda)}{2(1-\nu^2)}\left[\frac{e^{-y^*}}{\sqrt{\pi y^*}} + \frac{2}{\sqrt{\pi}}\int_0^{\sqrt{y^*}} e^{-t^2}\,dt\right]. \tag{25}$$

The solution (25) is shown by fig. 2 by a drawn line. It is in fact the FOURIER-transform of a pressure distribution which gives a deflection, independent of y^* on that part of the boundary of the elastic half-space,

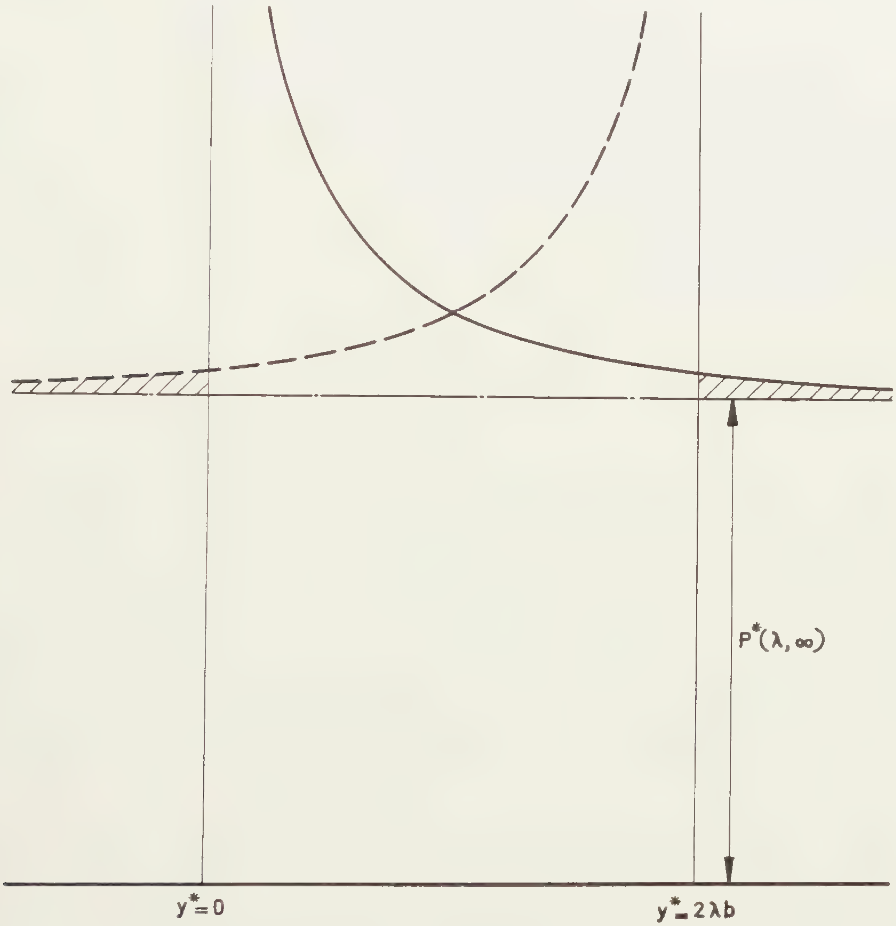

Fig. 2. Contact pressure according to the assumption that the deflection is a constant for $y^* > 0$.

for which $y^* > 0$. Actually we should have a deflection, which is independent of y^* on a segment $0 < y^* < 2\lambda b$. A qualitative picture of the actual solution is given in fig. 3.

A pressure distribution according to the drawn line in fig. 2, on which is superimposed a pressure distribution according to the dashed line (which has the same shape) gives a deflection, independent of y^* in the

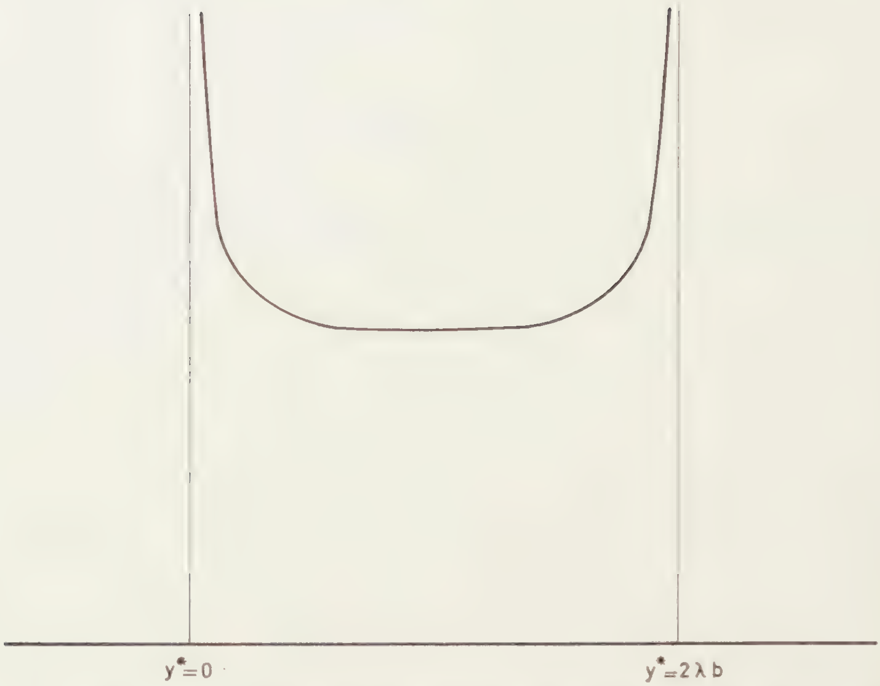

Fig. 3. Sketch of the actual contact pressure distribution over the width of the beam.

region $0<y^*<2\lambda b$, equal to twice the prescribed deflection, and which at infinity tends to the prescribed constant deflection. When we subtract from this combined pressure distribution a constant pressure, i.e. the value at infinity $P^*(\lambda, \infty)$ we have the prescribed deflection in the range $0<y^*<2\lambda b$ and an additional pressure in the ranges $y^*<0$ and $y^*>2\lambda b$, indicated by the shaded areas in fig. 2.

A good approximation for the FOURIER-transform $Q(\lambda)$ is now obtained if we neglect the effect of the shaded parts in fig. 2. We then get the approximation

$$Q(\lambda) = \frac{2}{\lambda} \int_0^{2\lambda b} P^*(\lambda, y^*)\, dy^* - \frac{1}{\lambda} \int_0^{2\lambda b} P^*(\lambda, \infty)\, dy^*. \tag{26}$$

Since the removal of the pressure, represented by the shaded areas would increase the pressure in the range $0<y^*<2\lambda b$, this approximation yields a *lower bound.*

Because

$$P^*(\lambda, \infty) = \frac{E\lambda W(\lambda)}{2(1-\nu^2)}.$$

the result is

$$Q(\lambda) > \frac{E W(\lambda)}{1-\nu^2} \left[(2\lambda b + \tfrac{1}{2})\, E_2(\sqrt{2\lambda b}) + \sqrt{\frac{2\lambda b}{\pi}} \cdot e^{-2\lambda b} - \lambda b \right], \tag{27}$$

in which $E_2(x)$ denotes the *error* function

$$(28) \qquad E_2(x) = \frac{2}{\sqrt{\pi}} \cdot \int_0^x e^{-t^2}\, dt.$$

An *upper bound* for $Q(\lambda)$ is obtained by adding the resultant of the shaded pressure distribution in fig. 2, i.e.

$$(29) \qquad Q(\lambda) < \frac{E\,W(\lambda)}{1-\nu^2}\,(\lambda b + \tfrac{1}{2}).$$

5. *The solution of the integral equation for arbitrary values of* λb

For arbitrary values of λb, $W(\lambda)$ can be written in the form

$$(30) \qquad W(\lambda) = \frac{Q_0}{\sqrt{2\pi}\left[\lambda^4 B + \frac{E}{1-\nu^2} f(\lambda b)\right]},$$

where

$$(31) \qquad f(\lambda b) = -\frac{\pi}{2}\,\frac{1-\frac{1}{4}(\lambda b)^2}{\log\left|\frac{\lambda b}{4}\right| + \gamma}, \qquad (\lambda b \text{ small}),$$

$$(32) \qquad f(\lambda b) = (2\lambda b + \tfrac{1}{2})\,E_2(\sqrt{2\lambda b}) + \sqrt{\frac{2\lambda b}{\pi}}\cdot e^{-2\lambda b} - \lambda b, \qquad (\lambda b \text{ large}),$$

as follows from (20) and (29).

In fig. 4 there has been plotted $f(\lambda b) - \lambda b$ against λb, using the asymptotic formula (32), and using the formula which is valid for small values of λb (31). For comparison there has been drawn also the curve for small values of λb which follows from the first approximation (14). These curves are given in dashed lines. They are connected by a drawn line from which the right values of $f(\lambda b)$ for arbitrary λb can be estimated with a good accuracy. The error of our interpolation in $f(\lambda b)$ apparently does not exceed 0,001 anywhere. The actual relative accuracy is even better, because in (30) the term $\lambda^4 B$ has to be added to $E f(\lambda b)/(1-\nu^2)$. Table 1

TABLE I

λb	0	2	4	6	8
0.3	0.763	0.786	0.808	0.830	0.853
0.4	0.875	0.896	0.918	0.939	0.961
0.5	0.982	1.003	1.024	1.045	1.066
0.6	1.086	1.107	1.128	1.148	1.169
0.7	1.190	1.210	1.231	1.251	1.272
0.8	1.292	1.313	1.333	1.353	1.374
0.9	1.394	1.415	1.435	1.455	1.476
1.0	1.496	1.516	1.536	1.557	1.577
1.1	1.597	1.617	1.637	1.657	1.677
1.2	1.698	1.718	1.738	1.758	1.778
1.3	1.798	1.818	1.838	1.858	1.879
1.4	1.899				

has been obtained from our graph; for $\lambda b < 0.3$ and $\lambda b > 1.4$ the asymptotic formulae are applicable with at least three-figure accuracy.

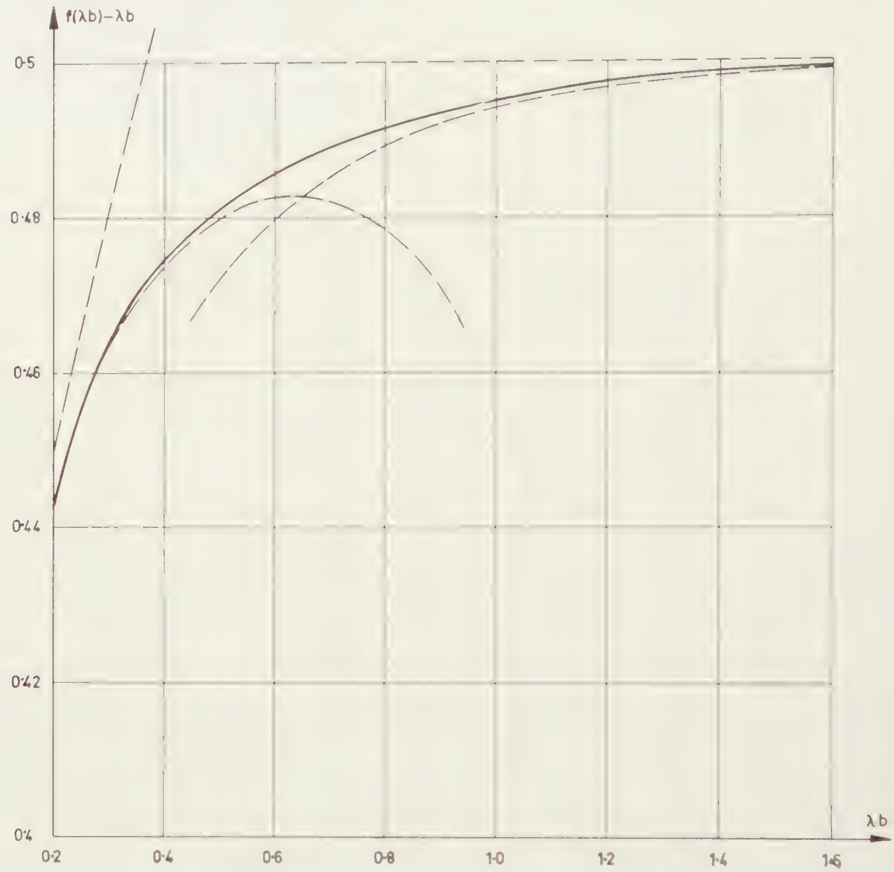

Fig. 4. The linking of the asymptotic solutions.

6. *The inverse transformation*

From $W(\lambda)$ we can derive the deflection $w(x)$ by the inverse FOURIER-transformation

$$w(x) = \frac{1}{\sqrt{2\pi}} \int_{-\infty}^{\infty} W(\lambda)\, e^{-i\lambda x}\, d\lambda. \tag{33}$$

Because $W(\lambda) = W(-\lambda)$ this is equivalent to

$$w(x) = \sqrt{\frac{2}{\pi}} \int_{0}^{\infty} W(\lambda) \cos \lambda x \, d\lambda. \tag{34}$$

We now introduce the following nondimensional variables

$$\frac{x}{b} = \bar{x}, \quad \lambda b = \varphi, \quad \frac{B(1-\nu^2)}{Eb^4} = \beta. \tag{35}$$

We then can write

$$w(\bar{x}) = \frac{1-\nu^2}{\pi} \cdot \frac{Q_0}{bE} \cdot \int_0^\infty \frac{\cos(\bar{x}\varphi)\, d\varphi}{\beta\varphi^4 + f(\varphi)}. \tag{36}$$

The bending moment M is equal to $B \cdot d^2w/dx^2$, so

$$M(\bar{x}) = -\frac{Q_0 b}{\pi} \cdot \beta \cdot \int_0^\infty \frac{\varphi^2 \cos(\bar{x}\varphi)\, d\varphi}{\beta\varphi^4 + f(\varphi)}. \tag{37}$$

The pressure $q(x)$ finally can be derived from the inverse transformation

$$q(x) = \sqrt{\frac{2}{\pi}} \int_0^\infty Q(\lambda) \cos(\lambda x)\, d\lambda, \tag{38}$$

and because

$$Q(\lambda) = \frac{E}{1-\nu^2} W(\lambda)\, f(\lambda b).$$

this is to be written

$$q(\bar{x}) = \frac{Q_0}{\pi b} \cdot \int_0^\infty \frac{f(\varphi) \cos(\bar{x}\varphi)\, d\varphi}{\beta\varphi^4 + f(\varphi)}. \tag{39}$$

To evaluate the integrals in (36), (37) and (39), we can split them up into a part for φ ranging from 0 to, say, 5, to be handled numerically and a part for φ ranging from 5 to infinity, to be handled analytically, by neglecting $f(\varphi)$ with respect to $\beta\varphi^4$. Dealing with (36), there is the difficulty, that the integrand has a (logarithmic) singularity at $\varphi = 0$. We can subtract out this singularity and the integral in (36) is evaluated as follows

$$\left\{ \begin{aligned} \int_0^\infty \frac{\cos(\bar{x}\varphi)\, d\varphi}{\beta\varphi^4 + f(\varphi)} = \int_0^5 \left\{ \frac{1}{\beta\varphi^4 + f(\varphi)} + \frac{2}{\pi} \log\varphi \right\} \cos(\bar{x}\varphi)\, d\varphi + \\ - \int_0^5 \frac{2}{\pi} \log\varphi \cos(\bar{x}\varphi)\, d\varphi + \int_0^\infty \frac{\cos(\bar{x}\varphi)\, d\varphi}{\beta\varphi^4}. \end{aligned} \right. \tag{40}$$

The integral in the expression (36) for $w(\bar{x})$ tends to $1/\bar{x}$, when $\bar{x}$ tends to infinity, which can be seen by partial integration:

$$\int_0^\infty \frac{\cos(\bar{x}\varphi)\, d\varphi}{\beta\varphi^4 + f(\varphi)} = \frac{\sin(\bar{x}\varphi)}{\bar{x}} \cdot \frac{1}{\beta\varphi^4 + f(\varphi)} \Bigg|_0^\infty + \frac{1}{\bar{x}} \int_0^\infty \frac{4\beta\varphi^4 + \varphi f'(\varphi)}{\{\beta\varphi^4 + f(\varphi)\}^2} \cdot \frac{\sin(\bar{x}\varphi)\, d\varphi}{\varphi}.$$

Since the quotient

$$\frac{4\beta\varphi^4 + \varphi f'(\varphi)}{\{\beta\varphi^4 + f(\varphi)\}^2}$$

satisfies the DIRICHLET conditions, the integral tends to $\pi/2$ times the value of this quotient, when φ tends to zero (see for ex. [7]). From (31)

it is clear that for small values of φ

$$f(\varphi) = -\frac{\pi}{2}\cdot\frac{1}{\log\varphi}, \quad f'(\varphi) = \frac{\pi}{2}\cdot\frac{1}{\log^2\varphi}\cdot\frac{1}{\varphi},$$

and

(41) $$\lim_{x\to\infty}\int_0^\infty \frac{\cos(\bar{x}\varphi)\,d\varphi}{\beta\varphi^3 + f(\varphi)} = \frac{1}{\bar{x}}.$$

Hence the asymptotic behaviour of the deflection for $\bar{x}\to\infty$ is

(42) $$w(\bar{x}) \to \frac{1-\nu^2}{\pi}\cdot\frac{Q_0}{bE}\cdot\frac{1}{\bar{x}}.$$

By differentiation we obtain the asymptotic behaviour of the bending moment

(43) $$M(\bar{x}) \to \frac{Q_0 b}{\pi}\cdot\beta\cdot\frac{2}{\bar{x}^3}.$$

7. *Numerical results and discussion*

Some results of numerical computations are represented in figs. 5, 6 and 7, showing the deflection curves and the bending moments for different values of β. For comparison with the present theory, the results of WINKLER's hypothesis are given in dashed lines, where WINKLER's foundation constant has been chosen in such a way that the maximum bending moment coincides with our result.

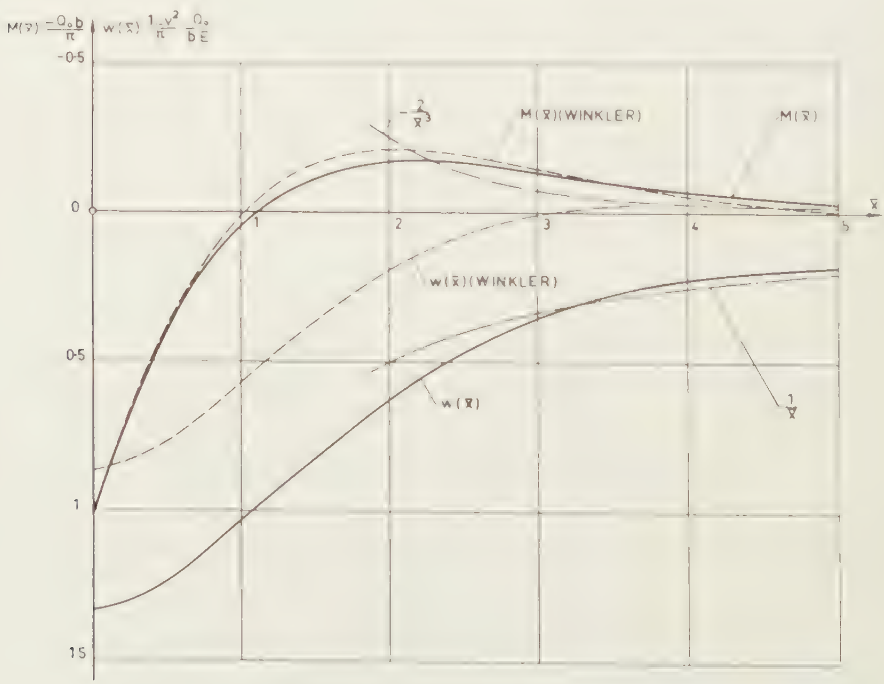

Fig. 5. Deflection and bending moment curves for $\beta = 1$.

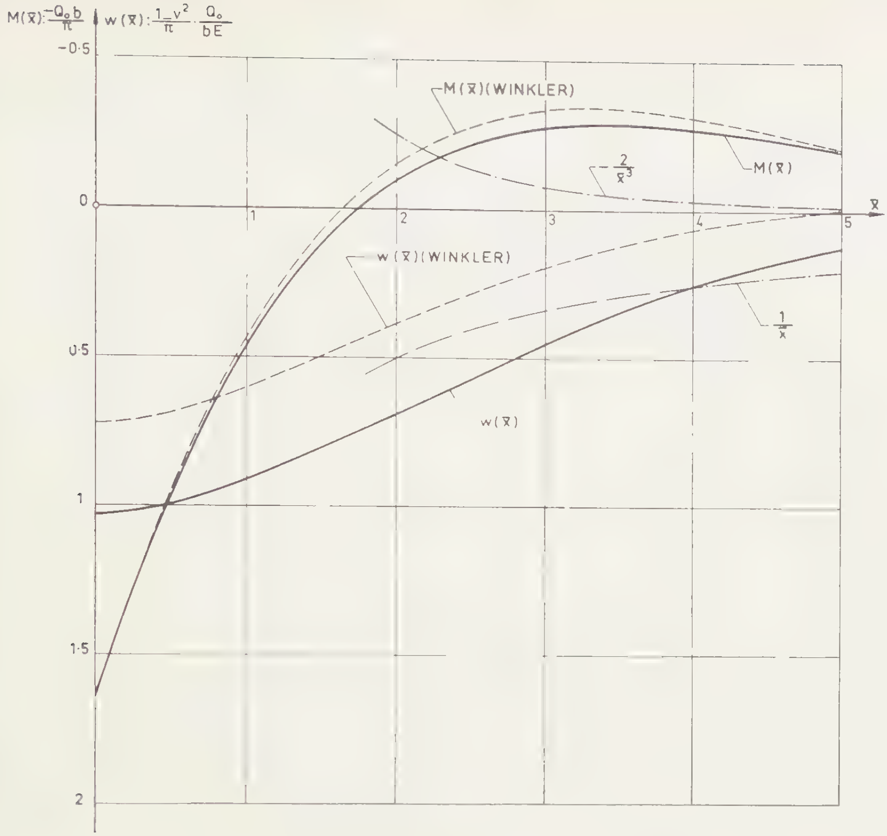

Fig. 6. Deflection and bending moment curves for $\beta = 5$.

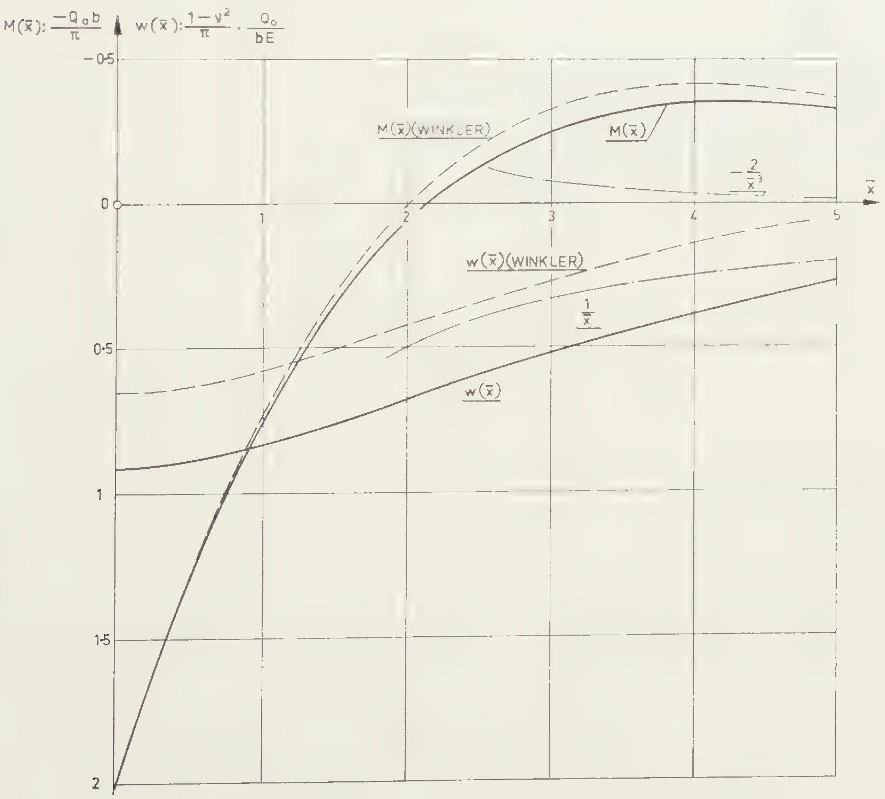

Fig. 7. Deflection and bending moment curves for $\beta = 10$.

Table II shows the comparison with BIOT's approximate results, which give a good approximation to his theory.

TABLE II

β	BIOT's results: $M_{\max} = Q_0 b/\pi \cdot 0.332\,\pi\ [C\,\beta]^{0,277}$ Uniform pressure over the width of the beam ($C = 1$)	Uniform deflection over the width of the beam ($C = 1.13$)	Present results
1	1.04 $Q_0 b/\pi$	1.08 $Q_0 b/\pi$	1.023 $Q_0 b/\pi$
5	1.63 ,,	1.69 ,,	1.641 ,,
10	1.97 ,,	2.04 ,,	2.005 ,,
25	2.54 ,,	2.63 ,,	2.609 ,,
50	3.08 ,,	3.19 ,,	3.170 ,,
75	3.45 ,,	3.57 ,,	3.552 ,,
100	3.74 ,,	3.86 ,,	3.848 ,,

Acknowledgement

The author is greatly indebted to Professor W. T. KOITER for many helpful suggestions and for his stimulating interest in the investigation. The investigation arose out of a problem on which the author worked for the Netherlands Railways Company, and the author is also indebted to this Company and Professor A. D. DE PATER for permission to publish the present results.

Appendix

Some integrals, which have been used, are listed below (see for the derivation of these integrals for ex. [6])

(A 1)
$$\int_{-b}^{+b} \frac{\log\{\frac{1}{2}|\lambda(\eta - y)|\}}{\sqrt{b^2 - \eta^2}}\, d\eta = \pi \log\left|\frac{\lambda b}{4}\right|,$$

(A 2)
$$\int_{-b}^{+b} \frac{d\eta}{\sqrt{b^2 - \eta^2}} = \pi.$$

(A 3)
$$\int_{-b}^{+b} \frac{\eta\, d\eta}{\sqrt{b^2 - \eta^2}} = 0.$$

(A 4)
$$\int_{-b}^{+b} \frac{\eta^2 d\eta}{\sqrt{b^2 - \eta^2}} = \frac{\pi}{2}\, b^2.$$

(A 5)
$$\int_{-b}^{+b} \frac{\{\frac{1}{2}\lambda(\eta - y)\}^2 \log\{\frac{1}{2}|\lambda(\eta - y)|\}}{\sqrt{b^2 - \eta^2}}\, d\eta = \frac{\lambda^2\pi}{8}\left\{(2y^2 + b^2)\log\left|\frac{\lambda b}{4}\right| + 3y^2 - \frac{b^2}{2}\right\}.$$

(A 6)
$$\int_{-b}^{+b} \frac{(b^2 - 2\eta^2)\,[\log\{\frac{1}{2}|\lambda(\eta - y)|\} + \gamma]\, d\eta}{\sqrt{b^2 - \eta^2}} = -\frac{\pi}{2}\,(b^2 - 2y^2).$$

REFERENCES

1. Biot, M. A., Bending of an Infinite Beam on an Elastic Foundation. Journal of Appl. Mech., **4**, A–1 (1937).
2. Föppl, A., Vorlesungen über Technische Mechanik, 10. Auflage. Leipzig, 268 (1927).
3. Koiter, W. T., Approximate solution of Wiener-Hopf type integral equations with applications. Proc. Kon. Ned. Akad. van Wetensch., Series **B 57**, 558–579 (1954).
4. Pater, A. D. de, Inleidend Onderzoek naar het dynamisch gedrag van Spoorstaven. Thesis, Delft, 9 (1948).
5. Rvachev, V. L., Pressure on an elastic Half-space of a Stamp, having the Form of a Strip (in russian). Prikladnaia Matematika i Mechanika, 248–254 (1956).
6. Schmeidler, W., Integralgleichungen mit Anwendungen in Physik und Technik. Leipzig, 58 (1950).
7. Sneddon, I. N., Fourier Transforms. McGraw-Hill Book Cy, Inc., 12 (1951).
8. Watson, G. N., A Treatise on the Theory of Bessel Functions. Cambridge, 185 (1952).
9. Wieghardt, K., Über den Balken auf nachgiebiger Unterlage. Zeitschr. für Angew. Math. und Mech., **2**, 165 (1922).
10. Winkler, E., Die Lehre von der Elastizität und Festigkeit. Prag, 182 (1867).

PALEONTOLOGY

UN DIAGRAMME POLLINIQUE SIMPLIFIE D'UNE COUCHE DE "GYTTJA", SITUEE A POUEYFERRE PRES DE LOURDES (PYRENEES FRANÇAISES CENTRALES), DATE PAR LA METHODE DU RADIO-CARBONE

PAR

HL. DE VRIES †, F. FLORSCHÜTZ ET JOSEFA MENÉNDEZ AMOR

(Communicated by Prof. I. M. VAN DER VLERK at the meeting of May 28, 1960)

Abstract

A simplified radiocarbon dated pollen diagram from the Central French Pyrenees.

This diagram reflects the development of the forests in the neighbourhood of Lourdes during the last part of the third stadial phase (Pleni-glacial C) of the Würm glaciation, the Late glacial and the beginning of the Holocene.

Vers la fin du Pléistocène il existait aux environs de Lourdes quelques lacs, formés dans des dépressions, probablement d'origine glaciaire. Ces lacs se remplissent graduellement d'argile, de "gyttja" et de tourbe. Les sédiments, déposés dans trois de ces lacs, situés dans le voisinage de Poueyferré, de Monge et de Lourdes (latitude ± 43°, longitude ± 0° Gr., altitude ± 420 m), ont été étudiés paléobotaniquement par les deux auteurs mentionnés en dernier lieu, en collaboration avec Mlle Prof. Dr H. Alimen qui s'occupait de la description des conditions géologiques. Les résultats définitifs seront publiés sous peu.

En anticipation, la partie inférieure du diagramme de Poueyferré, comprenant le trajet pléistocène et le commencement de l'Holocène, a été reproduite ici sous une forme simplifiée. Elle est pourvue de dates C 14 en six endroits, aux profondeurs d'à peu près 350, 445, 510, 645, 660 et 795 cm. Les échantillons prélevés pour la datation absolue, aux profondeurs de ± 445, 645 et 795 cm, ont été pris en 1957 à la même place que le matériel pour l'analyse pollinique, les autres, à ± 350, 510 et 660 cm, en 1958 à une distance de quelques mètres. Ces dates sont respectivement 9.260 ± 100 ans, 12.310 ± 130 ans, 12.930 ± 135 ans, 13.600 ± 110 ans, 18.790 ± 225 ans et 15.800 ± 120 ans avant le présent. Elles forment une suite logique, abstraction faite de celle à une profondeur d'environ 660 cm qui n'harmonise pas avec les autres. Il est possible que cette anomalie soit causée par une cryoturbation qui a occasionné une élévation de couches plus profondes.

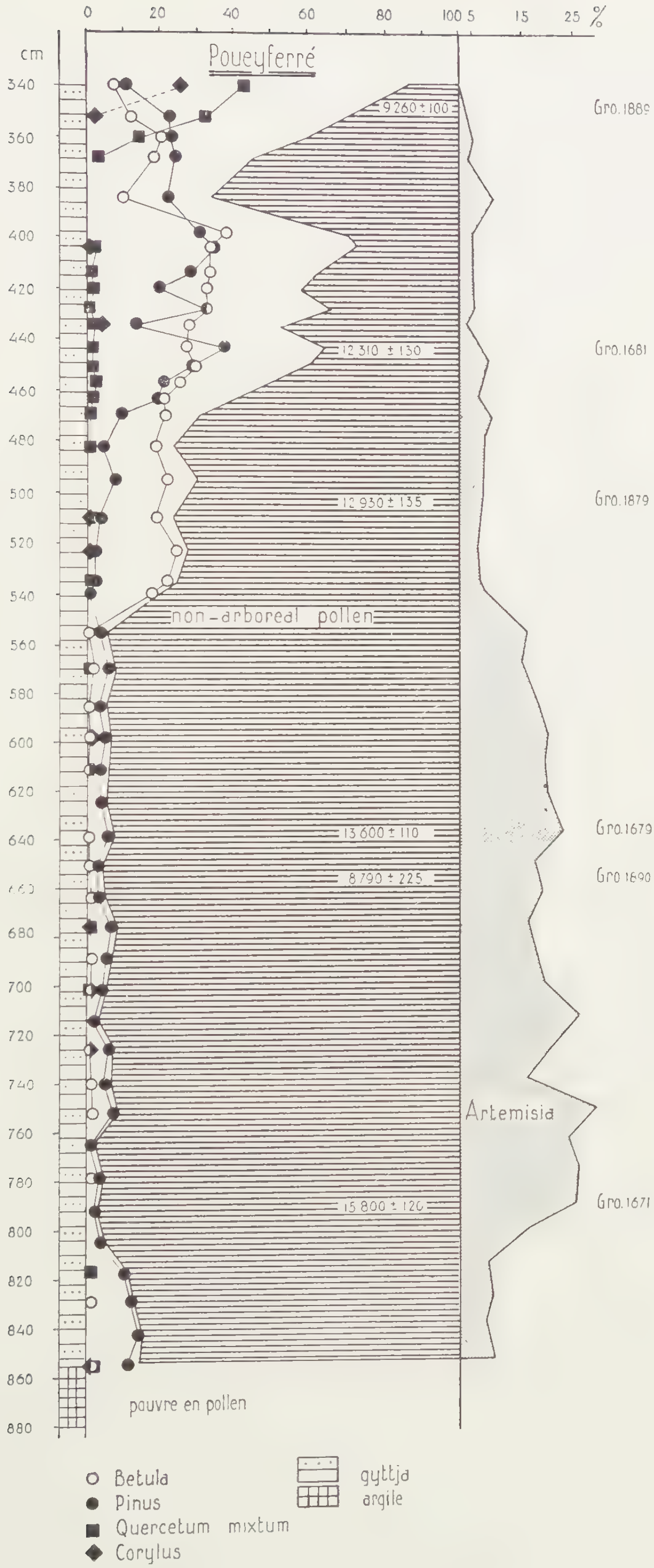
Poueyferré
cm
0
20
40
60
80
100
5
15
25
%
340
360
380
400
420
440
460
480
500
520
540
560
580
600
620
640
680
700
720
740
760
780
800
820
840
860
880
9 260 ± 100
12 310 ± 130
12 930 ± 135
13 600 ± 110
8 790 ± 225
15 800 ± 120
Gro. 1681
Gro. 1879
Gro. 1679
Gro. 1690
Gro. 1671
non-arboreal pollen
Artemisia
pauvre en pollen
Betula
Pinus
Quercetum mixtum
Corylus
gyttja
argile

Fig. 1

La plus ancienne des autres dates, 15.800, indique le début de la période tardiglaciaire, commençant, à notre avis, par le plus ancien Dryas. Par conséquent, la partie inférieure du diagramme, jusqu'à environ 800 cm, reflète probablement la fin de la troisième phase stadiale du Wurmien (Pléniglaciaire C). Il se peut que le lac date de ce temps-là.

La relation entre les pourcentages de grains de pollen d'arbres d'une part et d'arbustes et d'herbes de l'autre, est défavorable pour les premiers dans cette partie du diagramme. Elle permet de supposer qu'aux alentours de Poueyferré les arbres étaient rares. Parmi les arbustes et les herbes, *Artemisia* était évidemment assez fréquente. Les Chénopodiacées ne faisaient pas défaut non plus. Le paysage peut avoir eu un caractère steppique modéré.

Plus haut qu'environ 800 cm, la relation en question devient encore plus défavorable pour les grains de pollen d'arbres. Ce fait, combiné avec l'élévation des pourcentages d'*Artemisia*, pourrait démontrer une accentuation des conditions steppiques.

La date de 13.600 à une profondeur de $\pm$ 645 cm appartient manifestement encore au plus ancien Dryas. Vraisemblablement, le climat ne s'était pas amélioré. Quelques décimètres plus haut, cependant, là où les pourcentages de grains de pollen d'arbres montent jusqu'à peu près 25, suggérant la présence d'un paysage de parc, un tel adoucissement se manifeste. Les bouleaux dominaient, tandis qu'*Artemisia* était moins fréquente. Il semble justifié de tracer la limite entre le plus ancien Dryas et le Bolling à cette profondeur. Dans la seconde moitié du Bolling, finissant il y a à peu près 12.300 ans, l'espacement des arbres avait diminué. Des forêts de bouleaux et de pins se développèrent, subissant seulement une légère recurrence entre $\pm$ 440 et $\pm$ 435 cm, pendant l'ancien Dryas. Elles se rétablirent dans l'Allerod et devinrent même plus denses, comme le montre le spectre à $\pm$ 400 cm, dénotant une relation des pourcentages pollen d'arbres/pollen d'arbustes et d'herbes d'approximativement 70:30.

Encore une fois, pendant le Dryas récent, un paysage de parc, maintenant avec pins et bouleaux, s'installa et fut remplacé à son tour par des forêts de pins, de bouleaux et de chênes, indiquant le début de l'Holocène. La date supérieure, 9.260, se rapporte au deuxième siècle du Boréal.

L'auteur nommé en second offre ses remercîments sincères à l'Organisation Néerlandaise pour le Développement de la Recherche Scientifique (Z.W.O.) à La Haye et au Centre National de la Recherche Scientifique (C.N.R.S.) à Paris pour leurs subventions qui lui ont permis d'effectuer des sondages dans l'ancien lac de Poueyferré et ailleurs aux environs de Lourdes, afin de recueillir des échantillons pour l'analyse paléobotanique et la datation par le procédé du radio-carbone.

PHYSICS

STRUCTURE AND ZEEMAN EFFECT IN THE SPECTRA OF THE OSMIUM ATOM, Os I AND Os II

I

BY

TH. A. M. VAN KLEEF

Zeeman-laboratory, University of Amsterdam, the Netherlands

(Communicated by Prof. J. DE BOER at the meeting of January 30, 1960)

Synopsis

An investigation of published and unpublished data on the Os I spectrum resulted in the quantum interpretation of known energy levels and the detection of a number of new ones. In all, 154 of the 262 levels now known have been labelled, among which are practically all ground levels. These belong to the even electron configurations $5d^6 6s^2$ and $5d^7 6s$ whereas none could be attributed to $5d^8$. In the odd system most levels could be assigned to multiplets of the configurations $5d^6 6s6p$, $5d^5 6s^2 6p$ and $5d^7 6p$. Many of the high even states have been associated with the configurations $5d^6 6s7s$, $5d^5 6s^2 7s$ and $5d^6 6s6d$. Due to a former misinterpretation, the existing value for the ionization potential is too high. An improved value of $(8.5 \pm 0.1) V$ has been derived. Critical examination of the levels accepted by previous authors proved that 14 were fortuitous; several others not satisfying our requirements have been maintained tentatively. On the other hand 19 new levels could be established, namely 3 low even, 10 odd and 6 high even ones, so that the total numbers belonging to those three groups are now 45, 178 and 39 respectively. For practically all levels in the two groups and for about half of the high even states the g-factors are known. A complete table of all the relative energy levels with their properties is given. These account for 2968 observed lines classified as 3293 transitions, that is about 40 % of the total number of observed Os I-lines and a much bigger proportion of the total intensity. The classified lines and their intensities and observed Zeeman splittings have been listed.

Some improvement was also obtained in the analysis of the Os II spectrum. The lowest term of the $5d^5 6s^2$ configuration ($^6S_{5/2}$) could be identified. The odd system was extended with 4 new states, one of which could be interpreted as $5d^5 6s(^7S)6p\ ^8P_{9/2}$. Two existing levels have been recognized as the corresponding $^8P_{7/2}$ and $^8P_{5/2}$. This octet is the lowest odd multiplet. The number of classified Os II-lines is 162, being about 15 % of the total number of observed lines. The energy levels and classified lines have been tabulated.

1. *Introduction*

The first true regularities in the spectrum of neutral osmium were found by C. P. SNYDER in 1900, but never published. Independently a preliminary analysis of the spectrum of Os I resulting in the detection of 34 low even levels, 14 high even and 89 odd levels has been given by W. ALBERTSON [1]. His analysis was based on the wave-length data given by H. KAYSER [2], EXNER and HASCHEK [3] between 2251 Å and 4500 Å and those given

by W. F. MEGGERS [4] between 4500 Å and 8645 Å. The relative values of the levels were given to 6 figures. However, only 18 low even levels, 7 odd ones and 5 high even ones were interpreted in terms of the quantum theory. It was not possible to extend these assignments because no investigation of the Zeeman effect had been made. A number of these interpretations had to be changed in the course of our work (see sections 5–7). In 1938 ALBERTSON [5] reported that he had reobserved the spectrum at the Massachusetts Institute of Technology (M.I.T.) and recorded more than 4500 lines, of which 2169 were classified as combinations between 234 energy levels. Unfortunately he never published these results.

In 1949 J. C. VAN DEN BOSCH made observations at the M.I.T. especially on the Zeeman effect, in the region between 2350 Å and 4850 Å. Details of his experiments have been described elsewhere [6]. Magnetic fields up to about 80000 oersted have been used. In 1951 these observations were supplemented with zero field spectrograms in the region of shorter wave-lengths (<2500 Å) and Zeeman spectrograms in the region 2500 Å–4500 Å obtained by the author in the Zeeman laboratory. In 1954 H. HOOYKAAS and W. J. SURINGAR made observations in the region of longer wave-lengths (>4500 Å).

In 1952 we redetermined all term values mentioned by ALBERTSON [1] to 7 figures, by means of the data collected in the M.I.T. Tables [7], the measurements of VAN DEN BOSCH [8] and our own data (Albertson's additional unpublished data on wave lengths and terms were still unknown to us). One low even level and 6 odd ones detected by ALBERTSON were found to be erroneous. After that we extended the system with 8 new low levels and 50 new odd ones [9]. VAN DEN BOSCH made mention of these results at the Rydberg Centennial Conference on Atomic Spectroscopy in Lund in 1954 [10].

In 1954 Dr. ALBERTSON was kind enough to send all his unpublished wave-length data [11] to the Zeeman laboratory. By means of these VAN DEN BOSCH was able to extend the numerical analysis with 1 low level, 56 odd ones and 20 high even ones. Moreover he determined the g values of many levels. Of the odd levels found by the author [9] 8 were rejected. All levels and g values have finally been published in "Atomic Energy Levels" Volume III [12] (AEL). However, nothing had been done in the way of quantum interpretation since ALBERTSON's first publication [1]. Hence we attempted to extend the assignments with the aid of the complete record of data in AEL and all the wave-length and Zeeman effect material available in the Zeeman laboratory.

This investigation resulted in the detection of 3 even ground levels, 10 odd ones and 6 high even ones, and the interpretation of 40 low even levels, 95 odd ones and 19 high ones even. Details about the energy levels are given in section 3. In the sections 5–7 we shall discuss the assignments. In table I a historical survey of the progress in the analysis is given.

In section 8 the analysis of the Os II-spectrum will be considered.

TABLE I

Comparison of the results of various authors

	Total number of detected levels			Total number of observed g-values			Total number of interpreted levels		
	low even	odd	high even	low even	odd	high even	low even	odd	high even
ALBERTSON 1934	34(1) [1]	89(6)	14	—	—	—	18{5} [2]	7{2}	5{2}
VAN KLEEF 1952	41	133(8)	14	—	—	—	no changes		
V. D. BOSCH 1958	42	181(13)	34(1)	32	154	8			
VAN KLEEF 1959	45	178	39	42	174	22	40	95	19

[1]) A bracketed number denotes the number of levels rejected by the following author.
[2]) A number between braces denotes the number of misinterpreted levels.

2. *Experimental part*

The first series of experiments was made in 1951. Solid electrodes of 20 % osmium and 80 % silver made by high pressure treatment of the mixed powders were available for the purpose. The light-source was an *intermittent arc* (Back trembler) under reduced pressure. The vibrating cathode was a tungsten strip, the fixed anode a rod consisting of the osmium silver mixture. A Hilger *E* 1 *quartz prism spectrograph* was used for observations in the region 2100–2500 Å in zero magnetic field. Most of the observed lines belong to the Os II spectrum. The Zeeman effect was investigated in the region 2500–4500 Å by means of the $6\frac{1}{2}$ m *Wadsworth grating mounting*. The spectrum was not very bright and exposures of at least six hours had to be made to photograph the Zeeman patterns of the strongest lines. Moreover, the spectrograms showed a considerable number of *W*-lines owing to the tungsten counter electrode. The expectation that the M.I.T. Zeeman spectrograms could be extended in this region, was not confirmed. However, in the region above 4500 Å HOOYKAAS and SURINGAR [13] succeeded in supplementing the Zeeman effect observations considerably.

The *Weiss magnet* produced a field of about 38000 Oe at a current of 110 A, the diameter of the pole tips being 1 cm and their distance 0.6 cm. The mean current in the source was regulated at 3 A by means of a variable resistance. Exposure times varied from three to eight hours.

In order to improve the description and interpretation of the spectra it will be necessary to have the disposal of pure osmium in the form of solid metal rods. Especially in the regions above 6000 Å and below 2400 Å a good deal of new information might then be obtained, just as in the case of the iridium spectrum [14, 15].

3. *Energy levels*

In table II all levels of Os I and their properties have been displayed. The subsequent columns show 1. the level symbol established according

to a well-known system [16], 2. the numerical value in kayser (cm^{-1}) relative to the lowest state, 3. the J-value, 4. the g-factor and 5. the interpretation. The even and odd level groups have been listed separately; in each group the order is according to decreasing binding energy. Tentative identifications, g-values and levels have been denoted by a question-mark. The identifications will be discussed in the sections 5–7.

The new level values have been averaged from all reliable combinations involved after having converted the wave-lengths in air into vacuum wave number values by means of EDLEN's tables [17] and the values taken from Atomic Energy Levels [12] have been checked and re adjusted when necessary. Apart from a few misprints, which have been corrected, 13 odd levels and one high even level have been cancelled in the course of this analysis because of insufficient accuracy of the intervals, double classifications and disagreeing Zeeman patterns. They were located at 28609, 46947, 47845, 47957, 48338, 48546, 48999, 49461, 49680, 49903, 50453, 50530, 53758 (this is the high even level) and 57122 K. Only for the last a g-value was known. Some high even levels also found by Van den Bosch have been called in question, because the number of combinations is somewhat too low with regard to our standard and no confirming Zeeman effect data are available. Of 44 levels the g-values have been newly determined and of the 262 levels now known 154 levels could be interpreted.

TABLE II

Relative levels in Os I

Symbol	Value	J	g	Interpretation				Notes
				low even group				
0	0.00	4	1.44	$5d^6 6s^2$		$^5D_4$		
27	2740.49	2	1.44	$5d^6 6s^2$		$^5D_2$		
41	4159.32	3	1.47	$5d^6 6s^2$		$^5D_3$		
51	5143.92	5	1.38		$5d^7(a^4F)6s$		$^5F_5$	
57	5766.14	1	1.47	$5d^6 6s^2$		$^5D_1$		
60	6092.79	0	0/0	$5d^6 6s^2$		$^5D_0$		
87	8742.83	4	1.31		$5d^7(a^4F)6s$		$^5F_4$	
101	10165.98	2	1.45	$5d^6 6s^2$		$^3P_2$		1
110	11030.58	4	1.16		$5d^7(a^4F)6s$		$^3F_4$	
113	11378.00	3	1.26		$5d^7(a^4F)6s$		$^5F_3$	
127	12774.38	2	1.00		$5d^7(a^4F)6s$		$^5F_2$	1
130	13020.07	1	0.31		$5d^7(a^4F)6s$		$^5F_1$	
133	13364.83	2	0.94		$5d^7(a^4F)6s$		$^3F_2$	2
140	14091.37	3	1.10		$5d^7(a^4F)6s$		$^3F_3$	
143	14338.99	5	1.13	$5d^6 6s^2$		$^3G_5$		1
148	14848.05	4	1.08	$5d^6 6s^2$		$^3G_4$		1
149	14852.33	6	1.14	$5d^6 6s^2$		$^3H_6$		
152	15222.57	2	1.61		$5d^7(a^4P)6s$		$^5P_2$	2
153	15390.76	3	1.54		$5d^7(a^4P)6s$		$^5P_3$	2
162	16212.41	1	1.74		$5d^7(a^4P)6s$		$^5P_1$	2

TABLE II *(continued)*

Relative levels in Os I

Symbol	Value	J	g	Interpretation		Notes
				low even group *(continued)*		
176	17667.34	1	1.40	$5d^6 6s^2$	$^3P_1$	
183	18301.40	0	0/0	$5d^6 6s^2$	$^3P_0$	1
184	18417.12	5	1.12	$5d^6 6s^2$	$^3H_5$	3, 4
189	18901.94	3	1.20	$5d^7(a^2D)6s$	$^3D_3$	
190	19048.91	0	0/0	$5d^7(a^4P)6s$	$^3P_0$	
191	19108.87	4	1.03	$5d^6 6s^2$	$^3H_4$	
194	19410.66	2	0.97	$5d^7(a^2D)6s$	$^1D_2$	
198	19893.07	4	1.06	$5d^6 6s^2$	$^1G_4$	
210	21033.45	1	0.88	$5d^7(a^2D)6s$	$^3D_1$	
211	21123.66	3	0.94	$5d^6 6s^2$	$^3G_3$	
213	21303.36	2	1.26	$5d^7(a^2D)6s$	$^3D_2$	
225	22563.65	1	1.61	$5d^7(a^4P)6s$	$^3P_1$	5
233	23317.60	2	1.27	$5d^7(a^4P)6s$	$^3P_2$	
234	23322.66	4	1.04	$5d^7(a^2G)6s$	$^3G_4$	
239	23984.58	3	1.07	$5d^6 6s^2$	$^3F_3$	
242	24291.97	5	1.14	$5d^7(a^2G)6s$	$^3G_5$	5
250	25069.71	2	0.89	$5d^6 6s^2$	$^3F_2$	
255	25593.94	3	0.97	$5d^7(a^2G)6s$	$^3G_3$	5
256	25601.55	4	1.14	$5d^6 6s^2$	$^3F_4$	5
273	27350.96	3				3, 6
281	28139.52	3	1.24			
284	28411.95	2		$5d^7(a^2P)6s$	$^3P_2$	7
293	29394.30	4				
300	30056.79	2				
317	31765.12	3				3
				odd group		
2261	22615.69	4	1.62	$5d^6 6s(a^6D)6p$	$^7D_4$	
2346	23462.90	5	1.55	$5d^6 6s(a^6D)6p$	$^7D_5$	
2501	25012.93	3	1.73	$5d^6 6s(a^6D)6p$	$^7D_3$	
2527	25275.42	2	2.04	$5d^6 6s(a^6D)6p$	$^7D_2$	
2778	27786.79	1	2.77	$5d^6 6s(a^6D)6p$	$^7D_1$	3
2795	27954.32	2	2.04	$5d^5 6s^2(a^6S)6p$	$^7P_2$	2
2833	28331.77	4	1.59	$5d^5 6s^2(a^6S)6p$	$^7P_4$	1
2837	28371.68	3	1.74	$5d^5 6s^2(a^6S)6p$	$^7P_3$	1
2909	29099.41	6	1.48	$5d^6 6s(a^6D)6p$	$^7F_6$	
2938	29381.65	3	1.49	$5d^6 6s(a^6D)6p$	$^7F_3$	4
3007	30078.28	2	1.48	$5d^6 6s(a^6D)6p$	$^7F_2$	
3027	30279.95	5	1.47	$5d^6 6s(a^6D)6p$	$^7F_5$	
3049	30499.98	0	0/0	$5d^6 6s(a^6D)6p$	$^7F_0$	3
3052	30524.92	1	1.55	$5d^6 6s(a^6D)6p$	$^7F_1$	
3059	30591.45	4	1.54	$5d^6 6s(a^6D)6p$	$^7P_4$	
3245	32457.44	2	1.84	$5d^6 6s(a^6D)6p$	$^7P_2$	
3268	32684.61	4	1.47	$5d^6 6s(a^6D)6p$	$^7F_4$	
3312	33124.48	3	1.63	$5d^6 6s(a^6D)6p$	$^7P_3$	
3412	34125.40	3	1.44	$5d^6 6s(a^6D)6p$	$^5D_3$	
3436	34365.33	5	1.42	$5d^6 6s(a^6D)6p$	$^5F_5$	

TABLE II *(continued)*

Relative levels in Os I

Symbol	Value	J	g	Interpretation		Notes
				odd group *(continued)*		
3480	34803.82	4	1.37	$5d^66s(a^6D)6p$	$^5F_5$	
3509	35090.50	2	1.57	$5d^66s(a^6D)6p$	$^5P_2$	
3561	35615.92	3	1.51	$5d^66s(a^6D)6p$	$^5P_3$	
3591	35919.55	1	1.29	$5d^66s(a^6D)6p$	$^5F_1$	
3628	36289.85	0	0/0	$5d^66s(a^6D)6p$	$^5D_0$	3
3634	36345.81	2	1.15	$5d^66s(a^6D)6p$	$^5F_2$	
3663	36634.54	2	1.36	$5d^66s(a^6D)6p$	$^5D_2$	
3680	36806.27	3	1.48	$5d^66s(a^4D)6p$	$^5D_3$	
3681	36817.94	5	1.28	$5d^66s(a^4D)6p$	$^5F_5$	
3682	36826.39	4	1.41	$5d^66s(a^6D)6p$	$^5D_4$	
3697	36979.51	1	1.31	$5d^66s(a^6D)6p$	$^5D_1$	
3780	37808.58	3	1.26	$5d^66s(a^6D)6p$	$^5F_3$	
3790	37908.77	4	1.45	$5d^66s(a^4D)6p$	$^5D_4$	
3792	37921.71	2	1.45	$5d^66s(a^4D)6p$	$^5D_2$	
3813	38130.09	4	1.24	$5d^66s(a^4D)6p$	$^5F_4$	
3824	38244.20	1	1.55	$5d^66s(a^4D)6p$	$^5D_1$	
3826	38264.16	3	1.23	$5d^66s(a^4D)6p$	$^3D_3$	
3833	38330.75	2	1.41	$5d^66s(a^4D)6p$	$^5F_2$	
3848	38486.01	3	1.61	$5d^56s^2(a^6S)6p$	$^5P_3$	
3861	38613.44	1	0.29	$5d^66s(a^4D)6p$	$^5F_1$	
3874	38741.19	2	1.60	$5d^56s^2(a^6S)6p$	$^5P_2$	
3887	38875.97	1	1.90	$5d^56s^2(a^6S)6p$	$^5P_1$	
3938	39382.95	3	1.18	$5d^66s(a^4D)6p$	$^5F_3$	
3940	39405.98	5	1.18	$5d^66s(a^4H)6p$	$^5H_5$	
3949	39493.80	2	0.93	$5d^66s(a^4D)6p$	$^3D_2$	
3950	39505.28	0	0/0	$5d^66s(a^4D)6p$	$^5D_0$	3
3967	39674.89	2	1.91	$5d^66s(a^4D)6p$	$^5P_2$	
4003	40036.27	7	1.29	$5d^66s(a^4H)6p$	$^5H_7$	3
4008	40087.01	4	1.36	$5d^7(a^4F)6p$	$^5F_4$	
4029	40290.44	6	1.30	$5d^66s(a^4H)6p$	$^5G_6$	
4036	40361.92	4	1.32	$5d^66s(a^4D)6p$	$^3F_4$	
4049	40497.48	1	2.18	$5d^66s(a^6D)6p$	$^5P_1$	
4088	40888.05	2	0.82	$5d^66s(a^4D)6p$	$^3F_2$	
4102	41023.22	6	1.23	$5d^66s(a^4H)6p$	$^5H_6$	
4122	41225.02	5	1.27	$5d^7(a^4F)6p$	$^5F_5$	
4123	41231.98	3	1.08	$5d^66s(a^4D)6p$	$^3F_3$	
4172	41725.58	4	1.04	$5d^66s(a^4H)6p$	$^5H_4$	
4187	41875.93	3	1.30	$5d^66s(a^4D)6p$	$^5P_3$	
4229	42299.83	1	1.00	$5d^66s(a^4D)6p$	$^3P_1$	
4231	42310.25	4	1.22	$5d^66s(a^4H)6p$	$^5G_4$	
4232	42316.68	3	1.08	$5d^66s(a^4H)6p$	$^5G_3$	
4242	42422.36	1	1.86	$5d^66s(a^4D)6p$	$^5P_1$	
4258	42582.75	0	0/0	$5d^66s(a^4D)6p$	$^3P_0$	
4265	42658.36	2	1.41	$5d^66s(a^4D)6p$	$^3P_2$	
4274	42746.57	4	1.32	$5d^7(a^4F)6p$	$^5D_4$	
4301	43011.56	3	1.05	$5d^66s(a^4H)6p$	$^5H_3$	
4340	43401.82	5	1.22	$5d^66s(a^4H)6p$	$^5G_5$	

TABLE II *(continued)*

Relative levels in Os I

Symbol	Value	J	g	Interpretation	Notes
				odd group *(continued)*	
4343	43437.13	2	1.00	$5d^6 6s(a^4H)6p$ $^5G_2$	
4351	43515.75	3	1.21	$5d^7(a^4F)6p$ $^5F_3$	
4361	43610.81	2	1.05	$5d^7(a^4F)6p$ $^3F_2$	
4375	43754.64	4	1.05	$5d^6 6s(a^4H)6p$ $^3H_4$	
4386	43862.69	4	1.20	$5d^7(a^4F)6p$ $^3F_4$	
4387	43876.12	5	1.13	$5d^6 6s(a^4H)6p$ $^3H_5$	
4407	44075.34	2	1.16	$5d^7(a^4F)6p$ $^5F_2$	
4414	44144.14	3	1.13	$5d^7(a^4F)6p$ $^3F_3$	
4447	44474.88	1	1.01	$5d^7(a^4F)6p$ $^5F_1$	
4466	44662.97	2	1.31	$5d^7(a^4F)6p$ $^5D_2$	
4472	44729.93	1	1.01	$5d^7(a^4F)6p$ $^5D_1$	
4483	44839.09	6	1.19	$5d^6 6s(a^4H)6p$ $^3H_6$	
4486	44869.71	3	1.35	$5d^7(a^4F)6p$ $^5D_3$	
4489	44892.67	4	1.22	$5d^7(a^4F)6p$ $^5G_4$	
4492	44921.12	5	1.27	$5d^7(a^4F)6p$ $^5G_5$	
4511	45113.19	0	0/0	$5d^7(a^4F)6p$ $^5D_0$	3
4531	45315.88	6	1.30	$5d^7(a^4F)6p$ $^5G_6$	
4538	45388.69	4	1.07	$5d^6 6s(a^4H)6p$ $^3G_4$	
4550	45503.45	2	1.32		
4556	45561.99	3	1.00	$5d^6 6s(a^4H)6p$ $^3G_3$	
4574	45757.85	5	1.21	$5d^6 6s(a^4H)6p$ $^3G_5$	3
4575	45758.63	5	1.23	$5d^7(a^4F)6p$ $^3G_5$	
4577	45774.55	3	1.12	$5d^7(a^4F)6p$ $^5G_3$	
4616	46169.54	2	1.19	$5d^7(a^4F)6p$ $^3D_2$	
4620	46202.36	1	0.62	$5d^7(a^4F)6p$ $^3D_1$	
4626	46263.46	4	1.12	$5d^7(a^4F)6p$ $^3G_4$	
4632	46327.99	3	1.11	$5d^7(a^4F)6p$ $^3G_3$	
4640	46406.90	2	1.15		
4651	46515.45	1	1.19		
4677	46776.29	3	1.25	$5d^7(a^4F)6p$ $^3D_3$	
4681	46812.87	2	1.15		
4705	47057.29	3	1.21		
4715	47158.48	4	1.19		5
4720	47200.25	5	1.31		
4747	47477.05	1	1.14		
4753	47539.58	2	0.99	$5d^7(a^4F)6p$ $^5G_2$	
4761	47614.64	3	1.12		
4780	47802.23	0	0/0		3
4782	47827.68	3	1.11		
4785	47853.53	4	1.17		
4793	47934.89	2	1.21		
4806	48062.22	5	1.18		3
4813	48131.92	4			8
4830	48302.56	3	1.14		
4840	48409.32	1	0.98		
4852	48525.87	4	1.07		
4875	48756.10	4	1.16		

TABLE II *(continued)*

Relative levels in Os I

Symbol	Value	J	g	Interpretation	Notes
				odd group *(continued)*	
4877	48773.49	2	1.15		
4887	48874.93	3	1.28		
4905	49053.60	1	0.89		
4911	49112.10	2	1.10		
4913	49138.11	3	1.23		
4920	49202.03	3	1.50		5
4948	49481.99	4	1.20		
4953	49534.28	5	1.15		5
4961	49614.84	2	1.10		
4987	49872.57	2	0.93		
4994	49947.06	3	1.19		
5000	50007.36	1	1.42		
5015	50153.37	3	1.16		
5027	50274.91	4	1.12		
5029	50293.56	4	1.18		
5031	50311.71	2	1.15		
5032	50329.97	3	1.22		
5037	50377.19	5	1.19		
5050	50503.53	4	1.19		
5058	50589.09	1	1.06		
5063	50630.26	6	1.13		
5067	50670.83	1	1.19		
5090	50902.87	5	1.19		
5093	50937.24	4	1.18		
5098	50989.77	2	1.12		
5104	51042.76	3	1.25		
5115	51151.91	5	1.17		3
5116	51166.38	0	0/0		
5121	51217.74	1	0.66		
5122	51228.63	3	1.27		
5131	51311.24	2	0.90		
5132	51329.30	4	1.07		
5154	51545.88	2	1.50		
5165	51655.94	2	1.09		
5175	51758.65	3	1.13		
5204	52042.60	6	1.17		
5213	52138.11	3	1.08		
5216	52162.03	2	1.21		
5233	52337.78	2	1.05		5
5237	52374.93	1	1.14		
5249	42490.56	4	1.11		
5256	52563.51	3			
5260	52604.13	3	0.99		
5267	52677.58	3			
5271	52715.84	4	1.13		
5280	52801.90	6	1.13		
5293	52937.60	3	1.24		

TABLE II *(continued)*

Relative levels in Os I

Symbol	Value	J	g	Interpretation	Notes
				odd group *(continued)*	
5307	53073.24	2	1.20		
5313	53131.25	4	1.19		
5333	53338.22	3	1.39		
5342	53424.25	2	1.64		5
5344	53447.29	4	1.13		
5345	53454.11	1	1.78		5
5357	53572.09	6	1.10		
5364	53647.27	2	1.37		5
5388	53887.05	3	1.12		5
5404	54049.89	2	0.96		
5406	54064.40	2	1.03		5
5430	54302.45	1	1.57		
5432	54328.11	6	1.21		
5448	54484.27	1	0.59		
5475	54753.20	2			9
5480	54800.46	1	1.46		
5486	54867.89	2			
				high even group	
4719	47198.73	5	1.57	$5d^66s(a^6D)7s$ $^7D_5$	
4873	48737.44	4	1.50	$5d^66s(a^6D)7s$ $^5D_4$	1
5103	51038.49	4	1.59	$5d^66s(a^6D)7s$ $^7D_4$	1
5113	51138.13	3	1.71	$5d^66s(a^6D)7s$ $^7D_3$	
5214	52148.69	2	1.80	$5d^66s(a^6D)7s$ $^7D_2$	10
5240	52401.81	3	1.56	$5d^66s(a^6D)7s$ $^5D_3$	5
5346	53464.00	1	2.70	$5d^66s(a^6D)7s$ $^7D_1$	3,4
5359	53594.54	2	1.61	$5d^66s(a^6D)7s$ $^5D_2$	5
5467	54676.96	3	1.82	$5d^56s^2(a^6S)7s$ $^7S_3$	
5484	54847.38	1		$5d^66s(a^6D)7s$ $^5D_1$	11
5503	55034.31	5	1.46	$5d^66s(a^6D)6d$ $^7D_5$	3
5512	55126.96	4	1.56	$5d^66s(a^6D)6d$ $^7D_4$	3
5513	55131.63	6	1.45	$5d^66s(a^6D)6d$ $^7F_6$	3
5538	55388.87	3	1.78	$5d^66s(a^6D)6d$ $^7D_3$	
5540	55402.47	5	1.40	$5d^66s(a^6D)6d$ $^7F_5$	
5541	55419.00	4	1.47	$5d^66s(a^6D)6d$ $^7F_4$	5
5570	55702.49	0	0/0	$5d^66s(a^6D)7s$ $^5D_0$	3
5609	56092.46	2		$5d^66s(a^6D)6d$ $^7D_2$?	12
5622	56222.41	5		$5d^66s(a^6D)6d$ $^7G_5$	13
5672	56729.16	4			
5733	57334.37	? 3			
5782	57826.90	? 3			
5809	58098.19	? 4			
5864	58647.69	2	1.78		3
5868	58688.20	? 3			
5876	58768.76	4			
5890	58905.20	? 3			
5895	58957.24	3	2.04 ?		5

TABLE II *(concluded)*

Relative levels in Os I

Symbol	Value	J	g	Interpretation	Notes
				high even group *(concluded)*	
5907	59074.97 ?	3			
5910	59105.95 ?	2			
5914	59142.16 ?	2			
5917	59170.43	2			
5922	59229.84	2	1.44 ?		5
5928	59282.85	3			14
5955	59556.04	3			
5958	59582.97	3			
5960	59602.19	2			
5975	59750.04 ?	3			
6064	60649.49 ?	4			

NOTES TO TABLE II

1. Previous assignments [1, 12] changed.
2. First interpretation.
3. New level.
4. This and all following levels of the group had not been interpreted previously.
5. g-value determined for the first time.
6. $g = 1.04$ or 1.11.
7. $g = 1.35$ or 1.41.
8. $g = 0.99$ or 1.33.
9. $g = 1.08$ or 1.46.
10. Not labelled by Albertson, identified as $5d^6 6s(a^6D)7s\ ^5D_2$ in AEL, Vol. III [12].
11. Previous ambiguity of the J quantum number resolved.
12. $g = 1.42$ or 2.03.
13. $g = 1.20$ or 1.36.
14. $g = 1.35$ or 1.53.

4. *List of classified lines*

In table III the classified lines of Os I have been collected in the order of increasing wave-length. The total number is 2968, corresponding to 3293 transitions; 269 lines were doubly, 25 lines trebly and 2 lines quadruply classified. When not stated otherwise the wave-lengths have been taken from the M.I.T.Tables [7] and the intensities are the corresponding arc-values. A bracketed number belongs to a wave-length taken from other sources, as indicated in the last column: B stands for Van den Bosch [8], EH for Exner and Haschek [3], M for Meggers [4] and K for the author. Those intensity numbers are on a scale different from the rest. The wave-lengths observed by Albertson [11] only (A) are very weak but no intensity estimate was available. Letter symbols behind the intensity number have the usual meaning [7]. All vacuum wave-numbers are given to 7 figures irrespective of the accuracy of the wave-length. In the column headed "Classification" the highest level is always

mentioned first. The discrepancy $\delta\sigma$ is σ (observed) − σ (calculated). Below 4500 Å a classification is considered as tentative if the discrepancy is bigger than $|0.25|$ K in case the wave-length is given to 7 figures and $|0.40|$ K when it is given to 6 figures. Above 4500 Å 6 figure wave-lengths which are due to MEGGERS are very accurate so that the admitted discrepancy was changed into $|0.25|$ K. Completely resolved Zeeman patterns are given by the g-values derived from them. In case the pattern is unresolved but the intensity distribution is discernible, the strongest component is given (in Lorentz-units) with the position of the weaker components relative to the strongest indicated by three dots. The numbers in the last column relate to the notes collected at the end of the table. Of 1027 lines the splitting is given; of these 344 show resolved patterns.

TABLE III

Classified lines of Os I

Int.	λ_{air}	$\sigma_{vac.}$	Classification		$\delta\sigma$	Zeeman effect	Notes
15	2001.89	49936.63	5267(3)–	27(2)	—0.46		1
5	2003.73	49890.77	5404(2)–	41(3)	+0.20		2
20	2018.14	49534.59	4953(5)-	0(4)	+0.31		
10	2020.04	49488.01	5364(2)–	41(3)	+0.06		
15	2022.76	49421.48	5216(2)–	27(2)	—0.06		
10	2023.72	49398.03	5213(3)–	27(2)	+0.41		1
20	2028.23	49288.21	5344(4)–	41(3)	+0.24		
5	2029.18	49265.13	5342(2)–	41(3)	+0.20		
5	2032.51	49184.43	5432(6)–	51(5)	+0.24		
12	2032.73	49179.11	5333(3)–	41(3)	+0.21		
30	2034.44	49137.77	4913(3)–	0(4)	—0.34		
15	2035.93	49101.81	5486(2)–	57(1)	+0.06		
15	2038.72	49034.63	5480(1)–	57(1)	+0.31		
10	2040.68	48987.54	5475(2)–	57(1)	+0.48		1
8	2043.68	48915.64	5165(2)–	27(2)	+0.19		
25	2048.28	48805.80	5154(2)–	27(2)	+0.41		1
15	2049.42	48778.65	5293(3)–	41(3)	+0.37		
10	2052.40	48707.84	5480(1)–	60(0)	+0.17		
10	2058.78	48556.92	5271(4)–	41(3)	+0.40		
10	2059.65	48536.41	5430(1)–	57(1)	+0.10		
10	2060.08	48526.28	4852(4)–	0(4)	+0.41		1
10	2060.40	48518.75	5267(3)–	41(3)	+0.49		1
20	2061.69	48488.39	5122(3)–	27(2)	+0.25		
12	2062.16	48477.34	5121(1)–	27(2)	+0.09		
25	2063.55	48444.69	5260(3)–	41(3)	—0.12		
4	2064.24	48428.50	5357(6)-	51(5)	+0.33		
5	2065.80	48391.94	5448(1)-	60(0)	+0.46		1
10	2068.38	48331.58	5249(4)–	41(3)	+0.34		
25	2069.61	48302.86	4830(3)–	0(4)	+0.30		
12	2070.42	48283.97	5404(2)–	57(1)	+0.22		
15	2074.95	48178.57	5233(2)–	41(3)	+0.11		
25	2076.95	48132.18	4813(4)–	0(4)	+0.26		
40	2079.97	48062.30	4806(5)–	0(4)	+0.08		
20	2082.54	48003.00	5216(2)–	41(3)	+0.29		

TABLE III *(continued)*

Classified lines of Os I

Int.	λ_{air}	$\sigma_{vac.}$	Classification		$\delta\sigma$	Zeeman effect	Notes
15	2083.20	47987.79	5313(4)–	51(5)	+0.46		1
15	2083.58	47979.04	5213(3)–	41(3)	+0.25		
20	2087.84	47881.16	5364(2)–	57(1)	+0.03		
20	2089.03	47853.89	4785(4)–	0(4)	+0.36		
20	2089.21	47849.77	5058(1)–	27(2)	+0.37		
12	2096.28	47688.40	5345(1)–	57(1)	+0.43		1, 2
25	2097.60	47658.40	5280(6)–	51(5)	+0.42		1, 4
			5342(2)–	57(1)	+0.29		
10	2099.51	47615.05	4761(3)–	0(4)	+0.41		1
15	2100.63	47598.67	5032(3)–	27(2)	+0.19		
5	2108.44	47413.40	5015(3)–	27(2)	+0.32		
15	2110.74	47361.74	5345(1)–	60(0)	+0.42		1
10	2111.40	47346.94	5249(4)–	51(5)	+0.30		
5	2114.97	47267.03	5000(1)–	27(2)	–0.16		
40	2117.66	47206.99	4994(3)–	27(2)	+0.42		1
80	2117.96	47200.31	4720(5)–	0(4)	+0.06		
15	2119.31	47170.25	5132(4)–	41(3)	+0.27		
40	2123.84	47069.65	5122(3)–	41(3)	+0.34		
25	2124.39	47057.46	4705(3)–	0(4)	+0.17		
10	2132.26	46883.80	5104(3)–	41(3)	+0.36		
10	2132.67	46874.79	4961(2)–	27(2)	+0.44		1
25	2154.59	46397.95	4913(3)–	27(2)	+0.33		
25	2157.08	46344.39	5050(4)–	41(3)	+0.18		
30	2157.84	46328.08	4632(3)–	0(4)	+0.09		
50	2158.53	46313.27	4905(1)–	27(2)	+0.16		
60	2159.98	46282.18	5237(1)–	60(0)	+0.04		
25	2164.49	46185.75	5132(4)–	51(5)	+0.37		
40	2165.19	46170.83	5032(3)–	41(3)	+0.18		
20	2166.05	46152.50	5031(2)–	41(3)	+0.11		
20	2166.90	46134.40	4887(3)–	27(2)	—0.04		
			5029(4)–	41(3)	+0.16		
20	2171.65	46033.50	4877(2)–	27(2)	+0.50		1
15	2172.84	46008.29	5115(5)–	51(5)	+0.30		2
10	2173.49	45994.53	5015(3)–	41(3)	+0.28		2
(1)	2183.04	45793.35	5093(4)–	51(5)	+0.03		K
20	2183.69	45779.72	5154(2)–	57(1)	—0.02		
10	2183.94	45774.48	4577(3)–	0(4)	—0.07		
25	2184.68	45758.98	4575(5)–	0(4)	+0.35		
			5090(5)–	51(5)	+0.03		
50	2188.97	45669.31	4840(1)–	27(2)	+0.48		1
10	2194.11	45562.33	4556(3)–	0(4)	+0.34		
			4830(3)–	27(2)	+0.26		
(1)	2199.48	45451.10	5121(1)–	57(1)	—0.50		K, 1
25	2201.93	45400.54	5116(0)–	57(1)	+0.30		
25	2202.49	45389.00	4538(4)–	0(4)	+0.31		
25	2203.91	45359.76	5050(4)–	51(5)	+0.15		
15	2210.53	45223.92	5098(2)–	57(1)	+0.29		
40	2211.96	45194.69	4793(2)–	27(2)	+0.29		
25	2214.16	45149.78	5029(4)–	51(5)	+0.14		

TABLE III *(continued)*

Classified lines of Os I

Int.	λ_{air}	$\sigma_{vac.}$	Classification	$\delta\sigma$	Zeeman effect	Notes
20	2215.37	45125.12	5121(1)– 60(0)	+0.17		
20	2217.23	45087.28	4782(3)– 27(2)	+0.09		
30	2223.85	44953.08	4911(2)– 41(3)	+0.30		
25	2225.44	44920.96	4492(5)– 0(4)	—0.16		
20	2226.23	44905.02	5067(1)– 57(1)	+0.33		
25	2226.83	44892.92	4489(4)– 0(4)	+0.25		
30	2227.98	44869.75	4486(3)– 0(4)	+0.04		3
20	2230.27	44824.09	5058(1)– 57(1)	+0.34		
35	2234.61	44736.64	4747(1)– 27(2)	+0.08		
15	2235.65	44715.83	4887(3)– 41(3)	+0.22		
20	2239.72	44634.58	5480(1)– 101(2)	+0.10		
25	2241.62	44596.76	4875(4)– 41(3)	—0.02		
30	2242.10	44587.21	5475(2)– 101(2)	—0.01		
(4)	2252.02	44390.83	4953(5)– 51(5)	+0.47		K, 1, 5
10	2252.15	44388.27	5313(4)– 87(4)	—0.15		
12	2254.69	44338.26	4948(4)– 51(5)	+0.19		
10	2259.63	44241.33	5000(1)– 57(1)	+0.11		
(1)	2262.02	44194.59	5293(3)– 87(4)	—0.18		K
(8)	2264.63	44143.66	4414(3)– 0(4) 4830(3)– 41(3)	—0.48 +0.42		K, 5, 6
40	2268.28	44072.64	4681(2)– 27(2)	+0.26		
60	2270.17	44035.95	4677(3)– 27(2)	+0.15		
(1)	2275.42	43934.36	5267(3)– 87(4)	—0.39		K
30	2276.43	43914.86	5000(1)– 60(0)	+0.29		
(1)	2277.30	43898.09	5406(2)– 101(2)	—0.33		K
25	2278.44	43876.13	4387(5)– 0(4)	+0.01		
20	2279.85	43849.00	4961(2)– 57(1)	+0.30		
50	2283.67	43775.65	4793(2)– 41(3)	+0.08		
12	2284.76	43754.77	4375(4)– 0(4)	+0.13		
30	2286.517	43721.15	5388(3)– 101(2)	+0.08		
(4)	2289.30	43668.01	4782(3)– 41(3)	—0.35		K
15	2292.21	43612.58	4875(4)– 51(5)	+0.40		
20	2293.54	43587.29	4632(3)– 27(2)	—0.21		2, 3
(4)	2297.32	43515.58	4351(3)– 0(4)	—0.17		K, 5
15	2299.12	43481.51	5364(2)– 101(2)	+0.22		
(2)	2300.51	43455.24	4761(3)– 41(3)	—0.08		K
25	2301.88	43429.38	4616(2)– 27(2)	+0.33		
(1)	2303.344	43401.78	4340(5)– 0(4)	—0.04		B
12	2303.69	43395.27	5213(3)– 87(4)	—0.01		
40	2304.38	43382.27	4852(4)– 51(5)	+0.32		
10	2306.30	43346.16	4911(2)– 57(1)	+0.20		
40	2309.40	43287.98	5345(1)– 101(2)	—0.15		
10	2315.58	43172.45	5333(3)– 101(2)	+0.21		
30	2324.24	43011.61	4301(3)– 0(4)	+0.05		
4	2324.89	42999.58	4715(4)– 41(3)	+0.42		1
(1)	2325.50	42988.31	4813(4)– 51(5)	+0.31		K, 3
(4)	2326.98	42960.96	4905(1)– 60(0)	+0.15		K
12	2329.287	42918.42	4806(5)– 51(5)	+0.12		

TABLE III *(continued)*

Classified lines of Os I

Int.	λ_{air}	$\sigma_{vac.}$	Classification	$\delta\sigma$	Zeeman effect		Notes
	2329.890	42907.31	5307(2) – 101(2)	+0.05			A
(1)	2330.395	42898.20	4705(3) – 41(3)	+0.23			K
10	2332.64	42856.73	5388(3) – 110(4)	+0.26			
2h	2334.561	42821.47	4556(3) – 27(2)	—0.03			EH
10	2337.78	42762.51	4550(2) – 27(2)	—0.45			1
30l	2338.650	42746.61	4247(4) – 0(4)	+0.04			
	2340.677	42709.60	4785(4) – 51(5)	+0.01			A
30l	2341.949	42686.41	5406(2) – 113(3)	+0.01			
15	2343.758	42653.45	4681(2) – 41(3)	—0.10			
20	2344.330	42643.05	4840(1) – 57(1)	—0.13			
25	2345.770	42616.88	4677(3) – 41(3)	—0.09			
(1)	2347.42	42586.92	5132(4) – 87(4)	+0.45			EH, 1
25	2351.579	42511.60	5267(3) – 101(2)	0.00			
25	2351.732	42508.84	5388(3) – 113(3)	—0.21			
30l	2353.006	42485.83	5122(3) – 87(4)	+0.03	(0)	1.33	7
5	2355.648	42438.18	5260(3) – 101(2)	+0.03			
	2356.835	42416.81	5344(4) – 110(4)	+0.10			A
25	2357.267	42409.04	5115(5) – 87(4)	—0.04			
25	2362.411	42316.70	4232(3) – 0(4) 4840(1) – 60(0)	+0.02 +0.17			
50	2362.771	42310.26	4231(4) – 0(4)	+0.01	(... 0.83)	---	7a
	2362.900	42307.95	5333(3) – 110(4)	+0.31			A, 1
[illegible]	2363.346	42299.97	5104(3) – 87(4)	+0.04			EH, 8
15	2365.075	42269.04	5364(2) – 113(3)	—0.23			
14	2366.275	42247.61	4640(2) – 41(3)	+0.03			
	2368.428	42209.21	5237(1) – 101(2)	+0.26			A, 1
50	2369.255	42194.47	5093(4) – 87(4)	+0.06			
15	2370.523	42171.90	5233(2) – 101(2)	+0.10			
25	2370.699	42168.77	4632(3) – 41(3) 4793(2) – 57(1)	+0.10 +0.02	 (0)	 0.97	 9
50	2371.188	42160.08	5090(5) – 87(4)	+0.04	(0)	0.81	
25	2372.921	42129.30	4486(3) – 27(2)	+0.08			
25	2374.337	42104.16	4626(4) – 41(3)	+0.02			
25	2374.527	42100.80	5313(4) – 110(4)	+0.13			
	2376.303	42069.34	5344(4) – 113(3)	+0.05			A
50	2377.03	42056.47	4720(5) – 51(5)	+0.14	$g_1 = 1.31$	$g_2 = 1.38$	10
50	2377.618	42046.06	5342(2) – 113(3)	—0.19	(0)	1.29	
30	2378.151	42036.64	4780(0) – 57(1)	+0.05			
25	2378.746	42026.13	5480(1) – 127(2)	+0.05			
40	2379.393	42014.71	4715(4) – 51(5)	+0.15	(0)	2.04	
15	2379.642	42010.31	4616(2) – 41(3)	+0.09			
30	2380.823	41989.48	4472(1) – 27(2)	+0.04			
30	2382.479	41960.28	5333(3) – 113(3)	+0.06			
30	2384.632	41922.41	4466(2) – 27(2)	—0.07			
15	2385.502	41907.13	5293(3) – 110(4)	+0.11			
40	2387.292	41875.70	4187(3) – 0(4)	—0.23			
6	2388.874	41847.97	5486(2) – 130(1)	+0.15			

TABLE III *(continued)*

Classified lines of Os I

Int.	λ_{air}	$\sigma_{vac.}$	Classification	$\delta\sigma$	Zeeman effect		Notes
	2392.726	41780.61	5480(1)– 130(1)	+0.22			A
30	2393.866	41760.72	5050(4)– 87(4)	+0.02			
45	2394.292	41753.29	5313(4)– 113(3)	+0.04	(0)	1.07	
	2395.378	41734.35	4447(1)– 27(2)	—0.04			A
(4)	2395.439	41733.29	5475(2)– 130(1)	+0.16	(0)	1.31	B, 11
(20)	2395.880	41725.61	4172(4)– 0(4)	+0.03	g_1 = 1.03	g_2 = 1.45	B, 5
(1)	2396.725	41710.90	4747(1)– 57(1)	—0.01			B
100	2396.784	41709.87	5448(1)– 127(2)	—0.02			
20	2397.625	41695.25	5307(2)– 113(3)	+0.01			
25	2398.200	41685.25	5271(4)– 110(4)	—0.01	(—)	1.16	
	2400.405	41646.95	5267(3)– 110(4)	0.05			A
25	2401.127	41634.44	5037(5)– 87(4)	+0.08	(0)	0.60 ...	
10	2402.233	41615.27	4577(3)– 41(3)	+0.04			
(2)	2403.533	41592.76	5175(3)– 101(2)	+0.09			B
25	2403.853	41587.23	5032(3)– 87(4)	+0.09	(0)	1.51	
(1)	2404.642	41573.58	5260(3)– 110(4)	+0.03			K
(6)	2405.447	41559.67	5293(3)– 113(3)	+0.07	(0)	1.26	B
10	2405.960	41550.81	5029(4)– 87(4)	+0.08			
	2407.074	41531.59	5027(4)– 87(4)	—0.49			A, 1
	2407.267	41528.26	5430(1)– 127(2)	+0.19			A
	2409.483	41490.06	5165(2)– 101(2)	+0.10			A
(6)	2410.983	41464.25	5448(1)– 130(1)	+0.05	(0.32)	—	B
	2411.226	41460.07	5249(4)– 110(4)	+0.09			A
(2)	2414.097	41410.77	5015(3)– 87(4)	+0.03			B
25	2414.517	41403.57	4414(3)– 27(2)	—0.08			
(4)	1414.568	41402.69	4556(3)– 41(3)	+0.02			B, 5
	2415.643	41384.27	4747(1)– 60(0)	+0.01			A
20	2417.986	41344.17	4550(2)– 41(3)	+0.04	(0)	1.71	
(2)	2418.350	41337.95	5271(4)– 113(3)	+0.11			B
15	2418.529	41334.89	4407(2)– 27(2)	+0.04	g_1 = 1.17	g_2 = 1.45	
(1)	2420.602	41299.50	5267(3)– 123(3)	—0.08			K
($\frac{1}{2}$)	2421.157	41290.02	5406(2)– 127(2)	0.00			B
(—)	2421.59	41282.65	5430(1)– 130(1)	+0.27			EH, 3, 8
(1)	2422.012	41275.45	5404(2)– 127(2)	—0.06			B
20	2424.565	41231.99	4123(3)– 0(4)	+0.01	g_1 = 1.07	g_2 = 1.45	
3	2424.717	41229.41	4538(4)– 41(3)	+0.04			
50	2424.970	41225.11	4122(5)– 0(4)	+0.09	(0)	0.80	
(1)	2426.195	41204.29	4994(3)– 87(4)	+0.06			B
(—)	2429.675	41145.29	5131(2)– 101(2)	+0.03			EH, 8
40	2431.193	41119.60	4626(4)– 51(5)	+0.06	(—)	... 2.30	9
			5448(1)– 133(2)	+0.16			
40	2431.607	41112.60	5249(4)– 113(3)	+0.04	(0)	—	12
			5388(3)– 127(2)	+0.13			
(1)	2431.900	41107.64	5213(3)– 110(4)	+0.11			K
	2434.580	41062.40	5122(3)– 101(2)	—0.25			A
(6)	2435.516	41046.61	4681(2)– 57(1)	—0.12	(0)	0.85	B
(4)	2435.650	41044.35	5406(2)– 130(1)	+0.02	(—)	1.74	B

TABLE III *(continued)*

Classified lines of Os I

Int.	λ_{air}	$\sigma_{\text{vac.}}$	Classification	$\delta\sigma$	Zeeman effect		Notes
	2436.513	41029.82	5404(2)– 130(1)	0.00			A
(4)	2442.000	40937.64	5430(1)– 133(2)	+0.02			B
(1)	2445.638	40876.75	5104(3)– 101(2)	−0.03			B
8	2445.880	40872.70	5364(2)– 127(2)	−0.19			2
12	2446.023	40870.31	4361(2)– 27(2)	−0.01	$g_1 = 1.05$	$g_2 = 1.44$	
25	2450.738	40791.68	4953(5)– 87(4)	+0.23	(0)	0.92	
(4)	2451.199	40784.01	5216(2)– 113(3)	−0.02	(0)	—	B
125	2451.726	40775.24	4351(3)– 27(2)	−0.02	$g_1 = 1.21$	$g_2 = 1.44$	
(—)	2452.66	40759.71	5213(3)– 113(3)	−0.40			EH, 8
(1)	2453.287	40749.30	4651(1)– 57(1)	−0.01	(0)	—	B, 11
12	2453.895	40739.20	4948(4)– 87(4)	+0.04	(... 0.40)	—	
	2455.636	40710.33	4486(3)– 41(3)	−0.06			A
(1)	2456.305	40699.23	5406(2)– 133(2)	−0.34			K, 1
125	2456.462	40696.63	4343(2)– 27(2)	−0.01	$g_1 = 1.00$	$g_2 = 1.44$	
($\frac{1}{2}$)	2457.166	40684.97	5404(2)– 133(2)	−0.09			B
	2458.568	40661.78	5475(2)– 140(3)	−0.05			A
	2459.298	40649.71	5342(2)– 127(2)	−0.16			A
(?)	2459.842	40640.72	4640(2)– 57(1)	−0.04			B
	2460.667	40627.10	5364(2)– 130(1)	−0.10			A
50	2461.417	40614.71	4575(5)– 51(5)	0.00	$g_1 = 1.16$	$g_2 = 1.38$	
4	2464.501	40563.89	5333(3)– 127(2)	+0.05	(0.26)	1.78	
(?)	2467.057	40521.88	5388(3) 133(2)	−0.34			B, 1
(2)	2468.102	40504.72	5067(1)– 101(2)	−0.13			B
15s	2472.281	40436.25	4620(1)– 57(1)	+0.03	$g_1 = 0.63$	$g_2 = 1.47$	
	2473.112	40422.68	4651(1)– 60(0)	+0.02			A
	2474.289	40403.44	4616(2)– 57(1)	+0.04			A
(6)	2474.796	40395.17	4913(3)– 87(4)	−0.11	(0)	1.50	B
(2)	2475.688	40380.61	5175(3)– 113(3)	−0.04			B
25	2476.836	40361.90	4036(4)– 0(4)	−0.02	(... 0.46)	1.38	
	2480.717	40298.76	5132(4)– 110(4) 5307(2)– 127(2)	+0.04 −0.10			A
12w	2482.427	40271.00	4301(3)– 27(2)	−0.07	$g_1 = 1.05$	$g_2 = 1.44$	
($\frac{1}{2}$)	2484.049	40244.71	4538(4)– 51(5)	−0.06			B
(1)	2486.935	40198.02	5122(3)– 110(4)	−0.03			K
50w	2488.548	40171.96	4531(6)– 51(5)	0.00	(0)	0.74 ...	
(4)	2488.808	40167.76	5154(2)– 113(3)	−0.12			B
(6)	2489.045	40163.93	5032(3)– 101(2)	−0.06	(0)	—	B
8w	2491.021	40132.07	4887(3)– 87(4)	−0.03	(0)	1.33	
10	2491.689	40121.32	5115(5)– 110(4)	−0.01	(0)	1.25	13
(6)	2492.421	40109.53	4620(1)– 60(0)	−0.04	(0)	0.62	B
(1)	2493.824	40086.97	4008(4)– 0(4)	−0.04	(0.38)	—	B
	2495.551	40059.22	5342(2)– 133(2)	−0.20			A
	2495.918	40053.34	5307(2)– 130(1)	+0.17			A

(To be continued)

PHYSICS

STRUCTURE AND ZEEMAN EFFECT IN THE SPECTRA OF THE OSMIUM ATOM, Os I AND Os II
II

BY

TH. A. M. VAN KLEEF
Zeeman-laboratory, University of Amsterdam, the Netherlands

(Communicated by Prof. J. DE BOER at the meeting of January 30, 1960)

TABLE III *(continued)*
Classified lines of Os I

Int.	λ_{air}	σ_{vac}	Classification	$\delta\sigma$	Zeeman effect		Notes
20hl	2498.414	40013.33	4875(4)– 87(4)	+0.06	(... 0.50, 0.63)	1.25	
5h	2499.924	39989.16	5432(6)– 143(5)	+0.04	(o)	1.42	
(½)	2500.026	39987.53	5015(3)– 101(2)	—0.06			B
12	2500.911	39973.38	5333(3)– 133(2)	—0.01			
			5406(2)– 140(3)	+0.35			1
	2501.843	39958.49	5404(2)– 140(3)	—0.03			A
10s	2502.290	39951.35	5132(4)– 113(3)	+0.05	(0)	0.53, 0.71, 0.88 ...	
8	2504.387	39917.91	4265(2)– 27(2)	+0.04	(0)	1.43	
10	2504.507	39915.99	4407(2)– 41(3)	—0.03	$g_1 = 1.17$	$g_2 = 1.49$	
	2507.250	39872.33	5090(5)– 110(4)	+0.04			A
8s	2508.610	39850.71	5122(3)– 113(3)	+0.08	(0)	1.27	
(1)	2509.192	39841.46	5000(1)– 101(2)	+0.08			K
25	2509.936	39829.66	5260(3)– 127(2)	—0.09	(0)	0.97	
40	2512.873	39783.12	4852(4)– 87(4)	+0.08	$g_1 = 1.06$	$g_2 = 1.29$	
50	2513.246	39777.21	4492(5)– 51(5)	+0.01	(... 0.50, 0.63)	1.33	
40s	2515.044	39748.77	4489(4)– 51(5)	+0.02	(0)	... 2.06	
	2515.763	39737.42	4550(2)– 57(1)	+0.11			A
	2517.602	39708.38	5307(2)– 133(2)	—0.03			A
(½)	2517.714	39706.62	4987(2)– 101(2)	+0.03			B
12	2517.920	39703.37	4386(4)– 41(3)	0.00	$g_1 = 1.18$	$g_2 = 1.45$	
20	2518.441	39695.16	4483(6)– 51(5)	—0.01	$g_1 = 1.19$	$g_2 = 1.38$	
(2)	2519.287	39681.83	4242(1)– 27(2)	—0.04	$g_1 = 1.91$	$g_2 = 1.44$	B
	2520.372	39664.75	5104(3)– 113(3)	—0.01			A
	2521.623	39645.07	5486(2)– 152(2)	—0.25			A
	2523.743	39611.77	5098(2)– 113(3)	0.00			A
	2524.453	39600.64	5237(1)– 127(2)	+0.09			A
	2524.794	39595.29	4375(4)– 41(3)	—0.03			A
10	2526.013	39576.18	4232(3)– 27(2)	—0.01	(—)	0.37, 0.72, 1.10	

TABLE III *(continued)*

Classified lines of Os I

Int.	λ_{air}	$\sigma_{vac.}$	Classification	$\delta\sigma$	Zeeman effect		Notes
(1)	2526.827	39563.43	5233(2)– 127(2)	+0.03	(0.22)	1.00	B
			4229(1)– 27(2)	+0.02			
30r	2527.075	39559.36	4830(3)– 87(4)	—0.37			1
			5093(4)– 113(3)	+0.12			
	2527.321	39555.69	5364(2)– 140(3)	—0.21			A
	2528.924	39530.63	5475(2)– 152(2)	0.00			A
	2532.361	39476.98	5486(2)– 153(3)	—0.15			A
12	2532.436	39475.81	5432(6)– 149(6)	+0.03	(... 0.28)	1.18	
	2532.622	39472.91	5050(4)– 110(4)	—0.04			A
	2533.999	39451.47	4361(2)– 41(3)	—0.02			A
8	2534.166	39448.86	4961(2)– 101(2)	0.00	$g_1 = 1.09$	$g_2 = 1.43$	
	2536.925	39405.96	3940(5)– 0(4)	—0.02			A
—	2537.997	39389.32	4813(4)– 87(4)	+0.23			2, 3, 15
5	2538.102	39387.69	5216(2)– 127(2)	+0.04			
	2538.408	39382.93	3938(3)– 0(4)	—0.02			A
(½)	2539.648	39363.71	5213(3)– 127(2)	—0.02	(0.10)	1.10	B
			4351(3)– 41(3)	—0.50			1
(1)	2540.150	39355.93					B
			5344(4)– 140(3)	+0.01	(0.02)	1.15	9
			5037(5)– 110(4)	+0.16	(0)	1.24	9
40	2540.741	39346.77					
			4511(0)– 57(1)	—0.28			1, 6
(½)	2541.651	39332.69	5342(2)– 140(3)	—0.19	(0)	0.89	B, 11
50	2542.512	39319.37	4806(5)– 87(4)	—0.02	(0)	0.55	
	2542.944	39312.69	5267(3)– 133(2)	—0.06			A
10	2543.804	39299.40	5032(3)– 110(4)	+0.01	(0)	1.05	
	2545.206	39277.76	4343(2)– 41(3)	—0.05			A
(4)	2546.164	39262.98	5029(4)– 110(4)	0.00	(0)	1.17	B
	2547.212	39246.82	5333(3)– 140(3)	—0.03			A
	2547.374	39244.33	5027(4)– 110(4)	0.00			A
5	2547.700	39239.31	5260(3)– 133(2)	+0.01	(0)	1.03	
(2)	2548.100	39233.15	5357(6)– 143(5)	+0.05	(0)	1.01	B
	2554.035	39141.99	5216(2)– 130(1)	+0.03			A, 3
20	2554.465	39135.40	4187(3)– 27(2)	—0.04	(0)	1.09	
(4)	2555.113	39125.47	5050(4)– 113(3)	—0.06	(0)	1.08	B
10	2555.273	39123.02	5015(3)– 110(4)	+0.03	(0)	1.17	
10	2556.077	39110.72	4785(4)– 87(4)	+0.02	(... 0.50)	—	
	2556.234	39108.31	5344(4)– 143(5)	+0.01			A
10	2557.768	39084.86	4782(3)– 87(4)	+0.01			
12	2558.093	39079.89	5430(1)– 152(2)	+0.01	(0)	1.65	
	2560.715	39039.88	5313(4)– 140(3)	0.00			A
12	2562.665	39010.18	5237(1)– 133(2)	+0.08	$g_1 = 1.15$	$g_2 = 0.96$	
8	2564.369	38984.26	5175(3)– 127(2)	—0.01	(0)	1.27	
12	2565.167	38972.13	4913(3)– 101(2)	0.00	(0, 0.24, 0.48)	—	
(½)	2565.716	38963.79	4472(1)– 57(1)	0.00	(0.47)	—	
(8)	2566.497	38951.94	5032(3)– 113(3)	—0.03	(... 0.12)	1.23	
(6)	2566.883	38946.08	4911(2)– 101(2)	—0.04	$g_1 = 1.10$	$g_2 = 1.45$	
251	2568.834	38916.50	4994(3)– 110(4)	+0.02	(0)	1.12	
(½)	2568.898	38915.53	5029(4)– 113(3)	—0.03			B

TABLE III *(continued)*

Classified lines of Os I

Int.	λ_{air}	$\sigma_{vac.}$	Classification	$\delta\sigma$	Zeeman effect		Notes
	2570.139	38896.75	4466(2)– 57(1)	—0.08			A
			5027(4)– 113(3)	—0.16			
	2570.744	38887.60	4905(1)– 101(2)	—0.02			A
(1)	2571.144	38881.54	5165(2)– 127(2)	—0.02	(… 0.15)	1.08	B
25	2571.782	38871.90	4761(3)– 87(4)	+0.09	g_1 = 1.13	g_2 = 1.31	
	2573.085	38852.21	4301(3)– 41(3)	—0.03			A
	2573.482	38846.22	5293(3)– 140(3)	—0.01	(0)	—	A
	2573.772	38841.84	5406(2)– 152(2)	+0.01			A
	2574.736	38827.31	5404(2)– 152(2)	—0.01			A
(?)	2576.737	38797.15	5216(2)– 133(2)	—0.05			B
	2577.057	38792.33	5313(4)– 143(5)	+0.07	(0)	—	A
8	2578.164	38775.68	5015(3)– 113(3)	+0.11	(0)	—	
10	2578.321	38773.32	5213(3)– 133(2)	+0.04	g_1 = 1.12	g_2 = 0.96	3
(?)	2578.467	38771.13	5154(2)– 127(2)	—0.37			B, 1
25	2581.052	38732.30	4387(5)– 51(5)	+0.10	g_1 = 1.14	g_2 = 1.38	
(6)	2581.890	38719.73	5357(6)– 149(6)	—0.03	(… 0.21)	1.17	B
80s	2581.958	38718.71	4386(4)– 51(5)	—0.06	g_1 = 1.19	g_2 = 1.37	
(2)	2582.630	38708.63	4447(1)– 57(1)	—0.11	g_1 = 0.99	g_2 = 1.45	9, B
			4887(3)– 101(2)	—0.32			1
	2586.192	38655.32	5486(2)– 162(1)	—0.16			A
(½)	2587.420	38636.98	4472(1)– 60(0)	—0.16	(0)	1.01	B
8	2587.486	38636.00	5165(2)– 130(1)	+0.13	(0)	1.08	
(½)	2588.262	38624.41	5271(4)– 140(3)	—0.06			B
	2589.180	38610.71	4375(4)– 51(5)	—0.01			A
8	2589.391	38607.57	4877(2)– 101(2)	+0.06	(… 0.59)	—	
75	2590.755	38587.24	4274(4)– 41(3)	—0.01	(0)	0.84 …	
(6)	2591.975	38569.08	4994(3)– 113(3)	+0.02	(… 0.19)	1.25	B
(½)	2593.895	38540.53	5475(2)– 162(1)	—0.26	(0)	1.13	B, 1, 11
10	2594.143	38536.85	5131(2)– 127(2)	—0.01	(… 0.20)	0.96	
	2594.906	38525.52	5154(2)– 130(1)	—0.29			A, 1
(½)	2596.368	38503.83	4953(5)– 110(4)	+0.13			B
10	2596.692	38499.03	4265(2)– 41(3)	—0.01	(0)	1.56	
	2596.893	38496.05	5388(3)– 153(3)	—0.24			A
	2597.027	38494.07	4987(2)– 113(3)	—0.50			A, 1
5	2597.201	38491.48	4123(3)– 27(2)	—0.01	(0, 0.36, 0.69)	—	
4	2597.291	38490.15	5333(3)– 148(4)	—0.02			
(2)	2597.573	38485.97	3848(3)– 0(4)	—0.04			B
5	2599.129	38462.93	5280(6)– 143(5)	+0.02	(0)	1.12	
(½)	2599.505	38457.37	4720(5)– 87(4)	—0.05			B
	2599.710	38454.34	5122(3)– 127(2)	+0.09			A
12	2599.907	38451.42	4948(4)– 110(4)	+0.01	(… 0.14)	1.27	
8	2600.452	38443.36	5121(1)– 127(2)	0.00	g_1 = 0.66	g_2 = 1.00	
	2601.726	38424.55	5364(2)– 152(2)	—0.15			A
(2)	2602.337	38415.52	4715(4)– 87(4)	—0.13	(… 0.50)	—	B
	2603.434	38399.33	5249(4)– 140(3)	+0.14			A
(1)	2603.802	38393.91	5175(3)– 133(2)	+0.09	(0)	—	B
20	2604.604	38382.09	4447(1)– 60(0)	0.00	(0)	1.01	

TABLE III *(continued)*

Classified lines of Os I

Int.	λ_{air}	$\sigma_{vac.}$	Classification	$\delta\sigma$	Zeeman effect		Notes
(1)	2604.959	38376.86	5271(4)– 143(5)	+0.01	(0)	1.14	B
8	2609.203	38314.44	4705(3)– 87(4)	−0.02	(0)	1.48	
20	2609.560	38309.20	4407(2)– 57(1)	0.00	g_1 = 1.16	g_2 = 1.47	
20	2610.782	38291.27	5131(2)– 130(1)	+0.10	g_1 = 0.90	g_2 = 0.31	9
			5165(2)– 133(2)	+0.16			
8	2611.330	38283.23	5313(4)– 148(4)	+0.03	(... **0.40**)	1.15	
	2612.336	38268.49	5104(3)– 127(2)	+0.11			A
20	2612.630	38264.18	3826(3)– 0(4)	+0.02	g_1 = 1.23	g_2 = 1.46	
50	2613.058	38257.92	4340(5)– 51(5)	+0.02	g_1 = 1.21	g_2 = 1.37	
(?)	2613.837	38246.52	5233(2)– 140(3)	+0.11	(0)	—	B
(1)	2614.057	38243.30	4840(1)– 101(2)	−0.04	(**0**, 0.47)	—	B
	2614.493	38236.91	4961(2)– 113(2)	+0.07			A
5	2615.962	38215.45	5098(2)– 127(2)	+0.06	(0.25)	1.07	
	2616.916	38201.52	5342(2)– 152(2)	−0.16			A
(1)	2617.176	38197.72	5121(1)– 130(1)	+0.05	(0.36)	—	B
	2618.315	38181.11	5154(2)– 133(2)	+0.06			A
30	2619.944	38157.37	4232(3)– 41(3)	+0.01	g_1 = 1.08	g_2 = 1.47	
	2620.334	38151.69	5249(4)– 143(5)	+0.12			A
10	2620.619	38147.54	4088(2)– 27(2)	−0.02	g_1 = 0.82	g_2 = 1.45	
(2)	2620.698	38146.39	5116(0)– 130(1)	+0.08			B
5	2621.371	38136.60	4830(3)– 101(2)	+0.02			
25	2621.818	38130.10	3813(4)– 0(4)	+0.01	g_1 = 1.23	g_2 = 1.44	
	2623.368	38107.71	4913(3)– 110(4)	+0.18			A
(½)	2623.616	38103.97	4948(4)– 113(3)	−0.02	(0)	—	B
(½)	2624.574	38090.06	5430(1)– 162(1)	+0.02	g_1 = 1.56	g_2 = 1.75	B
	2625.905	38070.90	5216(2)– 140(3)	+0.24			A
20	2628.479	38033.47	4677(3)– 87(4)	+0.01	(0)	1.41	9
			5342(2)– 153(3)	+0.18			
			6064(4)–2261(4)	−0.33			1
5	2632.892	37969.73	5098(2)– 130(1)	+0.03	(0)	1.48	3
5	2634.291	37949.57	5280(6)– 149(6)	0.00	(0)	1.14	
4	2634.439	37947.44	5333(3)– 153(3)	−0.02			
150	2637.133	37908.67	3790(4)– 0(4)	−0.10	(0)	1.45	
(1)	2637.980	37896.50	5067(1)– 127(2)	+0.05	(0)	—	B
(1)	2639.981	37867.78	5271(4)– 148(4)	−0.01	(0.16)	—	B
	2640.256	37863.83	5122(3)– 133(2)	+0.03			A
(—)	2641.10	37851.74	5406(2)– 162(1)	−0.25			EH, 8
10	2641.174	37850.68	5307(2)– 152(2)	+0.01	(0.49, **0.85**)	—	
(4)	2641.598	37844.61	4361(2)– 57(1)	−0.06	g_1 = 1.05	g_2 = 1.47	9, B
			4887(3)– 110(4)	+0.26			1
	2642.101	37837.40	5404(2)– 162(1)	−0.08			A
	2642.646	37829.60	5267(3)– 148(4)	+0.07			A
	2643.033	37824.06	4920(3)– 113(3)	+0.03			A
6	2643.629	37815.53	5058(1)– 127(2)	+0.02	(0)	0.97	
75	2644.114	37808.59	3780(3)– 0(4)	+0.01	g_1 = 1.26	g_2 = 1.45	
15	2646.892	37768.91	4793(2)– 101(2)	0.00	g_1 = 1.21	g_2 = 1.46	
	2647.504	37760.19	4913(3)– 113(3)	+0.08			A

TABLE III *(continued)*

Classified lines of Os I

Int.	λ_{air}	$\sigma_{vac.}$	Classification	$\delta\sigma$	Zeeman effect		Notes
25	2647.730	37756.96	4049(1)– 27(2)	—0.03	$g_1 = 2.20$	$g_2 = 1.44$	
	2648.887	37740.46	5313(4)– 153(3)	—0.03			A
25	2649.335	37734.09	4911(2)– 113(3)	—0.01	$g_1 = 1.07$	$g_2 = 1.24$	
	2650.571	37716.49	4187(3)– 41(3)	—0.12			A
(2)	2650.675	37715.02	5293(3)– 152(2)	—0.01	(0, 0.34)	(0.51, 0.89, 1.26)	B
(½)	2651.478	37703.60	5204(6)– 143(5)	—0.01	(0)	—	B
10	2652.977	37682.29	5307(2)– 153(3)	—0.19	(0)	—	
(?)	2653.253	37678.36	5104(3)– 133(2)	+0.43			B, 1, 14
12	2653.776	37670.95	4343(2)– 57(1)	—0.04	$g_1 = 1.00$	$g_2 = 1.48$	
	2654.029	37667.35	5175(3)– 140(3)	+0.07			A
	2654.434	37661.61	4782(3)– 101(2)	—0.09			A
15	2655.198	37650.77	5067(1)– 130(1)	+0.01	(0.89)	—	
8	2655.780	37642.52	5249(4)– 148(4)	+0.01	(0.13)	1.09	
50	2658.600	37602.60	4274(4)– 51(5)	—0.05	(0)	1.50	
30	2659.833	37585.17	4632(3)– 87(4)	+0.01	$g_1 = 1.10$	$g_2 = 1.30$	
5	2660.918	37569.83	5058(1)– 130(1)	+0.01	(0.75)	—	
20	2661.179	37566.15	4172(4)– 41(3)	—0.11	$g_1 = 1.06$	$g_2 = 1.48$	
(1)	2661.931	37555.54	5032(3)– 127(2)	—0.05			B
(2)	2662.552	37546.78	5293(3)– 153(3)	—0.06	$g_1 = 1.23$	$g_2 = 1.52$	B
(2)	2663.226	37537.28	5031(2)– 127(2)	—0.05	(0.23)	1.05	B
	2664.401	37520.73	4626(4)– 87(4)	+0.10			A
5	2666.211	37495.25	4852(4)– 110(4)	—0.04	(... 0.32)	—	3, 23
	2669.069	37455.11	5267(3)– 152(2)	+0.10			A
8	2669.529	37448.65	4761(3)– 101(2)	—0.01	$g_1 = 1.12$	$g_2 = 1.46$	
2	2670.527	37434.66	5364(2)– 162(1)	—0.20			
	2673.321	37395.54	4877(2)– 113(3)	+0.05			A
15	2674.568	37378.10	4875(4)– 123(3)	0.00	(0)	0.95	
25	2674.885	37373.67	4753(2)– 101(2)	+0.07	(... 0.93)	(... 1.45, 1.95)	
(1)	2679.380	37310.98	4747(1)– 101(2)	—0.09			B
8	2679.735	37306.04	5067(1)– 133(2)	+0.04	$g_1 = 1.18$	$g_2 = 0.94$	
	2680.763	37291.74	5031(2)– 130(1)	+0.10			A
	2680.882	37290.08	5213(3)– 148(4)	+0.02			A
10	2682.187	37271.93	4830(3)– 110(4)	—0.05	(0)	1.18	
	2684.995	37232.97	5000(1)– 127(2)	—0.01			A
	2685.554	37225.20	5058(1)– 133(2)	+0.14			A
(½)	2686.541	37211.53	5342(2)– 162(1)	—0.31			B, 1
8	2688.077	37190.27	5204(6)– 149(6)	0.00	(... 0.15)	1.16	
5	2689.350	37172.67	4994(3)– 127(2)	—0.01	(0.12, 0.39, 0.67)	... 1.54	14
50	2689.816	37166.23	4231(4)– 51(5)	—0.10	$g_1 = 1.22$	$g_2 = 1.38$	
	2691.181	37147.38	4852(4)– 113(3)	—0.49			A, 1
(—)	2691.907	37137.36	5122(3)– 140(3)	+0.10			EH,3,8,15
10	2694.523	37101.31	4813(4)– 110(4)	—0.03	(... 0.69)	—	
5	2694.748	37098.21	4987(2)– 127(2)	+0.02	(... 0.22)	0.94	
(1)	2696.612	37072.57	4123(3)– 41(3)	—0.09			B
50	2699.589	37031.69	{4577(3)– 87(4) {4806(5)– 110(4)	—0.03 +0.05	$g_1 = 1.12$ (0)	$g_2 = 1.30$ 1.19	

TABLE III *(continued)*

Classified lines of Os I

Int.	λ_{air}	$\sigma_{vac.}$	Classification	$\delta\sigma$	Zeeman effect		Notes
10	2700.746	37015.82	4575(5)- 87(4)	+0.02			
	2702.600	36990.43	5132(4) 143(5)	+0.12			A
8	2702.830	36987.28	5000(1) 130(1)	—0.01	$g_1 = 1.41$	$g_2 = 0.31$	
10	2704.448	36965.15	5032(3) 133(2)	+0.01	$g_1 = 1.23$	$g_2 = 0.97$	
(1)	2705.452	36951.44	5104(3) 140(3)	+0.05			B
			5031(2)- 133(2)	+0.13			
(?)	2705.776	36947.01					B
			5233(2)- 153(3)	—0.01			
50	2706.702	36934.38	3967(2)- 27(2)	—0.02	$g_1 = 1.91$	$g_2 = 1.44$	
12	2707.421	36924.57	4830(3)- 113(3)	+0.01	(... 0.30)	—	
	2708.445	36910.61	5175(3)- 148(4)	+0.01			A
($\frac{1}{2}$)	2709.344	36898.37	5098(2)- 140(3)	0.03			B
20	2709.864	36891.28	4705(3)- 101(2)	0.03	$g_1 = 1.21$	$g_2 = 1.44$	
(?)	2713.203	36845.88	5093(4) 140(3)	+0.01			B
50r	2714.642	36826.35	3682(4)- 0(4)	—0.04	(... 0.11)	1.14	
(4)	2714.900	36822.86	4785(4) 110(4)	—0.09	(0)	1.17	B
(2)	2715.177	36819.10	4556(3)- 87(4)	—0.06			B
(4)	2715.268	36817.86	3681(5)- 0(4)	—0.08			B
			4258(0)- 57(1)	—0.05	(0)	1.47	9
12	2715.364	36816.56					
			5448(1)- 176(1)	—0.37			1
8	2715.636	36812.87	5115(5)- 143(5)	—0.05	(... 0.23)	—	
(—)	2716.16	36805.77	3680(3)- 0(4)	—0.05			EH, 1, 8
(2)	2716.805	36797.04	4782(3)- 110(4)	—0.06	(0)	1.24	B
($\frac{1}{2}$)	2717.422	36788.68	5015(3)- 133(2)	—0.06			B
(4)	2718.713	36771.21	5216(2)- 153(3)	—0.06	$g_1 = 1.22$	$g_2 = 1.54$	B
75	2720.044	36753.22	3949(2)- 27(2)	—0.09	$g_1 = 0.93$	$g_2 = 1.44$	
	2720.491	36747.18	5213(3)- 153(3)	—0.17			A
75	2721.862	36728.67	4088(2)- 41(3)	0.06	$g_1 = 0.82$	$g_2 = 1.47$	
	2727.246	36656.17	4242(1)- 57(1)	—0.05			A
(4)	2727.940	36646.85	4681(2)- 101(2)	—0.04	(0.60)	—	B
(1)	2728.010	36645.91	4538(4)- 87(4)	+0.05			B
			3938(3)- 27(2)	—0.07			
12	2728.272	36642.39			(0)	—	12
			5000(1)- 133(2)	—0.14			
(10)	2730.665	36610.28	4677(3)- 101(2)	—0.03	$g_1 = 1.25$	$g_2 = 1.45$	B, 5
($\frac{1}{2}$)	2731.829	36594.68	4961(2)- 130(1)	—0.09			B
	2732.620	36584.09	4761(3)- 110(4)	+0.03			A
75	2732.805	36581.61	4172(4)- 51(5)	—0.05	$g_1 = 1.04$	$g_2 = 1.38$	
($\frac{1}{2}$)	2734.652	36556.90	4793(2)- 113(3)	+0.01	(0)	1.31	B
	2736.208	36536.11	5175(3)- 152(2)	+0.03			A
(1)	2736.393	36533.64	4229(1)- 57(1)	—0.05			B
(1)	2738.338	36507.70	4987(2)- 133(2)	—0.04	(0)	0.92	B
15	2740.321	36481.28	5132(4)- 148(4)	+0.03	(0)	1.08	
8	2740.753	36475.53	4785(4)- 113(3)	0.00	(0)	—	
(1)	2742.698	36449.67	4782(3)- 113(3)	—0.01	(0.41)	—	B
	2743.901	36433.69	5165(2)- 152(2)	+0.32			A, 1, 14
	2745.530	36412.07	5050(4)- 140(3)	—0.09	(0)	1.27	A
(6)	2747.907	36380.58	5122(3)- 148(4)	0.00	$g_1 = 1.25$	$g_2 = 1.06$	B

TABLE III *(continued)*

Classified lines of Os I

Int.	λ_{air}	$\sigma_{vac.}$	Classification	$\delta\sigma$	Zeeman effect		Notes
12	2748.863	36367.92	5175(3)– 153(3)	+0.03	$g_1 = 1.12$	$g_2 = 1.54$	
15	2749.180	36363.73	4913(3)– 127(2)	0.00	$g_1 = 1.22$	$g_2 = 1.01$	
8	2751.147	36337.73	4911(2)– 127(2)	+0.01	(... 0.18)	1.04	
	2751.770	36329.51	4242(1)– 60(0)	—0.06	(0)	—	A
8	2753.722	36303.76	5115(5)– 148(4)	—0.10	(0)	1.49	
(½)	2754.667	36291.30	5063(6)– 143(5)	+0.03	(0)	1.13	B
(6)	2755.589	36279.18	4905(1)– 127(2)	—0.04	(0)	1.08	B
25	2757.808	36249.97	4961(2)– 133(2)	—0.04	$g_1 = 1.11$	$g_2 = 0.95$	
(4)	2758.502	36240.85	4640(2)– 101(2)	—0.07			B
(½)	2758.673	36238.61	5032(3)– 140(3)	+0.01			B
15	2758.821	36236.66	4761(3)– 113(3)	+0.02	(... 0.40)	1.18	
(½)	2760.059	36220.41	5031(2)– 140(3)	+0.07			B
20	2761.082	36206.99	4229(1)– 60(0)	—0.05	(0)	1.00	
50	2761.418	36202.58	4036(4)– 41(3)	—0.02	$g_1 = 1.32$	$g_2 = 1.46$	9
			5029(4)– 140(3)	+0.39			1
	2762.028	36194.59	5104(3)– 148(4)	—0.12			A
(½)	2762.928	36182.80	5448(1)– 183(0)	—0.07			B
25	2763.273	36178.28	4492(5)– 87(4)	—0.01	(0)	1.17	
20	2763.935	36169.62	4720(5)– 110(4)	—0.05	(... 0.36)	—	14
(1)	2764.326	36164.49	5050(4)– 143(5)	—0.05			B
	2764.470	36162.61	5237(1)– 162(1)	+0.09			A
(½)	2764.545	36161.63	4632(3)– 101(2)	—0.38			1
			4753(2)– 113(3)	+0.05			B
(8)	2765.042	36155.14	5154(2)– 153(3)	+0.02	(0)	1.60	B
10	2765.447	36149.84	4489(4)– 87(4)	0.00	(... 0.31)	1.21	
(1)	2766.550	36135.43	3887(1)– 27(2)	—0.05			B
10	2767.122	36127.96	4715(4)– 110(4)	+0.06	(0.21)	1.14	
(2)	2767.202	36126.92	4486(3)– 87(4)	+0.04			B
	2769.224	36100.54	4887(3)– 127(2)	—0.01			A
20	2769.875	36092.06	4911(2)– 130(1)	+0.03	$g_1 = 1.10$	$g_2 = 0.31$	
5	2770.098	36089.15	5093(4)– 148(4)	—0.04	(... 0.36)	—	9
			5131(2)– 152(2)	+0.48			1
(10)	2770.719	36081.06	4122(5)– 51(5)	—0.04	(0.46, 0.57)	1.35	B
(½)	2772.159	36062.31	5015(3)– 140(3)	+0.11			B
	2772.742	36054.73	5090(5)– 148(4)	—0.09			A
12	2773.069	36050.49	5090(5)– 149(6)	—0.05	(0)	1.01	
12	2774.016	36038.18	5037(5)– 143(5)	—0.02	(... 0.16)	1.07	
5	2774.151	36036.43	4620(1)– 101(2)	+0.05			
8	2774.375	36033.52	4905(1)– 130(1)	—0.01	$g_1 = 0.87$	$g_2 = 0.31$	
8s	2774.900	36026.70	4705(3)– 110(4)	—0.01	(0)	1.08	
	2776.485	36006.13	5122(3)– 152(2)	+0.07			A
(1)	2776.690	36003.47	4616(2)– 101(2)	—0.09			B
25	2776.910	36000.62	3874(2)– 27(2)	—0.08	$g_1 = 1.59$	$g_2 = 1.45$	9
			5430(1)– 183(0)	—0.43			1
(2)	2777.028	35999.09	4877(2)– 127(2)	—0.02			B

TABLE III *(continued)*

Classified lines of Os I

Int.	λ_{air}	$\sigma_{vac.}$	Classification	$\delta\sigma$	Zeeman effect		Notes
	2780.848	35949.64	5216(2)– 162(1)	+0.02			A
	2781.703	35938.59	5132(4)– 153(3)	+0.05			A
(1)	2781.903	35936.01	5027(4)– 143(5)	+0.09	(0)	1.17	B
40	2782.552	35927.63	4008(4)– 41(3)	—0.06	(0)	1.00 …	
	2783.101	35920.55	5131(2)– 153(3)	+0.07			A
25	2786.306	35879.23	4102(6)– 51(5)	—0.07	$g_1 = 1.22$	g_2 1.37	
40	2786.798	35872.89	3861(1)– 27(2)	—0.06	$g_1 = 0.28$	$g_2 = 1.44$	
(1)	2799.525	35837.83	5122(3)– 153(3)	—0.04			B
	2789.580	35837.12	4920(3)– 133(2)	—0.08			A
(2)	2790.898	35820.20	5104(3)– 152(2)	+0.01			B
(1)	2793.504	35786.79	5345(1)– 176(1)	+0.02			B
(4)	2793.940	35781.20	4987(2)– 140(3)	0.00			B
(6)	2793.992	35780.54	4715(4)– 113(3)	+0.06	(0)	1.17	B
(8)	2794.193	35777.96	5063(6)– 149(6)	+0.03	(0.07)	1.14	B
(1)	2794.557	35773.30	4913(3)– 133(2)	+0.02			B
(2)	2796.106	35753.49	4877(2)– 130(1)	+0.07	(0, 0.85)	—	B
100	2796.727	35745.55	3848(3)– 27(2)	+0.03	$g_1 = 1.61$	$g_2 = 1.44$	9
			4677(3)– 110(4)	—0.16			
(1)	2801.924	35679.25	4705(3)– 113(3)	—0.04	(0.11)	1.25	B
80	2804.067	35651.98	5104(3)– 153(3)	—0.02	$g_1 = 1.25$	$g_2 = 1.54$	
	2805.416	35634.83	4840(1)– 127(2)	—0.11			A
100w	2806.906	35615.93	3561(3)– 0(4)	+0.01	(0)	1.16 …	
(2)	2807.486	35608.57	4577(3)– 101(2)	0.00			B
(1)	2808.241	35598.99	5098(2)– 153(3)	—0.02			B
40	2808.935	35590.20	3833(2)– 27(2)	—0.06	(0.08)	1.43	
(8)	2813.769	35529.06	5037(5)– 148(4)	—0.08	(0)	1.46	B
10	2813.839	35528.18	4830(3)– 127(2)	0.00	(0)	1.41	
50	2814.200	35523.62	3826(3)– 27(2)	—0.05	$g_1 = 1.23$	$g_2 = 1.45$	9
			4961(2)– 140(3)	+0.15			
10	2814.839	35515.56	3967(2)– 41(3)	—0.01			
8	2815.272	35510.09	4887(3)– 133(2)	—0.01	(0, 0.34)	—	
40	2815.780	35503.69	3824(1)– 27(2)	—0.02	(0)	1.36	
(2)	2817.512	35481.86	5032(3)– 148(4)	—0.06			B
	2819.482	35457.07	5486(2)– 194(2)	—0.16			A
12	2820.178	35448.32	5067(1)– 152(2)	+0.06	$g_1 = 1.20$	$g_2 = 1.63$	
10	2820.555	35443.58	5165(2)– 162(1)	+0.05	$g_1 = 1.09$	$g_2 = 1.76$	
20	2821.251	35434.84	4681(2)– 113(3)	—0.03	(0)	1.43	
(½)	2821.887	35426.85	5027(4)– 148(4)	—0.01	(0.10)	1.10	
(?)	2823.558	35405.89	5307(2)– 176(1)	—0.01			B
(½)	2823.929	35401.24	4414(3)– 87(4)	—0.07			B
20	2824.166	35398.27	4677(3)– 113(3)	—0.02	(0)	1.26	
(2)	2824.367	35395.75	4556(3)– 101(2)	—0.26			B, 1
(2)	2824.777	35390.61	4948(4)– 140(3)	—0.01			B
(1)	2824.888	35389.23	4840(1)– 130(1)	—0.02			B
(2)	2829.035	35337.35	4550(2)– 101(2)	—0.12	(0.28)	—	B
40	2829.269	35334.43	3949(2)– 41(3)	—0.05	$g_1 = 0.93$	$g_2 = 1.48$	
(6)	2829.345	35333.48	5154(2)– 162(1)	+0.01	(0)	1.24	B

TABLE III *(continued)*

Classified lines of Os I

Int.	λ_{air}	$\sigma_{vac.}$	Classification	$\delta\sigma$	Zeeman effect		Notes
(1)	2831.590	35305.46	5015(3)– 148(4)	—0.06	(0)	0.94	9
			5876(4)–2346(5)	—0.40			B, 1
(8)	2832.238	35297.39	4632(3)– 110(4)	—0.02	(0)	1.24	B
	2835.783	35253.26	5430(1)– 190(0)	—0.28			A, 1
25	2837.422	35232.90	4626(4)– 110(4)	+0.02	(0)	1.16	
30	2838.173	35223.58	3938(3)– 41(3)	—0.05	$g_1 = 1.18$	$g_2 = 1.46$	
100R	2838.626	35217.96	4036(4)– 51(5)	—0.04	(0)	... 1.72	
(2)	2840.447	35195.38	4953(5)– 143(5)	+0.09	(... 0.47)	1.14	B
(8)	2841.596	35181.15	3792(2)– 27(2)	—0.07	(0)	1.45	B
(½)	2843.109	35162.42	5406(2)– 189(3)	—0.04			B
(½)	2843.268	35160.46	4793(2)– 127(2)	—0.05			B
	2843.710	35154.99	5357(6)– 184(5)	+0.02			A
	2843.890	35152.77	5345(1)– 183(0)	+0.06	(0)	—	A
50	2844.396	35146.52	4029(6)– 51(5)	0.00	(0)	0.89 ...	
15	2844.680	35143.01	4948(4)– 143(5)	+0.01	(0)	0.94	
	2845.463	35133.34	4387(5)– 87(4)	+0.05			A
40	2846.391	35121.89	4088(2)– 57(1)	—0.02	$g_1 = 0.81$	$g_2 = 1.46$	
12	2846.554	35119.88	4386(4)– 87(4)	+0.02	(... 0.43)	1.27	
(1)	2847.310	35110.55	4920(3)– 140(3)	—0.11			B
(1)	2847.569	35107.35	5032(3)– 152(2)	—0.05			B
30	2848.247	35099.00	4994(3)– 148(4)	—0.01	(0)	0.72 ...	9
			5131(2)– 162(1)	+0.17			
15	2849.046	35089.16	5031(2)– 152(2)	+0.02	$g_1 = 1.13$	$g_2 = 1.62$	
75	2850.762	35068.04	3780(3)– 27(2)	—0.05	$g_1 = 1.26$	$g_2 = 1.45$	
(+)	2851.961	35053.30	4782(3)– 127(2)	0.00			B
	2852.491	35046.78	4913(3)– 140(3)	+0.04			A
(½)	2853.851	35030.08	5344(4)– 184(5)	—0.09	(0)	1.11	B
25	2855.337	35011.85	4375(4)– 87(4)	+0.04	$g_1 = 1.05$	$g_2 = 1.30$	
	2855.872	35005.29	5121(1)– 162(1)	—0.04			A
5	2857.537	34984.90	5388(3)– 189(3)	—0.21	(0.22)	1.17	
25	2860.063	34954.00	5116(0)– 162(1)	+0.03	(0)	1.73	
100	2860.956	34943.09	4008(4)– 51(5)	0.00	(0)	1.41	
(2)	2861.278	34939.16	5032(3)– 153(3)	—0.05			B
(½)	2861.392	34937.76	4830(3)– 133(2)	+0.03			B
(?)	2861.939	34931.09	5015(3)– 152(2)	+0.09			B
	2863.272	34914.82	4793(2)– 130(1)	0.00			A
(+)	2864.251	34902.89	5029(4)– 153(3)	+0.09	(0, 0.38)	—	B
15	2865.680	34885.48	4626(4)– 113(3)	+0.02	(0)	0.89	
(1)	2865.787	34884.18	5027(4)– 153(3)	+0.03			B
(1)	2869.397	34840.30	4761(3)– 127(2)	+0.04			B
50	2872.405	34803.81	3480(4)– 0(4)	—0.01	(0.28)	1.42	
(5)	2873.421	34791.51	4616(2)– 113(3)	—0.03	(0)	1.37	B
(2)	2874.154	34782.64	4780(0)– 130(1)	—0.02	(0.09)	0.32	B, 16
	2874.587	34777.40	5098(2)– 162(1)	+0.04	(0, 0.62)	—	A
50	2874.955	34772.94	4351(3)– 87(4)	+0.02	(0)	... 1.68	
	2875.791	34762.84	5015(3)– 153(3)	+0.03	(... 1.15)	—	A
(2)	2877.258	34745.12	5364(2)– 189(3)	—0.21			B

TABLE III *(continued)*

Classified lines of Os I

Int.	λ_{air}	$\sigma_{vac.}$	Classification	$\delta\sigma$	Zeeman effect		Notes
30	2877.351	34743.99	4577(3)- 110(4)	+0.02	(0)	1.18	
40	2878.400	34731.33	4049(1)- 57(1)	−0.01	g_1 = 2.16	g_2 = 1.45	
	2878.962	34724.55	4994(3)- 152(2)	+0.06			A
	2879.830	34714.09	5313(4)- 184(5)	—0.04			A
	2880.362	34707.68	5237(1)- 176(1)	+0.09			A
(½)	2880.697	34703.64	4486(3)- 101(2)	−0.09	(0)	—	B
(1)	2880.780	34702.64	4747(1)- 127(2)	−0.03			B
			4877(2)- 140(3)	+0.01			
	2882.483	34682.13					A
			4953(5)- 149(6)	+0.18			
(?)	2883.414	34670.94	5233(2)- 176(1)	−0.50			B, 1
(?)	2883.932	34664.71	4875(4)- 140(3)	0.02			B
20	2884.408	34658.99	4340(5)- 87(4)	0.00	(0)	0.96	
	2884.842	34653.78	5406(2)- 194(2)	+0.04			A
(1)	2885.177	34649.76	4987(2)- 152(2)	—0.24			B
(½)	2886.062	34659.13	5404(2)- 194(2)	0.10	(0)	0.96	B
10	2890.849	34581.77	3874(2)- 41(3)	—0.10			
			4793(2)- 133(2)	—0.06	g_1 = 1.21	g_2 = 0.94	9
(1)	2891.833	34570.00					B
			5958(3)- 2501(3)	—0.04			
(8)	2892.342	34563.92	4472(1)- 101(2)	—0.03	g_1 = 1.01	g_2 = 1.46	B
(?)	2892.983	34556.27	4994(3)- 153(3)	—0.03			B
(½)	2893.914	34545.15	5344(4)- 189(3)	—0.20			B
25	2895.064	34531.43	4556(3)- 110(4)	−0.02	g_1 = 1.00	g_2 = 1.16	
40	2896.063	34519.52	4753(2)- 130(1)	+0.01	g_1 = 0.99	g_2 = 0.32	
	2897.956	34496.97	4466(2)- 101(2)	—0.02			A
	2899.224	34481.88	4987(2)- 153(3)	+0.07			A
	2899.698	34476.24	5388(3)- 194(2)	−0.15			A
(½)	2901.212	34458.25	5067(1)- 162(1)	0.17			B
10	2901.322	34456.95	4747(1)- 130(1)	−0.03	g_1 = 1.15	g_2 = 0.31	
	2903.066	34436.25	5333(3)- 189(3)	−0.03	(0)	1.20	A
(4)	2903.214	34434.49	4852(4)- 140(3)	−0.01	(0)	1.03	B
	2904.673	34417.20	4875(4)- 143(5)	+0.09			A
40	2905.730	34404.68	4049(1)- 60(0)	0.01	(0)	2.17	
	2906.415	34396.58	4577(3)- 113(3)	+0.03			A
	2906.767	34392.41	4961(2)- 152(2)	+0.14			A
5	2908.026	34377.51	5058(1)- 162(1)	+0.03	g_1 = 1.06	g_2 = 1.74	
500R	2909.061	34365.28	3436(5)- 0(4)	—0.05	(0.15)	1.36	16
12	2909.669	34358.10	4538(4)- 110(4)	— 0.01	(... 0.32)	—	
5	2911.341	34338.37	5344(4)- 191(4)	— 0.05	(... 0.40)	—	
			3848(3)- 41(3)	—0.03	g_1 = 1.61	g_2 = 1.46	9
50	2912.334	34326.66					
			5960(2)- 2527(2)	0.11			
30	2913.844	34308.88	4447(1)- 101(2)	—0.02	g_1 = 1.01	g_2 = 1.45	
10	2914.710	34298.68	5271(4)- 184(5)	—0.04	(0)	1.11	
(+)	2915.446	34290.02	4913(3)- 148(4)	—0.04			B
	2916.053	34282.89	4705(3)- 127(2)	—0.02			A
40	2917.258	34268.73	4301(3)- 87(4)	0.00	g_1 = 1.03	g_2 = 1.29	
10	2917.827	34262.04	3940(5)- 51(5)	—0.02			

TABLE III *(continued)*

Classified lines of Os I

Int.	λ_{air}	$\sigma_{vac.}$	Classification	$\delta\sigma$	Zeeman effect		Notes
100	2919.794	34238.97	3697(1)– 27(2)	—0.05	$g_1 = 1.30$	$g_2 = 1.44$	
			5313(4)– 189(3)	+0.10			
(?)	2920.609	34229.41					B
			5333(3)– 191(4)	+0.06			
(2)	2921.069	34224.02	4961(2)– 153(3)	—0.06	$g_1 = 1.10$	$g_2 = 1.54$	B
	2922.165	34211.19	4830(3)– 140(3)	0.00			A
(½)	2924.243	34186.88	4852(4)– 143(5)	0.00			B
(6)	2924.491	34183.98	4556(3)– 113(3)	—0.01	$g_1 = 1.00$	$g_2 = 1.26$	B
	2925.281	34174.75	4753(2)– 133(2)	0.00	(0.08)	0.94	A
			5307(2)– 189(3)	+0.09			
40	2925.568	34171.39					
			3833(2)– 41(3)	—0.04	(0)	1.53	9
			3412(3)– 0(4)	+0.05			
30	2929.507	34125.45					
			4550(2)– 113(3)	0.00	(0)	1.10	9
15	2930.566	34113.11	5672(4)–2261(4)	—0.36			1
(1)	2930.630	34112.38	4747(1)– 133(2)	+0.16			B
40	2931.280	34104.81	3826(3)– 41(3)	—0.03	$g_1 = 1.23$	$g_2 = 1.47$	
(½)	2931.758	34099.25	5031(2)– 162(1)	—0.05			B
(2)	2932.447	34091.24	4948(4)– 153(3)	+0.01	$g_1 = 1.18$	$g_2 = 1.52$	B
			5237(1)– 183(0)	—0.10	(0)	1.10	9
(2)	2933.980	34073.43					B
			5249(4)– 184(5)	—0.01			
30	2934.642	34065.74	3680(3)– 27(2)	—0.04	(0)	1.51	
	2934.958	34062.08	5907(3)–2501(3)	+0.04			A
(1)	2936.813	34040.56	4813(4)– 140(3)	+0.01			B
(8)	2936.986	34038.55	4681(2)– 127(2)	+0.06	$g_1 = 1.16$	$g_2 = 1.00$	B
(1)	2937.230	34035.73	5293(3)– 189(3)	+0.07			B
(2)	2938.376	34022.45	5313(4)– 191(4)	+0.07	$g_1 = 1.19$	$g_2 = 1.02$	B
(1)	2939.388	34010.74	4538(4)– 113(3)	+0.05			B
(1)	2939.682	34007.34	5928(3)–2527(2)	—0.09			B
(2)	2939.990	34003.77	4274(4)– 87(4)	+0.03			B
(1)	2940.149	34001.94	4677(3)– 127(2)	+0.03			B
(1)	2942.120	33979.16	4920(3)– 152(2)	—0.30	(0)	1.40	B, 1, 17
8	2942.204	33978.19	4414(3)– 101(2)	+0.03	$g_1 = 1.13$	$g_2 = 1.46$	
30	2942.848	33970.75	3813(4)– 41(3)	—0.02	$g_1 = 1.25$	$g_2 = 1.48$	
(1)	2944.270	33954.35	5922(2)–2527(2)	—0.07			B
(½)	2947.636	33915.58	4913(3)– 152(2)	+0.04			B
	2948.171	33909.42	4407(2)– 101(2)	+0.06			A
12	2948.229	33908.75	3967(2)– 57(1)	0.00			
(10)	2948.289	33908.10	4875(4)– 148(4)	+0.05			B
30	2949.532	33893.77	3663(2)– 27(2)	—0.28	(0.16)	1.41	1, 17
8	2949.810	33890.58	4492(5)– 110(4)	+0.04	(0)	1.55	
5	2949.896	33889.59	4911(2)– 152(2)	+0.06	$g_1 = 1.09$	$g_2 = 1.61$	
(½)	2950.856	33878.57	5154(2)– 176(1)	+0.03	(0)	1.55	B
	2952.290	33862.11	4489(4)– 110(4)	+0.02	(... 0.20)	1.17	A
(1)	2953.917	33843.47	4793(2)– 140(3)	—0.05	(0)	—	B
	2954.296	33839.13	4486(3)– 110(4)	0.00			A
8	2955.000	33831.06	4905(1)– 152(2)	+0.03	$g_1 = 0.89$	$g_2 = 1.62$	

TABLE III *(continued)*

Classified lines of Os I

Int.	λ_{air}	$\sigma_{\text{vac.}}$	Classification	$\delta\sigma$	Zeeman effect		Notes
	2955.246	33828.24	5293(3)– 191(4)	—0.49			A, 1
(½)	2956.495	33813.96	5271(4)– 189(3)	+0.06	(0)	1.00	B
	2957.797	33799.07	5907(3)–2527(2)	—0.48			A, 1
(1)	2958.157	33794.96	5000(1)– 162(1)	+0.01			B
8	2958.341	33792.86	4681(2)– 130(1)	+0.06	g_1 = 1.15	g_2 = 0.31	9
			4813(4)– 143(5)	—0.07			
	2959.847	33775.66	5267(3)– 189(3)	+0.02			A
(½)	2960.608	33766.98	5480(1)– 210(1)	—0.03			B
40	2961.012	33762.37	3792(2)– 41(3)	—0.02	(0)	1.48	9
			4785(4)– 140(3)	+0.21			
30	2962.148	33749.42	3790(4)– 41(3)	—0.03	(0)	1.41	
20	2962.327	33747.39	4913(3)– 153(3)	+0.04	g_1 = 1.22	g_2 = 1.55	
(1)	2962.877	33741.12	4651(1)– 127(2)	+0.05	g_1 = 1.17	g_2 = 0.99	B
(+)	2963.057	33739.07	3950(0)– 57(1)	—0.07	(0)	—	B
(+)	2963.291	33736.41	4782(3)– 140(3)	+0.10	(0)	—	B
25	2964.062	33727.63	3949(2)– 57(1)	—0.03	g_1 = 0.92	g_2 = 1.46	
8	2964.615	33721.34	4911(2)– 153(3)	0.00	(0, 0.40)	0.44, 0.89...	
	2964.759	33719.70	5475(2)– 210(1)	—0.05			A
	2966.300	33702.19	5260(3)– 189(3)	0.00			A
(½)	2967.160	33692.42	4705(3)– 133(2)	—0.04			B
5	2968.446	33677.82	4852(4)– 148(4)	0.00	(0)	1.08	
	2969.787	33662.62	5307(2)– 194(2)	+0.04	(... **0.45**)	—	A
8	2970.689	33652.40	4887(3)– 152(2)	+0.04	(0, 0.32, 0.65)	—	
40	2970.972	33649.19	3780(3)– 41(3)	—0.07	g_1 = 1.26	g_2 = 1.47	
12	2972.251	33634.71	5864(2)–2501(3)	—0.05	(0)	1.66	
	2972.446	33632.51	4640(2)– 127(2)	—0.01			A
(8)	2973.064	33625.52	5204(6)– 184(5)	+0.04	(0)	1.33	B
(+)	2974.729	33606.69	5271(4)– 191(4)	—0.28			1, B
			5622(5)–2261(4)	—0.03			
(?)	2974.847	33605.36	3634(2)– 27(2)	+0.04			B
	2976.329	33588.63	5249(4)– 189(3)	+0.01			A
30	2977.637	33573.88	4232(3)– 87(4)	+0.03	—	2.02	
(2)	2978.098	33568.68	5267(3)– 191(4)	—0.03			B
20	2978.208	33567.44	4231(4)– 87(4)	+0.02	(... **0.26**)	—	
(4)	2978.487	33564.30	5486(2)– 213(2)	—0.23			B
12	2979.432	33553.65	4632(3)– 127(2)	+0.04	(0)	1.28	
(+)	2979.677	33550.89	4877(2)– 152(2)	—0.03			B
			5121(1)– 176(1)	+0.49			1
(+)	2981.806	33526.94	5293(3)– 194(2)	0.00	(0, 0.28, 0.55)	—	B
8	2982.125	33523.35	4761(3)– 140(3)	+0.08	(0.06)	1.11	
40	2982.902	33514.62	4489(4)– 113(3)	—0.05			
			4785(4)– 143(5)	+0.08	(0)	1.10	9
5	2984.290	33499.03	5116(0)– 176(1)	—0.01	(0)	1.40	

TABLE III *(continued)*

Classified lines of Os I

Int.	λ_{air}	$\sigma_{vac.}$	Classification	$\delta\sigma$	Zeeman effect		Notes
			4651(1)– 130(1)	0.00			
(½)	2984.615	33495.38					B
			5260(3)– 191(4)	+0.12	(0)	—	9
(½)	2984.940	33491.74	4486(3)– 113(3)	+0.03	(... 0.27)	—	B
10	2985.614	33484.18	4887(3)– 153(3)	+0.01	$g_1 = 1.28$	$g_2 = 1.53$	
8	2988.262	33454.51	4830(3)– 148(4)	0.00			
	2988.597	33450.76	5448(1)– 210(1)	—0.06			A
(½)	2988.685	33449.77	5475(2)– 213(2)	—0.07			B
			4361(2)– 101(2)	0.00	(0, 0.44)	—	9
12	2989.127	33444.83					2
			5333(3)– 198(4)	—0.32			1
	2989.939	33435.75	5233(2)– 189(3)	—0.09			A
	2990.630	33428.02	4620(1)– 127(2)	+0.04			A
20	2992.112	33411.46	4677(3)– 133(2)	0.00	$g_1 = 1.25$	$g_2 = 0.94$	
	2992.922	33402.42	4961(2)– 162(1)	—0.01	(0, 0.67)	—	A
15	2993.571	33395.18	4616(2)– 127(2)	+0.02	$g_1 = 1.18$	$g_2 = 1.00$	
	2994.320	33386.83	4640(2)– 130(1)	0.00	$g_1 = 1.16$	$g_2 = 0.31$	A
	2994.659	33383.05	4877(2)– 153(3)	+0.32			A, 1
(½)	2994.785	33381.65	5249(4)– 191(4)	—0.04	(... 0.43)	—	B
(½)	2995.624	33372.29	5864(2)–2527(2)	+0.02	(... 0.52)	—	B
(2)	2996.256	33365.26	4875(4)– 153(3)	—0.08			B
40	2997.647	33349.77	4351(3)– 101(2)	0.00	$g_1 = 1.22$	$g_2 = 1.47$	
(1)	3000.107	33322.43	5098(2)– 176(1)	0.00	$g_1 = 1.13$	$g_2 = 1.40$	B
60	3003.482	33284.98	4466(2)– 113(3)	+0.01	(0)	1.20	
(2)	3003.580	33283.90	4813(4)– 148(4)	+0.03			B
	3004.733	33271.16	4343(2)– 101(2)	+0.01			A
	3004.929	33268.99	5430(1)– 210(1)	−0.01	$g_1 = 1.56$	$g_2 = 0.88$	A
(2)	3005.114	33266.91	5267(3)– 194(2)	−0.01			B
	3005.731	33260.11	5216(2)– 189(3)	+0.02	(0)	1.19	A
	3007.712	33238.20	5313(4)– 198(4)	+0.02			A
40	3007.896	33236.14	5213(3)– 189(3)	−0.03	(0.15)	1.16	
20	3009.896	33214.06	4806(5)– 148(4)	−0.11	(0)	1.42	
(½)	3010.275	33209.88	4806(5)– 149(6)	−0.01			B
(1)	3012.379	33186.68	4840(1)– 152(2)	−0.07	$g_1 = 0.99$	$g_2 = 1.62$	B
(1)	3012.773	33182.34	4620(1)– 130(1)	+0.05	(0.31)	—	B
150	3013.074	33179.06	3591(1)– 27(2)	0.00	$g_1 = 1.28$	$g_2 = 1.44$	
100	3015.653	33150.65	4651(1)– 133(2)	+0.03	$g_1 = 1.18$	$g_2 = 0.94$	
100	3017.247	33133.14	4187(3)– 87(4)	+0.04	(0)	1.31	
300R	3018.039	33124.45	3312(3)– 0(4)	—0.03	$g_1 = 1.62$	$g_2 = 1.45$	
(2)	3019.035	33113.52	4414(3)– 110(4)	—0.04	(0)	1.22	B
100	3019.375	33109.79	3887(1)– 57(1)	—0.04	$g_1 = 1.89$	$g_2 = 1.46$	
(2)	3022.098	33079.96	4830(3)– 152(2)	—0.03			B
(1)	3023.253	33067.32	4715(4)– 140(3)	+0.21			B
(1)	3025.355	33044.35	5293(3)– 198(4)	—0.18	(... 0.34)	1.12	B, 11
	3027.913	33016.46	5404(2)– 210(1)	+0.02			A
40	3028.917	33005.49	4785(4)– 148(4)	+0.01	(... 0.32)	1.13	
(½)	3029.400	33000.23	4577(3)– 127(2)	+0.06			B
500	3030.695	32986.13	3813(4)– 51(5)	—0.04	$g_1 = 1.24$	$g_2 = 1.38$	
30	3031.006	32982.74	4172(4)– 87(4)	—0.01	(... 1.09)	—	

TABLE III *(continued)*

Classified lines of Os I

Int.	λ_{air}	$\sigma_{\text{vac.}}$	Classification	$\delta\sigma$	Zeeman effect		Notes
40	3031.295	32979.60	4782(3)– 148(4)	—0.03	(0)	1.03	
(2)	3031.717	32975.01	3874(2)– 57(1)	—0.04			B
50	3032.806	32963.17	4632(3)– 133(2)	+0.01	$g_1 = 1.12$	$g_2 = 0.95$	
(1)	3036.117	32927.22	5233(2)– 194(2)	+0.10			B
(1)	3036.212	32926.19	5404(2)– 211(3)	—0.04	(0)	—	B
(1)	3036.544	32922.60	5058(1)– 176(1)	+0.05	$g_1 = 1.05$	$g_2 = 1.40$	B
(1)	3037.118	32916.37	5121(1)– 183(0)	+0.03	(0)	—	B
(?)	3037.560	32911.58	4830(3)– 153(3)	—0.22			B
200	3040.900	32875.43	3561(3)– 27(2)	0.00	(0)	1.59	
(½)	3042.223	32861.14	4720(5)– 143(5)	—0.12			B
(2)	3042.626	32856.79	5175(3)– 189(3)	+0.08			B
100	3043.505	32847.30	3861(1)– 57(1)	0.00	(1.17)	1.46	
	3043.665	32845.60	4387(4)– 110(4)	+0.06			A
			4301(3)– 101(2)	+0.02	(0)	1.04	9
30	3044.067	32841.23	4905(1)– 162(1)	+0.04	(0.86)	—	
50	3044.408	32837.55	4620(1)– 133(2)	+0.02	(0, 0.32)	1.27	
100	3044.910	32832.14	4386(4)– 110(4)	+0.03	(0.14)	1.18	
30	3045.777	32822.79	5271(4)– 198(4)	+0.02	(0.24)	1.10	
(1)	3046.081	32819.52	4715(4)– 143(5)	+0.03			B
(4)	3047.453	32804.74	4616(2)– 133(2)	+0.03	(0.46)	—	B
(4)	3047.605	32803.11	5541(4)–2261(4)	—0.20			B
40	3049.042	32787.65	4556(3)– 127(2)	+0.04	(0)	1.00	
(4)	3049.336	32784.49	5267(3)– 198(4)	—0.02			B
80	3049.456	32783.20	3887(1)– 60(0)	+0.02	(0)	1.91	
100	3050.386	32773.20	5538(3)–2261(4)	+0.02	(0)	1.53	
80	3051.166	32764.83	3790(4)– 51(5)	—0.02	(0)	1.19	
(½)	3051.670	32759.42	5622(5)–2346(5)	—0.09			B
(½)	3052.185	32753.88	5165(2)– 189(3)	—0.12			B
40	3052.418	32751.39	5216(2)– 194(2)	+0.02	$g_1 = 1.21$	$g_2 = 0.98$	
(½)	3052.889	32746.34	5404(2)– 213(2)	—0.19	$g_1 = 0.97$	$g_2 = 1.26$	B
(2)	3053.376	32741.11	4813(4)– 153(3)	—0.05			B
(2)	3053.977	32734.67	5115(5)– 184(5)	—0.12	(... 0.24)	—	B
(1)	3054.507	32728.99	4550(2)– 127(2)	—0.08	(0.33, 0.63)	—	B
(4)	3054.661	32727.34	5213(3)– 194(2)	—0.11			B
50	3054.968	32724.05	4375(4)– 110(4)	—0.01	(... 0.37)	1.04	
80	3055.211	32721.45	4681(2)– 140(3)	—0.05	(0)	1.04	
	3056.058	32712.41	4793(2)– 152(2)	+0.09			A
	3056.184	32711.06	5260(3)– 198(4)	0.00			A
(8)	3057.468	32697.29	4407(2)– 113(3)	—0.05	(0)	1.40	B
500R	3058.66	32684.55	3268(4)– 0(4)	—0.06	(0)	1.46	9
			4677(3)– 140(3)	—0.37			1, 18
100	3060.305	32666.98	3682(4)– 41(3)	—0.09	(0)	1.33	
(½)	3061.923	32649.72	5175(3)– 191(4)	—0.06			B
100	3062.192	32646.85	3680(3)– 41(3)	—0.10	(0)	1.47	
20	3062.468	32643.91	5031(2)– 176(1)	—0.46			1
			5154(2)– 189(3)	—0.03	$g_1 = 1.51$	$g_2 = 1.20$	9

TABLE III

Classified lines of Os I

Int.	λ_{air}	$\sigma_{vac.}$	Classification	$\delta\sigma$	Zeeman effect		Notes
	3065.319	32613.58	5364(2)– 210(1)	—0.24			A
50	3066.116	32605.07	4782(3)– 152(2)	—0.04	g_1 = 1.11	g_2 = 1.61	
30	3066.833	32597.45	5249(4)– 198(4)	—0.04	(... 0.21)	1.09	
(½)	3068.149	32583.47	5388(3)– 213(2)	—0.22			B
125	3069.936	32564.51	3833(2)– 57(1)	—0.10	(0)	1.38	
(4)	3070.260	32561.07	4877(2)– 162(1)	—0.01	g_1 = 1.14	g_2 = 1.75	B
(?)	3071.120	32551.95	5782(3)–2527(2)	+0.47			B, 1
(2)	3071.865	32544.06	4793(2)– 153(3)	—0.07	g_1 = 1.20	g_2 = 1.52	B
125	3074.08	32520.61	3861(1)– 60(0)	—0.04	(0)	0.29	9
			5093(4)– 184(5)	+0.49			1
125	3074.96	32511.30	5512(4)–2261(4)	+0.03	(0.25)	1.58	
30	3076.751	32492.38	4265(2)– 101(2)	0.00			
100	3077.056	32489.15	4123(3)– 87(4)	0.00	(0)	1.92	
80	3077.437	32485.13	4351(3)– 110(4)	—0.04	(0)	1.07	9
			4386(4)– 113(3)	+0.44			1
100	3077.720	32482.15	4122(5)– 87(4)	—0.04	(0)	1.22	
125	3078.113	32478.00	3824(1)– 57(1)	—0.06	(0)	1.51	
125	3078.383	32475.15	3663(2)– 41(3)	—0.07	(0)	1.61	
40	3079.560	32462.74	4785(4)– 153(3)	—0.03	(0, 0.35, 0.70)	—	
(4)	3082.015	32436.88	4782(3)– 153(3)	—0.04			B
(8)	3083.750	32418.64	5503(5)–2261(4)	—0.02	(0)	—	B
60	3084.596	32409.75	4577(3)– 133(2)	+0.03	(0)	—	9
			5131(2)– 189(3)	+0.45			1
50	3086.274	32392.12	4761(3)– 152(2)	+0.05	g_1 = 1.12	g_2 = 1.62	
50	3087.748	32376.66	4375(4)– 113(3)	+0.02	(0)	0.64	
60	3088.266	32371.23	4340(5)– 110(4)	—0.01	(0)	1.39	
(½)	3088.429	32369.52	5067(1)– 183(0)	+0.09	(0)	—	B
100	3090.085	32352.17	4720(5)– 148(4)	—0.03	(0)	1.80	
100	3090.296	32349.96	3509(2)– 27(2)	—0.05	(0.22)	1.52	
80	3090.492	32347.91	4720(5)– 149(6)	—0.01	(0)	0.74	9
			5175(3)– 194(2)	—0.08			
40	3091.248	32340.00	5000(1)– 176(1)	—0.02	(0, 0.35)	—	11
	3092.790	32323.91	5344(4)– 211(3)	+0.28			A, 1
	3093.385	32317.69	6064(4)–2833(4)	—0.03			A
125	3093.587	32315.56	4640(2)– 140(3)	+0.03	(0)	1.03	
30	3094.074	32310.47	4715(4)– 148(4)	+0.04			
(½)	3094.707	32303.86	5486(2)– 225(1)	—0.38			B, 1
40	3099.261	32256.40	4242(1)– 101(2)	+0.02	(0, 0.41)	—	
(½)	3099.435	32254.58	4747(1)– 152(2)	+0.10			B
(½)	3100.353	32245.03	5165(2)– 194(2)	—0.25			B
			5213(3)– 198(4)	—0.01			
(2)	3101.158	32236.66	4632(3)– 140(3)	+0.04	(0)	1.13	9, B
			5480(1)– 225(1)	—0.15			

TABLE III *(continued)*

Classified lines of Os I

Int.	λ_{air}	$\sigma_{\mathrm{vac.}}$	Classification	$\delta\sigma$	Zeeman effect		Notes
125	3101.528	32232.82	4361(2)– 113(3)	+0.01	$g_1 = 1.04$	$g_2 = 1.25$	
(6)	3102.380	32223.97	4761(3)– 153(3)	+0.09	$g_1 = 1.13$	$g_2 = 1.55$	B
20	3102.716	32220.48	5132(3)– 191(4)	+0.05	(0.20)	—	3
	3103.285	32214.60	5333(3)– 211(3)	+0.04			A
20	3103.415	32213.22	5063(6)– 184(5)	+0.08	(0)	1.14	
(2)	3103.807	32209.15	4705(3)– 148(4)	—0.09			B
200d	3104.980	32196.98	4556(3)– 133(2)	—0.18	(0)	1.07	19
			4840(1)– 162(1)	+0.07	(0.75)	1.75	
($\frac{1}{2}$)	3105.688	32189.64	5475(2)– 225(1)	+0.09			B
150	3105.992	32186.49	3634(2)– 41(3)	0.00	$g_1 = 1.16$	$g_2 = 1.47$	
40	3107.378	32172.14	4626(4)– 140(3)	+0.05	(0)	1.23	
125	3108.981	32155.56	3792(2)– 57(1)	—0.01	(0)	1.46	
125	3109.381	32151.42	3824(1)– 60(0)	+0.01	(0)	1.55	
20	3109.679	32148.34	4753(2)– 155(3)	—0.48			1, 15
(1)	3110.404	32140.84	5104(3)– 189(3)	+0.02	(0.19)	—	B
30	3110.618	32138.63	4550(2)– 133(2)	+0.01			
100	3111.09	32133.76	4229(1)– 101(2)	—0.09	$g_1 = 1.02$	$g_2 = 1.46$	
	3112.491	32119.32	5122(3)– 191(4)	—0.44			A, 1
50	3114.814	32095.34	4486(3)– 127(2)	+0.01	$g_1 = 1.35$	$g_1 = 1.02$	
(6)	3115.027	32093.14	4511(0)– 130(1)	+0.02	(0)	0.31	B
($\frac{1}{2}$)	3115.707	32086.14	5050(4)– 184(5)	—0.27			B, 1
50	3116.475	32078.23	4616(2)– 140(3)	+0.06	(0)	0.98	
80	3118.122	32061.29	5467(3)-2261(4)	+0.02	(0, 0.19, 0.40, 0.58)	—	
150	3118.328	32059.17	4343(2)– 113(3)	+0.04	$g_1 = 1.01$	$g_2 = 1.26$	9
			5733(3)–2527(2)	+0.22			
30	3119.895	32043.07	5115(5)– 191(4)	+0.03	$g_1 = 1.17$	$g_2 = 1.01$	
20	3120.650	32035.32	5093(4)– 189(3)	+0.02	(0)	1.16	
(8)	3120.690	32034.91	5333(3)– 213(2)	+0.05	(0.10)	—	B, 11
(1)	3123.339	32007.73	5313(4)– 211(3)	+0.14			B
(1)	3125.948	31981.03	4301(3)– 110(4)	+0.05			B
	3127.984	31960.21	5037(5)– 184(5)	+0.14			A
	3128.408	31955.91	5541(4)–2346(5)	—0.19	(0)	—	A
20	3128.439	31955.56	4472(1)– 127(2)	+0.01	(0)	1.01	
60	3129.229	31947.49	4961(2)– 176(1)	—0.01	$g_1 = 1.10$	$g_2 = 1.40$	
30	3130.002	31939.61	5540(5)–2346(5)	+0.04			
($\frac{1}{2}$)	3130.576	31933.75	5104(3)– 191(4)	—0.14			B
125	3131.115	31928.25	4677(3)– 148(4)	+0.01	$g_1 = 1.26$	$g_2 = 1.09$	
20	3131.481	31924.52	4626(4)– 143(5)	+0.05	(0)	1.10	
($\frac{1}{2}$)	3131.877	31920.48	5448(1)– 225(1)	—0.14	(0)	—	B, 11
(1)	3133.832	31900.57	5131(2)– 194(2)	—0.01	(0, 0.52)	—	B, 11
(1)	3135.017	31888.51	4466(2)– 127(2)	—0.08			B
(?)	3136.209	31876.39	5029(4)– 184(5)	—0.05			B

(To be continued)

PHYSICS

STRUCTURE AND ZEEMAN EFFECT IN THE SPECTRA OF THE OSMIUM ATOM, Os I AND Os II

III

BY

TH. A. M. VAN KLEEF

Zeeman-laboratory, University of Amsterdam, the Netherlands

(Communicated by Prof. J. DE BOER at the meeting of January 30, 1960)

TABLE III *(continued)*

Classified lines of Os I

Int.	λ_{air}	$\sigma_{vac.}$	Classification	$\delta\sigma$	Zeeman effect		Notes
(½)	3137.284	31865.47	5175(3)– 198(4)	—0.11			B
(4)	3138.036	31857.83	5027(4)– 184(5)	+0.04	(0)	1.15	B
60	3140.314	31834.73	4705(3)– 152(2)	+0.01	$g_1 = 1.22$	$g_2 = 1.62$	
50	3140.938	31828.40	5093(4)– 191(4)	+0.03	$g_1 = 1.18$	$g_2 = 1.03$	
(½)	3142.363	31813.97	5293(3)– 211(3)	+0.03			B
30	3143.043	31807.09	5121(1)– 194(2)	+0.01	$g_1 = 0.65$	$g_2 = 0.97$	
20	3144.338	31793.99	5090(5)– 191(4)	—0.01	$g_1 = 1.19$	$g_2 = 1.03$	
(1)	3146.726	31769.86	5307(2)– 213(2)	—0.02	(0.10)	1.11	B
(1)	3146.951	31767.59	4715(4)– 153(3)	—0.13			B
15	3149.807	31738.78	5430(1)– 225(1)	—0.02	(0.06)	1.59	
(½)	3151.428	31722.46	4793(2)– 162(1)	—0.02	(0)	0.70	B
80	3152.070	31716.00	4274(4)– 110(4)	+0.01	$g_1 = 1.31$	$g_2 = 1.15$	9
			5672(4)–2501(3)	—0.23			
150	3152.673	31709.93	4187(3)– 101(2)	—0.02	$g_1 = 1.30$	$g_2 = 1.45$	9
			4472(1)– 130(1)	+0.07			
	3153.087	31705.80	5000(1)– 183(0)	—0.16	(0)	—	A
125	3153.611	31700.50	4447(1)– 127(2)	0.00	(0)	1.00	
20	3155.328	31683.25	4577(3)– 140(3)	+0.07			
(?)	3155.402	31682.51	3682(4)– 51(5)	+0.04	(0.13)	1.50	B, 11
500R	3156.248	31674.02	3681(5)– 51(5)	0.00	(0.41)	1.33	
100	3156.775	31668.73	5513(6)–2346(5)	0.00	(0)	1.06	
(8)	3156.997	31666.51	4705(3)– 153(3)	—0.02	$g_1 = 1.23$	$g_2 = 1.56$	B
100	3157.238	31664.09	5512(4)–2346(5)	+0.03	(0)	1.53	
20	3159.356	31642.86	4486(2)– 130(1)	—0.04	(0)	1.26	
(2)	3160.226	31634.15	5293(3)– 213(2)	—0.09			B
30	3160.286	31633.55	4301(3)– 113(3)	—0.01			
20	3160.427	31632.14	5104(3)– 194(2)	+0.04			
80	3161.445	31621.95	5067(1)– 190(0)	+0.03	(0)	1.18	
100	3161.728	31619.12	4036(4)– 87(4)	+0.03	(0.06)	1.32	

TABLE III *(continued)*

Classified lines of Os I

Int.	λ_{air}	$\sigma_{vac.}$	Classification	$\delta\sigma$	Zeeman effect		Notes
			5050(4)– 189(3)	—0.14	(0)	1.20	9
(2)	3163.496	31601.45					B
			5955(3)–2795(2)	—0.27			1
(6)	3164.422	31592.20	5271(4)– 211(3)	+0.02	(0.32)	—	B, 11
			4681(2)– 152(2)	+0.01	$g_1 = 1.15$	$g_2 = 1.62$	9
60	3164.612	31590.31					
			4780(0)– 162(1)	—0.01			
200	3166.512	31571.35	5503(5)– 2346(5)	—0.10	(… 0.39)	1.50	
			4677(3)– 152(2)	0.00	$g_1 = 1.24$	$g_2 = 1.60$	9
100	3168.281	31553.72					
			5267(3)– 211(3)	—0.20			
(2)	3168.648	31550.07	5486(2)– 233(2)	—0.22			B
(2)	3169.560	31541.00	5058(1)– 190(0)	+0.02			B
100	3173.196	31504.86	4486(3)– 133(2)	—0.02	$g_1 = 1.35$	$g_2 = 0.96$	
(½)	3173.623	31500.62	5406(2)– 225(1)	—0.13			B
(1)	3175.082	31486.14	5404(2)– 225(1)	—0.10			B
(1)	3175.434	31482.65	5480(1)– 233(2)	—0.21	$g_1 = 1.45$	$g_2 = 1.26$	B
20	3175.648	31480.53	5260(3)– 211(3)	+0.06	(0.10)	0.98	
(?)	3176.656	31470.54	4556(3)– 140(3)	—0.08			B
150	3178.065	31456.59	3561(3)– 41(3)	—0.01	(0.14)	1.49	
80	3178.240	31454.86	4447(1)– 130(1)	+0.05	$g_1 = 1.00$	$g_2 = 0.29$	
20	3179.259	31444.77	4911(2)– 176(1)	+0.01	$g_1 = 1.11$	$g_2 = 1.41$	
(8)	3180.128	31436.18	5132(4)– 198(4)	—0.05	(0)	1.07	B
(4)	3180.213	31435.34	5475(2)– 233(2)	—0.26	0.38	—	B, 1
	3180.972	31427.87	5032(3)– 189(3)	—0.16			A
(2)	3181.565	31421.99	4681(2)– 153(3)	—0.12			B
(8)	3181.806	31419.60	4575(5)– 143(5)	—0.04			B
100	3181.879	31418.88	4574(5)– 143(5)	+0.02	(0.43)	1.17	
20	3182.229	31415.43	4626(4)– 148(4)	+0.02	(… 0.24)	—	
100	3182.567	31412.09	4550(2)– 140(3)	+0.01	$g_1 = 1.34$	$g_2 = 1.10$	
40	3182.803	31409.76	5031(2)– 189(3)	—0.01	(0)	—	
10	3184.337	31394.63	5050(4)– 191(4)	—0.03	(0.53, 0.67)	—	
(4)	3184.654	31391.50	5029(4)– 189(3)	—0.12	(0)	1.12	B
(8)	3185.199	31386.13	4905(1)– 176(1)	—0.13	$g_1 = 0.89$	$g_2 = 1.38$	B
150	3185.327	31384.88	3412(3)– 27(2)	—0.03	(0)	1.45	
	3185.979	31378.48	5975(3)–2837(3)	+0.12			A
15	3186.402	31374.29	5267(3)– 213(2)	+0.07			2, 3
30	3186.533	31373.00	5027(4)– 189(3)	+0.03			
(6)	3186.875	31369.63	4414(3)– 127(2)	—0.13			B
100	3186.980	31368.59	4274(4)– 113(3)	+0.02	(0)	… 1.59	
(6)	3187.152	31366.90	5249(4)– 211(3)	0.00			B
80	3187.335	31365.01	4472(1)– 133(2)	—0.09	(0)	0.90	
125	3189.459	31344.22	4008(4)– 87(4)	+0.04	(… 0.20)	1.33	
(½)	3190.341	31335.55	5122(3)– 198(4)	—0.01			B
	3191.041	31328.71	5928(3)–2795(2)	+0.18			A
20	3191.191	31327.21	4753(2)– 162(1)	+0.04	$g_1 = 0.99$	$g_2 = 1.74$	
			4407(2)– 127(2)	0.00	$g_1 = 1.16$	$g_2 = 1.00$	9
40l	3193.867	31300.96					
			5260(3)– 213(2)	+0.19			

TABLE III *(continued)*

Classified lines of Os I

Int.	λ_{air}	$\sigma_{vac.}$	Classification	$\delta\sigma$	Zeeman effect		Notes
125	3194.234	31297.36	4538(4)– 140(3)	+0.04	(0)	1.04	
50	3194.687	31292.92	4651(1)– 152(2)	+0.04	$g_1 = 1.20$	$g_2 = 1.62$	
100	3195.382	31286.12	4232(3)– 110(4)	+0.02	(0)	1.35	
30	3195.966	31280.40	4265(2)– 113(3)	+0.04	$g_1 = 1.43$	$g_2 = 1.27$	
(8)	3196.048	31279.60	4231(4)– 110(4)	—0.07	(0.29)	—	B
40s	3197.200	31268.33	5037(5)– 191(4)	+0.01	$g_1 = 1.20$	$g_2 = 1.05$	9
			6064(4)–2938(3)	+0.49			1
(?)	3197.618	31264.24	4747(1)– 162(1)	—0.40			B, 1
(1)	3198.050	31260.02	5067(1)– 194(2)	—0.15	(0, 0.19)	—	B
(4)	3198.178	31258.77	5115(5)– 198(4)	—0.07	(0)	0.54	B, 11
(?)	3198.924	31251.48	5015(3)– 189(3)	—0.15			B
			5958(3)–2833(4)	+0.28			1
(?)	3202.046	31221.01	5032(3)– 191(4)	—0.09			B
(8)	3202.757	31214.08	5232(2)– 211(3)	—0.04			B
40	3202.834	31213.33	3697(1)– 57(1)	—0.04	(0.15)	1.35	
	3203.045	31211.30	5958(3)–2837(3)	+0.01			A
10	3205.777	31184.68	4640(2)– 152(2)	+0.35			1
			5029(4)– 191(4)	—0.01	(0.45, 0.58)	—	9
			5955(3)–2837(3)	+0.32			1
	3206.339	31179.24	5058(1)– 194(2)	+0.01			A
(1df)	3207.640	31166.56	5448(1)– 233(2)	—0.11			B
(2)	3209.390	31149.57	5104(3)– 198(4)	—0.12	(0, 0.19, 0.38)	—	B
(4)	3211.559	31128.53	5216(2)– 210(1)	—0.05	$g_1 = 1.21$	$g_2 = 0.88$	B
(1)	3212.365	31120.72	5907(3)–2795(2)	+0.07			B
40	3212.720	31117.28	4953(5)– 184(5)	+0.12	(0.53)	—	
20	3213.463	31110.09	4447(1)– 133(2)	+0.04			
(6)	3213.869	31106.16	4877(2)– 176(1)	+0.01			B
	3213.942	31105.48	4632(3)– 152(2)	+0.06			A
(2)	3216.227	31083.35	5364(2)– 225(1)	—0.27	(0, 0.23)	—	B, 1, 17
(1df)	3216.631	31079.45	5609(2)–2501(3)	—0.08	(0, 0.30, 0.60)	—	B
20	3218.023	31066.01	4123(3)– 101(2)	+0.01	(0, 0.37, 0.76)	—	
25	3219.135	31055.28	4407(2)– 130(1)	+0.01	$g_1 = 1.17$	$g_2 = 0.32$	
(1)	3219.726	31049.58	4538(4)– 143(5)	—0.12	(0)	—	B
30	3220.189	31045.12	4994(3)– 189(3)	0.00	(0)	1.19	9
			5015(3)– 191(4)	+0.42			1
(12)	3220.296	31044.08	5093(4)– 198(4)	—0.09	(0.24, 0.37, 0.48)	—	B
(zdf$\frac{1}{2}$)	3220.891	31038.35	5216(2)– 211(3)	—0.02			B
(?)	3223.205	31016.06	4640(2)– 153(3)	—0.08			B
	3223.409	31014.13	5213(3)– 211(3)	—0.32			A, 1
100	3223.858	31009.78	5090(5)– 198(4)	—0.02	$g_1 = 1.18$	$g_2 = 1.06$	
(2)	3226.447	30984.90	5430(1)– 233(2)	+0.05			B
(?)	3226.984	30979.74	4620(1)– 152(2)	—0.05			B
125	3227.280	30976.90	4531(6)– 143(5)	+0.01	$g_1 = 1.29$	$g_2 = 1.13$	
125	3229.206	30958.43	5000(1)– 190(0)	—0.02	(0)	1.42	
40	3230.399	30946.99	4616(2)– 152(2)	+0.02	$g_1 = 1.19$	$g_2 = 1.63$	

TABLE III *(continued)*

Classified lines of Os I

Int.	λ_{air}	$\sigma_{vac.}$	Classification	$\delta\sigma$	Zeeman effect		Notes
(4)	3231.271	30938.64	4232(3)– 113(3)	—0.04	(... 0.56)	—	B
150	3231.417	30937.25	4632(3)– 153(3)	+0.02	$g_1 = 1.11$	$g_2 = 1.54$	
(30)	3231.937	30932.27	4231(4)– 113(3)	+0.02	(0)	1.24	B
500R	3232.055	30931.14	3509(2)– 41(3)	—0.04	(0)	1.36	
150	3232.540	30926.50	4577(3)– 148(4)	0.00	(0)	1.02	
	3233.286	30919.39	5032(3)– 194(2)	+0.08			A
150	3234.196	30910.66	4575(5)– 148(4)	+0.08	(0)	1.13	
(8)	3234.654	30906.29	4575(5)– 149(6)	—0.01	(0)	0.93	B
100	3234.731	30905.55	4574(5)– 149(6)	+0.03	(0)	0.82	
(2)	3235.206	30901.01	5031(2)– 194(2)	—0.04	(0.30)	—	B
(½)	3236.312	30890.45	5345(1)– 225(1)	—0.01			B
(½)	3237.070	30883.22	5486(2)– 239(3)	—0.09			B
(6)	3238.172	30872.71	4626(4)– 153(3)	+0.01	$g_1 = 1.14$	$g_2 = 1.53$	B
100	3238.628	30868.37	3663(2)– 57(1)	—0.03	$g_1 = 1.40$	$g_2 = 1.54$	
(½)	3239.469	30860.35	5342(2)– 225(1)	—0.25	(0)	—	B
(2)	3239.645	30858.68	5216(2)– 213(2)	+0.01	(0.08)	1.24	B
80	3241.044	30845.36	4187(3)– 110(4)	+0.01	$g_1 = 1.30$	$g_2 = 1.16$	
15	3241.796	30838.20	4994(3)– 191(4)	+0.01	(0)	—	
15	3241.982	30836.43	4361(2)– 127(2)	0.00	(... 0.09)	—	
(2)	3242.157	30834.77	5213(3)– 213(2)	+0.02	(0)	—	B
(½)	3243.992	30817.32	5609(2)–2527(2)	+0.28			B, 1
4	3245.678	30801.32	4489(4)– 140(3)	+0.02			
	3245.948	30798.76	5917(2)–2837(3)	+0.01			A
1	3247.996	30779.33	4414(3)– 133(2)	+0.02	$g_1 = 1.13$	$g_2 = 0.95$	
(6)	3248.087	30778.47	4486(3)– 140(3)	+0.13			B
			4616(2)– 153(3)	—0.31			1
	3248.902	30770.78	5914(2)–2837(3)	+0.30			A, 1
(1zdf)	3249.120	30768.69	5475(2)– 239(3)	+0.07	(0)	—	B
(4)	3250.863	30752.19	4905(1)– 183(0)	—0.01	(0)	0.90	B
(2)	3251.431	30746.82	5406(2)– 233(2)	+0.02			B
50	3252.006	30741.41	4351(3)– 127(2)	+0.04	$g_1 = 1.22$	$g_2 = 1.02$	
(½)	3252.986	30732.13	5404(2)– 233(2)	—0.16	(0.60)	—	B
(1)	3254.054	30722.04	4088(2)– 101(2)	—0.03			B
60	3254.914	30713.92	4556(3)– 148(4)	—0.02	(0)	... 1.38	
(8)	3255.024	30712.88	4961(2)– 189(3)	—0.02	(0)	1.37	B
10h	3255.270	30710.56	4407(2)– 133(2)	+0.05	(0.45)	—	
(?)	3255.999	30703.69	5907(3)–2837(3)	+0.40			B, 1, 3, 14
80	3256.924	30694.97	4172(4)– 110(4)	—0.03	$g_1 = 1.04$	$g_2 = 1.16$	
60	3260.299	30663.19	3940(5)– 87(4)	+0.04	$g_1 = 1.18$	$g_2 = 1.30$	9
			4343(2)– 127(2)	+0.44			1
500R	3262.290	30644.48	3480(4)– 41(3)	—0.02	(0)	0.94 ...	
100	3262.751	30640.15	3938(3)– 87(4)	+0.03	(0)	... 1.75	
100h	3264.686	30621.99	5165(2)– 210(1)	—0.50			1
(?)	3265.924	30610.38	5050(4)– 198(4)	—0.08			B
400R	3267.945	30591.45	3059(4)– 0(4)	0.00	(0.30, 0.46)	1.51	

TABLE III *(continued)*

Classified lines of Os I

Int.	λ_{air}	σ_{vac}	Classification	$\delta\sigma$	Zeeman effect		Notes
200	3269.209	30579.62	3634(2)– 57(1)	—0.05	$g_1 = 1.15$	$g_2 = 1.46$	9
			4948(4)– 189(3)	—0.43			1
8	3269.887	30573.28	5890(3)–2833(4)	—0.15			
15h	3270.851	30564.28	5388(3)– 234(4)	—0.11	(0)	—	
15	3271.984	30553.69	4489(4)– 143(5)	+0.01			
(10)	3272.160	30552.05	4577(3)– 152(2)	+0.07	$g_1 = 1.12$	$g_2 = 1.61$	B
15	3273.384	30540.63	4538(4)– 148(4)	—0.01	(0)	1.08	
200	3275.201	30523.68	3628(0)– 57(1)	—0.03	(0)	1.46	
3	3276.411	30512.41	5154(2)– 210(1)	—0.02	(0)	—	
(½)	3276.694	30509.77	5307(2)– 225(1)	+0.18			B
(½)	3277.727	30500.16	4483(6)– 143(5)	+0.06			B
80	3277.966	30497.93	4187(3)– 113(3)	0.00	(0.13)	1.28	
(1)	3279.453	30484.14	5037(5)– 198(4)	+0.02			EH
	3281.666	30463.58	4531(6)– 149(6)	+0.03			A
	3281.829	30462.07	4987(2)– 194(2)	+0.16			A
	3282.552	30455.36	5175(3)– 213(2)	+0.07			A
6	3284.537	30436.92	5032(3)– 198(4)	+0.02			
			5876(4)–2833(4)	—0.07			
30	3286.674	30417.13	4343(2)– 130(1)	+0.07	$g_1 = 1.00$	$g_2 = 0.31$	
(1df)	3287.874	30406.04	5541(4)–2501(3)	—0.03			B
(2)	3288.480	30400.43	5029(4)– 198(4)	—0.06	(... 0.43)	1.30	B
30	3288.837	30397.13	5876(4)–2837(3)	+0.05	(0.33)	1.56	11
200	3290.263	30383.96	3312(3)– 27(2)	—0.03	$g_1 = 1.62$	$g_2 = 1.44$	9
			4577(3)– 153(3)	+0.17			
10	3291.127	30375.98	5538(3)–2501(3)	+0.04	(0.11)	—	
(1df)	3291.439	30373.10	4948(4)– 191(4)	—0.02	(0)	1.00	B, 11
(1df)	3294.217	30347.49	4172(4)– 113(3)	—0.09			B
(1)	3295.095	30339.40	4556(3)– 152(2)	—0.02			B
			4875(4)– 184(5)	+0.42			1
(½)	3295.942	30331.61	4049(1)- 101(2)	+0.11			B
(20)	3301.460	30280.91	4550(2)– 152(2)	+0.03	$g_1 = 1.32$	$g_2 = 1.62$	B
500R	3301.559	30280.00	3027(5)– 0(4)	+0.05	(0)	1.50	
(½)	3301.985	30276.09	5864(2)–2837(3)	+0.08			B
(6)	3302.918	30267.54	4793(2)– 176(1)	—0.01	$g_1 = 1.22$	$g_2 = 1.40$	B
(1)	3303.687	30260.50	5015(3)– 198(4)	0.00			B
(?)	3305.272	30245.98	4361(2)– 133(2)	0.00			B
(zdf8)	3305.661	30242.43	5154(2)– 213(2)	—0.09			B
80	3306.233	30237.20	4301(3)– 127(2)	+0.02	(0)	1.11	
(?)	3308.070	30220.41	5960(2)–2938(3)	—0.13	(0.29)	—	B, 11
(df½)	3309.192	30210.16	4911(2)– 189(3)	0.00			B
10	3309.667	30205.83	5132(4)– 211(3)	+0.19	$g_1 = 1.06$	$g_2 = 0.94$	
(½)	3309.842	30204.23	4961(2)– 194(2)	+0.05			B
(?)	3310.165	30201.28	4123(3)– 110(4)	—0.12			B
			5958(3)–2938(3)	—0.04			

TABLE III *(continued)*

Classified lines of Os I

Int.	λ_{air}	$\sigma_{\text{vac.}}$	Classification	$\delta\sigma$	Zeeman effect		Notes
200	3310.912	30194.47	4122(5)– 110(4)	+0.03	$g_1 = 1.27$	$g_2 = 1.14$	9
			4640(2)– 162(1)	—0.02			
8	3312.027	30184.30	5121(1)– 210(1)	+0.01	(0.21)	—	
10	3313.459	30171.26	4556(3)– 153(3)	+0.03	$g_1 = 1.00$	$g_2 = 1.54$	
50	3315.421	30153.41	3591(1)– 57(1)	0.00	$g_1 = 1.29$	$g_2 = 1.46$	
40	3315.688	30150.98	4351(3)– 133(2)	+0.06	$g_1 = 1.20$	$g_2 = 0.93$	
6	3317.276	30136.54	5345(1)– 233(2)	+0.03	$g_1 = 1.78$	$g_2 = 1.27$	
(½)	3317.403	30135.39	4780(0)– 176(1)	0.00			B
6	3318.590	30124.61	5344(4)– 234(4)	—0.02	(... **0.25**)	—	
(½)	3319.763	30113.97	5512(4)–2501(3)	—0.06			B
4	3319.902	30112.71	4550(2)– 153(3)	+0.02	(**0**, 0.22, 0.45)	—	2
(1)	3320.342	30108.72	4852(4)– 184(5)	—0.03	(0)	—	B
10	3320.425	30107.96	4840(1)– 183(0)	+0.04	(0)	0.99	
(?)	3320.548	30106.85	5342(2)– 233(2)	0.00			B
(1)	3320.747	30105.04	5122(3)– 211(3)	+0.07	(**0**, 0.28)	—	B, 11
10	3322.051	30093.23	4920(3)– 191(4)	+0.07			
(2)	3323.527	30079.86	5406(2)– 239(3)	+0.04	(0.11)	—	B, 11
(4)	3324.279	30073.06	4492(5)– 148(4)	—0.01			B
50d	3324.356	30072.39	4343(2)– 133(2)	+0.09	(**0.11**)	0.97	
15	3324.749	30068.81	4492(5)– 149(6)	+0.02	—	0.66	
(½)	3325.149	30065.19	5404(2)– 239(3)	—0.12			B
15	3326.386	30054.01	4994(3)– 198(4)	+0.02	(**0**, 0.12, 0.25, 0.36)	—	
12	3326.517	30052.83	4414(3)– 140(3)	+0.06	(... **0.09**)	1.10	
80	3327.425	30044.63	4489(4)– 148(4)	+0.01	$g_1 = 1.22$	$g_2 = 1.09$	
(?)	3328.368	30036.12	5432(6)– 242(5)	—0.02	(0)	—	B
20	3329.126	30029.28	4913(3)– 191(4)	+0.04	$g_1 = 1.24$	$g_2 = 1.05$	
(½)	3330.097	30020.52	5333(3)– 233(2)	—0.10			B
(1)	3330.652	30015.52	5333(3)– 234(4)	—0.04			B
(½)	3332.612	29997.87	4538(4)– 153(3)	—0.06			B
(½)	3333.483	29990.03	4620(1)– 162(1)	+0.08			B
12	3333.849	29986.74	4483(6)– 149(6)	—0.02	(... **0.23**)	—	
15	3334.151	29984.02	4407(2)– 140(3)	+0.05	(0)	1.00	
(6)	3335.376	29973.01	4887(3)– 189(3)	+0.02	(... **0.24**)	—	B
200R	3336.150	29966.05	3412(3)– 41(3)	—0.03	(**0.06**)	1.46	
2	3337.138	29957.18	4616(2)– 162(1)	+0.05			2
2	3340.689	29925.34	5122(3)– 213(2)	+0.07	(0)	1.32	2
	3341.386	29919.13	5104(3)– 211(3)	+0.03			A
10	3341.914	29914.37	5121(1)– 213(2)	—0.01	$g_1 = 0.66$	$g_2 = 1.25$	
	3343.265	29902.32	5388(3)– 239(3)	—0.15			A
(½)	3343.399	29901.09	5928(3)–2938(3)	—0.11			B
(½)	3346.633	29872.19	4753(2)– 176(1)	—0.05			B
			5782(3)–2795(2)	—0.39			1
(1)	3346.709	29871.51	4877(2)– 189(3)	+0.06	(0)	—	B
	3347.308	29866.20	5098(2)– 211(3)	+0.09			A

TABLE III *(continued)*

Classified lines of Os I

Int.	λ_{air}	$\sigma_{vac.}$	Classification	$\delta\sigma$	Zeeman effect		Notes
			4123(3)– 113(3)	+0.11			
30	3348.662	29854.09					
			4875(4)– 189(3)	—0.07	(0)	1.11	9
50	3351.735	29836.72	3591(1)– 60(0)	—0.04	(0)	1.29	
(1)	3353.474	29811.25	5237(1)– 225(1)	—0.03			B
(df)	3353.775	29808.58	5313(4)– 234(4)	—0.01			B
(½)	3354.943	29798.20	5486(2)– 250(2)	+0.02			B
	3356.298	29786.20	5240(3)–2261(4)	+0.08			A
(1)	3357.662	29774.07	5233(2)– 225(1)	—0.06			B
100	3357.969	29771.35	4386(4)– 140(3)	+0.03	g_1 = 1.20	g_2 = 1.09	
			4887(3)– 191(4)	—0.02			
(½)	3358.568	29766.04					B
			5809(4)–2833(4)	—0.38			1
8	3359.743	29755.63	5307(2)– 233(2)	—0.01	(... 0.12)	—	2
80	3361.149	29743.19	3848(3)– 87(4)	+0.01	g_1 = 1.60	g_2 = 1.29	
(6)	3361.576	29739.41	5104(3)– 213(2)	+0.01	(0)	1.23	B
2	3362.559	29730.72	5480(1)– 250(2)	—0.03	g_1 = 1.46	g_2 = 0.88	2
5	3362.926	29727.47	4913(3)– 194(2)	+0.02	(0)	—	
100	3364.122	29716.90	3245(2)– 27(2)	—0.05	g_1 = 1.85	g_2 = 1.45	
10	3364.362	29714.78	4813(4)– 184(5)	—0.02			
15	3365.872	29701.45	4911(2)– 194(2)	+0.01	g_1 = 1.10	g_2 = 0.98	
	3367.957	29683.09	5475(2)– 250(2)	—0.40			A, 1
(2)	3370.130	29663.93	5467(3)–2501(3)	—0.10			B
50	3370.202	29663.29	4375(4)– 140(3)	+0.02	(0)	0.95	
300R	3370.588	29659.90	3480(4)– 51(5)	0.00	(0)	1.39	
(4)	3371.948	29647.93	4242(1)– 127(2)	—0.05			B
			4486(3)– 152(2)	+0.03			
(8)	3372.035	29647.17					B
			4875(4)– 191(4)	—0.06			
40	3372.083	29646.75	4301(3)– 133(2)	+0.02	g_1 = 1.04	g_2 = 0.92	
3	3372.524	29642.87	4905(1)– 194(2)	—0.07	(0)	—	
15	3373.038	29638.35	4265(2)– 130(1)	+0.06	(0, ...)	—	
6	3373.204	29636.89	5067(1)– 210(1)	—0.49			1, 2
3	3375.131	29619.97	5293(3)– 233(2)	—0.03	(0)	1.24	2
6	3377.593	29598.38	5216(2)– 225(1)	0.00	(0, 0.41)	—	
50	3378.679	29588.88	4948(4)– 198(4)	—0.04	g_1 = 1.20	g_2 = 1.06	
	3380.621	29571.90	5484(1)–2527(2)	—0.06			A
15	3381.669	29562.71	4258(0)– 130(1)	+0.03	(0)	0.31	
80	3384.003	29542.32	4232(3)– 127(2)	+0.02	(—)	0.95, 1.08, 1.20	
20	3384.596	29537.15	4387(5)– 143(5)	+0.02	(0)	1.12	
40	3385.940	29525.42	4229(1)– 127(2)	—0.03	(0)	1.01	
			4386(4)– 143(5)	—0.01	(0)	0.95	9
30	3386.138	29523.69	5890(3)–2938(3)	+0.14			
			5960(2)–3007(2)	—0.22			
(½)	3386.401	29521.40	3826(3)– 87(4)	+0.07			B
10	3386.627	29519.43	4361(2)– 140(3)	—0.01	(0)	—	
100	3387.836	29508.90	3967(2)– 101(2)	—0.01	g_1 = 1.91	g_2 = 1.45	
(8)	3388.007	29507.41	4472(1)– 152(2)	+0.05	(0, 0.62)	—	B

TABLE III *(continued)*

Classified lines of Os I

Int.	λ_{air}	$\sigma_{vac.}$	Classification	$\delta\sigma$	Zeeman effect		Notes
(zdf?)	3388.327	29504.62	5958(3)–3007(2)	—0.07			B
3	3388.639	29501.90	4489(4)– 153(3)	—0.01			
2	3391.286	29478.88	4486(3)– 153(3)	—0.07	(... 0.58)	—	2
	3391.399	29477.92	5955(3)–3007(2)	+0.16			A
(4)	3392.961	29464.32	4887(2)– 194(2)	+0.05			B
(2)	3393.149	29462.69	5344(4)– 239(3)	—0.02			B, 15
40	3395.719	29440.39	4466(2)– 152(2)	—0.01	$g_1 = 1.30$	$g_2 = 1.61$	
	3396.179	29436.44	4785(4)– 184(5)	+0.03			A
(2)	3398.431	29416.90	4852(4)– 191(4)	—0.10	(0.20)	—	B
20	3398.575	29415.65	4375(4)– 143(5)	0.00	(0)	—	
20	3400.117	20402.32	4242(1)– 130(1)	+0.03	(—)	... 1.84	
(1)	3400.206	29401.55	5467(3)–2527(2)	+0.01			B
(1)	3400.320	29400.56	4830(3)– 189(3)	—0.06			B
40	3401.174	29393.18	5271(4)– 234(4)	0.00	(... 0.25)	1.08	
200	3401.859	29387.26	3813(4)– 87(4)	0.00	(0.25)	1.28	9
			5876(4)–2938(3)	+0.15			
200	3402.511	29381.63	2938(3)– 0(4)	—0.02	(0)	1.39	
(6)	3402.720	29379.82	5050(4)– 211(3)	—0.05	$g_1 = 1.20$	$g_2 = 0.95$	9
			5733(3)–2795(2)	—0.23			B
	3404.209	29367.00	5067(1)– 213(2)	—0.47			A, 1
(df$\frac{1}{2}$)	3404.687	29362.85	4877(2)– 194(2)	+0.02	(0)	1.23	B, 11
(1)	3405.030	29359.89	5267(3)– 233(2)	—0.09			B
30	3406.667	29345.79	4343(2)– 140(3)	+0.03	$g_1 = 0.99$	$g_2 = 1.10$	
	3408.366	29331.19	4036(4)– 110(4)	—0.15			A
40	3408.756	29327.80	3949(2)– 101(2)	—0.02	$g_1 = 0.93$	$g_2 = 1.46$	
	3411.270	29306.22	5868(3)–2938(3)	—0.33			A, 1
15	3412.740	29293.57	4265(2)– 133(2)	+0.04	(0)	0.94	
(?)	3413.043	29290.96	4550(2)– 162(1)	—0.08			B
(1)	3413.572	29286.43	5058(1)– 213(2)	—0.10			B
			5260(3)– 233(2)	—0.10			
(4)	3414.157	29281.41	5260(3)– 234(4)	—0.06	(0.13)	—	B
(1)	3414.349	29279.76	4229(1)– 130(1)	0.00			B
			5357(6)– 242(5)	—0.36			1
($\frac{1}{2}$)	3414.529	29278.22	5031(2)– 210(1)	—0.04			B
5	3415.224	29272.26	4466(2)– 153(3)	+0.05	(0.22)	—	2
	3415.960	29265.99	5864(2)–2938(3)	—0.05			A
	3417.553	29252.34	4447(1)– 152(2)	+0.03			A
($\frac{1}{2}$)	3418.413	29244.95	4913(3)– 198(4)	—0.09			B
(2)	3419.850	29232.67	5430(1)– 250(2)	—0.07	$g_1 = 1.59$	$g_2 = 0.90$	B
(1)	3420.175	29229.89	4813(4)– 189(3)	—0.09			B
(1)	3421.173	29221.36	3436(5)– 51(5)	—0.05			EH
30	3421.687	29216.97	3938(3)– 101(2)	0.00	$g_1 = 1.18$	$g_2 = 1.44$	
(2)	3425.080	29188.03	5031(2)– 211(3)	—0.02			B
(2)	3426.539	29175.60	4747(1)– 183(0)	—0.05	(0)	1.13	B
($\frac{1}{2}$)	3427.209	29169.89	5029(4)– 211(3)	—0.01			B

TABLE III *(continued)*

Classified lines of Os I

Int.	λ_{air}	$\sigma_{vac.}$	Classification	$\delta\sigma$	Zeeman effect		Notes
30	3427.438	29167.95	5249(4)– 234(4)	+0.05	(... 0.25)	1.07	
80	3427.671	29165.97	3790(4)– 87(4)	+0.03	$g_1 = 1.45$	$g_2 = 1.31$	
(?)	3428.928	29155.28	5344(4)– 242(5)	—0.04			B
	3429.382	29151.44	5027(4)– 211(3)	+0.19			A
			5922(2)–3007(2)	—0.12			
—	3429.987	29146.27	5313(4)– 239(3)	—0.40			1, 2
4	3430.066	29145.60	4681(2)– 176(1)	+0.07	(0)	—	2
20	3435.256	29101.57	4187(3)– 127(2)	+0.02	$g_1 = 1.31$	$g_2 = 1.01$	
(½)	3436.358	29092.24	5165(2)– 225(1)	—0.05			B
			5917(2)–3007(2)	+0.09			
(1)	3436.787	29088.60	5307(2)– 239(3)	—0.06			B
40	3439.486	29065.78	3780(3)– 87(4)	+0.03	(0)	1.39	
15	3439.831	29062.86	4340(5)– 143(5)	+0.03	(0.42)	—	
(20)	3440.594	29056.42	4008(4)– 110(4)	—0.01	$g_1 = 1.36$	$g_2 = 1.16$	B
(1)	3443.378	29032.93	4793(2)– 189(3)	—0.02	(0)	—	B
(8)	3443.955	29028.07	4387(5)– 148(4)	0.00	(0)	1.24	B
	3444.030	29027.46	5910(2)–3007(2)	—0.21			A
(½)	3444.130	29026.59	5032(3)– 213(2)	—0.02	(0)	1.13	B
50	3444.460	29023.81	4387(5)– 149(6)	+0.02	(0)	1.18	
(2)	3444.552	29023.04	4813(4)– 191(4)	—0.01			B
(½)	3444.891	29020.18	5233(2)– 233(2)	0.00			B
80	3445.551	29014.62	4386(4)– 148(4)	—0.02	$g_1 = 1.20$	$g_2 = 1.09$	
(2)	3447.457	28998.58	4840(1)– 194(2)	—0.08	(0)	0.98	B
	3447.910	28994.80	5406(2)– 250(2)	+0.11			A
100	3449.196	28983.96	4036(4)– 113(3)	+0.04	(0)	1.46	
	3449.432	28982.01	4887(3)– 198(4)	+0.15			A
			5154(2)– 225(1)	—0.22			
10	3450.390	28973.93	5000(1)– 210(1)	+0.02	$g_1 = 1.43$	$g_2 = 0.88$	
(2)	3451.442	28965.10	3312(3)– 41(3)	—0.06			B
(2)	3452.850	28953.29	5293(3)– 239(3)	+0.27			1
							B
			4806(5)– 191(4)	—0.06	(0, 0.15 ...)	—	9
20s	3453.054	28951.58	4232(3)– 133(2)	—0.27			1
			4785(4)– 189(3)	—0.01	(0)	1.11	9
50	3455.031	28935.01	4229(1)– 133(2)	+0.01	(0)	0.91	
20	3456.139	28925.73	4782(3)– 189(3)	—0.01	(0.25)	—	
(?)	3458.430	28906.55	4375(4)– 148(4)	—0.04	(0.11)	1.06	B
(½)	3460.195	28891.83	4830(3)– 194(2)	—0.07			B
	3463.636	28863.16	4875(4)– 198(4)	+0.13			A
15	3464.881	28852.76	4407(2)– 152(2)	—0.01	(... 0.94)	—	
(½)	3465.195	28850.14	5015(3)– 213(2)	—0.07			B
60	3465.435	28848.15	4651(1)– 176(1)	+0.04	$g_1 = 1.19$	$g_2 = 1.40$	
(½)	3465.883	28844.42	5216(2)– 233(2)	—0.01			B

TABLE III *(continued)*

Classified lines of Os I

Int.	λ_{air}	$\sigma_{vac.}$	Classification	$\delta\sigma$	Zeeman effect		Notes
(1)	3466.523	28839.09	4987(2)– 210(1) 5313(4)– 242(5)	—0.03 —0.19	(0)	0.90	9 B
12	3469.368	28815.44	5213(3)– 234(4)	—0.01	(0)	—	
20	3476.852	28753.42	4414(3)– 153(3)	+0.04	(0.81, 1.22)	—	
	3477.394	28748.97	4987(2)– 211(3)	+0.06			A
(½)	3477.568	28747.50	5131(2)– 225(1)	—0.09			B
(2)	3477.917	28744.61	4785(4)– 191(4)	—0.05			B
(½)	3478.316	28741.32	4715(4)– 184(5)	—0.04			B
100	3478.529	28739.55	4640(2)– 176(1)	—0.01	$g_1 = 1.15$	$g_2 = 1.39$	
(½)	3479.548	28731.14	5271(4)– 239(3)	—0.12			B
	3481.790	28712.67	4761(3)– 189(3)	—0.03			A
40	3482.112	28709.98	3887(1)– 101(2)	—0.01	$g_1 = 1.90$	$g_2 = 1.45$	3
20	3482.231	28709.01	4008(4)– 113(3)	0.00			
(1)	3482.844	28703.95	5000(1)– 213(2)	—0.05			B
(½)	3485.198	28684.57	4407(2)– 153(3)	—0.01			B
40	3487.248	28667.70	4351(3)– 148(4)	0.00	$g_1 = 1.22$	$g_2 = 1.08$	
30	3488.765	28655.24	4274(4)– 140(3)	+0.04	$g_1 = 1.33$	$g_2 = 1.10$	
10d	3488.906	28654.11	5121(1)– 225(1)	+0.02	$g_1 = 0.67$	$g_2 = 1.61$	
	3490.904	28637.71	4753(2)– 189(3)	+0.07			A
30	3491.495	28632.83	4852(4)– 198(4)	+0.03	(0)	1.06	
	3493.109	28619.63	5260(3)– 239(3)	+0.08			A
	3493.362	28617.56	5914(2)–3052(1)	+0.32			A, 1
	3494.352	28609.45	5868(3)-3007(2)	—0.47			A, 1
(1)	3497.780	28581.38	4961(2)– 210(1) 5359(2)-2501(3) 5910(2)-3052(1)	—0.01 —0.23 +0.35			B 1
80	3498.536	28575.21	3874(2)– 101(2)	0.00	$g_1 = 1.60$	$g_2 = 1.46$	
3	3499.266	28569.25	4987(2)– 213(2) 5864(2)–3007(2)	+0.04 —0.16			
10	3499.535	28567.05	4265(2)– 140(3)	+0.06			
100	3501.162	28553.78	4340(5)– 148(4)	+0.01	$g_1 = 1.22$	$g_2 = 1.09$	
30	3501.687	28549.49	4340(5)– 149(6)	0.00	(0)	—	
15	3503.451	28535.12	4620(1)– 176(1)	+0.10	$g_1 = 0.62$	$g_2 = 1.40$	
300	3504.659	28525.28	3268(4)– 41(3)	—0.01	(0)	1.45	
—	3505.014	28522.40	5113(3)-2261(4)	—0.04	(0)	—	2
	3506.408	28511.09	4187(3)– 133(2)	—0.01			A
(1)	3506.547	28509.93	5280(6)– 242(5)	0.00			B
10	3507.049	28505.85	4761(3)– 191(4) 5249(4)– 239(3)	+0.08 —0.13			
8	3508.851	28491.21	4961(2)– 211(3)	+0.03			2
30	3511.225	28471.95	4386(4)– 153(3)	+0.02			
—	3512.988	28457.66	4123(3)– 127(2)	+0.06	(0)	1.20	2
	3513.224	28455.78	5404(2)– 255(3)	—0.17			A
	3513.862	28450.58	4466(2)– 162(1)	+0.02	$g_1 = 1.31$	$g_2 = 1.75$	A
(1)	3515.045	28441.00	5175(3)– 233(2)	—0.05			B
	3515.630	28436.30	5175(3)– 234(4)	+0.31			A, 1

TABLE III *(continued)*

Classified lines of Os I

Int.	λ_{air}	$\sigma_{vac.}$	Classification	$\delta\sigma$	Zeeman effect		Notes
20	3516.630	28428.19	4747(1)– 190(0)	+0.05	(0)	1.14	
	3516.943	28425.68	5098(2)– 225(1)	—0.44			A, 1
8	3517.164	28423.87	5271(4)– 242(5)	0.00	(0)	1.18	
15	3517.292	28422.83	5103(4)–2261(4)	+0.03	(0.13)	—	
(?)	3518.023	28416.93	4782(3)– 194(2)	—0.09			B
20	3518.942	28409.51	4830(3)– 198(4)	+0.02			
15	3519.176	28407.62	4274(4)– 143(5)	+0.04			
	3520.485	28397.09	5672(4)–2833(4)	—0.30			A, 1
10	3523.167	28375.44	3940(5)– 110(4)	+0.04			
150	3523.636	28371.66	2837(3)– 0(4)	—0.02	$g_1 = 1.74$	$g_2 = 1.44$	
4	3525.290	28358.35	4948(4)– 211(3)	+0.02			2
	3525.398	28357.51	5672(4)–2837(3)	+0.03			A
	3525.794	28354.33	5342(2)– 250(2)	—0.21			A
80	3526.035	28352.36	3938(3)– 110(4)	—0.01	(0)	1.11	
(?)	3527.793	28338.24	5165(2)– 233(2)	—0.10			B
400R	3528.602	28331.74	2833(4)– 0(4)	—0.03	$g_1 = 1.59$	$g_2 = 1.44$	
100	3530.062	28320.01	3848(3)– 101(2)	—0.02	$g_1 = 1.62$	$g_2 = 1.46$	
15	3531.129	28311.46	4961(2)– 213(2)	—0.02	(0.17, 0.31)	—	
100	3532.800	28298.07	3245(2)– 41(3)	—0.05	$g_1 = 1.84$	$g_2 = 1.46$	
(2)	3532.947	28296.89	3967(2)– 113(3)	0.00			B
			4351(3)– 152(2)	+0.02	$g_1 = 1.21$	$g_2 = 1.61$	9
40	3533.408	28293.20					
			5388(3)– 255(3)	+0.09			
	3534.350	28285.69	5388(3)– 256(4)	+0.19			A
(?)	3536.514	28268.35	5333(3)– 250(2)	—0.16			B
1	3537.988	28256.58	4715(4)– 189(3)	+0.04			2
(?)	3540.200	28238.92	4813(4)– 198(4)	+0.07			B
(½)	3541.549	28228.16	5154(2)– 233(2)	—0.12			B
20	3541.906	28225.32	4232(3)– 140(3)	+0.01	(0.11)	1.18	11
(zdf10)	3542.589	28219.88	4361(2)– 153(3)	—0.17			B
150	3542.711	28218.91	4231(4)– 140(3)	+0.03	(0, 0.13, 0.27, 0.41)	1.56	
			4343(2)– 152(2)	—0.46			1
(½)	3543.315	28214.10					B
			4651(1)– 183(0)	+0.05			
12	3544.582	28204.01	4761(3)– 194(2)	+0.03			
	3545.293	28198.39	5249(4)– 242(5)	—0.20			A
1	3547.876	28177.83	5216(2)– 239(3)	+0.38			1, 2
	3547.923	28177.48	5876(4)–3059(4)	+0.17			A
(6)	3549.523	28164.75	3833(3)– 101(2)	—0.02	(0.09)	—	B
20	3549.684	28163.48	4301(3)– 148(4)	—0.03	(0)	1.13	
15	3550.714	28155.31	4705(3)– 189(3)	—0.04	(0)	1.21	
6	3550.939	28153.52	5213(3)– 239(3)	—0.01			2, 14
	3552.894	28138.03	5609(2)–2795(2)	—0.11			A
8	3554.048	28128.90	4753(2)– 194(2)	—0.02	(0)	0.98	2
8	3554.544	28124.97	4351(3)– 153(3)	—0.02			
10	3555.707	28115.77	3949(2)– 113(3)	—0.03			
30	3555.973	28113.67	4088(2)– 127(2)	0.00	$g_1 = 0.82$	$g_2 = 1.01$	
	3556.788	28107.28	5067(1)– 225(1)	+0.10			A

TABLE III *(continued)*

Classified lines of Os I

Int.	λ_{air}	$\sigma_{\text{vac.}}$	Classification	$\delta\sigma$	Zeeman effect		Notes
(1)	3557.940	28098.16	3826(3)– 101(2)	—0.02			EH
4h	3558.805	28091.30	4720(5)– 191(4)	—0.08			
150	3559.786	28083.55	3682(4)– 87(4)	—0.01	(... 0.44)	1.41	
(?)	3560.410	28078.63	4911(2)– 210(1)	—0.02			B, 3
			3824(1)– 101(2)	—0.04			
1	3560.468	28078.18					2
			4920(3)– 211(3)	—0.19			
150R	3560.855	28075.12	3681(5)– 87(4)	+0.01	(0)	1.23	
50	3562.337	28063.44	3680(3)– 87(4)	0.00	$g_1 = 1.48$	$g_2 = 1.32$	
5	3564.092	28049.62	4715(4)– 191(4)	+0.01			2
(1)	3567.078	28026.18	5058(1)– 225(1)	—0.06			EH
	3567.833	28020.24	4905(1)– 210(1)	+0.09			A
2	3568.566	28014.46	4913(3)– 211(3)	+0.01			2
	3569.544	28006.81	5132(4)– 234(4)	+0.17			A
100	3569.775	28004.98	3938(3)– 113(3)	+0.03	(0.20)	1.22	
	3571.879	27988.51	4911(2)– 211(3)	+0.07			A
30	3574.079	27971.25	4231(4)– 143(5)	—0.01	(0)	0.72 ...	14
	3575.451	27960.55	4785(4)– 198(4)	+0.09			A
	3576.945	27948.87	4705(3)– 191(4)	+0.45			A, 1
(vdf4)	3581.195	27915.67	5570(0)–2778(1)	—0.30	(0)	—	B, 1
			4681(2)– 189(3)	+0.07			
5	3581.794	27911.00			(0)	—	2, 12
			5122(3)– 233(2)	—0.03			
20	3583.091	27900.90	4620(1)– 183(0)	—0.06	(0)	0.62	
			4274(4)– 148(4)	—0.01			
15	3583.398	27898.51					
			4920(3)– 213(2)	—0.16			
15	3584.404	27890.68	5622(5)–2833(4)	+0.04			2,14
30	3586.506	27874.33	4677(3)– 189(3)	—0.02	(... 0.15)	1.24	
			4088(2)– 130(1)	+0.07	$g_1 = 0.82$	$g_2 = 0.31$	9
60	3587.315	27868.05					
			5293(3)– 250(2)	+0.16			
(1)	3587.974	27862.93	4407(2)– 162(1)	0.00			B
	3589.214	27853.33	5344(4)– 255(3)	—0.02			A
30	3590.107	27846.38	4626(4)– 184(5)	+0.04	(0)	1.07	
	3591.441	27836.06	4550(2)– 176(1)	—0.05			A
2	3591.602	27834.78	4913(3)– 213(2)	+0.03			2
	3592.205	27830.14	5342(2)– 255(3)	—0.17			A
20	3592.317	27829.25	5115(5)– 234(4)	0.00	$g_1 = 1.18$	$g_2 = 1.05$	
15	3597.519	27789.01	4301(3)– 152(2)	+0.02			
			3052(1)– 27(2)	0.00	(0, 0.12)	—	
300	3598.111	27784.43					
			4187(3)– 140(3)	—0.13	(0.39, 0.61)	... 1.09, 1.32 ...	20
	3599.462	27774.04	5175(3)– 239(3)	—0.03			A
60	3601.833	27755.72	3792(2)– 101(2)	—0.01	(0)	1.45	
			4905(1)– 213(2)	+0.47			1
15	3602.484	27750.71					
			5204(6)– 242(5)	+0.08	(0)	1.28	9

TABLE III *(continued)*

Classified lines of Os I

Int.	λ_{air}	$\sigma_{vac.}$	Classification	$\delta\sigma$	Zeeman effect		Notes
(2)	3602.827	27748.06	5031(2)– 225(1)	0.00			B
	3603.357	27744.01	5333(3)– 255(3)	—0.27			A, 1
(?)	3603.866	27740.07	4877(2)– 210(1)	+0.03			B
(1)	3604.305	27736.69	5333(3)– 256(4)	+0.02			B
(1)	3605.783	27725.32	5104(3)– 233(2)	+0.16			EH
	3612.718	27672.13	5098(2)– 233(2)	—0.04			A
	3612.763	27671.78	5165(2)– 239(3)	+0.42			A, 1
30	3613.329	27667.42	4677(3)– 191(4)	0.00	$g_1 = 1.25$	$g_2 = 1.03$	
(½)	3615.631	27649.80	4877(2)– 211(3)	—0.03			B
	3616.083	27646.38	4705(3)– 194(2)	—0.25			A
150	3616.574	27642.60	3780(3)– 101(2)	0.00	$g_1 = 1.26$	$g_2 = 1.45$	
60	3619.431	27620.78	4301(3)– 153(3)	—0.02	$g_1 = 1.06$	$g_2 = 1.54$	
15	3620.241	27614.60	5093(4)– 234(4)	+0.02	(0.38, **0.50**)	—	
(4)	3621.123	27607.87	5267(3)– 250(2)	0.00			B
(df2)	3625.367	27575.55	5103(3)–2346(5)	—0.04			B
(2)	3625.885	27571.61	4887(3)– 213(2)	+0.04			B
(1)	3627.240	27561.31	5154(2)– 239(2)	+0.01			B
40	3629.953	27540.71	3268(4)– 51(5)	+0.02			
(½)	3630.393	27537.37	5313(4)– 255(3)	+0.06			B
(½)	3630.777	27534.46	5260(3)– 250(2)	+0.04			B
(1)	3631.402	27529.73	5313(4)– 256(4)	+0.03			B
	3632.255	27523.29	4088(2)– 133(2)	+0.07			A
	3634.429	27506.83	5809(4)–3059(4)	+0.09			A
(1)	3634.675	27504.93	4640(2)– 189(3)	—0.03			B
(1)	3638.056	27479.37	5307(2)– 255(3)	+0.07			B
(1)	3639.290	27470.06	4877(2)– 213(2)	—0.07			EH
(4)	3639.471	27468.69	4232(3)– 148(4)	+0.06	(0)	—	B
(2)	3639.695	27467.00	4651(1)– 190(0)	+0.46			B, 1
200	3640.329	27462.22	4231(4)– 148(4)	+0.02	$g_1 = 1.22$	$g_2 = 1.08$	
30	3641.227	27455.44	3848(3)– 110(4)	+0.01			
20	3642.505	27445.81	4511(0)– 176(1)	—0.04	(0)	1.40	
	3643.974	27434.78	5538(3)–2795(2)	+0.23			A
(?)	3645.116	27426.15	4632(3)– 189(3)	+0.10			B
			4681(2)– 194(2)	—0.02			
1	3648.304	27402.19	4852(4)– 211(3)	—0.02			
			5475(2)– 273(3)	—0.05			
100	3648.806	27398.42	4361(2)– 162(1)	+0.02	$g_1 = 1.04$	$g_2 = 1.73$	
	3650.090	27388.81	5240(3)–2501(3)	—0.07			A
15	3650.381	27386.60	4172(4)– 143(5)	+0.01			
	3653.162	27365.75	4677(3)– 194(2)	+0.12			A
	3653.484	27363.37	3874(2)– 113(3)	+0.18			A
30	3653.725	27361.53	4626(4)– 189(3)	+0.01	(0)	1.03	
100	3654.492	27355.79	4274(4)– 153(3)	—0.02	$g_1 = 1.33$	$g_2 = 1.54$	
(1)	3654.838	27353.23	5067(1)– 233(2)	0.00			EH
	3655.928	27345.07	5132(4)– 239(2)	+0.35			A, 1
(1)	3656.404	27341.48	4575(5)– 184(5)	—0.03			B
	3656.516	27340.68	4574(5)– 184(5)	—0.05			A
150	3656.902	27337.76	3007(2)– 27(2)	—0.03	(**0.09**)	1.46	
(+)	3657.128	27336.07	5293(3)– 256(4)	+0.02			B

TABLE III *(continued)*

Classified lines of Os I

Int.	λ_{air}	$\sigma_{vac.}$	Classification	$\delta\sigma$	Zeeman effect		Notes
(1)	3660.778	27308.85	4987(2)– 225(1)	—0.07			EH
	3661.024	27307.01	4720(5)– 198(4)	—0.17			A
10	3661.252	27305.28	5237(1)– 250(2)	+0.06	$g_1 = 1.14$	$g_2 = 0.88$	
	3663.002	27292.27	5975(3)–3245(2)	—0.33			A, 1
	3665.745	27271.85	5058(1)– 233(2)	—0.44			A, 1
			4265(2)– 153(3)	+0.02			
40	3666.309	27267.62	4616(2)– 189(3)	+0.02	(0)	1.22	9
			5233(2)– 250(2)	—0.45			1
	3666.585	27265.59	4715(4)– 198(4)	+0.18			A
	3667.892	27255.88	5733(3)–3007(2)	—0.21			A
(1)	3669.473	27244.13	5122(3)– 239(3)	+0.08			EH
	3670.644	27235.45	5782(3)–3059(4)	0.00			A
200	3670.891	27233.59	3826(3)– 110(4)	+0.01	(0)	1.00	
	3672.111	27224.57	4343(2)– 162(1)	—0.15			A
(1)	3672.86	27218.99	4632(3)– 191(4)	—0.13			EH
40	3675.451	27199.80	4241(1)– 152(2)	+0.01	$g_1 = 1.86$	$g_2 = 1.62$	
10	3678.016	27180.83	5050(4)– 234(4)	—0.04	(… 0.58)	—	
(1)	3678.260	27179.03	4830(3)– 211(3)	+0.13			B
30	3681.568	27154.61	4626(4)– 191(4)	+0.02	$g_1 = 1.09$	$g_2 = 0.96$	
(10)	3683.460	27140.66	4123(3)– 140(3)	+0.05	(0)	1.09	B
(1)	3684.127	27135.75	5214(2)–2501(3)	—0.01			B
15	3684.546	27132.66	4049(1)– 133(2)	+0.01	(0)	—	
(1)	3685.372	27126.61	5240(3)–2527(2)	+0.22			EH
(2)	3686.003	27121.94	5271(4)– 255(3)	+0.04			B
(2)	3687.042	27114.29	5271(4)– 256(4)	0.00	(0)	1.13	B
(1)	3687.90	27107.98	3848(3)– 113(3)	—0.03			EH
	3688.155	27106.14	4840(1)– 213(2)	+0.18			A
200	3689.058	27099.48	3813(4)– 110(4)	—0.03	(… 0.28)	1.21	
	3689.776	27094.23	4232(3)– 152(2)	+0.12			A
15	3690.724	27087.24	5541(4)–2833(4)	+0.01			2
	3692.129	27076.96	4229(1)– 152(2)	—0.30			A, 1
(1)	3692.26	27075.98	5267(3)– 256(4)	—0.05			EH
(1)	3692.991	27070.64	5540(5)–2833(4)	—0.06			EH
(1)	3694.357	27060.61	5484(1)–2778(1)	+0.02	(0)	1.09	B, 11
(1)	3695.182	27054.57	5037(5)– 234(4)	+0.04			B
(½)	3695.646	27051.17	4961(2)– 225(1)	—0.02			B
	3697.536	27037.37	5132(4)– 242(5)	+0.04			A
20	3698.832	27027.87	4187(3)– 148(4)	—0.01	$g_1 = 1.30$	$g_2 = 1.08$	
5h	3700.299	27017.15	5538(3)–2837(3)	—0.04			
	3700.910	27012.70	5032(3)– 233(2)	+0.33			A, 1
(1)	3701.253	27010.19	5260(3)– 255(3)	0.00	(0)	0.98	B
(½)	3701.647	27007.32	5032(3)– 234(4)	+0.01			B
4	3702.763	26999.17	4830(3)– 213(2)	—0.03			
100	3703.247	26995.65	4466(2)– 176(1)	+0.02	$g_1 = 1.31$	$g_2 = 1.40$	
50	3706.556	26971.55	4538(4)– 184(5)	—0.02	(0)	1.27	
(1)	3706.644	26970.91	5029(4)– 234(4)	+0.01			B, 3
4	3709.145	26952.72	3833(2)– 113(3)	—0.03	$g_1 = 1.40$	$g_2 = 1.25$	9
			5093(4)– 239(3)	+0.06			

TABLE III *(continued)*

Classified lines of Os I

Int.	λ_{air}	$\sigma_{\text{vac.}}$	Classification	$\delta\sigma$	Zeeman effect		Notes
(1)	3709.205	26952.28	5027(4)– 234(4)	+0.03			B
50	3712.838	26925.91	4232(3)– 153(3)	—0.01	$g_1 = 1.09$	$g_2 = 1.54$	
100	3713.726	26919.47	4231(4)– 153(3)	—0.02	(0, 0.14, 0.31, 0.60)	—	
(1)	3714.022	26917.33	4632(3)– 194(2)	0.00			B, 15
(2)	3716.229	26901.35	4793(2)– 210(1)	—0.09	(0, 0.33)	—	B
12	3716.336	26900.57	3967(2)– 127(2)	+0.06			
(1)	3716.879	26896.67	5249(4)– 253(3)	+0.05			EH
(1)	3717.441	26892.60	5484(1)–2795(2)	—0.46			EH, 1
10	3717.926	26889.07	5249(4)– 256(4)	+0.06	(0)	1.12	2
30	3718.339	26886.08	3826(3)– 113(3)	—0.08	(0.07)	1.25	9
			4122(5)– 143(5)	+0.05			
(1)	3718.744	26883.18	4677(3)– 198(4)	—0.04			EH
(8)	3719.436	26878.15	3790(4)– 110(4)	—0.04	(0.62, 0.87, 1.14)	—	B
40	3719.522	26877.53	4172(4)– 148(4)	0.00	(... 0.16)	1.06	
80	3720.132	26873.12	3561(3)– 87(4)	+0.03	$g_1 = 1.51$	$g_2 = 1.30$	9
			5214(2)–2527(2)	—0.15			
	3720.375	26871.40	5955(3)–3268(4)	—0.03			A
30	3721.959	26859.93	5115(5)– 242(5)	—0.01	(... 0.15)	1.17	
15	3725.284	26835.96	5015(3)– 233(2)	—0.01	$g_1 = 1.15$	$g_2 = 1.27$	
20	3728.411	26813.45	3697(1)– 101(2)	—0.08	$g_1 = 1.33$	$g_2 = 1.46$	
(½)	3728.719	26811.24	4793(2)– 211(3)	+0.01			B
30	3729.220	26807.63	4447(1)– 176(1)	+0.09	$g_1 = 1.01$	$g_2 = 1.40$	
40	3730.731	26796.78	4088(2)– 140(3)	+0.10	$g_1 = 0.84$	$g_2 = 1.12$	
(2)	3733.344	26778.02	3780(3)– 110(4)	+0.02			B
(1)	3734.559	26769.31	4780(0)– 210(1)	+0.03			B
	3736.048	26758.67	4616(2)– 194(2)	—0.21			A
	3736.529	26755.23	5512(4)–2837(3)	—0.05			A
(4)	3736.964	26752.08	3813(4)– 113(3)	—0.01	(0)	1.21	B
(2)	3740.066	26729.89	4785(4)– 211(3)	+0.02			B
(1)	3740.24	26728.65	5486(2)– 281(3)	+0.28			EH, 1
40	3741.085	26722.62	5467(3)–2795(2)	—0.02	$g_1 = 1.82$	$g_2 = 2.04$	
20	3741.529	26719.44	3949(2)– 127(2)	+0.02	(... 0.14)	—	
	3742.727	26710.92	5609(2)–2938(3)	+0.11			A
(1)	3743.681	26704.11	4782(3)– 211(3)	+0.09			EH
(1)	3743.890	26702.62	5503(5)–2833(4)	+0.04			EH
(1)	3744.394	26699.03	5404(2)– 273(3)	+0.10			EH
	3745.399	26691.87	3245(2)– 57(1)	+0.47			A, 1
(½)	3745.698	26689.71	5000(1)– 233(2)	—0.05	(0)	—	B
(1)	3745.800	26688.98	5175(3)– 250(2)	+0.04	(0)	—	B
100	3746.466	26684.24	4102(6)– 143(5)	+0.01	$g_1 = 1.23$	$g_2 = 1.13$	9
			5914(2)–3245(2)	—0.48			1
4	3749.073	26665.68	4577(3)– 191(4)	0.00			
(1)	3749.84	26660.22	4556(3)– 189(3)	+0.17			EH
15	3750.590	26654.89	3967(2)– 130(1)	+0.07			

TABLE III *(continued)*

Classified lines of Os I

Int.	λ_{air}	$\sigma_{vac.}$	Classification	$\delta\sigma$	Zeeman effect		Notes
15	3750.804	26653.37	4187(3)– 152(2)	+0.01			
20	3751.315	26649.74	4575(5)– 191(4)	—0.02	(0, 0.16, 0.31, 0.51, 0.67)	—	
15	3751.943	26645.28	5093(4)– 242(5)	+0.01	(0)	1.03	
400R	3752.524	26641.16	2938(3)– 27(2)	0.00	(0)	1.53	
(50)	3752.640	26640.33	3680(3)– 101(2)	+0.04	(0)	1.51	B
(1)	3753.877	26631.55	4793(2)– 213(2)	+0.02			B
	3754.734	26625.51	5975(3)–3312(3)	—0.05			A
(1)	3756.795	26610.87	5090(5)– 242(5)	—0.03			B
40	3757.116	26608.60	3938(3)– 127(2)	+0.03	$g_1 = 1.19$	$g_2 = 1.02$	
(1)	3758.121	26601.48	4550(2)– 189(3)	—0.03			B
20	3760.274	26586.25	5165(2)– 250(2)	+0.02	$g_1 = 1.09$	$g_2 = 0.87$	
(½)	3764.705	26554.96	4987(2)– 233(2)	—0.01			B
100	3766.301	26543.71	3792(2)– 113(3)	0.00	$g_1 = 1.46$	$g_2 = 1.26$	9
			5213(3)– 255(3)	—0.46			1
80	3768.138	26530.77	3790(4)– 113(3)	0.00	(0, 0.19, 0.38, 0.57)	—	
	3769.871	26518.60	5050(4)– 239(3)	—0.35			A, 1
20	3771.640	26506.13	4753(2)– 210(1)	0.00	(0, 0.12)	1.07	
40s	3771.944	26504.00	4492(5)– 184(5)	0.00			
	3772.573	26499.61	5895(3)–3245(2)	—0.19			A
12	3773.780	26491.10	4761(3)– 211(3)	+0.12	(0.37, 0.51)	—	
60	3774.400	26486.75	4538(4)– 189(3)	0.00	$g_1 = 1.08$	$g_2 = 1.20$	
60	3774.619	26485.21	4187(3)– 153(3)	+0.04			
			3950(0)– 130(1)	0.00	(0)	0.30	9
	3775.703	26477.64	5960(2)–3312(3)	—0.07			A
(1)	3775.912	26476.18	5154(2)– 250(2)	+0.01			EH
(1)	3776.011	26475.45	4489(4)– 184(5)	—0.10			B
50	3776.254	26473.75	3949(2)– 130(1)	+0.02	$g_1 = 0.93$	$g_2 = 0.31$	
150	3776.992	26468.58	3663(2)– 101(2)	+0.02	$g_1 = 1.36$	$g_2 = 1.45$	
	3778.418	26458.62	5958(3)–2312(3)	+0.13			A
	3779.193	26453.18	4556(3)– 191(4)	+0.06			A
	3780.028	26447.35	5890(3)–3245(2)	—0.41			A, 1
20	3780.214	26446.02	4265(2)– 162(1)	+0.07	$g_1 = 1.42$	$g_2 = 1.75$	
(½)	3780.568	26443.54	4747(1)– 210(1)	—0.06			B
(½)	3781.800	26434.92	4632(3)– 198(4)	0.00			B
400R	3782.195	26432.16	3059(4)– 41(3)	+0.03	(0)	... 1.80	
(1)	3782.420	26430.59	3780(3)– 113(3)	+0.01			B
(?)	3782.717	26428.52	4472(1)– 183(0)	—0.01			B
20	3783.658	26421.94	4483(6)– 184(5)	—0.03			
(4)	3785.657	26407.99	4407(2)– 176(1)	—0.01	(0, 0.23)	—	B
	3788.222	26390.14	5907(3)–3268(4)	—0.22			A
	3788.467	26388.44	5480(1)– 284(3)	—0.07			A

(To be continued)

CONTENTS

PRINTED IN THE NETHERLANDS

DRUKKERIJ HOLLAND N.V., AMSTERDAM